




京都大学化学研究所 国際共同利用・共同研究拠点

化学関連分野の深化・連携を基軸とする
先端・学際グローバル研究拠点

令和2年度
成果報告書

京都大学化学研究所 国際共同利用・共同研究拠点

化学関連分野の深化・連携を基軸とする
先端・学際グローバル研究拠点



令和2年度
成果報告書

まえがき

京都大学化学研究所は、平成22年度から「化学関連分野の深化・連携を基軸とする先端・学際研究拠点」（平成28年度から第二期）として国内外の共同利用・共同研究を推し進め、それを新たな糧としてより多様でグローバルな化学研究の展開と若手研究者の育成・輩出を図って参りました。特に本拠点では、化学関連コミュニティの研究者の皆様からの要請を踏まえながら、化学研究所の研究分野の広がりと深さに加えて、これまでの様々な連携実績を活かし、国内外の研究機関の相互協力を担保するハブ環境も提供しています。先端・学際的分野深耕にあたっては、関連コミュニティの研究者の皆様と化学研究所の教員が推進する分野選択型、課題提案型、施設・機器利用型、連携・融合促進型等の多彩な共同研究と、拠点として主催・共催する各種国際会議、シンポジウム、研究会等を通じて、多様性と先進性を担保し、さらに、国際的視点に基づいて次代の化学関連分野を担う若手研究者の育成にも注力しています。また、拠点運営では、所外、学外の関連分野有識者と化学研究所の教員を委員とする共同研究委員会および運営評議会を核として、共同研究課題の公募・採択などを戦略的に遂行しております。

このようなグローバルな拠点活動が評価され、化学研究所は、平成30年11月13日文部科学大臣から国際共同利用・共同研究拠点に認定され、「化学関連分野の深化・連携を基軸とする先端・学際グローバル研究拠点」として活動を強化しています。国際拠点活動の三年目にあたる令和2年度には、化学研究所教員が一丸となって、203件の応募の中から採択された132件の共同研究を遂行しました。そのうち、グローバルな化学研究の展開と人材育成のため、国際共同研究枠を令和元年度の55件から62件（若手国際枠3件を含む）に増やしました。しかし、世界的な新型コロナウイルス感染症拡大のため、従来のように国際・国内共同研究を推進できない状況が未だ続いております。まだ終息が見通せないコロナ禍での拠点活動を支援するため、拠点ではリモート実験環境整備やハイブリッド会議システム導入など、研究・教育環境整備に取り組んで参りました。今後とも、国際的ハブ機能を活用し、国際共同利用・共同研究の一層の促進、国際学術ネットワークの充実、国際的・先進的視野をもつ若手研究者の育成に取り組むことで、化学を中心とする研究分野の深化と境界学術分野の新規開拓を一層推進して参ります。皆様にはさらなるご支援・ご協力のほどよろしくお願い申し上げます。

本報告書は、令和2年度の本拠点における研究成果をとりまとめたものです。本報告書をご一読頂き、今後の本拠点の目指すべき方向や活動の推進方法などに関する忌憚のないご意見・ご提案などをお聞かせ下されば幸甚に存じます。

化学研究所
所長 辻井 敬亘

令和2年度 共同利用・共同研究報告書 目次

1. 共同研究成果報告

分野選択型共同研究

ビーム科学分野

2020-1	化学的手法に基づくキラルプラズモニックナノ構造体の作製および設計技術	大阪産業技術研究所	中川 充	1
2020-2	中赤外レーザーを用いた振動強結合による反応性変化の解明	北海道大学	平井 健二	2
2020-3	X-ray structural studies on ligand complexes of maleylacetate reductase	Kansai University	Tadao Oikawa	3
2020-4	レーザープラズマ密度制御による金属表面機能性付与加工	大阪産業大学	草場 光博	4
2020-5	2色パルス誘起微細周期構造形成過程の研究	摂南大学	長島 健	5
2020-6	ナノ構造を持つ ISOL 用標的の開発	理化学研究所	大西 哲哉	6
2020-7	電子散乱による短寿命不安定核の奇妙な構造の解明	東北大学	須田 利美	7

元素科学分野

2020-8※	Gas sensing properties research of transition-metal oxides	Chinese Academy of Sciences	Haichuan Guo	8
2020-9※	Separation and evaluation of thiolate protected metal clusters with atomic precision by using LC/MS	Tokyo University of Science	Yuichi Negishi	9
2020-10※	Small molecule activation using anionic crypto-FLPs	University of Bonn	Rainer Streubel	10
2020-11※	Design and tailoring advanced functional materials: Symmetry operation and high pressure synthesis	National Taiwan University	Wei-tin Chen	11
2020-12※	Development of unsymmetrical π -electron systems of heavier main group elements and elucidation of their property	Tohoku University	Takeaki Iwamoto	12
2020-13※	Optical control of high-order harmonic generation from solids	University of Tsukuba	Shunsuke Sato	13
2020-14※	Iron-catalyzed C-H borylation	Visva-Bharati University	Alakananda Hajra	14
2020-15※	Electrochemically engineered peptide based organic-inorganic nanohybrids for electrocatalytic conversion of biomass into value added chemicals	Indian Institute of Technology Indore	Apurba K. Das	15
2020-16※	Iron-catalyzed enantioselective carbometalation and ring-opening reactions of oxabicycloalkenes and other related substrates and mechanistic consideration	Indian Institute of Engineering Science and Technology	Laksmikanta Adak	16
2020-17	Study on the stability of novel ternary nanoparticles by doping 3 rd elements	Meio University	Yasutomi Tatetsu	17

※ 国際共同利用・共同研究

2020-18	固体における高効率極端非線形光学のための極短中赤外光源の開発 量子科学技術研究開発機構	石井 順久	18
2020-19	マルチフェロイック物質における高強度テラヘルツパルスを用いたマグノン・フォノン励起	東京工業大学	佐藤 琢哉 19
2020-20	ラジカル重合停止反応機構の包括的な理解とモデル化 物質・材料研究機構	中村 泰之	20
2020-21	Development of dinuclear nickel complexes based on a monoanionic tridentate pincer-type ligand Yokohama National University	Yoshitaka Yamaguchi	21
2020-22	磁性微粒子を用いたウルシオール塗膜の機能発現 京都市産業技術研究所	橘 洋一	22
2020-23	Creation of effective oxidation scavenger for efficient perovskite-based solar cells University of Tsukuba	Takahiro Sasamori	23
バイオ情報学分野			
2020-24※	A study on statistical machine learning for efficient graph structured data analysis Nagoya Institute of Technology	Masayuki Karasuyama	24
2020-25※	Integrating omics data and module-based network with deep learning to develop cancer type predictive models National Chiao Tung University	Jinn-Moon Yang	25
2020-26※	Next-generation bioinformatics approaches for the accurate identification of protease-specific substrate cleavage sites Monash University	Jiangning Song	26
2020-27※	Revealing associations between giant viruses and eukaryotes in the global ocean through community networks inference and mining CNRS UMR6004	Samuel Chaffron	27
2020-28※	Unveiling the genomic contents of ecologically important marine giant viruses CNRS UMR8030	Tom O. Delmont	28
2020-29	Development of predictive methods for marine microbial communities based on remote sensing data National Institute of Advanced Industrial Science and Technology	Kentaro Tomii	29
2020-30	Control and analysis of complex networks via probabilistic minimum dominating sets Toho University	Jose C. Nacher	30
2020-31	Genomics and transcriptomics of giant viruses Tokyo University of Science	Masaharu Takemura	31
2020-32	Whole genome analyses of marine bacterivorous heterotrophic nanoflagellates Fukui Prefectural University	Takafumi Kataoka	32
2020-33	Comparative genome analysis of Parmales and diatoms: Looking for the ancestral genomic feature Fukui Prefectural University	Shinya Sato	33
2020-34	分子ネットワーク解析の統計的機械学習による解法と応用 帯広畜産大学	茅野 光範	34
物質合成分野			
2020-35※	Light emission from halide perovskites and related materials National Taiwan University	Ru-Shi Liu	35

2020-36※	Exploration of cycloaddition properties of guanidine functionalized anthracenes	Rudjer Boskovic Institute Davor Margetic	36
2020-37※	Development of new blue TADF emitters with horizontal molecular orientations	University of St Andrews Eli Zysman-Colman	37
2020-38※	Coupling of nanographenes and curved π -systems and elucidation of their electronic and optical interactions	Okinawa Institute of Science and Technology Graduate University Akimitsu Narita	38
2020-39※	Development of hole transport materials for tin-perovskite and device characterization	Osaka University Akinori Saeki	39
2020-40	Development of π -conjugated nickel complexes for high performance n-type thermoelectric materials	Osaka Institute of Technology Michihisa Murata	40
2020-41	ヘテロアズレンの特性を活かした新規機能性色素の創製	久留米工業高等専門学校 黒飛 敬	41
2020-42	Preparation of chiral silica via chiral transfer	Osaka Institute of Technology Tomoyasu Hirai	42
2020-43	マクロ環骨格内に導入した反応中間体の化学	広島大学 安倍 学	43
2020-44	有機分子触媒を用いるN-N軸不斉化合物の速度論的光学分割法の開発	名城大学 吉田 圭佑	44
現象解析分野			
2020-45※	Molecular understanding on the structures and dynamics of ionic end-aggregation polymers	Suraneree University of Technology Visit Vao-soongnern	45
2020-46※	Observation of orbital Hall effect in ferromagnet/nonmagnet bilayers	University of Ulsan Sanghoon Kim	46
2020-47※	High frequency response of polymeric liquids: Rheology and dielectric relaxation	Yamagata University Sathish K. Sukumaran	47
2020-48※	Dissolved and particulate Fe isotopic composition in the North Pacific Ocean: Sources and internal cycling	Academia Sinica Tung-Yuan Ho	48
2020-49※	Revealing exciton quenching mechanisms in thermally activated delayed fluorescent devices	University of St. Andrews Ifor D. W. Samuel	49
2020-50※	Fabrication of low bandgap semiconductor films and their light induced interfacial charge transfer and charge transport dynamics	RMIT University Yasuhiro Tachibana	50
2020-51※	Dynamics of shear-induced concentration fluctuation in polymer solutions	Stony Brook University Maya Endoh	51
2020-52	GISAXS-CT法による硫黄系高分子薄膜材料における硫黄元素の不均一分布評価	関西学院大学 藤原 明比古	52
2020-53	基部陸上植物・ゼニゴケにおける活性型ジベレリンの単離と同定	京都大学 河内 孝之	53
2020-54	Origin analysis of atmospheric aerosol of mountainous areas by trace metal analysis	Kindai University Yuzuru Nakaguchi	54
2020-55	部分フッ素化両親媒性分子の膜物性・構造に対するRf鎖長依存性の解析	群馬大学 園山 正史	55

2020-56	Dynamic viscoelasticity and tensile properties of thermoplastic elastomers	Nagoya University Atsushi Noro	56
2020-57	プラズモニク合金ナノ粒子を設計するための理論的指針の構築	北海道大学 飯田 健二	57
2020-58	Study on transportation of metal ions through a polymer membrane containing ionic liquid	Kyoto University of Education Hiroshi Mukai	58
2020-59	Exploration of hierarchical dynamics of amorphous polymers by broadband dielectric spectroscopy	Osaka University Osamu Urakawa	59
課題提案型共同研究			
2020-60※	Dielectric relaxation of type-A rouse chain under end-adsorption/desorption equilibrium: Effect of motional coupling	Sungkyunkwan University Youngdon Kwon	60
2020-61※	Molecular mechanisms for the inactivation of a growth hormone in rice	Chinese Academy of Science Zuhua He	61
2020-62※	Well-defined AIE-based polymer brush for the application of the electrochemical luminescence biosensors	South China University Ying Ma	62
2020-63※	Role of phosphoinositide signaling in pollen development	Peking University Sheng Zhong	63
2020-64※	Role of PX-PH-type phospholipase Ds in plant intracellular membrane traffic	MRC Yohei Ohashi	64
2020-65※	Proteomic approach to discovering specific inhibitors for bile-acid interacting enzymes	Peking University Xiaoguang Lei	65
2020-66※	Transfer of redox sensitive elements across the sediment-water interface in a hypoxia area near the East Chia Sea	Xiamen University Pinghe Cai	66
2020-67※	Application of artificial viral capsid to intracellular delivery	Tottori University Kazunori Matsuura	67
2020-68※	Structural and functional analysis of curvature-inducing peptides and application	Karlsruhe Institute of Technology Anne S. Ulrich	68
2020-69※	Site-selective protein acetylation by a small molecule	Fudan University Lu Zhou	69
2020-70※	Modulation of ferrimagnetic spin waves by electric field	KAIST Kab-Jin Kim	70
2020-71※	Novel strategy for intracellular delivery of nanomedicines	IBEC Silvia Pujals	71
2020-72※	Revealing exciton quenching mechanisms in thermally activated delayed fluorescent devices	Tsinghua University Lian Duan	72
2020-73※	Fabrication of nanotopographical polymer surfaces for bactericidal properties-II	Stony Brook University Maya Endoh	73
2020-74※	Synthesis of polyether nanocomposite solid polymer electrolytes for lithium ion batteries	Michigan State University Robert C. Ferrier, Jr.	74

2020-75※	Structural and functional analysis of the surface glycolipids of outer membrane vesicles released by bacteria	University of Naples Federico II	Maria Michela Corsaro	75
2020-76※	Construction of heterologous protein secretion system at low temperatures by using cold-adapted microorganisms	Southwest University	Xianzhu Dai	76
2020-77※	Molecular mechanisms governing gene expression regulation in plant plasticity	National Center of Biotechnology	Rubio Vicente	77
2020-78※	Formation of supramolecular complexes through a host-guest interaction between cycloparaphenylene and azacorannulenes	Nanyang Technological University	Shingo Ito	78
2020-79※	Research of multi-qubit diamond quantum processors	Australian National University	Marcus W. Doherty	79
2020-80※	Research toward stable NV centers at shallow region in diamond	Leibniz institute for surface engineering	Gopalakrishnan Balasubramanian	80
2020-81※	Advanced iodine-mediated stereoselective flow electrochemistry	Cardiff University	Thomas Wirth	81
2020-82※	Cation- π interaction in enolate chemistry	University of Bristol	Jonathan Clayden	82
2020-83※	Interdisciplinary approach to nanostructured materials for applications	Universite de Strasbourg	Jean-Pierre Bucher	83
2020-84※	Relationship between chain orientation, amount of defects, and toughness of glassy polystyrene materials	Changchun Institute of Applied Chemistry	Quan Chen	84
2020-85※	Search for four-wave-mixing in the vacuum - Unveiling dark components in the Universe -	Hiroshima University	Kensuke Homma	85
2020-86	Fine synthesis of polymer brush on ferromagnetic nano-platelet for magnetophotonic LC	Osaka University	Yoshiaki Uchida	86
2020-87	自己集積型希土類錯体の薄膜化とその機能解析	大阪市立大学	三枝 栄子	87
2020-88	Study on the regulatory network of plant epidermal cell differentiation	Hiroshima University	Rumi Tominaga	88
2020-89	免疫賦活化するナノ集合体	大阪大学	山崎 晶	89
2020-90	Functional analysis of non-canonical strigolactones as plant hormones and root-derived signals	Meiji University	Yoshiya Seto	90
2020-91	Analysis of phase equilibrium and molecular dynamics in mixture of nematic liquid crystal and solvent	Japan Women's University	Ryoko Shimada	91
2020-92	イネのストリゴラクトン生合成におけるCYP711Aファミリーの機能解析	東京大学	井澤 毅	92
2020-93	Analysis of the physiological functions of extracellular vesicles produced by intestinal bacteria and fermented food-derived bacteria and their application	Kindai University	Atsushi Kurata	93
2020-94	自己集合性分子による心筋細胞移植の効率化	信州大学	柴 祐司	94

2020-95	Observation of spin wave propagation in polycrystalline YIG thin films prepared by coprecipitation method	Gifu University Keisuke Yamada	95
2020-96	抗腫瘍性膜透過ペプチドによるがん進展調節	慶応義塾大学 大橋 若奈	96
2020-97	Giant exchange reaction from H to D terminating on nanocrystalline silicon surface and their use	Nagoya City University Takahiro Matsumoto	97
2020-98	界面活性剤を用いた溶媒含浸樹脂による金属イオンの固相抽出	大阪府立大学 倉橋 健介	98
2020-99	Anomalous Hall effect of ultrathin Pt films grown on magnetic oxide	Hokkaido University Taro Nagahama	99
2020-100	異常高原子価イオンを含む機能性酸化物合成とその構造物性研究	高エネルギー加速器研究機構 齊藤 高志	100
2020-101	メビウストポロジを有する環状パラフェニレンの芳香族性の検討	大阪大学 藤塚 守	101
2020-102	Study on electronic and magnetic behavior of perpendicularly magnetized cobalt ferrite films	Nagoya Institute of Technology Masaaki Tanaka	102
2020-103	マルチスケールシミュレーションによる p 型有機半導体材料群の電荷移動度予測	山形大学 城戸 淳二	103
2020-104	DArP法を用いた新規 π 共役系ポリマーの開発と有機薄膜太陽電池への応用	広島大学 尾坂 格	104
2020-105	Au ₂₅ スピン・価数依存強磁性単電子トランジスタ	東京工業大学 真島 豊	105
2020-106	高強度レーザーと構造的媒質の相互作用による高エネルギー密度プラズマの生成・保持に関する実験研究	京都大学 岸本 泰明	106
2020-107	酢酸菌の外的ストレス耐性における膜脂質の機能解析	立命館大学 豊竹 洋佑	107
2020-108	セルロースの氷形成挙動の解明と表面修飾による着氷防止制御	産業技術総合研究所 榊原 圭太	108
2020-109	ダイヤモンドの数ナノレベルにおける表面近傍のNV中心作製	金沢大学 徳田 規夫	109
2020-110	ダイヤモンド中のNV中心スピンの電氣的制御と電氣的検出	産業技術総合研究所 牧野 俊晴	110
2020-111	4-ピロリジン-ピリジン型分子触媒による化学選択的アシル化反応の理論的解析	立教大学 山中 正浩	111
2020-112	動的不斉の発現を基盤とする不斉極性転換型炭素—炭素結合形成反応の開発	千葉大学 森山 克彦	112
2020-113	Studies on enantioselective total syntheses of marine natural product bohémamines and their derivatives	Kanazawa University Tomoyuki Yoshimura	113
2020-114	再生可能資源・木質バイオマスの先端化学材料への効率的変換法の開発	奈良県立医科大学 秦野 修	114

連携・融合促進型共同研究

- 2020-115※ Determine the three-dimensional structure of ^{13}C labeled α -synuclein(61-95) in the Langmuir-Blodgett film and supported phospholipids bilayers by p-MAIRS FT-IR
Middle Tennessee State University Chengshan Wang 115
- 2020-116※ Hydrophilic dendrimers as additive for polyvinylidene fluoride based membranes
University of Montpellier Mona Semsarilar 117
- 2020-117※ Resolving percolation dynamics responsible for mechanical reinforcement in polymer nanocomposites under uniaxial stretching
Stony Brook University Tadanori Koga 119
- 2020-118※ The 16th International Workshop for East Asian Young Rheologists
Osaka University Tadashi Inoue 121

施設・機器利用型共同研究

- 2020-119※ Study on the mechanism of the crystal structural evolution of polydimethylsiloxane
University of Science and Technology of China Liangbin Li 123
- 2020-120※ High-pressure synthesis of potential multiferroic oxides
University of Edinburgh Kunlang Ji 124
- 2020-121※ Micro- and nano-structural characterization by advanced transmission electron microscopy of novel functional materials for battery development
Chiang Mai University Torranin Chairuang Sri 125
- 2020-122※ Electron energy loss spectroscopy analysis of hexagonal multilayer graphene
National Taiwan University Cheng-Yen Wen 126
- 2020-123※ Electronic excitations in charge-density-wave systems
National Taiwan University Ming-Wen Chu 127
- 2020-124※ Synthesis and characterization of novel organoselenium and -tellurium compounds
Rikkyo University Mao Minoura 128
- 2020-125 単結晶X線構造解析を用いた、含フッ素共役分子の結晶構造におけるフルオラス相互作用の解明
茨城大学 吾郷 友宏 129
- 2020-126 Synthesis and structural characterization of low-valent species of heavier group 14 elements
Kindai University Tsukasa Matsuo 130
- 2020-127 DNP-NMRを利用した炭素材料表面官能基解析法の開発
岡山大学 後藤 和馬 131
- 2020-128 平面シリセンナノリボンの理論設計と新しい動作原理の探究
東北大学 高橋 まさえ 132
- 2020-129 核融合プラズマ対向材料中の水素・ヘリウム挙動の高精度測定
島根大学 宮本 光貴 133
- 2020-130 Synthesis and structures of cationic aromatics bearing thiopyrylium units
Fukuoka University Noriyoshi Nagahora 134
- 2020-131 FT-ICR-MSを用いた湖沼及び土壌環境中溶存有機物の化学特性および起源解析
京都工芸繊維大学 布施 泰朗 135
- 2020-132 2次元物質欠陥の束縛励起子のSTEM-EELS解析
九州大学 斉藤 光 136

2. 国際学会、シンポジウム・研究報告会

新型コロナウイルス感染拡大防止のため、令和2年度は開催せず。

3. 成果発表論文

137

(令和3年2月までに刊行された論文で、平成22–令和元年度の成果報告書に掲載されていないもの)

紙数の都合により、*を付けた論文のみについて、別刷りを本報告書に記載する。

- 1)* Highly Luminescent CsPbBr₃@Cs₄PbBr₆ Nanocrystals and Their Application in Electroluminescent Emitters, *J. Phys. Chem. Lett.*, 11, 10196–10202 (2020).
- 2)* Effect of Head-to-Head Association/Dissociation on Viscoelastic and Dielectric Relaxation of Entangled Linear Polyisoprene: An Experimental Test, *Macromolecules*, 53, 1070–1083 (2020).
- 3) Helicenes Fused with Hexafluorocyclopentene (HFCP): Synthesis, Structure, and Properties, *Eur. J. Org. Chem.*, 2020, 1871–1880 (2020).
- 4) Development of P- And N-Chirogenic Ligands Based on Chiral Induction from a Phosphorus Donor to a Nitrogen Donor in Palladium Complexes, *Organometallics*, 39, 1672–1677 (2020).
- 5) Reaction of germabenzeylpotassium with TBDMSCl: Unusual trimerization of germabenzene skeletons, *Phosphorus Sulfur Silicon Relat. Elem.*, 195, 936–939 (2020).
- 6) Visible-Transparent Aromatic Polymers Obtained by the Polycondensation of a Bis(trifluorovinyl)benzene with Bisphenols, *Macromolecules*, 53, 2942–2949(2020).
- 7) Insertion reaction of chalcogens into an Al-P bond, *Heterocycles*, 100, 1084–1093 (2020).
- 8) Facile preparation of α,ω -diynes bearing a perfluoroalkylene linker $-(CF_2)_n-$ ($n = 4,6$) and their application for Co- or Rh-catalyzed [2+2+2]cycloaddition reactions affording aromatic compounds with perfluoroalkylene units, *J. Fluorine Chem.*, 234, 109512 (2020).
- 9) Additive-Free Conversion of Internal Alkynes by Phosphanylalumanes: Production of Phosphorus/Aluminum Frustrated Lewis Pairs, *ChemPlusChem*, 85, 933–942 (2020).
- 10) 1,2-Insertion reactions of alkynes into Ge-C bonds of arylbromogermylene, *Dalton Trans.*, 49, 7189–7196 (2020).
- 11) Discovery of Self-Assembling Small Molecules as Vaccine Adjuvants, *Angew. Chem. Int. Ed.*, 60, 961–969 (2020).
- 12) A Single H₂O Molecule inside Hydrophobic Carbon Nanocavities: Effect of Local Electrostatic Potential, *Chem. Lett.*, 49, 244–247 (2020).
- 13) Precise synthesis of double-armed polymers with fullerene C₆₀ at the junction for controlled architecture, *Polym. Chem.*, 11, 4417–4425 (2020).
- 14) Cation Recognition on a Fullerene-Based Macrocyclic, *Chem. Sci.*, 11, 12428–12435 (2020).
- 15) Doubly-Holed Fullerenes, *J. Am. Chem. Soc.*, 142, 20572–20576 (2020).
- 16) Aluminum-Based Initiators from Thiols for Epoxide Polymerizations, *Macromolecules*, 53, 8181–8191 (2020).
- 17) Room Temperature Electrically Detected Nuclear Spin Coherence of NV Centres in Diamond, *Sci. Rep.*, 10, 792 (2020).
- 18) Charge state control by band engineering, *Semicond. Semimet.*, 103, 137–159 (2020).
- 19) Switchable giant nonreciprocal frequency shift of propagating spin waves in synthetic antiferromagnets, *Sci. Adv.*, 6, eaaz6931 (2020).

- 20) Enhanced antiferromagnetic resonance linewidth in NiO/Pt and NiO/Pd, *Phys. Rev. B*, 101, 060402(R) (2020).
- 21) Fabrication of ferrimagnetic Co/Gd/Pt multilayers with structural inversion symmetry breaking, *J. Mag. Soc. Japan*, 44, 9–14 (2020).
- 22) Dependence of Gilbert damping constant on microstructure in nanocrystalline YIG coatings prepared by co-precipitation and spin-coating on a Si substrate, *J. Magn. Magn. Mater.*, 513, 167253 (2020).
- 23) Observation of superconducting diode effect, *Nature*, 584, 373–376 (2020).
- 24) Tailoring THz antiferromagnetic resonance of NiO by cation substitution, *Phys. Rev. Mater.*, 4, 074402 (2020).
- 25) Chromatic aberration effect in refraction of spin waves, *J. Mag. Soc. Japan*, 44, 133–136 (2020).
- 26) Laser stimulated THz emission from Pt/CoO/FeCoB, *App. Phys. Lett.*, 117, 192403 (2020).
- 27) An Artificial Amphiphilic Peptide Promotes Endocytic Uptake by Inducing Membrane Curvature, *Bioconjug. Chem.*, 31, 1611–1615 (2020).
- 28) Enhancing the activity of membrane remodeling epsin-peptide by trimerization, *Bioorganic Med. Chem. Lett.*, 30, 127190 (2020).
- 29) Strigolactone biosynthesis, transport and perception, *Plant J.*, 105, 335–350 (2020).
- 30) Effects of a pyroglutamyl pentapeptide isolated from fermented barley extract on atopic dermatitis-like skin lesions in hairless mouse, *Biosci. Biotechnol. Biochem.*, 84, 1696–1705 (2020).
- 31) Lysophosphatidic acid acyltransferase from the thermophilic bacterium *Thermus thermophilus* HB8 displays substrate promiscuity, *Biosci. Biotechnol. Biochem.*, 84, 1831–1838 (2020).
- 32) Chemoproteomic Profiling of a Pharmacophore-Focused Chemical Library, *Cell Chem. Biol.*, 27, 708–718.e10 (2020).
- 33) Discovery of a Small-Molecule-Dependent Photolytic Peptide, *J. Am. Chem. Soc.*, 142, 1142–1146 (2020).
- 34) Tris(triazolo)triazine-based emitters for solution-processed blue thermally activated delayed fluorescence organic light-emitting diodes, *Mater. Adv.*, 1, 2862–2871 (2020).
- 35) Conformation Control of Iminodibenzyl-Based Thermally Activated Delayed Fluorescence Material by Tilted Face-to-Face Alignment With Optimal Distance (tFFO) Design, *Front. Chem.*, 8, 530 (2020).
- 36) Mechanistic study of silane alcoholysis reactions with self-assembled monolayer-functionalized gold nanoparticle catalysts, *Catalysts*, 10, 1–17 (2020).
- 37) Detailed structural characterization of the lipooligosaccharide from the extracellular membrane vesicles of *Shewanella vesiculosa* HM13, *Mar. Drugs*, 18, 231 (2020).
- 38) Characterization of a novel class of glyoxylate reductase belonging to the β -hydroxyacid dehydrogenase family in *Acetobacter aceti*, *Biosci. Biotechnol. Biochem.*, 84, 2303–2310 (2020).
- 39) Thermodynamic Effect on Viscosity and Density of a Mixture of 4-Cyano-4'-pentylbiphenyl (5CB) with dilute Dimethyl Phthalate (DMP), *J. Soc. Rheol. Japan*, 48, 199–206 (2020).

- 40) Rheo-Optical and Dielectric Study on Dynamics of Bottlebrush-like Polymacromonomer Consisting of a Polyisoprene Main Chain and Polystyrene Side Chains, *Macromolecules*, 53, 7096–7106 (2020).
- 41) Dielectric relaxation of type-a rouse chains undergoing reversible end-adsorption and desorption, *Nihon Reorogi Gakkaishi*, 48, 27–35 (2020).
- 42) Surface roughness and crystallinity of silicon solar cells irradiated by ultraviolet femtosecond laser pulses, *Electron. Commun. Jpn.*, 104, 3–9 (2020).
- 43) Development of intense terahertz light source for forming periodic structures on material surface, *Electron. Commun. Jpn.*, 103, 3–8 (2020).
- 44) Rotaxanes comprising cyclic phenylenedioxydiacetamides and secondary mono- And bis-dialkylammonium ions: Effect of macrocyclic ring size on pseudorotaxane formation, *Org. Chem. Front.*, 7, 513–524 (2020).
- 45) Iron-Catalyzed Chemoselective C–N Coupling Reaction: A Protecting-Group-Free Amination of Aryl Halides Bearing Amino or Hydroxy Groups, *Asian J. Org. Chem.*, 9, 372–376 (2020).
- 46) Regio- and stereoselective synthesis of 1,4-enynes by iron-catalysed Suzuki-Miyaura coupling of propargyl electrophiles under ligand-free conditions, *Org. Biomol. Chem.*, 18, 3022–3026 (2020).
- 47) Spin and orbital magnetic moments in perpendicularly magnetized $\text{Ni}_{1-x}\text{Co}_{2+y}\text{O}_{4-z}$ epitaxial thin films: Effects of site-dependent cation valence state, *Phys. Rev. B*, 101, 224434 (2020).
- 48) Charge disproportionation and interchange transitions in twelve-layer BaFeO_3 , *Phys. Rev. B*, 102, 054404 (2020).
- 49) Ruddlesden-Popper phases of lithium-hydroxide-halide antiperovskites: Two dimensional Li-ion conductors, *RSC Adv.*, 10, 41816–41820 (2020).
- 50) Oxygen Reduction Reaction Catalytic Activities of Pure Ni-Based Perovskite-Related Structure Oxides, *Chem. Mater.*, 32, 8694–8699 (2020).
- 51) Mixed-Ligand Approach to Palladium-Catalyzed Direct Arylation Polymerization: Synthesis of Donor-Acceptor Polymers Containing Unsubstituted Bithiophene Units, *Macromolecules*, 53, 158–164 (2020).
- 52) Biogeography of marine giant viruses reveals their interplay with eukaryotes and ecological functions, *Nat. Ecol. Evol.*, 4, 1639–1649 (2020).
- 53) KofamKOALA: KEGG Ortholog assignment based on profile HMM and adaptive score threshold, *Bioinformatics*, 36, 2251–2252 (2020).
- 54) An optimized metabarcoding method for mimiviridae, *Microorganisms*, 8, 506 (2020).
- 55) DeepCleave: A deep learning predictor for caspase and matrix metalloprotease substrates and cleavage sites, *Bioinformatics*, 36, 1057–1065 (2020).
- 56) Comprehensive review and assessment of computational methods for predicting RNA post-transcriptional modification sites from RNA sequences, *Brief. Bioinformatics*, 36, 1676–1696 (2020).
- 57) PeNGaRoo, a combined gradient boosting and ensemble learning framework for predicting non-classical secreted proteins, *Bioinformatics*, 36, 704–712 (2020).

4. 参考資料

4-1.令和 2 年度公募要領	158
4-2.令和 2 年度採択課題一覧	162

1. 共同研究成果報告

化学的手法に基づくキラルプラズモニックナノ構造体の 作製および設計技術

中川 充 大阪産業技術研究所

[目的] キラルな構造を有する貴金属ナノ構造体は、局在表面プラズモン共鳴に基づく特異な光学活性を示すキラルプラズモニックナノ構造体として盛んに研究されている。キラルプラズモニックナノ構造体は主に電子線リソグラフィーなどを用いた微細加工によって作製されるが、最近では化学合成法に関する研究が特に注目を集めている。しかしながら、化学合成によって作製可能なナノ構造体のバリエーションは非常に限られることから、より多様な構造に対応できるナノ構造体の合成および設計技術が求められている。そこで、以前我々が報告したキラルな構造を有する分子集合体を鋳型とするらせん状金ナノワイヤーの合成法を発展させることで本課題の検討を行った。

[実験] 調製した分子集合体の存在下で塩化金(III)酸を金前駆体、L-アスコルビン酸を還元剤として、金ナノワイヤーを合成した。このとき、還元剤の濃度を変化させることで、異なる条件のもと金ナノワイヤーを合成した。形成された金ナノワイヤーについて反応後 14 日後の構造を透過型電子顕微鏡 (TEM) により観察し、ナノワイヤーの光学特性評価および電子顕微鏡による電子エネルギー損失スペクトル測定 (EELS) を行った。

[結果と考察] 金前駆体 / 還元剤濃度比が 1 未満の場合、直径 \sim 3 nm、長さが数百から数千 nm 程度の金ナノワイヤー (NW-3, Fig. 1a) が形成し、還元剤濃度を調節しても形成される金ナノワイヤーの直径および長さに大きな変化は見られなかった。一方、金前駆体 / 還元剤濃度比が 2 のとき、直径 \sim 7 nm かつ、長さが 400 nm 未満のナノワイヤー (NW-7, Fig. 1b) が多く生成した。NW-3 の分散液は中-遠赤外領域にブロードな光吸収を示したのに対し、NW-7 では 1350 nm (0.92 eV) 付近の近赤外領域に吸収ピークを示し、それに伴い円偏光二色性スペクトルも変化した。また、同一試料内で長さおよび直径の異なる金ナノワイヤーについて EELS を測定したところ (Fig. 1c, d)、短いまたはアスペクト比の小さいワイヤーほど、高エネルギー側にエネルギー損失を示した。これらの結果から金ナノワイヤーの形状変化に伴う光学特性変化の主な原因は、ナノワイヤーの長さまたはアスペクト比の減少であることを明らかにした。

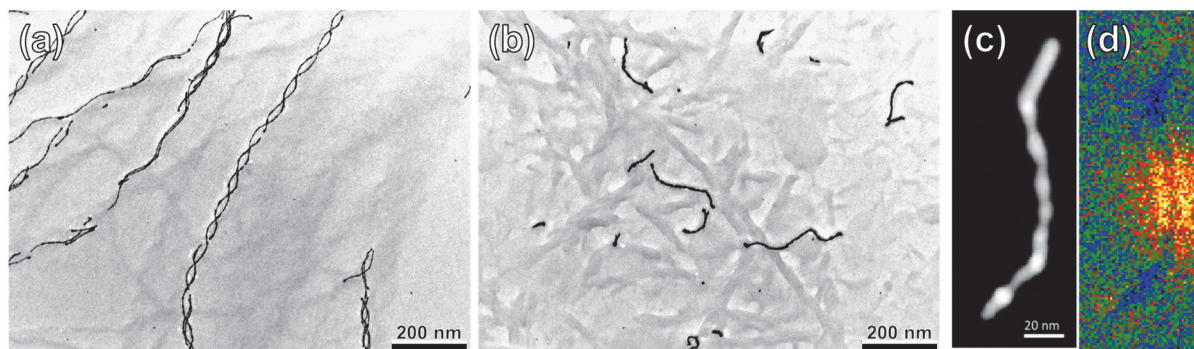


Fig. 1. (a) [金前駆体] / [還元剤] = 0.4で合成した太さ \sim 3 nmのらせん状金ナノワイヤーおよび、(b) [金前駆体] / [還元剤] = 2.0で合成した太さ \sim 7 nmのらせん状金ナノワイヤーのTEM像。(c) 直径 \sim 8 nm、長さ154 nmの金ナノワイヤーのHAADF-STEM像。(d) 0.79–0.89 eVにおけるEELSマッピング像。 $m=2$ のプラズモン振動にもとづくエネルギー損失を示していると考えられる。

中赤外レーザーを用いた振動強結合による反応性変化の解明

平井健二 北海道大学電子化学研究所

物質の振動準位や電子準位と光が強く結合すると新たに混成状態が生成し興味深い特性を示す。最近、量子光学の分野で、共振器（キャビティ）光子と物質の超強結合が注目されている。超強結合とは、真空ラビ周波数が光子周波数に近づく領域を指し、光子ドレッシング超伝導体や空洞増強相転移などのいくつかの興味深い現象が提案されている。これまで、ファブリペロー共振器、フォトニック結晶、プラズモン共振器を使用して、超強結合が広く研究されてきた。これらの研究の多くは、励起子、サブバンド間遷移、ランダウ準位など、電子に関連するエネルギー準位を対象としてきた。最近では、分子の振動準位とキャビティの超強結合が化学反応への影響を与えることが報告され、振動強結合化学の分野が急速に発展している。固体における結晶の振動（フォノン）はテラヘルツ（THz）から中赤外領域に位置し、この周波数帯の振動強結合が基礎的、応用的な観点から興味を持たれている。

本研究では、ギャップ幅を 100nm に狭めたスプリットリング共振器（SRR、図 1）の LC 共鳴とペロブスカイト半導体のフォノンモードとの間の超強結合が 0.95 THz ($\lambda \approx 300 \mu\text{m}$) で達成できることを示した。この小さなギャップの結合強度は 0.24 であった。SRR 構造は、電子ビームリソグラフィで作製した。強結合状態におけるラビスプリッティングのギャップサイズ依存性は、テラヘルツ時間領域分光法による透過率測定を行うことによって調べた。ギャップ内の電界増強係数をシミュレートすることによって解析した。ギャップサイズが小さくなると、電界増強係数の増加がギャップの中に含まれるフォノンの数の減少を上回ることにより、結合強度の全体的な増加につながることを示された。この結果は、SRR が、結合強度のギャップサイズ依存性がない他のキャビティと比較して、真空場のより効率的な閉じ込めが可能なことを示している。このようなサブミクロンギャップのキャビティによって得られた超強結合状態は、非線形光学や化学反応の研究に役立つプラットフォームとなる可能性がある。

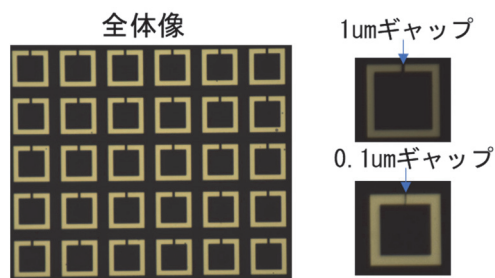


図 1. 自作した THz 金属スプリットリング共振器構造

X-ray structural studies on ligand complexes of maleylacetate reductase

Tadao Oikawa Kansai University

Rhizobium is a genus of tubercle-forming bacteria. It grows in the root of a plant in symbiosis with other bacteria to fix nitrogen from the air. Although considerable attention has been paid to *Rhizobium* genes and gene products, there is still little information available on the molecular structures, functions, and properties of the enzymes involved in the metabolic pathways. *Rhizobium* sp. strain MTP-10005 was isolated from natural river water during a screening experiment. Enzymological and genetic studies showed that the translational products of the *graA*, *graB*, *graC*, and *graD* genes (GraA, GraB, GraC, and GraD, respectively) could be potentially involved in the resorcinol degradation pathway. To reveal the structure and function of all these proteins, I have performed X-ray structural studies of the proteins in collaboration with Dr. Tomomi Fujii and Prof. emeritus Dr. Yasuo Hata, Institute for Chemical Research, Kyoto University. In this study, we focused on maleylacetate reductase (GraC), which catalyzes the NADH- or NADPH-dependent reduction of maleylacetate to 3-oxoadipate and attempted to determine the structure of GraC-cofactor-ligand complex.

N-terminal His-tagged GraC was overexpressed in *Escherichia coli* BL21 (DE3), purified, and used for crystallization. The GraC-NADH complex crystals were prepared using the sitting-drop vapor-diffusion method with a protein solution containing NADH and a reservoir solution consisted of 20% (w/v) PEG1500 and 0.1 M Bis-Tris pH 6.5. The crystals were soaked in cryoprotectant solutions consisted of 30% (w/v) PEG1500, 5 mM NADH, 0.1 M Bis-Tris pH 6.5, and each of several substrate analogs. Each soaked crystal was picked up in a cryoloop and frozen immediately in liquid nitrogen. Diffraction experiments were performed on beamline BL-5A, Photon Factory, KEK, Japan. Diffraction data for each crystal were collected under cryogenic conditions. The electron density maps were calculated using the data collected for each crystal and the phases derived from the previously determined structural model of the GraC-NADH complex. The electron density map of the crystal soaked in the cryoprotectant solution containing 10 mM adipic acid dipotassium salt showed a blob of density at the active site. An adipate molecule was modeled in the blob, and the structure was refined at 1.9 Å resolution.

In the present crystal, one homodimeric GraC molecule exists in the *P*1 unit cell, and each subunit binds an NADH molecule and an adipate molecule. The subunit of GraC molecule consists of two domains: an N-terminal domain with an α/β structure formed by residues 1–159 and a C-terminal α -helical domain formed by residues 160–351. The adipate molecule is located in the vicinity of NADH bound to the active site cleft between the domains of the subunit. The superposition of subunit C α atoms between GraC-NADH-adipate and GraC-NADH complexes results in the root mean square deviations of 0.49 Å. No significant conformational changes are observed in the protein backbone upon the binding of adipate to the GraC-NADH complex. In the active site, one of the carboxyl groups of the adipate molecule forms hydrogen bonds with the side-chains of Asn170, His243, His253, and His257. These residues might be involved in substrate binding or catalysis.

レーザープラズマ密度制御による金属表面機能性付与加工

草場光博 大阪産業大学

1. はじめに

チタン(Ti)はインプラント材として広く用いられているが、金属材料であるが故に長期的な使用時に問題点を有している。この問題点を解決するために Ti 表面に新機能を付加する必要がある。これまでの研究において、Ti 基板上にフェムト秒レーザーを照射することにより形成した周期的微細構造(Laser Induced Periodic Surface Structuring, LIPSS)が細胞伸展に有効であることを報告されている¹⁾。特に、細胞伸展制御を行なうにあたって LIPSS の周期が重要であることが示唆された。LIPSS の形状は材料特性、レーザー波長、表面雰囲気等の照射条件によって変わることがわかっており、金属表面の雰囲気(誘電率の異なる透明樹脂を表面に設置)を人工的に変化させることで LIPSS の周期を制御することにも成功している²⁾。しかしこれらの手法で得られる LIPSS の形状は限定的であり、微細構造物の均一な周期性を得ることは成功していなかった。そこで我々は、フェムト秒レーザーの基本波と二倍波を用いた二ビーム複合照射により Ti 基板に高い周期性の LIPSS 形成を試みた。二波長のパルスの異なる過渡応答により LIPSS の形状制御を行い、また、パルス間の遅延時間が LIPSS の形状(特に周期性)に与える影響を調べたので報告する。

2. 実験方法

Cyber Laser 社製のフェムト秒レーザー装置からのレーザーパルス(波長 800 nm, 繰り返し周波数 1 kHz, パルス幅 150 fs)をハーフミラーにより分岐させ、一方は光路差(遅延時間)を調節し、もう一方は二倍波(偏光は基本波に対して直交)に変換し、基本波と同軸にアライメントした後に Ti 基板へ集光照射した。スポット径はともに 25 μm (FWe-1M)となるように調整した。二倍波が先に基板に到達する条件を正の遅延時間と定義し、 ± 700 ps の間で変化させ実験を行った。30~300 パルス照射し、走査型電子顕微鏡(SEM)を用いて表面形状を計測した。

3. 実験結果

Fig. 1 (a)および(b)に基本波のみを 60 パルス照射したときおよび遅延時間を 0ps に設定し、基本波と二倍波を 60 ペア照射したときの SEM 画像をそれぞれに示す。二ビーム複合照射の照射条件(遅延時間、フルエンス)を最適化することで LIPSS の周期性が向上したことが分かった。

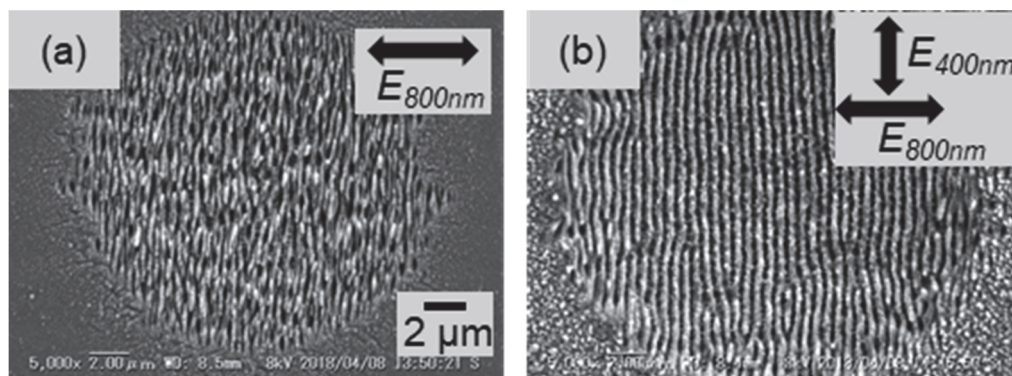


Fig.1 SEM images of Ti surface after (a) only fundamental wavelength pulse irradiation and (b) two color double pulse beam irradiation.

参考文献

- 1) T. Shinonaga, M. Tsukamoto, T. Kagwa, P. Chen, A. Nagai, T. Hanawa, Appl. Phys. B, **119** (2015) 493.
- 2) K. Takenaka, M. Tsukamoto, Y. Sato, T. Ooga, S. Asai, K. Murai, Appl. Phys. A, **124** (2018) 410.

成果報告

[1] M. Hashida, Y. Furukawa, S. Inoue, S. Sakabe, S. Masuo, M. Kusaba, H. Sakagami, M. Tsukamoto, J. Laser Applications **32**(2020)022054.

2 色パルス誘起微細周期構造形成過程の研究

長島健 摂南大学

1つのフェムト秒レーザーパルスをチタン表面に照射した後に、時間差（遅延時間）をつけてもう1つのレーザーパルスを照射する「ダブルパルス照射」により得られる表面微細周期構造について、1つのパルスのみを照射（シングルパルス照射）した場合と比較した。特に、組み合わせるパルスの波長を変えた「二波長ダブルパルス照射」（図1）を行い、アブレーションの深さやナノ周期構造の形状が、遅延時間やフルエンスの組み合わせによって変化することを明らかにした。紙面の都合上ここでは述べないが、二波長ダブルパルス照射を行うことでアブレーションの深さがシングルパルス照射時の約1/3に抑制され、光の反射率や侵入長の違いがアブレーションの抑制に寄与していることが示唆された¹⁾。周期構造の均一性は、微細周期構造 SEM 画像の2次元FFTから得られる広がり角 $\delta\theta$ （DOLA: dispersion in the LIPSS orientation angle）を用いて評価した（図2、均一性が高いほど $\delta\theta$ は小さくなる）。二波長ダブルパルス照射により形成された微細周期構造は高い周期性を持つことが分かった（図3）。図3(a)は閾値の1.5倍のフルエンスに調整された400 nmのフェムト秒レーザーパルスを60パルス照射して形成された周期構造を示す。400 nmパルスで作られる微細構造は格子間隔が nm オーダーで、溝の向きは偏光方向（青の矢印）に対しほぼ垂直であった。均一性を示す指標は $\delta\theta = 26^\circ$ であった。図3(b)に遅延時間を0 psに設定し、先の400 nmパルスに800 nmパルスを同軸状に調整し60ペア照射したときに形成される周期構造を示す。800 nmパルスのフルエンスは閾値の0.9倍であり、偏光方向（赤の矢印）は400 nmパルスと直交させた。形成された周期構造の格子間隔及び溝の向きは800 nmパルスで決まっていることがわかった。 $\delta\theta = 12^\circ$ となり、図3(a)の400 nmパルスのみの場合より均一性が向上した。また、パルスの役割を明らかにするためアブレーション抑制時間とレーザー波長の関係を調べた。第2パルスの波長が短いほど抑制時間は短くなり、表面に生じるプラズマの密度が関わっている可能性が示唆された。

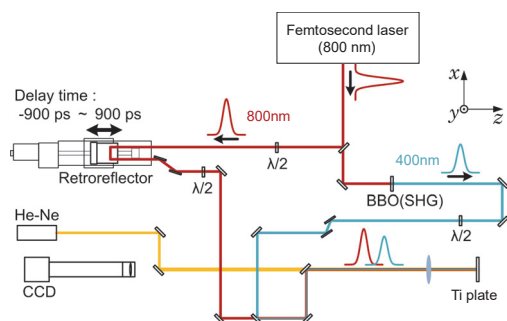


Fig.1 Experimental setup for two color double pulse beams.

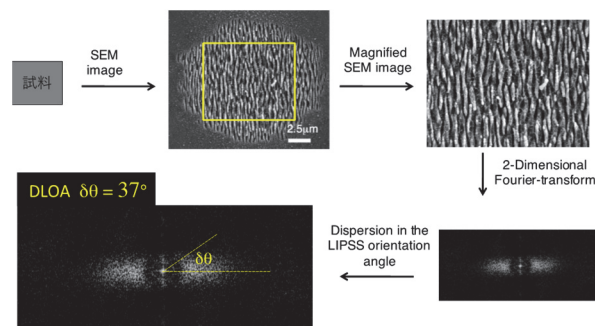


Fig. 2 The uniformity of LIPSS were determined by dispersion in the LIPSS orientation angle (DLOA) for obtaining 2D-FFT spectrum.

参考文献

- 1) Takenaka, K. Tsukamoto, M. Hashida, M. Masuno, S. Sakagami, H. Kusaba, M. Sakabe, S. Inoue, S. Furukawa, Y. Asai, S.: Ablation suppression of a titanium surface interacting with a two-color double-pulse femtosecond laser beam, Appl. Surf. Sci. **478**, (2019) 882-886
- 2) Hashida, M. Furukawa, Y. Inoue, S. Sakabe, S. Masuno, S. Kusaba, M. Sakagami, H. Tsukamoto, M. : Uniform LIPSS on titanium irradiated by two color double-pulse beam of femtosecond laser, J. Laser Appl. **32** (2020)022054-1-022054-4.

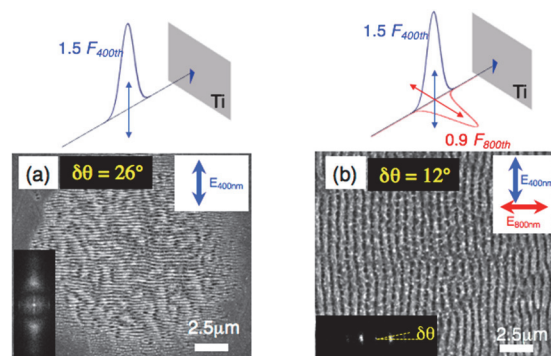


Fig. 3 High periodicity LIPSS on titanium surface irradiated by two-color double pulse beam²⁾.

ナノ構造を持つ ISOL 用標的の開発

大西哲哉 理化学研究所仁科加速器科学研究センター

〔目的〕 不安定核生成法の一つである ISOL 法では、標的内で生成した不安定核を、標的を高温（～2000℃）にすることで取り出している。そのため、高温でも蒸気圧が低くかつ融点も高い、炭化物が標的として用いられることが多い。しかし、これまでの研究によって、炭化物標的の寿命が約一週間程度であることが分かっている。これは、高温環境下では炭化物の焼結が進むため、標的内部の隙間が小さくなり、不安定核が出てこなくなるためである。解決策として、近年カーボンナノチューブを用いた炭化物標的が提案されるが、燃焼しやすく、取り扱いには専用の設備が必要である。本研究の目的は、カーボンナノチューブやグラフェン等のナノ構造をもつ新たな炭化物を用いて、取り扱いやすい ISOL 用標的を開発することである。

〔実験手法〕 対象とする元素の化合物(酸化物など)を炭素材料と混合し、高圧をかけ、厚さ 1 mm、直径 20 mm 程度の円板標的を作成する。作成した標的は真空チェンバー内で高温に加熱し、炭化物へと変換する。作成した炭化物標的は、電子顕微鏡を用いて、そのナノ構造を調べる。その後、電子ビームもしくは陽子ビームを照射し、不安定核生成量の変化から標的寿命や生成効率などを調べる。本年度はグラフェンを用いた円板標的の作成及び炭化作業を行った。作業場所は核燃物質取り扱いの必要から、理化学研究所仁科加速器研究センターにて、仁科センター市川進一氏と共に作業を行った。手順としては、まず酸化ウランを硝酸に溶解し硝酸ウラニル溶液を作成する。次に硝酸ウラニル溶液をグラフェンに含浸後、脱硝・酸化する。酸化物に必要なに応じてグラフェンを追加後、プレス機を用いて円板標的を作成する。作成した円板標的は、真空チェンバー内で高温に熱することで、炭化物へと変換する。

〔結果〕 酸化ウラン(U3O8:4.15g)を硝酸ウラニル溶液に転換後、グラフェンに含浸し、脱硝・酸化作業を経て、円板標的(UO3+グラフェン、直径 20mm、厚み～1mm)を作成した。この段階では U:C モル比が 1:8 になるようにグラフェン量を調整し、炭化作業後に U:C モル比が 1:4 程度になることを目指した。

作成した円板標的は真空チェンバー内で約 1100℃程度まで昇温し、炭化反応が終了するまで約 10 日高温状態を維持した。昇温作業中は、 $6\text{UO}_3 + \text{C} \rightarrow 2\text{U}_3\text{O}_8 + \text{CO}_2$, $\text{U}_3\text{O}_8 + \text{C} \rightarrow 3\text{UO}_2 + \text{CO}_2$, $\text{UO}_2 + 3\text{C} \rightarrow \text{UC} + 2\text{CO}$ といった一連の反応を経て、炭化ウラン(UC)が形成されていると考えられる。

炭化作業終了後の標的を写真 1-1)に示した。従来の炭素粉で形成した標的と同様に金属光沢が見られた。しかしながら、観察中に急激に酸化が始まってしまい(写真 1-2)参照)、ものの数分ですべて酸化ウランに変換された。酸化後は写真 1-3)に示すように層構造らしきものが見られたが、グラフェンの特性によるものなのかは、さらなる調査が必要である。



写真 1: 1) 炭化作業直後の炭化ウラン標的、 2) 標的の酸化中の様子、 3) 酸化後の標的の様子

〔考察〕 グラフェンを用いた円板標的の生成には成功したが、炭化後ここまですぐに酸化反応が起きてしまうのは、予想外であった。とはいえ、今回の結果は、作成した標的が不安定核の導出に必要な隙間構造を備えていることも示唆しており、標的の性質として期待が持てるものである。今後は素早い酸化反応に対応するべく、取り扱い装置の開発を進めていく予定である。

〔成果報告〕 特になし。

電子散乱による短寿命不安定核の奇妙な構造の解明

須田利美 東北大学電子光理学研究センター

【目的と研究方法】

本研究は、化学研究所・先端ビームナノ科学センター・粒子ビーム科学研究領域の若杉氏とともに電子散乱により短寿命不安定核の内部構造の解明を目標としている。電子散乱は、電子ビームを原子核に照射し散乱電子の観測より原子核内部構造の情報を引き出す単純な測定方法であるが、電子は原子核と電磁相互作用が量子電磁気学で完全に理解されているため測定から曖昧さなく内部構造をあぶり出すことができる。したがって、天然に存在する安定原子核の構造解明では電子散乱は決定的な役割を果たしてきた。実験技術の進展により天然には存在しない短寿命な不安定核が実験室で研究対象になり、過去の安定核で培われた常識を覆す構造を示唆する研究やこれらの構造理解が宇宙での物質進理解に必要であることから世界各地で鎬を削る研究が展開されている。

【本研究と今年度の成果】

不安定核構造研究にも電子散乱が王道であるが、生成困難かつ短寿命で崩壊するため十分な標的数確保が困難な不安定核の電子散乱による構造研究は不可能と考えられてきた。私たちはこの壁を打ち破る SCRIT 法とよぶ電子散乱用新標的生成法を編み出し、世界初の不安定核研究用電子散乱施設を建設・運用を始めている。

今年度の共同利用費申請書では東北大研究者が京都大学を2回訪問し新規研究を含む今後の研究についての打ち合わせを実施することを提案していたが、残念ながらコロナ禍のため実現できなかった。現場での議論はできなかったが、リモート会議システムを利用し定期的に会合を行い、共同研究を進めることと今後の研究計画を議論することはできた。また関連した研究に関する検討も理研研究者を含む15名の参加を得てリモートで実施した。

並行して、東北大サイドでは鈴木により提案された電子弾性散乱で決定する電荷密度分布を利用した陽子と中性子分布の分布情報を決定する新しい解析方法の検討ならびに実験可能性の検討を継続した。この研究の結果を今年度論文として発表した。

“The mean square radius of the neutron distribution and the skin thickness derived from electron scattering”

H. Kurasawa, T. Suda and T. Suzuki, Progress in Experimental and Theoretical Physics, 2021 (in press).

【今後の予定】

年度末3月には東北大学電子光理学研究センターの支援も得て、全国の研究者に声をかけたリモート研究会を開催する予定である。また、来年度も本研究についての検討を継続し、実験可能性や電子散乱で決定できる分布情報精度について京都大学の共同研究者と詰めて行く予定としている。

Gas sensing properties research of transition-metal oxides

Haichuan Guo Ningbo Institute of Industrial Technology

Introduction

The perovskite-type oxides are widely used to detect poisonous and harmful gases because of high sensitivity and excellent selectivity, which demonstrates excellent application potential in the field of gas sensors. Herein, a new design of sensor array (Fig. 1) was realized by integrating a series of transition-metal oxides LnFeO_3 ($\text{Ln} = \text{La}, \text{Pr}, \text{Nd}, \text{Sm}$), which revealed excellent recognition ability for various VSCs (H_2S , CS_2 , DMS, and DMDS), showing promise for real time monitoring [1].

Experiments and results

LnFeO_3 materials were synthesized by the citrate sol-gel method. As-prepared oxide powders were dispersed in deionized water and drop-coated on alumina ceramic substrates with comb-type Au electrodes. The ceramic chips were calcined at $300\text{ }^\circ\text{C}$ for 1 h to strengthen the stability and repeatability. Gas sensing properties were measured using an intelligent gas sensing analysis system by the static volumetric method. The recognition abilities of the LnFeO_3 sensors were investigated by the sensor array and the principal component analysis (PCA) were conducted to distinguish four typical VSCs.

The results (Fig. 1 inset) clearly show that different concentrations, the region of plots and various shape for each kind of VSCs. It can be obviously seen that the data points of sensor array could be clustered and four different VSCs can be obviously distinguished. Therefore, the result indicates that the footprints of different VSCs gases were successfully determined, which demonstrated the possibility of detecting and discriminating the VSCs in air pollution by the LnFeO_3 sensor array.

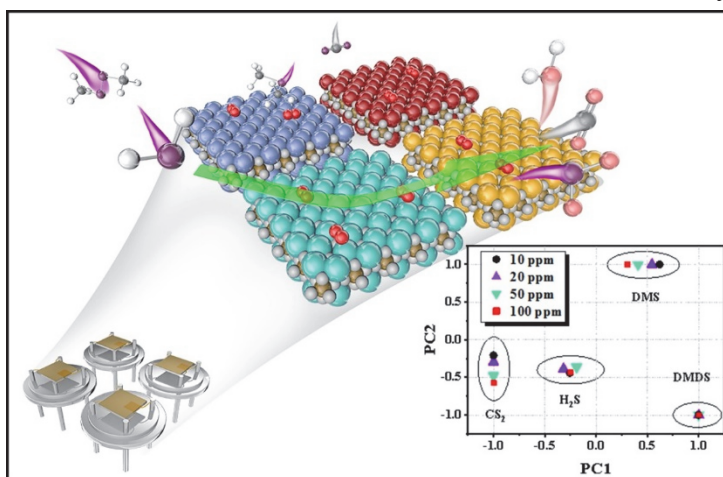


Fig. 1 Schema of the sensor array and the result of PCA analysis

[1] Z. Zhang, S. Zhang, C. Jiang, H. Guo, F. Qu, Y. Shimakawa, and M. Yang, Integrated sensing array of the perovskite-type LnFeO_3 ($\text{Ln} = \text{La}, \text{Pr}, \text{Nd}, \text{Sm}$) to discriminate detection of volatile sulfur compounds. *Journal of Hazardous Materials*, 2021, in press.

Separation and evaluation of thiolate protected metal clusters with atomic precision by using LC/MS

Yuichi Negishi Tokyo University of Science

Objectives Thiolate-Protected gold nanoclusters ($\text{Au}_n(\text{SR})_m$) have size-specific physical and chemical properties. In these nanoclusters, ligand-exchange reaction is commonly used to induce further functionality. In recent years, although it was reported that ligand-exchange reaction proceed with size-conversion at the same time, mechanism of this reaction is not revealed. For elucidation of size-conversion mechanism, it is necessary to obtain the information of intermediate products in reaction.

Experimental methods In our work, we tried to track ligand-exchange reaction with the size-conversion of $\text{Au}_{25}(\text{SR})_{18}$ cluster to $\text{Au}_{28}(\text{SR})_{20}$ cluster by introducing LC/MS which was directly connected the chromatograph with the mass spectrometer. We used reversed-phase high-performance liquid chromatography (RP-HPLC) and electrospray ionization mass spectrometry (ESI-MS) under guidance by ICR partner researchers. The ligand-exchange reaction started at addition of 4-*tert*-butylbenzenethiol (HSPhtBu) to $[\text{Au}_{25}(\text{SC}_2\text{H}_4\text{Ph})_{18}]^-$ dissolved in toluene. The products at each reaction time were evaluated by LC/MS.

Results and discussion Figure 1 shows the UV chromatograms of the crude product at each reaction time. In these chromatograms, multiple peaks were observed. The reaction time of peaks were longer than that of Au_{25} (Figure 1a) with the progress of the reaction time (Figure 1b–e). It is considered that polarity of the cluster change to lower as the number of ligand-exchange increased. Figure 2a shows the UV chromatogram of the crude product after 30 minutes of reaction at 80 °C. Figure 2b shows the UV-visible absorption spectra of the separated products at typical peaks in Figure 2a. In spectra i–iv, the disappeared and the new specific peak of Au_{28} clusters was observed at 365 nm. From these results, it was revealed that products of ligand-exchange reaction could be separated and the electronic structure change could be tracked by our method.

Publications

- [1] Y. Negishi *et al.*, *Nanoscale*, **12**, 8017-8039 (2020).
 [2] K. Isozaki, Y. Negishi, T. Hasegawa, M. Nakamura, K. Miki *et al.*, *Catalysts*, **10**, 908 (2020).

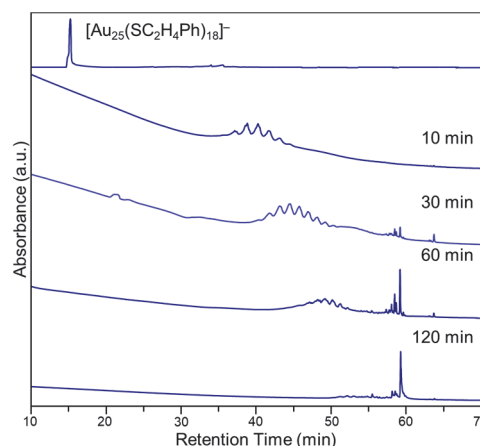


Figure 1. UV chromatograms of $[\text{Au}_{25}(\text{SC}_2\text{H}_4\text{Ph})_{18}]^-$ clusters (a) before and after reaction at (b) 10 min, (c) 30 min, (d) 60 min and (e) 120 min.

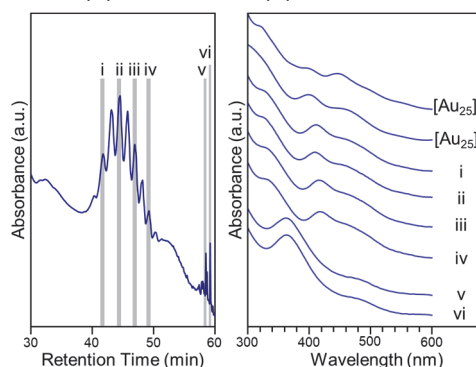


Figure 2. (a) UV chromatograms at 380 nm of the crude product after reaction for 30 min and (b) UV-vis absorption spectra of the products at typical peaks in (a).

Small molecule activation using anionic crypto-FLPs

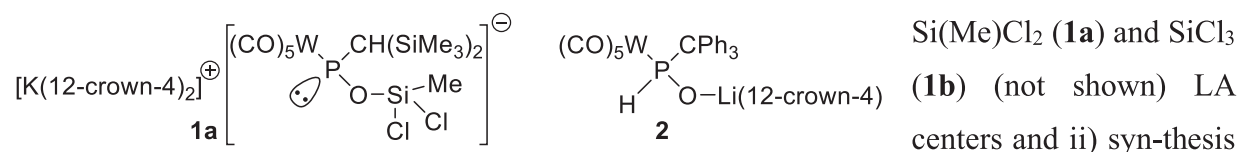
Rainer Streubel University of Bonn

This collaborative research project was carried out with Prof. Norihiro Tokitoh (ICR, University of Kyoto) but due to Covid-19 travel restrictions the planned exchange of 2 PhD students (from Bonn) and 1 PhD student (from Japan) could not be pursued. Despite this problem we have continued our efforts on a smaller level in Germany to advance the project.

Objectives: The purpose of the project is to develop novel chemistry using anionic FLPs, featuring group 14/15 elements with an anionic phosphorus as Lewis base and a group 14 element (E = C-Pb) in tetravalent coordination with E-halogeno functionality, in small molecule activation.

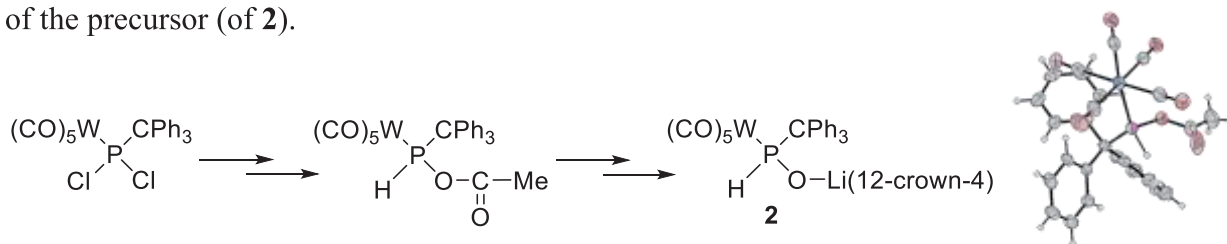
Experimental methods: Inert-gas synthesis techniques, analytical methods (NMR, IR, UV/vis, CV, X-ray)

Experimental results: The studies focused on i) synthesis of new crypto-FLPs containing and



of a new precursor (**2**) bearing a *P*-CPh₃ group that should enable to access products with a greater tendency to crystallize.

Discussion: Synthesis of **1a,b** was achieved, but crystals couldn't be obtained, unfortunately. Also no further studies on the reactivity of **1a,b** were performed. In case of **2**, we also arrived there recently via the multistep route shown in the scheme. Here, we could confirm the structure of the precursor (of **2**).



Depending on the progress of our reactivity studies using the new FLPs (**1a,b**, and those derived from **2**) we still plan to expand our synthetic approach by using SiBr_n containing FLP derivatives.

Publication: R. Kunzmann, Y. Omatsu, G. Schnakenburg, A. Espinosa Ferao, T. Yanagisawa, N. Tokitoh, R. Streubel, *A synthon for unknown 1,3-zwitterions? – A K/OR phosphinidenoid complex with an additional Si-Cl function*, *Chem. Commun.* **2020**, 56, 3899-3902. DOI: 10.1039/d0cc00024h.

Design and tailoring advanced functional materials: Symmetry operation and high pressure synthesis

Wei-tin Chen National Taiwan University

[Introduction] The exploration of fascinating functionalities and phenomena of novel materials is essential in modern condensed matter sciences which is motivated much by the succession needs of novel technology applications. High pressure synthesis techniques are one of most important methods in preparation of such novel materials. The previous supported project has successfully demonstrated the unique ability to prepare novel materials with high-pressure synthesis, and this project proposes to continue the utilization of such unique techniques for novel materials exploration. It is targeted to design and investigate, for instance, compounds containing unusual high valence state or showing exotic structural/charge/orbital/spin phase transitions. With the 6-8 two-stage Kawai-type 111 geometry and cubic anvil DIA-type high-pressure apparatus equipped at Advanced Solid State Chemistry Laboratory (Shimakawa lab), extreme pressure and temperature synthesis conditions were realized for novel materials synthesis.

[Results and discussion] The joint research became difficult under the situation of pandemic in year 2020. Nevertheless, various projects were carried out with utilizing the unique high-pressure apparatus at Prof. Shimakawa's lab, and high resolution synchrotron x-ray powder diffraction experiment were performed at Taiwan Photon Source, NSRRC (Taiwan) with beamline joint research proposal. For compounds containing unusual high valence state, successive complex site-selective charge-redistribution transitions were revealed in hexagonal 12-layered BaFeO₃ perovskite.[1] Li-hydroxide halides with antiperovskite structure LiBr(Li₂OHBr)₂ was prepared with solid state reaction, and it was shown that the Li⁺ ions primarily contribute in two-dimensional ion conduction.[2] In order to further understand the intriguing structural phase transitions observed in HgMn₇O₁₂ quadruple perovskite,[3] e⁻/h⁺ doping effect and chemical pressure effect were investigated with introducing various cation into A site (Fig. 1). Apparent change of the LT structure and transition temperature were observed and detailed structure analysis is ongoing to understand the origin of the modification.

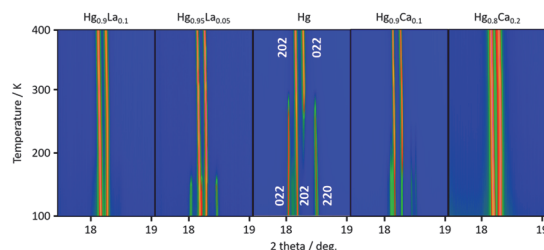


Fig. 1 T-dependent SXR patterns of the doped quadruple perovskite (Hg_xA_{1-x})Mn₇O₁₂.

[References]

1. Z. Tan *et. al.*, *Phys. Rev. B*, **102**, 054404 (2020)
2. A. Koedtrud *et. al.*, *RSC Adv.*, **10**, 41816 (2020)
3. W.-T. Chen *et. al.*, *Phys. Rev. B*, **97**, 144102 (2018)

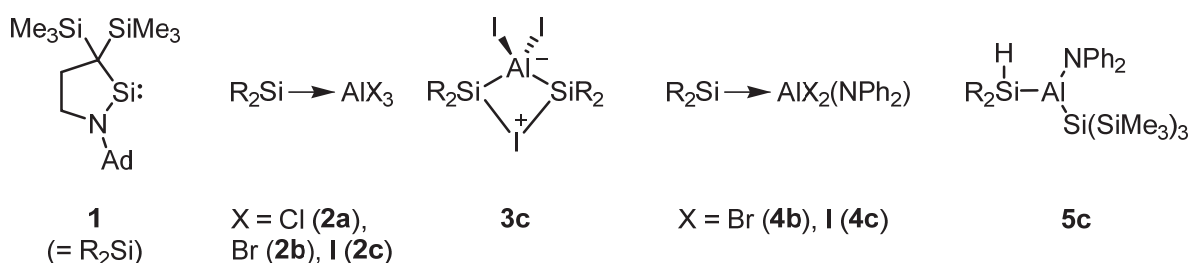
Development of unsymmetrical π -electron systems of heavier main group elements and elucidation of their property

Takeaki Iwamoto Tohoku University

Objectives: π -Electron systems containing multiple bonds of heavier main group elements have been studied as prospects for advanced materials and reagents for small molecule activation. We aimed at developing unsymmetrical π -electron systems containing a double bond between group-14 and group-13 elements, which remain scarce compared to other heavier π -electron systems.

Experimental methods: To synthesize the unsymmetrical π -electron systems $R_2Si=AlR'$, we investigated the preparation of the corresponding precursor containing an Si–Al bond using the reaction of cyclic (alkyl)(amino) silylene **1** with halogenated alanes.

Experimental Results and Discussion: We prepared a series of trihaloalanes coordinated by silylene **1** (**2a–2c**), all of which were fully characterized by a combination of NMR spectroscopy, elemental analysis, and X-ray single-crystal diffraction (XRD) analysis. Notably, in the presence of an excess amount of **1** for the reaction of AlI_3 , we obtained a 2:1 adduct **3c** as colorless crystals. Compound **3** is a product resulting from the formal insertion of silylene **1** into the Al–I bond of **2c**. **3** is stable only in the solid state and dissociates into **2c** and **1** in solution, indicating that the reaction of **1** and **2c** is reversible. During the investigation of the reactions of **2a–2c** with various bulky nucleophiles to introduce a protecting group for an Si=Al bond, we obtained diphenylamino-substituted silylalanes **4b** and **4c**. Although the reductive dehalogenation of **4b** and **4c** by the reducing agent such as KC_8 , Na, etc. provided essentially a complex mixture, the reaction of **4c** with unsolvated $(Me_3Si)_3SiK$ provided a product assignable to **5c**. Although the mechanism for the formation of **5c** remains unclear at this time, unsolvated silyl anion may be a suitable reagent for the dehalogenation reaction of the silylhaloalane precursors to provide the desired Si=Al species.



This project was done in collaboration with Professor Norihiro Tokitoh (ICR Partner Researcher) and Professor Shigeyoshi Inoue (International Collaborating Researcher, Technical University of München, Germany).

Optical control of high-order harmonic generation from solids

Shunsuke Sato University of Tsukuba

Objectives

High-order harmonic generation (HHG) is an extreme photon-up-conversion process via extremely-nonlinear light-matter interactions. Thanks to the high coherence of the HHG process in gas-phase targets, a technology of ultra-short laser generation has been established. Recently, HHG from solid-state materials has been observed, and it has been gathering much interest as a promising candidate for novel light sources beyond the gas-phase HHG. However, the microscopic mechanism of the solid-state HHG is still highly controversial. In this research, we aim (i) to clarify the microscopic mechanism of the solid-state HHG and (ii) to establish a procedure to optimally-control HHG through optimization of driving laser fields, together with the partner ICR researchers Prof. Kanemitsu and Dr. Hirori.

Theoretical results

To obtain microscopic insight into the HHG, we simulated the electron dynamics in graphene under elliptically-polarized light with the quantum master equation. Figure 1 shows the computed intensity of the 7th order harmonics from graphene as a function of the ellipticity of the driving laser fields. As seen from the figure, the HHG can be enhanced by elliptically polarized light. Based on the microscopic analysis, we clarified that the enhancement of the HHG with elliptically-polarized light originates from the complex interplay among the field-induced intraband and interband transitions.

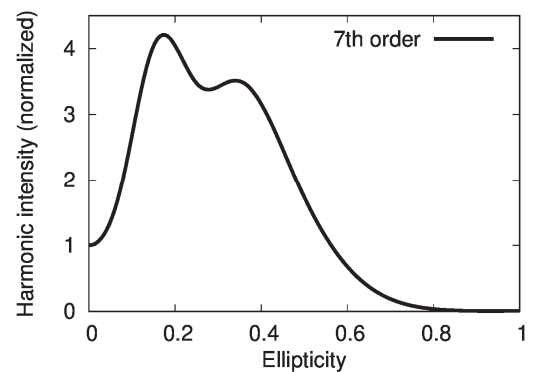


Fig. 1 The 7th-order harmonic intensity from graphene as a function of light ellipticity.

Discussion

Having clarified the microscopic mechanism of the HHG in solids based on the interplay of intraband and interband transitions, we further developed a way to control the HHG by manipulating the interplay through the laser parameter optimization, e.g., the relative phase control of two-color lasers. The experiment-theory joint project along these lines is already under a way.

Outcome

Shunsuke A. Sato, Hideki Hirori, Yasuyuki Sanari, Yoshihiko Kanemitsu, Angel Rubio, "High-order harmonic generation in graphene: Nonlinear coupling of intraband and interband transitions", Phys. Rev. B 103, L041408 (2021).

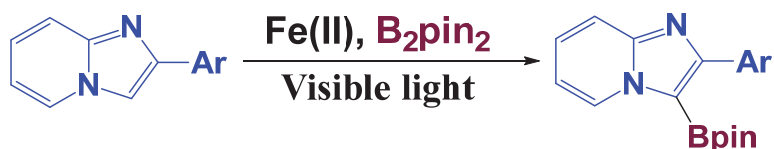
Iron-catalyzed C-H borylation

Alakananda Hajra Visva-Bharati University

Objective: Fe-catalyzed sp²-C-H Borylation of alkenes and Imidazo[1,2-*a*]pyridines

Imidazopyridine, an important class of nitrogen containing heterocycles, shows a wide range of biological activities such as antitumor, antiparasitic, antiviral, antimicrobial, fungicidal, anti-inflammatory, hypnotic etc. In addition, this motif is the core structure of some marketed drugs such as necopidem, zolpidem, olprinone, saripidem, zolimidine, alpidem, etc. Furthermore, few of them exhibit excited-state intramolecular proton transfer. Organoboron reagents are important synthetic intermediates that have a key role in the construction of natural products, pharmaceuticals and organic materials. The development of simpler approaches to organoborons can open additional routes to diverse substances.

An efficient and practical borylation protocol has been developed for the synthesis of borylated imidazo[1,2-*a*]pyridines *via* cost-effective and environmentally benign Fe-catalyzed C-H functionalization. A library of C3-borylated imidazo[1,2-*a*]pyridines were synthesized.



Presently we are focusing on the precise role of FeCl₃ and visible light, and late stage modification of the compound. To the best of our knowledge this is the first report for the synthesis of borylated imidazo[1,2-*a*]pyridines. Easy availability of basic chemicals as starting materials, less expensive metal catalyst tolerance of a wide range of functional groups, operational simplicity and practical applicability on a gram-scale are the notable advantages of this present protocol.

Electrochemically engineered peptide based organic-inorganic nanohybrids for electrocatalytic conversion of biomass into value added chemicals

Apurba K. Das Indian Institute of Technology Indore

The large-scale use of urea in the environment as a key ingredient of fertilizers and bio-waste results in environmental pollution. The urea oxidation reaction (UOR) is an effective way to clean urea rich wastewater with the production of hydrogen.

Objectives: The main aims of this project proposal are:

- (a) Design and develop electrochemically engineered peptide-anchored electrocatalyst
- (b) Experimental validation of electrocatalytic biomass conversion to value added chemicals
- (c) To study the mechanistic insights for electrocatalytic biomass conversion

Experimental Methods: An aromatic benzo[2,1,3]selenadiazole-5-carbonyl protected dipeptide BSeFL (BSe = benzoselenadiazole) suitable for electrodeposition method has been synthesized, purified and characterized. The electrochemical deposition of the BSeFL/Ni(OH)₂ electrocatalyst on carbon paper (CP) was carried out by the pulse-electrodeposition technique.

Experimental Results: In this study, simultaneous pulses of oxidation potential and reduction potential were applied to prepare the electrocatalyst. The BSeFL/Ni(OH)₂ was pulse electrodeposited at different reduction potentials. The SAED and XRD pattern confirmed the amorphous nature of nanosheets. The EDS and XPS analysis reveals uniform distribution of Ni, C, O, Se and N over cross-linked nanosheets of organic-inorganic nanohybrids. The catalytic urea electro-oxidation activity of the pulse electrodeposited BSeFL/Ni(OH)₂ (-1.0 V) electrocatalyst was evaluated using the three-electrode cell. The LSV curves were recorded in 1 M KOH solution containing 0.5 M urea at a scan rate of 2 mV s⁻¹. Gas chromatography analysis was employed to identify the gaseous product during the electrochemical UOR process. The gas chromatogram of the UOR process shows the evolution of O₂ and N₂.

Discussion: The Ni²⁺ ions present in the deposition bath interact with OH⁻ ions and carboxylate of BSeFL present on the electrode substrate surface by coulombic interactions which results in the simultaneous deposition of BSeFL/Ni(OH)₂. At a lower pH gradient and low reduction potential of -1.0 V, pulse-electrodeposition provides a denser film of electrically interconnected nanospheres with low charge transfer resistance for efficient electrocatalytic OER and UOR activity.

Publications: Jadhav R. G., Das A. K., Pulsed electrodeposited, morphology controlled organic-inorganic nanohybrids as bifunctional electrocatalyst for urea oxidation, *Nanoscale*, **2020**, 12, 23596-23606.

Iron-catalyzed enantioselective carbometalation and ring-opening reactions of oxabicycloalkenes and other related substrates and mechanistic consideration

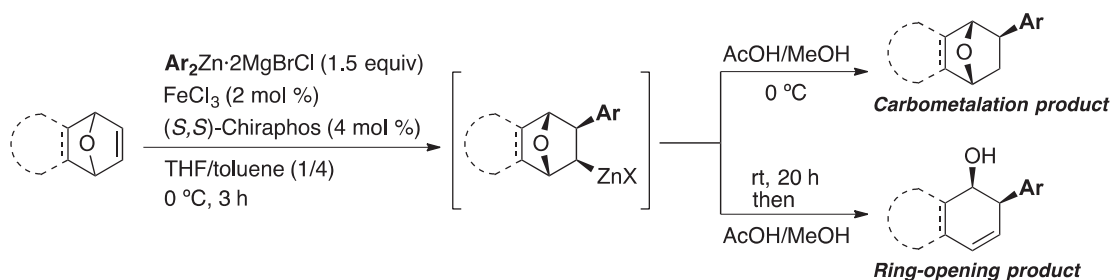
Laksmikanta Adak Indian Institute of Engineering Science and Technology

Introduction:

The transition-metal-catalyzed carbometalation of alkenes has attracted considerable interest among synthetic organic chemists, as it offers a useful pathway for the efficient and selective construction of carbon-carbon bonds. Because of the importance of asymmetric reaction for the synthesis of pharmaceuticals and natural products, significant efforts have been made to develop catalytic enantioselective carbometalation reactions of olefins. Palladium, rhodium, copper, and iridium-catalyzed (*Acc. Chem. Res.* **2003**, 36, 48; *Angew. Chem. Int. Ed.* **2012**, 51, 5400; *Org. Lett.* **2002**, 4, 2703; *Chem. Commun.* **2013**, 49, 9959) asymmetric transformations of oxa- and azabicyclic alkenes have been extensively studied, where enantioposition-selective addition of oxygen, nitrogen, and carbon nucleophiles brings about subsequent ring-opening reactions provide access to enantioenriched compounds bearing multiple stereocenters. Only one example was found for the catalytic asymmetric addition of terminal alkynes to oxabenzonorbornadienes without the ring opening, which was achieved by use of a chiral phosphine-cobalt catalyst system (*Chem. Commun.* **2012**, 48, 6106).

Although the use of iron catalysts in organic synthesis are attracting increased attention due to its economic and ecological points, but there application in enantioselective carbometalation has been limited to only highly strained cyclopropene derivatives (*J. Am. Chem. Soc.* **2000**, 122, 978). Nakamura and his group previously reported the iron-catalyzed diastereoselective ring opening of oxabicyclic alkenes with Grignard reagents (*Org. Lett.* **2003**, 5, 1373) and also the highly diastereoselective carbometalation of oxa- and azabicyclic alkenes with arylzinc reagents in which zinc reagents are used to trap carbometallated products prior to ring opening (*Angew. Chem. Int. Ed.* **2011**, 50, 454). With collaboration of Prof. Nakamura's group we developed iron-catalyzed enantioselective carbometalation and asymmetric ring opening reactions of oxabicyclic alkenes using a single catalyst system (Scheme 1).

Scheme 1. Iron-Catalyzed Enantioselective Carbometalation and Ring-opening of Oxabicyclic Alkenes



Results and Discussion:

The screening of reaction conditions for iron-catalyzed enantioselective carbozincation of oxabicyclic alkene with phenylzinc reagent were performed. Various chiral ligands and metal salts were used for the screening and optimization of reaction condition. Finally, it was found that 2 mol% FeCl_3 and 4 mol% (*S,S*)-Chiraphos provided the best result for the enantioselective carbometalation reaction.

Next Plan:

- (1) Based on the optimization of reaction conditions, the substrates scope for enantioselective carbometalation reactions will be performed
- (2) Substrates scope for the ring opening products will be done

Publications:

- (1) Adak, L.; Hatakeyama, T.; Nakamura, M. Iron-Catalyzed Cross-Coupling Reactions Tuned by Bulky *ortho*-Phenylene Bisphosphine Ligands, *Bull. Chem. Soc. Jpn.* **2021**, 94, 1125-1141.

Study on the stability of novel ternary nanoparticles by doping 3rd elements

Yasutomi Tatetsu Meio University

Many scientists have been investigating the possibility of creating novel materials by introducing third elements into stable binary nanoparticles with advanced chemical synthesis techniques that might increase the system's magnetic properties due to the change of its crystal structure. Recently, a new Z3-type Fe(Pd,In)₃ crystal structure was discovered by Teranishi's group in Kyoto University [1]. The new structure was synthesized by introducing a third element of In into L1₂-FePd₃, which is the thermodynamically stable phase of binary Fe–Pd systems. Although the addition of In might be the key behind this new finding, the physical aspects of In in stabilizing the new structure is unclear and cannot be understood deeply only through experiments.

In this report, we conducted theoretical analyses for the stability of an In-doped novel Fe–Pd phase. We calculated formation energies of In-doped L1₂- and Z3-Fe–Pd systems using first-principles calculation code, OpenMX [2], and compared the obtained energies in order to check the systems' stability against the concentration of In. The model structures for the calculations were based on the chemical composition ratio of Z3-FePd₃ obtained from experiments. The In sites were chosen by replacing Fe or Pd sites with a special-quasirandom-structure method implemented in the Alloy Theoretic Automate Toolkit [3]. We investigated stable sites for In in the L1₂- and Z3-FePd₃ structures by comparing formation energies and we found that an In stably is substituted for Fe and Pd at the e sites respectively. One of the interesting findings is that the most stable structure changes from L1₂-(Fe, In)Pd₃ to Z3-Fe(Pd, In)₃ when the concentration of In is around 20 % which is illustrated in the figure below. Same tendency can be seen in the experimental results from XRD, EXAFS, and STEM-EDS analyses. This indicates that the new nanoparticles with the Z3-type crystal structure, in which In atoms replace Pd atoms at the e sites, can be stably synthesized in a narrow range of In concentrations. Further theoretical analyses are needed for deeper understanding of how the magnetic properties are affected by the In concentration in Z3-type Fe(Pd,In)₃.

[1] K. Matsumoto, R. Sato, Y. Tatetsu, T. Teranishi, *et al.*, submitted.

[2] <http://www.openmx-square.org>

[3] A. van de Walle *et al.*, *Calphad Journal* **42**, 13 (2013).

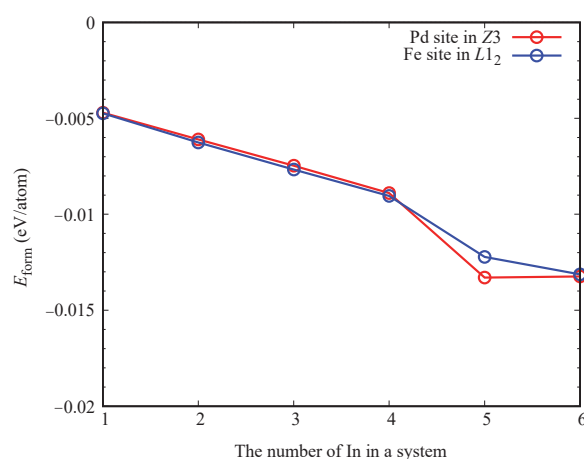


Figure: Formation energies for L1₂-(Fe, In)Pd₃ and Z3-Fe(Pd, In)₃ depending on the concentration of In.

マルチフェロイック物質における高強度テラヘルツパルスを用いたマグノン・フォノン励起

佐藤琢哉 東京工業大学

電荷に代わる新たな情報キャリアとしてマグノンが注目されており、磁性絶縁体薄膜を中心に精力的に研究が行われてきた。これらの磁性体薄膜のスピン波共鳴周波数は GHz 帯域であるが、昨今の通信速度の発展を考えるとさらに高い周波数応答が不可欠である。そこで、THz 帯の共鳴周波数を持つ反強磁性絶縁体中のマグノンが新たな研究対象として提案され、超高速スピントロニクスデバイス実現のため研究が行われている。反強磁性体の中にはマルチフェロイクスを発現する材料もあり、磁場による電気分極の制御、電場による磁化の制御といった電気磁気効果を使った超省電力デバイスへの応用が期待されている。近年、室温でマルチフェロイクスを発現する反強磁性材料として BiFeO_3 が非常に注目されている。薄膜において、DC 電場を印加することでマグノン周波数を変調できることが確認されている。また、フォノンとマグノンが結合しているため、瞬間誘導ラマン散乱によりコヒーレントフォノンを励起するとマグノンも同時に観測される。高速電場によるマグノン制御が期待できるが、実現のためにはフォノン-マグノン間の相関をより深く理解することが不可欠である。本研究では、廣理英基準教授、金光義彦教授と共同で、キャビティ構造を用いてフォノンをさらに強励起・変調した際のマグノン応答を調べた。

キャビティ構造に共鳴周波数の電場を照射すると、キャビティ近傍の局所部分でのみ電場増幅が生じる。そのため、局所部分からの信号のみを検出できる装置の開発が必要になる。そこで我々は、時間分解磁気光学顕微鏡を反射配置で用いることにより、試料局所部分でのファラデー測定を行う(図1)。励起光として 1300 nm(パルス時間幅: 50 fs、直線偏光)、検出光として 800 nm(パルス時間幅 100 fs, 円偏光)の光を用いた。現在コヒーレントフォノン(2.4 THz)を確認することが出来ており、今後キャビティを作製しマグノン応答を測定する。

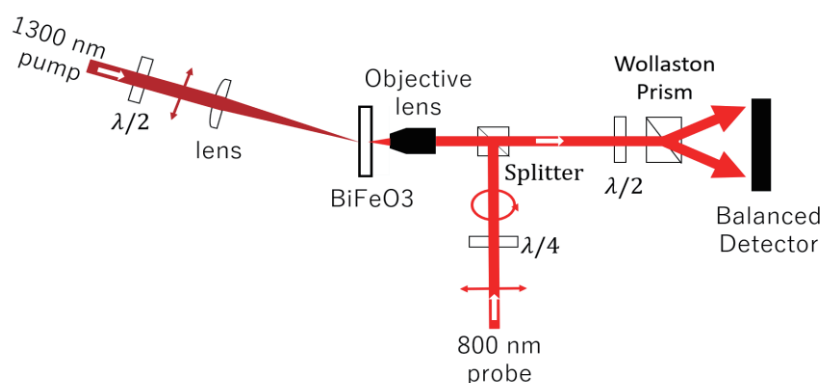


図 1.磁気光学顕微鏡の概要図。白矢印は進行方向を表す。検出光は対物レンズにより試料局所部分に集光される。その後反射光をバランス検出器でファラデー測定を行う。

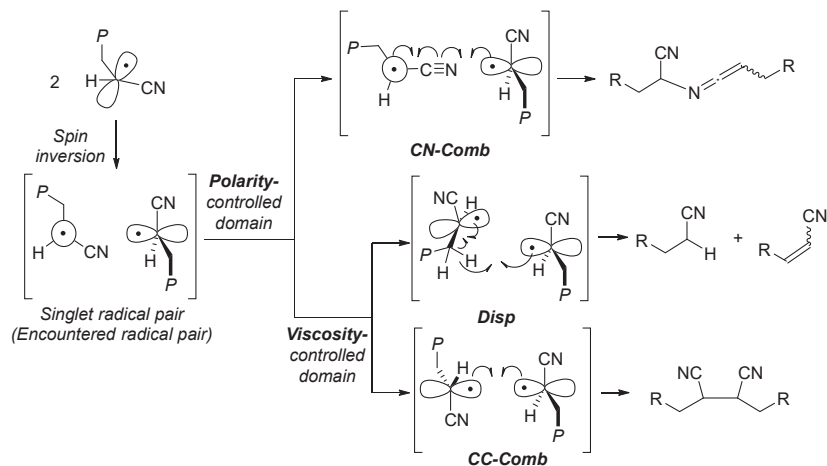
ラジカル重合停止反応機構の包括的な理解とモデル化

中村泰之 物質・材料研究機構

研究の目的: ラジカル重合反応を構成する基本反応の一つである重合停止反応について近年各種モノマーの停止反応機構や、反応機構を決定する要素など理解が不十分であったものが我々の研究により明らかになりつつある。本課題では化学研究所の山子茂教授と共同し、主要モノマー群の重合停止機構、およびそれにかかわる反応や機構に関与する要素についての調査を行い、機構に関する包括的な理解を得ることに取り組んだ。

結果と考察: まず、昨年度 (R1) 共同研究より継続して (メタ) アクリロニトリルのラジカル重合停止機構について検討を行った。アクリロニトリルの重合成長末端ラジカルおよびそれを模したモデルラジカルの停止反応では不均化、C-C 結合に加えて C-N 結合反応が起こることを昨年度研究により明らかにした。各種溶媒を用いてこれら 3 反応の起こる割合を生成物の収率分析から決定したところ、不均化と C-C 結合の割合は溶媒粘度により決定されるのに対し、全体の反応に対する C-N 結合の割合は溶媒の極性に依存することを明らかにした。C-N 結合の割合と溶媒の Polarity index (PI) は良い相関を示し、PI が大きいほど C-N 結合の割合は小さくなった。

メタクリロニトリルの選択性においても同様の傾向が見られ、不均化と C-C 結合の選択性は溶媒粘度に依存し、C-N 結合は溶媒極性に依存した。これらの結果は (メタ) アクリロニトリルの重合停止においては機構に二段階あり、溶媒極性に依存する段階に溶媒粘度に依存する段階が続くことを示唆した。一方、これらを説明する理論モデルについて計算化学による検討を行ったが現時点では合理的なモデルを得ることはできておらず、より多角的な検討が必要とされた。

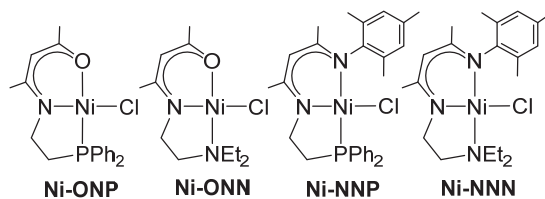


発表等 : 1) X. Li, T. Ogihara, T. Kato, Y. Nakamura, S. Yamago, Evidence for Polarity- and Viscosity-Controlled Domains in the Termination Reaction in the Radical Polymerization of Acrylonitrile, submitted. 2) X. Li, T. Kato, Y. Nakamura, S. Yamago, The Effect of Viscosity on the Coupling and Hydrogen-Abstraction Reaction between Transient and Persistent Radicals, *Bull. Chem. Soc. Jpn.* in press.

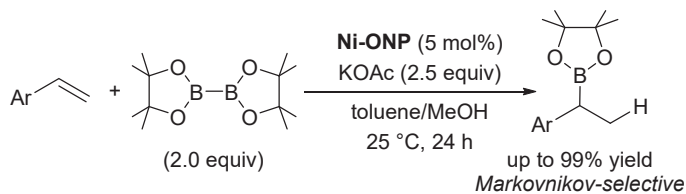
Development of dinuclear nickel complexes based on a monoanionic tridentate pincer-type ligand

Yoshitaka Yamaguchi Yokohama National University

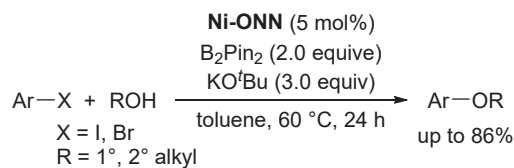
Tridentate pincer-type complexes have generated a lot of interest because the pincer-type ligand stabilizes the metal complexes and its properties can be tuned to achieve the best reactivity of the complex. We have recently reported the synthesis of a series of pincer-type nickel(II) complexes utilizing a combination of β -aminoketonato or β -diketiminato frameworks with a third donor such as a phosphino or amino group. Our systematic study on these nickel(II) complexes revealed that the modification of the ligand framework has a significant influence on the catalytic performance in the cross-coupling reaction of aryl halides or allylic ethers with arylmagnesium reagents (*Dalton Trans.* **2018**, 47, 8003.; *Eur. J. Inorg. Chem.* **2019**, 126.; *Molecules* **2019**, 24, 2296.). We have focused our attention on catalytic transformations promoted by well-defined these nickel(II) complexes.



Organoboronic acids and esters represent versatile synthetic intermediates in modern organic synthesis, particularly in cross-coupling reactions. Therefore, synthetic routes to organoboron compounds have been extensively explored. We were interested in developing the hydroboration reaction of vinylarenes using our nickel(II) complexes as catalysts. We found that β -aminoketonato-based *O,N,P*-coordinate tridentate pincer-type nickel(II) complex, **Ni-ONP**, shows high catalytic activity for the hydroboration of vinylarenes with bis(pinacolato)diboron (B_2Pin_2) in the presence of KOAc as a base. These reactions proceeded in a regioselective manner under mild conditions and afforded the corresponding Markovnikov products in high yield [1].



Alkyl aryl ethers are fundamental structural units for natural products, medicinal compounds and so on. Various synthetic methods have been developed for the preparation of alkyl aryl ethers. Transition-metal-catalyzed cross-coupling reactions of aryl halides with aliphatic alcohols are one of the most efficient approach for the construction of C-O bonds. During the study on the hydroboration reaction as mentioned above, we found that the *O,N,N*-coordinate nickel(II) complex, **Ni-ONN**, shows high catalytic activity for the cross-coupling of aryl halides with primary and secondary aliphatic alcohols in the presence of B_2Pin_2 and KO^tBu as a base [2].



Further investigations on the application to catalytic reactions and the modification of the ligand framework to construct dinuclear complexes are currently underway in our laboratory.

[1] Hashimoto, T.; Shiota, K.; Yamaguchi Y. “Selective Synthesis of Secondary Alkylboronates: Markovnikov-Selective Hydroboration of Vinylarenes with Bis(pinacolato)diboron Catalyzed by a Nickel Pincer Complex”, *Org. Lett.* **2020**, 22, 4033.

[2] Hashimoto, T.; Shiota, K.; Funatsu, K.; Yamaguchi Y. “Cross-Coupling Reactions of Aryl Halides with Primary and Secondary Aliphatic Alcohols Catalyzed by an *O,N,N*-Coordinated Nickel Complex”, *Adv. Synth. Catal.* **2021**, 10.1002/adsc.202001346.

磁性微粒子を用いたウルシオール塗膜の機能発現

橘洋一 京都市産業技術研究所

【目的】

古来より、漆に鉄粉を混合し攪拌することで黒色の漆を作製してきた。これは、漆の主成分であるウルシオール（長鎖炭化水素を有するカテコール誘導体）と鉄イオンの錯体形成によるものとされている¹⁾。漆の硬化反応に寄与するカテコールは鉄イオンとの反応により一部失われるが、得られる黒漆塗膜は、漆本来の光沢・高級感を維持した状態となる。そこで、天然漆を用い、鉄イオンの割合を変化させることで、得られる塗膜の評価を行い、鉄イオンの影響について検討した。

【実験】

初めに、天然の漆に対し水酸化鉄(II)を所定の割合（0, 0.1, 0.25, 0.5, 0.75, 1.5, 3.0 wt%）で混合し、室温条件下にて3分間攪拌することで黒漆を得た。さらに、得られた黒漆を20℃/80%の条件下で乾燥させ、黒漆塗膜を形成させた。塗膜の膜厚は、濡れ膜厚で50μmとした。同時に、乾燥時間の測定を行った。得られた黒漆塗膜の光沢の評価（スガ試験機社製）及び色差測定により黒味の評価（日本電色社製）を行った。

【結果】

初めに、乾燥時間の測定を行った。水酸化鉄(II)を加えていない天然漆のみの場合、指触乾燥時間は0.8時間であった。水酸化鉄(II)の割合を増加させていくと、0.75 wt%までは0.8～1時間となり、天然漆のみと比較して差は見られなかった。一方、それ以上の濃度では、黒漆の粘度の増加が見られ、1.5 wt%では0.5時間となり、3.0 wt%では増粘により測定不可となった。これより、分子内だけでなく分子間での錯形成が示唆された。

次に、得られた塗膜の光沢度及び色差測定を行った（図1）。水酸化鉄(II)の増加に従い、わずかに光沢度の減少が見られ、最終的に3.0 wt%では全く光沢のない塗膜となった。これは、前述のように粘度の増加に起因する。また、色差（L*）測定において、L*の値が小さいほど黒色を示す。図1の結果より、水酸化鉄(II)の添加量が少ない場合（0.1, 0.25 wt%）では、L*は5以上となり、得られた塗膜は飴色であった。一方、0.5 wt%以上の水酸化鉄(II)を添加した場合では、L*は1以下となり錯形成による黒色を確認された。本結果より、水酸化鉄(II)を0.5～0.75 wt%添加し錯形成させることで、塗膜として実用に耐えうるということがわかった。

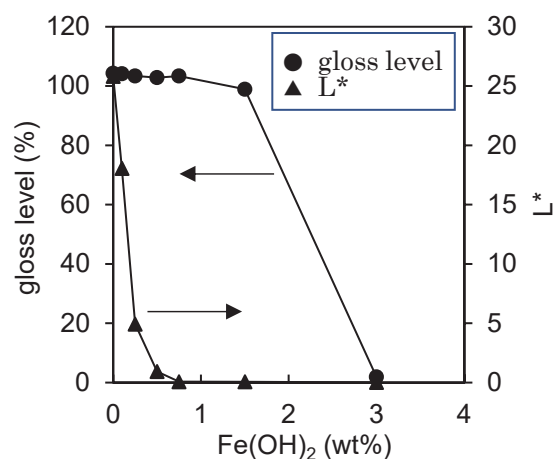


図 1. 水酸化鉄(II)の割合に対する光沢度及び色差（L*）測定

【参考文献】

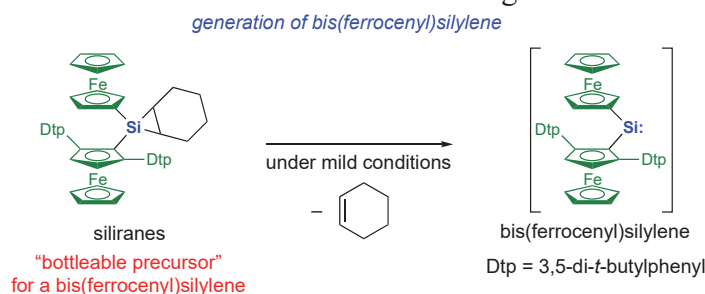
- 1) 漆—その科学と実技 寺田 晃, 小田 圭昭, 大藪 泰, 阿佐見 徹 1999, p87.

Creation of effective oxidation scavenger for efficient perovskite-based solar cells

Takahiro Sasamori University of Tsukuba

The goal of our collaborative research with Prof. Dr. Atsushi Wakamiya (ICR, Kyoto University) is development of an organic oxidation scavenger for the creation of efficient lead-free perovskite-based solar cells, and pioneering research achievements on the basis of the fusion of elemental science and functional physical chemistry. Challenges for lead-free efficient perovskite-based solar cells such as Sn(II)-based ones compared with their Pb counterparts predominantly include the facile oxidation of divalent Sn(II) into Sn(IV) which leads to the increased nonradiative charge recombination in the perovskite films. Thus, we have focused our research targets on the creation of low-coordinated main group element species as effective oxidation scavengers, which exhibit redox-active property and considerable solubility in organic solvents.

Silylenes, organosilicon compounds with an Si(II) center, are known to be easily oxidized under ambient conditions, suggesting their possible ability of working as effecting oxidation scavengers. Isolable stable silylenes remain scarce, and in most hitherto reported examples, the silicon center is stabilized by electron-donating substituents (e.g., heteroatoms such as nitrogen), which results in electronic perturbation. In order to avoid such electronic perturbation, we have been interested in the chemistry of redox-active silylenes with carbon-based substituents such as ferrocenyl groups. Due to the presence of a divalent silicon center and the redox-active transition metal iron, ferrocenylsilylenes can be expected to work as an active oxidation scavenger. In this research project, we have successfully synthesized bis(ferrocenyl)siliranes as a precursor for a bis(ferrocenyl)silylene, which could be a bottleable precursor for the bis(ferrocenyl)silylene under mild conditions. We are grateful to Prof. Wakamiya (ICR, Kyoto Univ.), Prof. Yoshida (Nagoya Univ.), Prof. Mitsudo (Okayama Univ.), and Prof. Tsuchiya (Kitasato Univ.) for their support on the research, and fruitful discussions.



1. Nakamura, T.; Yakumaru, S.; Truong, M. A.; Kim, K.; Liu, J.; Hu, S.; Otsuka, K.; Hashimoto, R.; Murdey, R.; Sasamori, T.; Kim, H. D.; Ohkita, H.; Handa, T.; Kanemitsu, Y.; Wakamiya, A. *Nature Communications* **2020**, *11*, 3008.
2. Pan, Y.; Morisako, S.; Aoyagi, S.; Sasamori, T. *Molecules* **2020**, *25*, 5917.

A study on statistical machine learning for efficient graph structured data analysis

Masayuki Karasuyama Nagoya Institute of Technology

For a variety of scientific fields such as biology, chemistry, and materials science, effective methodologies for analyzing their complicated data are strongly demanded. In particular, we focus on a graph-based representation, which enables us to handle data with interactions among each one of objects [1]. For example, a chemical compound is often represented as a graph in which an atom is a graph-vertex and a chemical bond is a graph-edge. Although graph is a versatile tool for data representation, analyzing its statistical property is usually difficult because of its combinatorial nature. In this study, we consider developing statistical machine learning methods for efficiently analyzing graph structured data by combining several techniques from data-mining, machine learning, and numerical optimization. For this inter-disciplinary topic, we have worked with the researchers including prof. Mamitsuka in the bio-knowledge engineering research laboratory of ICR.

We mainly focus on a task that statistically predicts a property associated with a given graph. For instance, predicting toxicity of a compound is a well-known example in this type of problems. We construct an algorithm that identifies sub-structures of the graph strongly contributing to the target property [2], which can provide insight about the underlying correlation structure. However, naive calculation is computationally infeasible because the number of possible sub-structures are usually extremely large. To overcome this difficulty, we extend a feature selection algorithm called Least Absolute Shrinkage and Selection Operator (LASSO), which has been widely used in statistical data analysis. LASSO is a linear model in which a small number of important features can be automatically detected through sparsity inducing penalty on the parameters. In our problem setting, the features are all the possible sub-graphs, and thus, can be intractable even just to enumerate. We propose an optimization algorithm that efficiently prunes unnecessary sub-graphs in the graph mining tree. Our pruning criterion is based on the optimality conditions from the numerical optimization problem of the LASSO penalty-based sub-graph selection model, by which the optimality of the result can be guaranteed. Effectiveness of the proposed approach in terms of computational efficiency and prediction accuracy is demonstrated by using several graph benchmark datasets.

[1] M. Karasuyama, and H. Mamitsuka, Factor Analysis on a Graph, *Proceedings of the 21th International Conference on Artificial Intelligence and Statistics*, vol.84, pp.1117-1126, 2018.

[2] T. Yoshida, I. Takeuchi, and M. Karasuyama, Distance Metric Learning for Graph Structured Data, *arXiv*, 2002.00727, 2020.

Integrating omics data and module-based network with deep learning to develop cancer type predictive models

Jinn-Moon Yang National Chiao Tung University

Objective: Classification of cancer types has been a major topic in biomedicine and bioinformatics. To classify cancer types, various machine learning approaches have been developed to better analyze mRNA expression data and improve the classification accuracy. However, current studies focus on dealing with unbalanced data, but not emphasize on exploring mechanism across multiple cancer types. A crucial step toward understanding cellular systems properties is to analyze the topology of biological networks and biochemical progress in cells. To construct the protein-protein interaction (PPI) network as completely as possible, genome-scale interaction discovery approaches, such as high-throughput yeast two-hybrid screening and co-affinity purification, have been proposed. However, current approaches are not satisfactory for the integrated analysis of mRNA expression data, PPI data, and other omics data. Therefore, we need to develop more flexible and accurate methods.

Results. In this year, we have done the following two studies as sub-projects. (1) Identification of active sites for small molecules. Identifying active sites of ligands for kinase proteins might lead to development of novel drugs for such difficult diseases as cancer. Therefore, we have been developing a novel method for the purpose, using graph convolutional networks. Currently, we are evaluating our developed method using several data sets and trying to improve it. (2) Prediction of human dicer cleavage sites. It is reported that miRNAs are related to different types of cancers such as lung, breast, and thyroid cancers. Understanding how dicer (enzyme) specifically selects cleavage sites may be useful to interpret the effects of mutations in miRNA coding genes. Therefore, several computational methods have been developed for predicting dicer cleavage sites. In this study, we developed a novel method, ReCGBM, by combining (i) new relational features to combine each sequence and its complementary strand, (ii) class features obtained via affinity propagation, and (iii) gradient boosting machine (a machine learning method). The results using benchmark data sets suggest that ReCGBM is an accurate and interpretable predictor.

Publication.

P. Liu, J. Song, C-Y, Lin, T. Akutsu: ReCGBM: a gradient boosting-based method for predicting human dicer cleavage sites, BMC Bioinformatics, vol. 22, paper ID. 63, 2021.

Next-generation bioinformatics approaches for the accurate identification of protease-specific substrate cleavage sites

Jiangning Song Monash University

In collaboration with Prof Tatsuya Akutsu and his research group at the Bioinformatics Center, we have carried out research activities, which are briefly summarized as follows:

Objectives:

Understanding of the mechanisms of regulation of proteolysis by proteases is very important for elucidation of cellular processes. The key to this understanding is to identify the complete repertoire of specific substrates that each protease targets.

Experimental methods:

We design the Procleave methodology to enhance protease substrate cleavage site prediction by incorporating 3D structural features of substrate cleavage segments. Procleave uses the data curated from the MEROPS database and maps substrate sequences to PDB structures by performing BLAST search, thereby generating an extensive 3D structural substrate dataset. Multifaceted sequence and structural features are then extracted, which are further integrated into a conditional random field algorithm with a data-smoothing strategy to train prediction models.

Experimental results and discussions:

We also assessed the performance of Procleave with several state-of-the-art approaches. The comparison results demonstrate that Procleave outperforms these methods, and the LOWESS smoothing optimization is critical to the performance of Procleave. A user-friendly webserver of Procleave is available as an implementation of the proposed approach. All predicted cleavage sites of the human proteome with structure data are provided for protease biology research. This work was published in the top journal *Genomics, Proteomics & Bioinformatics* in February 2020.

Publications:

- [1] Li F, Leier A, Liu Q, Wang Y, Xiang D, Akutsu T, Webb GI, Smith AI, Marquez-Lago T, Li J, Song J: Procleave: Predicting Protease-specific Substrate Cleavage Sites by Combining Sequence and Structural Information. *Genomics Proteomics Bioinformatics*. 18(1):52-64 (2020)
- [2] Mei S, ..., Akutsu T, ..., Song J. A comprehensive review and performance evaluation of bioinformatics tools for HLA class I peptide-binding prediction. *Briefings in Bioinformatics* 21(4):1119-1135 (2020)
- [3] Chen Z, ..., Akutsu T, Webb GI, ..., Song J. iLearn: an integrated platform and meta-learner for feature engineering, machine-learning analysis and modeling of DNA, RNA and protein sequence data. *Briefings in Bioinformatics* 21(3):1047-1057 (2020)
- [4] J Zhu Y, Li F, Xiang D, Akutsu T, Song J, Jia C. Computational identification of eukaryotic promoters based on cascaded deep capsule neural networks. *Briefings in Bioinformatics*, doi: 10.1093/bib/bbaa299 (2020)

Revealing associations between giant viruses and eukaryotes in the global ocean through community networks inference and mining

Samuel Chaffron CNRS UMR6004

Nucleocytoplasmic DNA viruses (NCLDV) are a monophyletic group of eukaryotic viruses that are highly diverse and abundant in marine environments. NCLDV are known to infect a broad range of eukaryotes, from unicellular eukaryotes to animals. However, the knowledge of their hosts is largely unknown. The number of viruses and hosts isolated in the laboratory represents a very small fraction of existing interactions in the ocean. Therefore, more consideration should be put into cultivation-independent approaches. In our collaborative project, taking advantage of the recent Tara Oceans large-scale marine metagenomics census, we used *in silico* network-based host prediction approaches to fill the gap and further expand our knowledge of the unknown viral world.

First, we built co-occurrence networks of NCLDV and eukaryotic taxa to predict virus-host interactions using Tara Oceans sequencing data (1). In total, 47,978 NCLDV-eukaryote associations were inferred using FlashWeave, an efficient probabilistic learning algorithm for network inference. Then, we applied a LR+ (positive likelihood ratio) based strategy to assess the accuracy of NCLDV host prediction from these co-occurrence networks. For the first time, we demonstrated that the prediction of NCLDV-eukaryote relationships based on co-occurrence networks is four times better than random expectation. To further improve the performance of co-occurrence-based predictions and extract meaningful pairs from high-dimensional co-occurrence networks, we developed a phylogeny-informed filtering method, Taxon Interaction Mapper (TIM). We showed it further improved the host prediction of NCLDV, and lead to a more concise list of candidate host lineages for three NCLDV families, which can be used to generate novel hypotheses to be tested in future experimental studies.

Moreover, using network-based host predictions combined with TIM-based refinement, we demonstrated that viruses explaining a large fraction of the variation of CEE (carbon export efficiency) may infect hosts that are important in marine ecosystems, such as chlorophytes, haptophytes, diatoms, and copepods. These findings imply that viral shunt and shuttle processes could depend on viral host interactions (2). We also used the co-occurrence network approach to predict the associations between NCLDV and virophage, known as NCLDV's "parasites". The virophage-NCLDV associations further supported our previous statement that co-occurrence networks inference and related analysis are appropriate for investigating NCLDV involved interactions in marine metagenomic data.

Publications:

- [1] Meng L, Endo H, Blanc-Mathieu R, Chaffron S, Hernández-Velázquez R, Kaneko H, Ogata H. 2020. Quantitative assessment of NCLDV–host interactions predicted by co-occurrence analyses. bioRxiv doi.org/10.1101/2020.10.16.342030
- [2] Kaneko H, Blanc-Mathieu R, Endo H, Chaffron S, Delmont TO, Gaia M, Henry N, Hernández-Velázquez R, Nguyen CH, Mamitsuka H, Forterre P, Jaillon O, De Vargas C, Sullivan MB, Suttle CA, Guidi L, Ogata H. 2021. Eukaryotic virus composition can predict the efficiency of carbon export in the global ocean. iScience 29;24(1):102002.

Unveiling the genomic contents of ecologically important marine giant viruses

Tom O. Delmont CNRS UMR8030

Objectives. Nucleocytoplasmic large DNA viruses (NCLDV) possess complex genomes and large particles. The PI has been constructing metagenome assembled genomes (MAGs) of NCLDVs based on *Tara* Oceans metagenomic data. Using this new resource, PI's group worked with the ICR partner lab (Hiroyuki Ogata's lab) to investigate various issues around uncultured marine NCLDVs, including their phylogenetic diversity, genomic features, infection strategies, biogeography, possible hosts and deep evolution.

Methods. NCLDV MAGs were generated from *Tara* Oceans metagenomes. MAGs were built using CONCOCT, HUMMER and the bioinformatics platform anvi'o.

Results. 745 NCLDV MAGs (average size 283 kb, ranging 101 kb to 1.4Mb) were generated. First, we identified 1038 protein domains in the NCLDV MAGs that have been previously unidentified in isolated viruses. These included myosin domains. These myosin genes were scattered in the phylogeny of NCLDVs but formed a monophyletic group when analyzed with homologs from various eukaryotes. Second, we used the MAGs to predict the hosts for the NCLDVs that were identified as important predictors of the biological carbon pump in the oceans (Kaneko *et al.*, 2021). Third, we are currently performing a systematic study to investigate the relationships between NCLDV MAGs and their eukaryotic hosts using the co-occurrence based the FlashWeave and Taxon Interaction Mapper (TIM) software.

Discussion

The MAG curation/cleaning is a time-consuming process, but it is nearly the final stage. The NCLDV MAG resource that PI's group generated is a valuable resource to address evolutionary and ecological questions on uncultured marine NCLDVs. This was already in part demonstrated by the above works that PI's group performed in collaboration with ICR's partner laboratory.

Publication

Kaneko H., Blanc-Mathieu R., **Endo H.**, Chaffron S., **Delmont T.O.**, **Gaia M.**, Henry N., Hernández-Velázquez R., Nguyen C.H., Mamitsuka H., Forterre P., Jaillon O., de Vargas C., Sullivan M.B., Suttle C.A., Guidi L., **Ogata H.** Eukaryotic virus composition can predict the efficiency of carbon export in the global ocean. *iScience*, 24, 102002 (2021).

Development of predictive methods for marine microbial communities based on remote sensing data

Kentaro Tomii National Institute of Advanced Industrial Science and Technology

It is important to realize the real-time monitoring of the global dynamics of marine microbiome for various aspects such as knowing the function of each species of microorganism, predicting the changes in the global climate and searching for novel industrial applicable microorganisms. The main problem to overcome is the low temporal and spatial resolution of the sampling using research vessels due to the limitation with cost and labor power. Satellite remote sensing is able to solve this problem because of its automatic, periodic and global sensing. The information obtained from satellite is the spectrum of reflected light (i.e., ocean color data). Though it has the information of the sunlight absorption by the pigments harbored in phytoplankton, a large gap exists between ocean color data and microbial composition. We aim to fill this gap by developing a method for predicting microbial composition from ocean color data using state-of-the-art bioinformatics and machine learning technologies.

In the development of the method for predicting microbial composition, global marine metagenomes of *Tara* Oceans are used as a prediction target. We are using following procedure considering the small number of *Tara* Oceans samples. 1) Make a regression model for predicting microbial composition from pigment data, which has ten times greater number of samples than *Tara* Oceans. 2) Pre-train a neural network using ocean color data as input and microbial composition predicted from pigment data as target. 3) Fine-tune the higher-level layers of pre-trained network with the target of real microbial composition data (transfer learning). We have implemented the first step of the procedure and found only the small part of the microbial community can be predicted from pigment data. This result suggests we will get a method for predicting relative abundance of some special microorganisms not a whole community when we finalize the procedure. To overcome this problem, we are exploring other ways to develop a prediction method, for example by detecting the patterns of microbial composition throughout the oceanic regions and seasons.

Research achievements

金子博人, 富井健太郎 他 宇宙から海洋生態系を観測する：リモセン × メタゲノム
生命情報科学若手の会 第12回研究会（優秀発表賞）

金子博人, 富井健太郎 他 深層学習を利用した人工衛星によるリモートセンシングに
基づく海洋微生物組成予測法の開発 第9回生命医薬情報学連合大会

Control and analysis of complex networks via probabilistic minimum dominating sets

Jose C. Nacher Toho University

Objective. In recent years, we have been focusing on structural controllability of complex networks and developing theory and methods based on the minimum dominating set (MDS), which is a well-known concept in graph theory. In particular, we developed a new concept, the probabilistic minimum dominating set (PMDS), by extending the MDS for handling weighted networks in which edges have some weights. In the last year, we developed a novel method for analyzing metabolic networks by combining PMDS with stoichiometric matrices and successfully applied to analysis of several cancer-related networks. However, our previous method for computing PMDS needs considerable computation time and some improvements are needed. Another major graph theoretic approach to structural controllability is based on maximum matching on bipartite graphs. In this model (MM model), it is assumed that a single driver node can send signals to many other nodes (driven nodes). However, such assumption may not be appropriate for certain kinds of biological networks. Therefore, it is needed to develop methods for identifying and analyzing driven nodes.

Results. We got the following two results. (1) In order to improve the efficiency of our previous method for identifying critical/intermittent/redundant nodes in PMDS, we have developed a novel method which combines some pre-processing procedure and integer linear programming, where critical, intermittent, and redundant nodes are nodes appearing in every PMDS, some PMDS, and no PMDS, respectively. In the pre-processing phase, many critical and redundant nodes are identified using some propositions, and then all kinds of nodes are identified using integer linear programming [1]. (2) As for the MM model, Pequito et al. developed a method (IEEE Trans. Automatic Control, 2016) for identifying a set of driven nodes, using maximum matching for bipartite graphs and strongly connected components of directed graphs. However, this method cannot identify critical/intermittent/redundant node categories (under the MM model). Therefore, we developed a novel method to identify critical/intermittent/redundant nodes using integer linear programming [2].

Presentations (talks only).

[1] E. Yamaguchi, T. Akutsu, J. C. Nacher: Analysis of human brain transcriptomics data across the lifespan using probabilistic network controllability, 7th International Conference on Biomedical and Bioinformatics Engineering, 2020.

[2] Y. Shinzawa, T. Akutsu, J. C. Nacher: Identification and analysis of driven nodes to efficiently control metabolic pathways, 7th International Conference on Biomedical and Bioinformatics Engineering, 2020.

Genomics and transcriptomics of giant viruses

Masaharu Takemura Tokyo University of Science

The giant virus is known for its large genome and viral particle size. Based on isolated giant viruses, I worked with the ICR partner lab (Hiroyuki Ogata's lab) to investigate the genomic and transcriptomics of isolated giant viruses.

Transcriptomic study of medusavirus. Meduavirus was isolated from a hot spring in Japan. A 48-hour time-course RNA-seq experiment was done to investigate the expression profile of viral and host genes. Viral expression profiles were clustered into 5 temporal clusters, which allowed us to identify the temporal tendency of functional category and subcellular localization of viral genes across time. Putative promoter motifs that may account for the regulation of viral gene expression were also predicted. The host transcriptional profile was greatly altered. We identified suppressed and activated groups during the infection course by doing K-means clustering-based Gene Ontology analysis and KEGG pathway enrichment analysis. Our study provides an insight into the transcriptional shift of both medusavirus and its host.

Genomic study of medusavirus stheno. Medusavirus stheno, the 2nd member of the proposed Medusaviridae, was isolated from freshwater sediment samples from the Tatakai River, Uji, Japan (Yoshida, et al., 2021). Medusavirus stheno has a 362,811 bp contig, which showed a high similarity with the original medusavirus genome. The isolation of medusavirus stheno in freshwater indicates a wider habitat of this virus.

Recombination. Recently, we have isolated and assembled 14 new members of the Marseilleviridae from Niigata and Kyoto prefectures, Japan. This presented the opportunity to study important genomic interactions between related closely giant viruses. Using a recombination detection tool, we have detected genome recombination events between these newly isolated viruses, and with other existing Marseilleviruses with nearly complete to complete genomes. Several recombination events are found only between giant viruses isolated in Japan. However, some of these signals are also shared with viruses not isolated in Japan, suggesting an ancestral recombinant. Our study provides insights on how recombination may be involved for the evolutionary stability of large genomes of giant viruses.

Publication

Yoshida K, Zhang R, Garcia KG, Endo H, Gotoh Y, Hayashi T, Takemura M, Ogata H. 2021. Draft Genome Sequence of Medusavirus Stheno, Isolated from the Tatakai River of Uji, Japan. Microbiol Resour Announc 10:10–12.

Whole genome analyses of marine bacterivorous heterotrophic nanoflagellates

Takafumi Kataoka Fukui Prefectural University

Heterotrophic nanoflagellates (HNFs) are known as the main consumers of bacteria in the aquatic ecosystems. They constitute important members to the microbial food web, which transfers energy and materials from small organisms to higher trophic levels¹. Thus, detailed studies on their diversity, ecology, and physiological characteristics are needed to better understand the marine biogeochemical cycles. However, there are only few studies that examined the genomic and ecophysiological aspect of marine HNFs².

Recently, I succeeded to isolate several environmental clones of HNFs from a saline lake, Lake Hiruga. As a result of phylogenetic analysis using 18S rRNA gene, it was suggested that an isolated clone (named HIYC8) represent a novel independent lineage within the subclass Bicosoecida, a member of heterokonts. To further understand the detailed phylogeny and potential function of this clone, it is essential to determine the whole genome sequence and to annotate genes from the genome. In this study, I and the ICR collaborator Dr. Hisashi Endo made use of the state-of-art long fragment sequencing technology and associated bioinformatics tools to make a high-quality draft genome of HIYC8.

Genomic DNA was extracted using a proteinase K/PCI method. The average fragment of the extracted DNA was 48.3 kbp and the quality (DNA Integrity Number, DIN) score measured by the TapeStation system (Agilent) was 7.6. To generate ultra-long reads from the extracted and purified genomic DNA, the Oxford Nanopore Technologies MinION sequencer was used with the library preparation kit SQR-LSK109 and the flow cell R9.4. The raw sequence reads were quality filtered and then assembled using the program Flye³. As a result, we obtained 221 contigs, which had an N50 of 2.0 Mbp, the total length of 76.8 Mbp, and the mean coverage of 52.1. A total of 19,053 genes were predicted from these contigs, although these included genes likely derived from prokaryotes. The genomes completeness was measured with BUSCO and the result indicated that 87.5% of the single-copy orthologous genes of eukaryotes were recovered in the assembly. The similarity between known 18S rRNA gene sequence of this clone and the sequences in the assembly were consistently 99.94% (1,736/1,737 residues). These results indicates that our draft genome is highly completed and accurate, although additional refinement is needed to exclude contaminations from other organisms.

References

- Azam, F. et al. (1983) *Mar. Ecol. Prog. Ser.*, 10, 257-263.
- Jürgens, K. and Massana, R. (2008) Chapter 11, In *Microbial ecology of the oceans*. Wiley.
- Kolmogorov, M. et al. (2019) *Nat. Biotechnol.*, 37, 540–546.

Comparative genome analysis of Parmales and diatoms: Looking for the ancestral genomic feature

Shinya Sato Fukui Prefectural University

Objectives. The order Parmales is a unicellular eukaryotic phytoplankton with a cell wall made of silica. Recent studies revealed that palmales are a sister group of diatoms that also have silica cell wall.

Diatoms are one of the most diverse and successful groups of microalgae sustaining the food web in the ocean. On the other hand, although parmales are widely distributed in the world's oceans from polar to subtropic, their diversity and abundance are extremely low compared to diatoms. A comparative study of parmales and diatoms has a potential to address several important issues, such as the physiological characteristics that made differences in ecological roles between them in the current ocean, the origin of cell walls and their early evolution.

Methods. We newly generated 7 parmales genome assemblies and conducted comparative genome analyses together with 8 parmales and 5 diatom genomes publicly available.

Results. A comparison of the genetic composition of the diatoms showed that the parmales are phagocytotic mixotrophs and there was a large gene loss event related to phagocytosis in the early stages of the diatom lineage. Parmales possess more genes related to lipid-fatty acid metabolism and storage than diatoms, suggesting the existence of physiological processes unique to Parmales. Furthermore, parmales have plastocyanin gene that functions in photosystems under poor iron conditions. These genomic features suggest that parmales are tolerant to oligotrophic conditions. On the other hand, a comparison of genes involved in nutrient uptake, such as nitrogen compound transporters and silicate transporters, suggested that diatoms have efficient nutrient uptake ability. The genomic composition of the diatoms also suggested a high tolerance to nitrogen depletion, highly regulated cell cycle control processes, and the existence of peculiar stress response processes. Comparison of genes involved in the formation of silica structures suggests that diatoms have more complex regulation of structure formation processes than parmales. These results show that the evolution of these traits supports the adaptation of diatoms to dynamic environments.

.

分子ネットワーク解析の統計的機械学習による解法と応用

茅野光範 帯広畜産大学

本研究では、機械学習と統計学を融合させた統計的機械学習の観点から、効率的な分子ネットワーク解析法を提案する。分子レベルとして、主に、ゲノム・遺伝子・代謝に焦点を当て、遺伝子ネットワークや代謝ネットワーク（代謝パスウェイ）の推定や、それらのネットワークへのゲノムの影響、実験条件（健常者と患者等）による違い等を検証するための解析方法を提案する。

まず、問題を明らかにする。図 1 は、5つの遺伝子 A-E の発現量のうち2つの遺伝子の散布図（図 1 左）、全ての5遺伝子の発現量のヒートマップである。図 1 において、Sample 1-50（例えば、健常者）では、遺伝子群 A-E の任意の対は互いに相関している（図 1 左の×印）が、Sample 51-100（例えば、がん患者）では、遺伝子群は互いに相関が無く、ランダムに発現している（図 1 左の◆印）。いくつかの遺伝子が互いに相関している（Sample 1-50）。Sample 51-100 では、この相関構造が崩壊しており、すなわち、これらの遺伝子機能が、がんなどにより崩壊していることを意味する。本研究では、このような相関変化をもつ遺伝子群を効率的に検出するための機械学習・統計的な解析方法を提案する。

我々は、これまで、手法の提案、数値実験による提案手法の評価、公共の遺伝子発現データ（Gene Expression Omnibus ; GEO から入手した延べ約 100 万個の遺伝子群）に提案手法を適用し、生物学的に意義のある遺伝子群が検出出来ることを確認した。また、先行研究で報告されている、相関ネットワークが変化する遺伝子群の具体例を集め始め、これらの成果を元に研究代表者と共同研究者との共著論文を執筆し、修正を重ねている。今後、提案手法をさらに発展させ、グラフネットワーク理論（馬見塚教授、Nguyen 講師）、計算機統計学（Wicker 教授）、アルゴリズムやマイニング理論（中村准教授、瀧川准教授）を駆使した機械学習・統計学的な分子ネットワーク解析法の提案が考えられる。また、これらの解析法の、医学分野（特に加齢研究）および農学分野（大西准教授）における具体的な生命科学現象への応用を検討している。

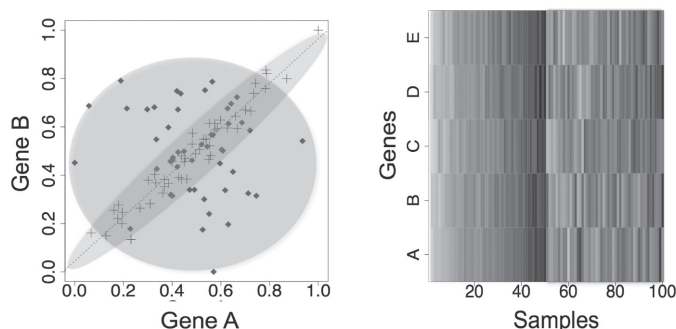


図 1 case/control により相関構造が変化する遺伝子対 A, B（左）と、同様な相関構造変化を持つ遺伝子群 A-E のヒートマップ（右。濃いほど発現量が高い）。遺伝子 A-E の中から任意の対をとると左図のような相関構造の変化が見られる。[Kayano M., Shiga M. and Mamitsuka H., IEEE/ACM Trans. Comp. Biol. Bioinform., 11(1): 154-167, 2014 より転載]

Light emission from halide perovskites and related materials

Ru-Shi Liu National Taiwan University

Objectives: Recently, zero-dimensional perovskite nanocrystals (NCs), which have relatively high thermal stability and narrow luminescence spectral width, are considered to be applied to light-emitting diodes and displays. The emission mechanism of this new material is under debate, and thus studying the photoluminescence (PL) properties is quite important in this kind of research.

Experimental methods: The high-quality Cs₄PbBr₆ zero-dimensional perovskite NCs, whose PL quantum yield (PLQY) reached up to 59%, were obtained by tuning the synthesis process of the hot-injection method. To further explore the emission mechanism of our samples, the time-resolved PL (TRPL) and transient absorption measurements were conducted by using a streak camera system and a pump-probe method.

Experimental results: The TRPL decay curves depend on the excitation photon fluences. A fast decay component appears under strong photoexcitation, and this signal corresponds to the trion recombination. By analyzing the PL decay curves at long delay times, the exciton lifetime τ_x of 4.4 ns and the absorption cross-section σ of $1.8 \times 10^{-15} \text{ cm}^2$ were obtained.

Discussion: The obtained values of τ_x and σ are almost the same order as the reported values for CsPbBr₃ NCs. Taking these PL properties and XRD diffraction data into account, we conclude that the emission of Cs₄PbBr₆ NCs originates from very small CsPbBr₃ NCs embedded in Cs₄PbBr₆ NCs. The photon fluence dependence of the TRPL spectra also suggests the reduction of trion formation comparing to the standard CsPbBr₃ NCs. The surface passivation of CsPbBr₃ NCs can be well improved by Cs₄PbBr₆ matrices, and the reduction of trion formation leads to the enhancement of PLQY.

Publication: Z. Bao, H. D. Chiu, W. Wang, Q. Su, T. Yamada, Y. C. Chang, S. Chen, Y. Kanemitsu, R. J. Chung, and R. S. Liu, “Highly Luminescent CsPbBr₃@Cs₄PbBr₆ Nanocrystals and Their Application in Electroluminescent Emitters” *J. Phys. Chem. Lett.* **2020**, *11*, 10196–10202.

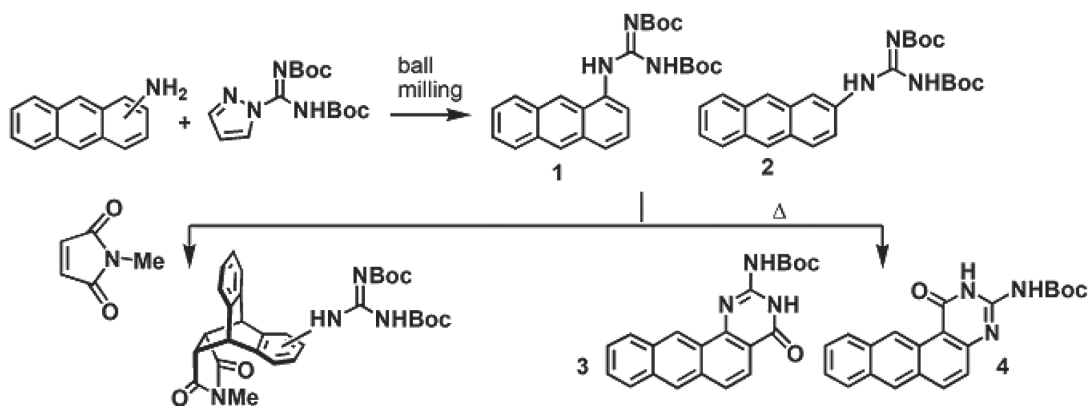
Exploration of cycloaddition properties of guanidine functionalized anthracenes

Davor Margetic Rudjer Boskovic Institute

Objectives

Synthesis of novel guanidinium anthracene reagents and investigation of their reactivity for fullerene derivatization with partner ICR researcher Professor Murata Yasujiro.

Experimental results. Guanylation reaction of aminoanthracenes was carried out in ball mill mechanochemically using *N,N'*-bis-Boc-1-pyrazole-1-carboxamidine as guanylation reagent (Scheme 1). Several experiments were carried out to investigate cycloaddition reactivity of guanidinoanthracenes **1** and **2**. Thermally promoted cycloadditions of anthracenes **1** and **2** with *N*-methylmaleimide afforded mixtures of *exo/endo* cycloadducts, whereas cycloadditions with fullerene showed lower reactivity. Unexpected thermal rearrangement of anthracenes to heterocycles **3** and **4** via intramolecular 6π electrocyclization process was also investigated.



Scheme 1.

Theoretical results. Density functional (DFT) calculations using B3LYP/6-31G* and M062X/6-31G* models were carried out to predict reactivity of anthracene-guanidine derivatives. Relative Diels-Alder reactivity of anthracenes was estimated from the transition state calculations of reactions with two dienophiles (*N*-methylmaleimide and fullerene). Located TS structures corresponding to concerted, synchronous $[4\pi+2\pi]$ cycloaddition mechanism. Overall, activation energies for cycloadditions with C_{60} are higher than reactions with *N*-methylmaleimide, which is in accordance with experimental observations. Electron donating amino and guanidine substituents on anthracene have small effect on the activation energies E_{act} . In addition, intramolecular 6π electrocyclization of aromatic guanidines was investigated computationally. Planned travel to ICR and lecture was not possible due to COVID-19 pandemic.

Development of new blue TADF emitters with horizontal molecular orientations

Eli Zysman-Colman University of St Andrews

This project focused on a novel type of acceptor, [1,2,4]-triazolo-[1,3,5]-triazine core (TTT). 1,2,4-Triazoles and 1,3,5-triazines have each been widely applied as acceptor motifs in thermally activated delayed fluorescence (TADF) materials due to their relatively weak electron-withdrawing character and the combination of both, namely the TTT core, has previously been employed within TADF emitters. However, the previous TTT-based organic light-emitting diodes (OLEDs) showed relatively poor performance with maximum external quantum efficiency (EQE_{MAX}) of less than 10%. Here, we designed two novel TADF emitters (**3,4,5-3TCz-TTT** and **3DMAC-TTT**, Figure 1a). The corresponding OLEDs successfully exhibited improved device performances.

Our group designed these emitters. Prof. Kaji's group conducted photophysical characterization and device fabrications. We identified CzSi as an appropriate host matrix for the TTT-based OLEDs and a doping concentration of 15 wt% was chosen as photoluminescence (PL) quantum yield (Φ_{PL}) was highest. Both compounds present sky-blue emission at 485 nm and 475 nm (Figure 1b), and high Φ_{PL} under N_2 of 80% and 79%, for **3,4,5-3TCz-TTT** and **3DMAC-TTT**, respectively. Both emitters present prompt fluorescence, with similar lifetimes reflecting tri-exponential decay kinetics, of 14.5 ns [$\tau_1 = 26.14$ ns (12.35%), $\tau_2 = 12.97$ ns (63.43%), $\tau_3 = 22.71$ ns (24.22%)] for **3,4,5-3TCz-TTT** and bi-exponential decay kinetics, of 11.9 ns [$\tau_1 = 6.95$ ns (34.7%), $\tau_2 = 14.6$ ns (65.3%)] for **3-DMAC-TTT**. Both compounds also show very long delayed PL (Figure 1c) with bi-exponential decay kinetics and lifetimes of 3.1 ms [$\tau_1 = 1.17$ ms (54.27%), $\tau_2 = 5.30$ ms (45.73%)] for **3,4,5-3TCz-TTT** and 4.7 ms [$\tau_1 = 1.16$ ms (46.84%), $\tau_2 = 7.84$ ms (53.16%)] for **3-DMAC-TTT**. **3,4,5-3TCz-TTT** and **3DMAC-TTT** based solution-processed OLEDs exhibited blue emission with Commission Internationale de l'Éclairage coordinates of (0.17, 0.28) and (0.16, 0.23), and EQE_{max} of 5.8% and 11.0%, respectively (Figure 1d).

[Published paper by this joint work]

The paper highlighting this work has now been published: Hundemer, F.; Crovini, E.; Wada, Y.; Kaji, H.; Bräse, S.; Zysman-Colman, E. Tris(Triazolo)-Triazine-Based Emitters for Solution- Processed Blue Thermally Activated Delayed Fluorescence Organic Light-Emitting Diodes. *Mater. Adv.* **2020**, *1* (8), 2862–2871. Other collaborative work for diindorocarbazole-based TADF emitters is currently ongoing and a manuscript related to this work will be submitted shortly.

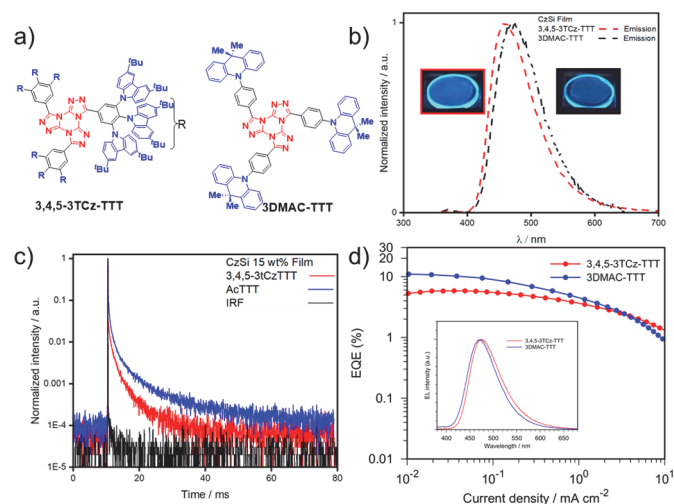


Figure 1: a) Molecular structures of **3,4,5-3TCz-TTT** and **3DMAC-TTT**. b) Emission spectra of **3,4,5-3TCz-TTT** and **3DMAC-TTT** in CzSi doped film (15 wt%) ($\lambda_{\text{exc}} = 340$ nm); c) Time-resolved PL decay of **3,4,5-3TCz-TTT** and **3DMAC-TTT** in spin-coated CzSi film (15 wt%) and; d) EQE-J curves of OLEDs containing **3,4,5-3TCz-TTT** (red) and **3DMAC-TTT** (blue) as emitters. Inset: EL spectra of OLEDs at the current density of 1 mA cm⁻².

Coupling of nanographenes and curved π -systems and elucidation of their electronic and optical interactions

Akimitsu Narita Okinawa Institute of Science and Technology Graduate University

Objective: To achieve the coupling of nanographenes with the curved π -systems developed by the ICR partner researchers, Prof. Takashi Hirose and Prof. Yasujiro Murata, the initial objective in this project has been to prepare adequately functionalized nanographenes. To this end, we have worked on syntheses of nanographenes with halogen or triflate groups that can be used for the transition-metal-catalyzed coupling reactions for the further functionalizations.

Results and discussion: We have previously prepared 5-bromobenzo[*rst*]pentaphene (**2**) during our attempts to synthesized $N = 8$ armchair graphene nanoribbons on surface [BCSJ, **2021**, doi:10.1246/bcsj.20200382], and considered benzo[*rst*]pentaphene as a model case to study the coupling with curved π -systems by the ICR partner researchers. To increase the solubility, 5-bromo-8-mesitylbenzo[*rst*]pentaphene (**4**) was prepared through the Suzuki coupling of **3** with mesitylboronic acid, followed by bromination (Figure). The possibility to use **4** for further coupling reactions could be verified by model reactions, namely Suzuki coupling with mesitylboronic acid to give 5,8-dimesitylbenzo[*rst*]pentaphene (**5**) in 82% yield as well as homocoupling to provide dimer **6** in 76% yield. Interestingly, chiral HPLC analysis of dimer **6** revealed the presence of enantiomers, and attempts on the optical resolution is currently ongoing. On the other hand, we have also prepared dibromo-substituted dibenzo[*hi,st*]ovalene (DBOV), following our previously reported procedure [Chem. Asian J. **2019**, 14, 1703.], and is ready for the further functionalization.

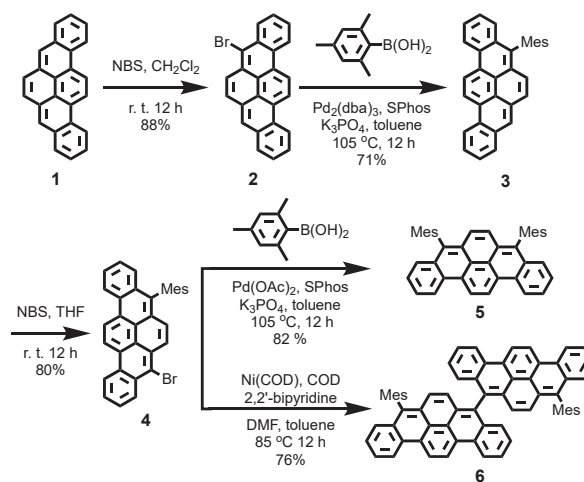


Figure: Synthesis of bromobenzo[*rst*]pentaphene **4** and its coupling towards **5** and **6**.

Conclusion: Bromobenzo[*rst*]pentaphene **4** and dibromo-DBOV have been prepared and are ready for the further coupling studies together with the ICR partner researchers. Although the planning of the research visits and stays at ICR needed to be postponed due to the Covid-19, the synthesis of novel bibenzo[*rst*]pentaphene **6** could be achieved. Optical resolution of **6** as well as investigation of its photophysical and electrochemical properties are currently ongoing.

Development of hole transport materials for tin-perovskite and device characterization

Akinori Saeki Osaka University

Tin iodide perovskite (ASnI_3) is one of the most feasible, less toxic alternatives to lead halide perovskite (APbX_3), owing to its readily formed three-dimensional (D) structure and more suited bandgap (1.2–1.4 eV) of the solar cell application than APbX_3 (1.5–2.3 eV). Here, we report the effect of ternary mixing organic A-site cations (GA, FA, and PEA) on the solar cell performance and charge carrier dynamics that are evaluated using time-resolved microwave conductivity (TRMC) (Fig. 1).^[1] $(\text{GA}_x\text{FA}_{1-x})_{0.9}\text{PEA}_{0.1}\text{SnI}_3$ exhibit the maximum power conversion efficiency (PCE) of 7.90% at $x = 0.15$ and a drastic decrease with increasing GA content. Notably, our TRMC measurements of ASnI_3 with/without a hole transport layer reveal the same trend with the devices. From the analyses, we suggest that a variation of electron mobility affected by the location of the GA cation in the grains significantly impacts the PCE. Our work sheds light on the role of mixed A-site cations and directs a route towards the further development of Sn perovskite solar cells.

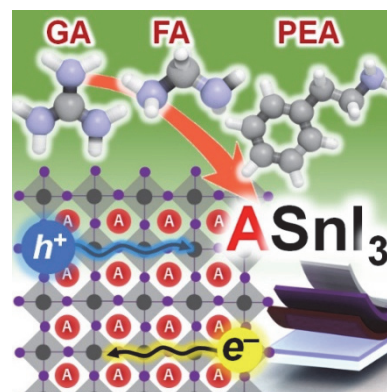


Fig. 1. A-site cation mixing effect on the charge carrier dynamics of tin-based perovskites.

Silver-bismuth-iodide (Ag-Bi-I) semiconductors have increasingly gathered much attention as an alternative to lead halide perovskites. However, Ag-Bi-I has not been thoroughly investigated owing to the complexity in its composition and solution process, and the PCE of its solar cell devices has still stayed at a low level. We report a rigorous exploration of the Ag-M-I composition and III-V elements ($M = \text{bismuth, antimony, indium, and gallium}$) via effective guidance of TRMC measurements (Fig. 2).^[2] Screening of Ag:Bi precursor ratio reveals the superior TRMC transients at the low Bi content to that at the high Bi content, which relates to the predominant Ag_2BiI_5 and AgBiI_7 phases, respectively and leads to the higher PCE in the former. The addition of hydroiodic acid (HI) and mixing of the III-V elements show dramatic effects on the charge carrier dynamics. We obtain an improved PCE of 1.82% in the Ag-(Bi/Sb)-I composite compared to the initial 0.78% of Ag-Bi-I without additive, which broadens the library of Ag-M-I semiconductors for a further evolution of lead-free solar cells.

11	13 (III)	14 (IV)	15 (V)	17
29 Cu	31 Ga	32 Ge	33 As	35 Br
47 Ag	49 In	50 Sn	51 Sb	53 I
79 Au	81 Tl	82 Pb	83 Bi	

Monovalent cation
Trivalent cation

$\text{Ag}_x(\text{III-V})_y\text{I}_{x+3y}$

Fig. 2. Screening of Ag-(III-V)-I semiconductors for solution-processed solar cell.

- [1] E. Nakanishi, R. Nishikubo, A. Wakamiya, A. Saeki, *J. Phys. Chem. Lett.* **2020**, *11*, 4043.
 [2] F. Iyoda, R. Nishikubo, A. Wakamiya, A. Saeki, *ACS Appl. Energy Mater.* **2020**, *3*, 8224.

Development of π -conjugated nickel complexes for high performance n-type thermoelectric materials

Michihisa Murata Osaka Institute of Technology

Introduction

Flexible thermoelectric generators are convenient and low-cost energy-harvesting devices that have recently received increasing attention. Especially organic and organometallic semiconducting materials are suited for this purpose due to their very low thermal conductivity. Moreover, relatively large films can be fabricated easily using low-cost solution-based processes. For the generation of flexible thermoelectric modules, p- and n-type organic semiconducting materials are of vital importance. While solution-processable high-performance p-type organic materials have been intensively studied, the development of the corresponding n-type materials has been hampered partially due to their instability upon doping with an n-dopant under atmospheric conditions. One promising example of an n-type material that can be used as a thermoelectric generator are nickel-ethenetetrathiolate (Ni-ETT) complexes, albeit that they are virtually insoluble in common organic solvents.

Results and Discussion

In this work, we have developed an efficient solution-based process for the fabrication of air-stable n-type thermoelectric films. A Ni-ETT complex (**2**) was synthesized and used to generate an aqueous dispersion (Scheme 1). A film fabricated via a simple drop-casting method with ethylene glycol (EG) as the key additive, exhibited a remarkably high thermoelectric n-type power factor ($PF = 33 \mu\text{W m}^{-1} \text{K}^{-2}$), which remains largely undiminished after 10 days under atmospheric conditions. This environmentally benign process stands in stark contrast to previously reported methods that use organic solvents during the film-forming process. The information obtained in part through the collaboration with Prof. Yasujiro Murata and co-workers should thus strongly contribute to the advancement of flexible thermoelectric modules.

Scheme 1

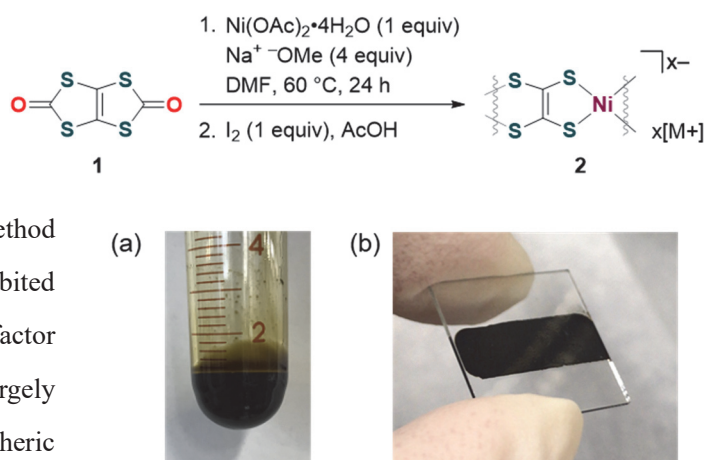


Figure 1. Images of (a) water-dispersed nickel complex **2** ($M = \text{Na}$) and (b) the drop-cast film.

References:

- 1) K. Ueda, Y. Yamada, T. Terao, K. Manabe, T. Hirai, Y. Asaumi, S. Fujii, S. Kawano, M. Muraoka, M. Murata, *J. Mater. Chem. A* **2020**, 8, 12319-12322.
- 2) M. Murata, 2020 27th International Workshop on Active-Matrix Flatpanel Displays and Devices (AM-FPD), Kyoto, Japan, **2020**, 48-49. (IEEE Xplore)

ヘテロアズレンの特性を活かした新規機能性色素の創製

黒飛敬 久留米工業高等専門学校

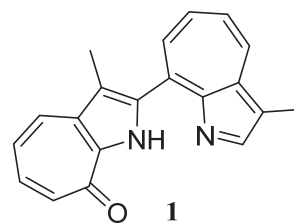
【目的】

これまでに我々はヘテロアズレン類の金属化反応について検討しており、幾つかの知見を得ている。しかし、有効な金属化反応の確立には至っていない。本研究ではヘテロアズレンの2位の反応に着目して、新たな機能性発現への方法論の確立を第一の目的とする。

既存の含窒素複素環からなる交互炭化水素化合物は、電子材料のみならず、金属錯体配位子や生理活性物質など、多種多様な機能性を有する。この複素環に非交互系のアズレン骨格を導入したヘテロアズレンを基本ユニットに使用し、磁性材料や分子認識を活用したセンサーなどへの応用を指向した分子設計を行い、ベンゼン系芳香族では見られない電子構造を利用した機能性の発現を試みる。具体的には1-アザアズレンダイマーの誘導体 **1** および 1,3-ジアザアズレンのアミノ架橋体 **2** の合成といくつかの物性について検討した。**1** はジピロメテンの部分構造を有しておりその発光挙動等に興味が持たれた。

【実験方法】

本研究に使用するヘテロアズレンユニットは 1-アザアズレン及び 1,3-ジアザアズレンとこれらの誘導体である。主な反応部位はアズレン骨格の 2, 4, 6 位とし、触媒反応を用いた分子間の直接カップリングおよびアミノ架橋による共役拡張を行った。1-アザアズレンとその誘導体を直接結合させた **1** の合成法については、これまでに Stille カップリングによる反応条件を精査し報告している。本研究では数種類のアルキル側鎖を有するものについて検討した結果、特にメチル体について合成および物性の検討を行った。また、1,3-ジアザアズレンについては、2-アミノ体と 2-ヨード体の Ullmann 型カップリングによって、2 位で結合した二置換体および三置換体の合成を検討した。



【結果と考察】

1 についてクロロホルムを溶媒に用いて吸収スペクトルを測定したところ、長波長側の吸収末端は 650 nm に達し、1-アザアズレンに比べ大幅な長波長シフトを示した。一方、蛍光は観測されず、アズレン骨格に由来する消光が原因と考えられた。しかし、過剰量の過塩素酸マグネシウムを加えることによって、蛍光 ($\lambda_{em}=330\text{ nm}$, $\lambda_{ex}=600\text{ nm}$) が観測されたことから、金属錯体の形成による構造変化によって発光していることが推測された。そこで、**1** と三フッ化ホウ素との反応を検討したところ、NMR および MS スペクトルの測定結果より、フッ化ホウ素錯体を形成していることがわかった。しかし、酸素原子が配位した構造と窒素原子が配位した BODIPY 構造の混在が示唆された。熱による構造変化が期待されることから、今後、発光挙動について精査する予定である。また、1,3-ジアザアズレンのアミノ架橋体 **2** の合成については、NMP 中で Ullmann 触媒を用いて種々検討したところ、アルゴン雰囲気下 120 °C で、二置換体と三置換体の混合物の生成を確認した。今後、各成分の単離と物性の調査を進める予定である。

Preparation of chiral silica via chiral transfer

Tomoyasu Hirai Osaka Institute of Technology

Silica-based chiral materials such as helical mesoporous silica has been attracted considerable attention in the fields such catalyst, template, chiral recognition. These materials are prepared by sol-gel transcription using an organic chiral structure as template. However, preparation of preferred -handed helical silica derivatives using an achiral polymer as a template has not been reported yet. Polyhedral oligomeric silsesquioxane (POSS) is an organic–inorganic hybrid nanoparticle. Methacrylate-functionalized POSS (MAPOSS) is commercially available and its polymers (PMAPOSS) with a well-controlled primary structure were obtained by controlled radical and living anionic polymerization. It is anticipated that if controlling of the helical conformation in PMAPOSS domains could keep the helical structure during the calcinating process, then it gives a simple and cost-effective preparation method for chiral silica materials.

isotactic PMAPOSS (*it*-PMAPOSS) was prepared on the basis of a living anionic polymerization using a Grignard initiator. To control the secondary structure in *it*-PMAPOSS, *it*-PMAPOSS and chiral dopant (*R* or *S*-BN) were mixed and subsequently the molecular aggregation state was elevated using vibration circular dichroism (VCD) spectroscopy measurements (Figure 1). Split-type Cotton effect could be observed at 1730, 1240~1000 cm^{-1} , which can be assigned to carbonyl, ester, and Si-O-Si stretching vibration, and they showed mirror image between *R* and *S*-BN. This suggests that *it*-PMAPOSS formed preferred-handed helical conformation by mixing of chiral dopant. The samples thus obtained were annealed at 620°C at a heating rate of 10°C / min under air, the residue evaluated using VCD spectroscopy measurements (Figure 2). The peaks ranging from 1000 to 1240 cm^{-1} , which can be assigned to Si-O-Si vibration, were dominant. The two bands centered at 1131 and 1047 cm^{-1} due to the cage and network Si-O bond stretching, respectively, broadened to a single unresolved band, showing a silica structure owing to cage crosslinking. Hence, it is clear that most of the organic segments were removed from the *it*-PMAPOSS. Interestingly, the split-type Cotton effect could still be observed in this region and was more striking than that of the unannealed sample, indicating that the distance between Si-O-Si decreased. The VCD results suggest that the induced preferred helical structure in the PMAPOSS and BN mixture can be used as a chiral template and maintained during the calcination process, leading to the formation of silica with exclusive optical activity.

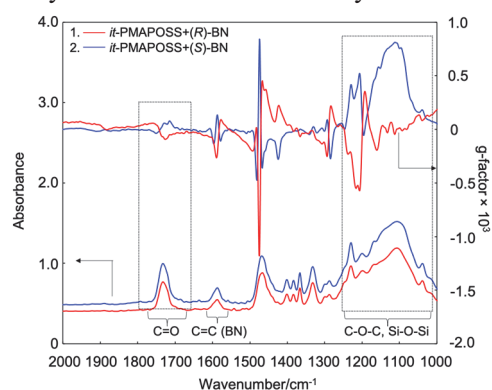


Figure 1. VCD spectrum of *it*-PMAPOSS with *R* and *S*-BN.

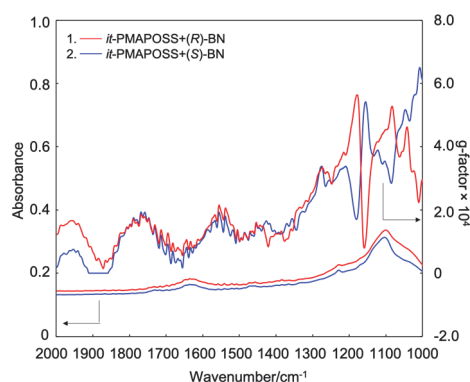


Figure 2. VCD spectrum of calcinated samples prepared using *it*-PMAPOSS with *R* and *S*-BN.

マクロ環骨格内に導入した反応中間体の化学

安倍学 広島大学

【諸言】近年、環状骨格内に湾曲した π 共役系が広がった分子の研究が盛んに行われている。例えば、全てのベンゼン環がパラ位で結合し、環構造を形成したシクロパラフェニレン(CPP)は、ベンゼン環の数が少なくなるにつれ、HOMO-LUMO ギャップが小さくなるという特異的な挙動が報告されている。この特異性は、ベンゼン骨格が湾曲することによって生じるジラジカル性に起因したキノイド構造の寄与に由来する。本研究では、

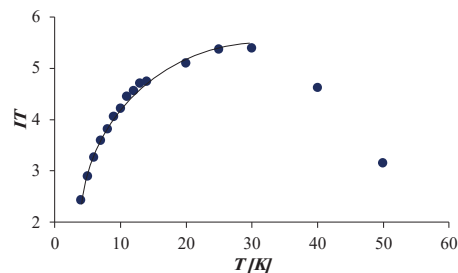
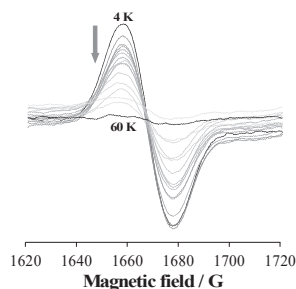
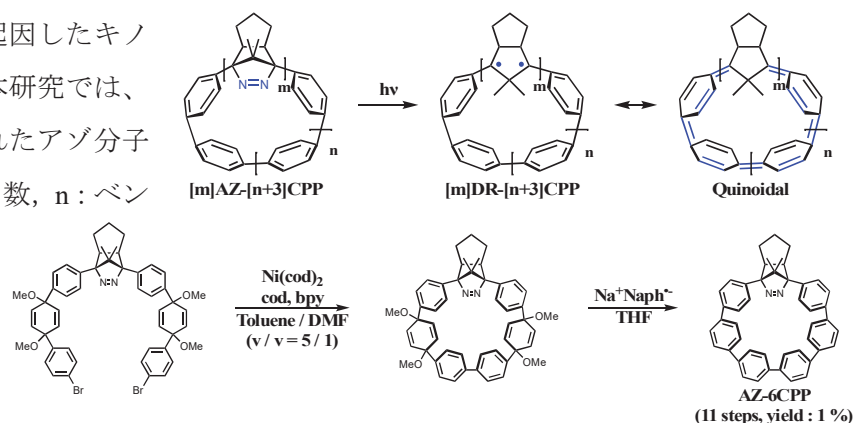
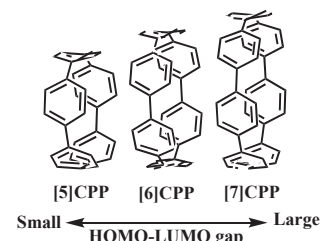
パラフェニレンで環状に繋がれたアゾ分子 **[m]AZ-[n]CPP** (m: アゾ骨格の数, n: ベンゼン環の数) を設計した。湾曲効果の影響を受けるマクロ環骨格内のマルチラジカルは、非環状状態のものの挙動とは異なり、キノイド構造の形成や環全体での芳香族性の発現、高い反応性など直鎖状とは異なる性質を有することが予想される。また、湾曲した環状骨格中でのジラジカルに関する研究報告は少なく、そのスピン状態と反応挙動にも興味を持たれるため、そのスピン多重度と構造に対する π 電子系の湾曲効果を調査した。

湾曲効果の影響を受けるマクロ環骨格内のマルチラジカルは、非環状状態のものの挙動とは異なり、キノイド構造の形成や環全体での芳香族性の発現、高い反応性など直鎖状とは異なる性質を有することが予想される。また、湾曲した環状骨格中でのジラジカルに関する研究報告は少なく、そのスピン状態と反応挙動にも興味を持たれるため、そのスピン多重度と構造に対する π 電子系の湾曲効果を調査した。

とは異なり、キノイド構造の形成や環全体での芳香族性の発現、高い反応性など直鎖状とは異なる性質を有することが予想される。また、湾曲した環状骨格中でのジラジカルに関する研究報告は少なく、そのスピン状態と反応挙動にも興味を持たれるため、そのスピン多重度と構造に対する π 電子系の湾曲効果を調査した。

状態と反応挙動にも興味を持たれるため、そのスピン多重度と構造に対する π 電子系の湾曲効果を調査した。

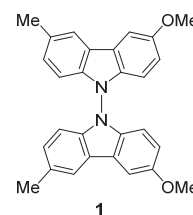
【結果と考察】¹⁾ マルチラジカル前駆体となる環状アゾ化合物の合成を試みた。Ni 触媒による分子内環化、還元的芳香族化を経て、**AZ-6CPP** の合成を達成し、X 線構造解析にて、その構造を確認した。2-MTHF 中、4 K で **AZ-6CPP** の光照射(Hg ランプ)を行うことにより、1650 G 付近に光脱窒素反応によって生じたジラジカル Triplet 種に由来する特徴的なシグナルが発生することが明らかになった。このシグナルをモニターし、温度可変 EPR 測定を行い、Bleaney-Bowers の式を用いたフィッティングを行うことにより、基底一重項であることが求められた。直鎖分子では、基底三重項であることから、湾曲効果によりスピン多重度が変化していることが明らかになった。また、このシグナルは、30 K を超えると徐々に減少していく様子が確認され、反応性に富むことが示唆された。1) Miyazawa, Y.; Wang, Z.; Antol, E.; Kayahara, E.; Yamago, S.; Abe, M. *J. Am. Chem. Soc.* in minor revision.



有機分子触媒を用いる N-N 軸不斉化合物の速度論的光学分割法の開発

吉田圭佑 名城大学

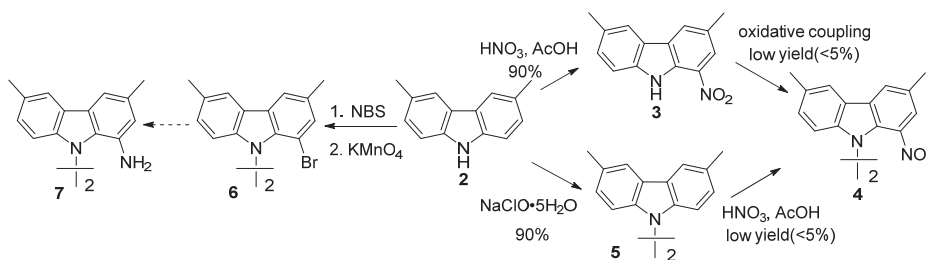
【目的】BINOL、BINAP に代表される C-C 軸不斉化合物は、数多くの研究報告が存在し、その利用方法も不斉リガンド、有機分子触媒、分子認識化学、材料化学など多岐にわたる。一方、N-N 結合による軸不斉の研究は、非常に例が少なくその性質も明らかになっていない。当研究室では三環性芳香族化合物のカルバゾールあるいはアクリドン誘導体に対し、CH₃CN-*t*BuOH 混合溶媒中、次亜塩素酸ナトリウム五水和物を作用させると、窒素上でホモカップリング反応が円滑に進行することを見出した。さらに本反応を用いて当大学で単離された N-N 結合を有する構造未確定天然物 **1** の構造決定にも成功し、N-N 軸上に軸不斉が存在する知見を得た。このような N-N 軸不斉化合物は、置換基に多様性を持たせることで様々な分野において利用価値のある化合物になると考え、現在更なる研究を進めているが、N-N 軸不斉化合物を光学活性体として得る触媒的方法論は皆無である。そこで今回、有機分子触媒による N-N 軸不斉化合物の速度論的光学分割法の開発を計画した。また、カルバゾールからなる N-N 軸不斉の安定性を見積もるためにラセミ化障壁およびラセミ化半減期を求めた。



【実験結果】

最初に化合物 **1** の軸不斉の存在をキラル HPLC で確認したのち、キラル分取カラムによって得られた各エナンチオマーを旋光度、CD スペクトルを用いて明確にした。また本化合物の一方のエナンチオマーを 110 °C で加熱し、時間経過による ee の変化の様子を測定、アイリングプロットからラセミ化半減期、ラセミ化障壁をそれぞれ算出し、27 日、34.6 kcal/mol という結果を得た。これは BINOL のように強固な C-C 軸不斉を持つ化合物に匹敵する結果であり、N-N 軸からなるキラル化合物のラセミ化障壁を初めて実測値として明らかに出来た。本光学活性体がある程度の熱条件に安定であることが分かったため、N-N 軸不斉化合物の速度論的光学分割の反応条件には耐えられると判断し、次に速度論的光学分割の基質合成を行った。アニリン化合物 **7** を反応の基質とするべく、その合成に取り

組んだ。**2** を出発原料にモノニトロ体 **3** を得た後、様々な酸化的カップリングを試みた



が **4** はほとんど得られなかった。また、**5** を得た後、位置選択的なニトロ化を試みたが、こちらも低収率であった。そこで現在、**2** のモノブロモ化の後、KMnO₄ によって **6** を得、臭素からアミノ基への返還を試みている。化合物が合成出来次第、川端研究室で開発されたアシル化触媒を用いて、速度論的光学分割を試みる予定である。

【成果報告】日本薬学会第 141 年会 口頭発表 28V03-am11

Molecular understanding on the structures and dynamics of ionic end-aggregation polymers

Visit Vao-soongnern Suranaree University of Technology

We collaborate with ICR faculties through an iJURC project to investigate structures and dynamics of monofunctional polymers undergoing head-to-head association and dissociation.

Objective: To study the effect of head-to-head association/dissociation on molecular dynamics by computational and experimental techniques

Methods

1. Monte Carlo (MC) simulation of coarse-grained monofunctional polymer model on a high coordination lattice.
2. Molecular Dynamic (MD) simulation of the fully atomistic model of carboxylated poly(cis-1,4-isoprene) and the neutralized form with cation (PICOOM).
3. Synchrotron X-Ray Absorption Spectroscopy (XAS) of carboxylated poly(cis-1,4-isoprene) neutralized with cation (PICOOM) where $M = K$ and Ca .

Results and Discussion

1. **MC simulation:** For the association/disassociation of monofunctional polymer as a function of interaction strength, slower dynamics was seen at the scale of molecular (the mean square displacement for the center of mass and decorrelation of the end-to-end vectors), chain segment (head-to-mid vector and mid-to-end vector) and beads near the interacting group.
2. **MD simulation:** For fully atomistic model of carboxylated poly(cis-1,4-isoprene) and the neutralized form with/without cation (PICOOH and $PICOO^-$ & Li^+ , K^+ , Ca^{++}), we can obtain the information of the local aggregated structures (distance and number of solvated atoms) and short time dynamics of ion, functional group and chain segment (up to 100 nanosecond).
3. **XAS experiment:** synchrotron XAS studies of carboxylated poly(cis-1,4-isoprene) neutralized with cation (K^+ and Ca^{++}) were performed to get results for the cation solvation structures.

Publication

1. Y. Matsumiya, H Watanabe*, N. Sukhonthamethirat, V. Vao-soongnern, Viscoelastic and Dielectric Behavior of Polyisoprene Monofunctionally Head-modified with Associative Metal-Carboxylate Group, NIHON REOROJI GAKKAISHI (2021, *In Press*)
2. Monte Carlo simulation of structures and dynamics of monofunctional polymer with head-to-head association/dissociation (*In Preparation*)

Activity

We have organized the first International Rheology Symposium at Thailand during February 23-26, 2021 (on-line due to Covid19) <https://iumrs-ica2020.com/symposium-detail.php?id=23>

Observation of orbital Hall effect in ferromagnet/nonmagnet bilayers

Sanghoon Kim University of Ulsan

Recently proposed orbital-Hall-induced torque (OHT) can be a candidate to enhance magnetization switching efficiency because the orbital current j^{orbital} , as a result of the orbital Hall effect (OHE), has been expected to be quite larger than the j^{spin} in some elements. The OHE is originated from the orbital texture, which is ubiquitous in condensed matters. If the j^{charge} is injected into NM, in other words, NM is in the non-equilibrium state with an introduction of an electric field, the orbital angular momentum $\pm L$ can be accumulated at edges against orbital quenching. As a result, the transverse j^{orbital} , flows by diffusion of L s. In order to observe such effect, we have conducted research to find such large OHE collaborating prof. Teruo Ono's group in ICR of Kyoto University.

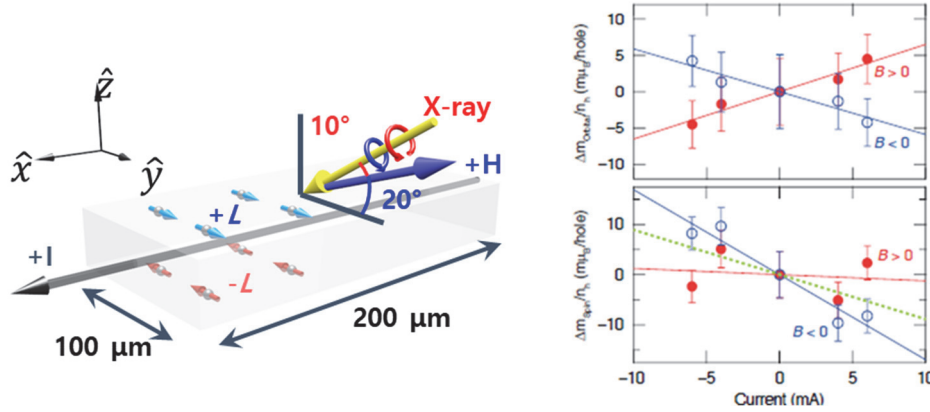


Figure 1. (left) Measurement Scheme to observe the orbital accumulation. (right) Current dependence of the orbital and spin accumulation in terms of the field direction.

Previously, we observed much larger torque efficiency of 3.28 in the Gd/Cr bilayer system than SHA of 0.09 in the Co/Cr bilayer system by conducting the harmonic Hall measurement. Here, we note that the torque efficiency in the Gd/Cr system is much higher than the Co/Cr system. In other words, large orbital accumulation can occur in the Gd/Cr system. Through the ICR international joint research, we succeeded in observation of the current-driven orbital modulations in the Gd/Cr bilayer from the XMCD study. Figure 1 shows the measurement setup to observe the orbital accumulation at the Gd/Cr interface. The low incident angle of the polarized X-ray can detect whether the spin or orbital angular momentum is parallel or antiparallel in a system. Gd M_5 and M_4 edges of Gd/Cr films were scanned varying current density with different current ($\pm x$) and magnetic field directions ($\pm y$) at 17K as shown in Fig. 1. We could observe clear current-density-dependence of the orbital magnetic moment Δm_o . This result is now under preparation for submission to a physical journal. This will be the first observation of the current-driven orbital generation.

High frequency response of polymeric liquids: Rheology and dielectric relaxation

Sathish K. Sukumaran Yamagata University

To investigate the dynamics of polymer chains and their response to imposed fields, experiments are typically performed under isothermal (constant temperature) conditions. To simplify the analysis, it is assumed, often implicitly, that the system temperature is not affected by the imposed field and remains uniform throughout the system. Therefore, the theoretical analysis of polymer dynamics uses isothermal response functions. However, the constant temperature assumption might not be valid for the high frequency response due to the insufficient time for the thermal equilibration of the relevant dynamical processes. Under these conditions, the adiabatic response functions might even be more appropriate. Therefore, combining the experimental and theoretical expertise of ICR (Hiroshi Watanabe, Yumi Matsumiya), and the computational, modelling and theoretical expertise of international (Jorge Ramierz, Madrid; Manlio Tassieri, Glasgow) and domestic (Yuichi Masubuchi, Nagoya) researchers, we have initiated a collaboration between ICR and several international and domestic research partners.

We began our investigations by studying the effect of imposing isothermal and adiabatic conditions on the linear rheology of an unentangled (short chain) polymer melt. We used a simple bead-spring model for the polymer and simulated it at high densities using molecular dynamics simulations (the so called Kremer-Grest model). The isothermal simulations were performed by controlling the temperature using a Langevin thermostat. The adiabatic simulations were performed at constant energy, i.e., without using a thermostat. Oscillatory shear deformation was imposed at several frequencies while ensuring that the amplitude of the deformation was small enough for the response to remain in the linear regime. Our results indicated that the storage modulus, G' , and the loss modulus, G'' , under both the isothermal and the adiabatic conditions were rather close to each other. This also indicated that the relaxation times of the polymer chains were not significantly affected. Therefore, at least in the linear regime, preliminary results suggest that the imposed conditions did not substantially modify the dynamics. However, under adiabatic conditions, as expected, the temperature of the system progressively increased with time. In addition, the temperature increase under high frequency oscillatory shear deformation was significantly larger than under low frequencies. The increase in temperature under adiabatic conditions cannot be sustained indefinitely without any effect on the system response. If nothing else, eventually the system is likely to undergo a change in state due to the heat generated by the imposed oscillatory shear deformation. We are currently further exploring this regime both to confirm our preliminary results and also to elucidate the response when the oscillatory shear is applied for longer times.

Dissolved and particulate Fe isotopic composition in the North Pacific Ocean: Sources and internal cycling

Tung-Yuan Ho Academia Sinica

Objectives:

The major objective of this joint study is to investigate the sources and internal cycling of dissolved and particulate Fe in the water column of the Northwestern and subarctic Pacific Ocean and to evaluate the impact of anthropogenic aerosols originating from East Asia on the processes. My host at ICR, Kyoto University, is Prof. Yoshiki Sohrin.

Methods:

Seawater samples were taken on Japanese GEOTRACES cruises, KH11-7 and KH15-3 with Prof. Yoshiki Sohrin's and other Japanese PIs' research groups in the subarctic North Pacific Ocean. Both dissolved and suspended particulate samples were collected for trace metal elemental and isotopic composition analysis. Elemental and isotopic composition of trace metals were determined by HR-ICPMS and MC-ICPMS, respectively. The detailed information of the sampling and pretreatment are described in the following papers.

Result and Discussions:

The details of the results and discussions are described in the following two papers. Chih-Chiang Hsieh, my Ph.D. student, has measured Fe isotopic composition in the samples and is preparing the other manuscript. In brief, we have observed lighter Fe isotopic composition in the suspended particles, indicating the important roles of anthropogenic aerosol Fe input in the oceanic region.

Publications:

Due to the impact of Covid-19, it was pity that I could not visit ICR, Kyoto University in 2020. However, Sohrin-san and my laboratory have still kept close interaction in the research topics. During the past year, we have submitted the following two papers. Both of them have received positive review comments and are currently under final revision. Another paper about the proposed research topic is under preparation.

Liao, W.-H., S. Takano, H.-A. Tian, H.-Y. Chen, Y. Sohrin, and **T.-Y. Ho*** (in revision) Zn elemental and isotopic features in the sinking particles of the South China Sea: the implications to its sources and sinks *Geochimica et Cosmochimica Acta*

Zheng, L.*, T. Minami, S. Takano, **T.-Y. Ho**, and Y. Sohrin. (final revision) Sectional distribution patterns of Cd, Ni, Zn, and Cu in the North Pacific Ocean: systematic importance of scavenging. *Global Biogeochemical Cycles*

Revealing exciton quenching mechanisms in thermally activated delayed fluorescent devices

Ifor D. W. Samuel University of St. Andrews

Highly efficient organic light-emitting diodes (OLEDs) especially at high brightness are desired for outdoor display and lighting application. As emitter materials, thermally activated delayed fluorescence (TADF) materials can theoretically achieve 100% of exciton conversion into light and it has been expected to use TADF materials in place of conventional emitters in OLEDs. However, TADF materials suffer from efficiency roll-off at high brightness mainly because of singlet-triplet annihilation (STA) and triplet-triplet annihilation (TTA). Therefore, we have tried to establish quantitative analysis method for STA and TTA by ultra-fast transient photo luminescence (Tr-PL) and transient electroluminescence (Tr-EL) measurements.

In our collaborating researchers, Yoshimasa Wada and Hironori Kaji have prepared neat films and host-free OLEDs using a highly efficient blue TADF material, MA-TA. The OLEDs exhibited high efficiency at low brightness and severe efficiency roll-off at high brightness, which is suitable for our research. To analyze STA of MA-TA, transient singlet exciton densities were estimated by Tr-PL measurement for neat MA-TA film using streak camera with pico-second time resolution and frequency adjustable laser (Figure 1). The laser frequencies were modulated from 2 kHz to 10, 50, and 200 kHz, where STA was expected to occur only at high frequency. From the following equations (1) and (2), we have determined Förster radii, R_0 , which will be used for the calculation of rate constant for STA (γ_{STA}). Here, $N_{S1}^{X \text{ kHz}}$, A , t , N_{T1} and τ are singlet exciton density at X kHz, prefactor, time, triplet exciton density, and fluorescent decay lifetime, respectively.

$$\frac{N_{S1}^{X \text{ kHz}}}{N_{S1}^{2 \text{ kHz}}} = A e^{-\beta \sqrt{t}} \quad (1)$$

$$\beta = \frac{4}{3} \pi^{\frac{3}{2}} R_0^3 N_{T1} \tau^{-0.5} \quad (2)$$

Slopes of the figure tell β , from which we calculated $R_0 = 4.7\text{--}6.3$ nm. For the determination of γ_{STA} , we need further investigation of other parameters, a and γ_{enc} , which are the distance between singlet and triplet excitons and their encounter rate constant, respectively as shown in eqs. (3) and (4).

$$k_{FRET} = \tau^{-1} \left(\frac{R_0}{a} \right)^6 \quad (3)$$

$$\gamma_{STA} = \frac{\gamma_{enc} k_{FRET}}{k_d + k_{FRET}} \quad (4)$$

We will continue this analysis as well as Tr-EL experiments for TTA analysis.

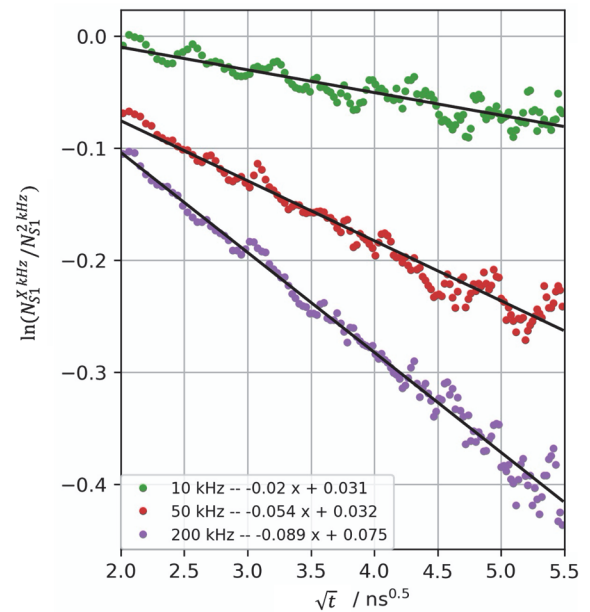


Figure 1. Normalized intensity of $N_{S1}^{X \text{ kHz}} / N_{S1}^{2 \text{ kHz}}$ as a function of \sqrt{t} .

Fabrication of low bandgap semiconductor films and their light induced interfacial charge transfer and charge transport dynamics

Yasuhiro Tachibana RMIT University

Introduction

Low bandgap semiconductors such as metal halide perovskite and metal chalcogenide semiconductor quantum dots have been recognised as the most promising material for next generation photovoltaic devices after the era of crystalline Si solar cells. They can be easily prepared with a solution processed method, and therefore applied for solar cells. However, the prepared solar cells may not necessarily indicate optimal solar cell performance. In this project, we employ different types of solution processed semiconductor films, and assess charge carrier mobilities and interfacial charge transfer dynamics. We have conducted this project with Professor Teranishi at the ICR, characterising low bandgap semiconductor films.

Experimental

Methylammonium lead iodide perovskite (MAPbI_3) nanocrystals were synthesized with the injection method. PbS quantum dots (PbS QDs) were synthesized using the method developed by us previously.[1] PbS QD sensitized TiO_2 films were prepared by first attaching mercaptopropionic acid (MPA) on the TiO_2 surface, and subsequently attached QD to MPA. Photo-induced charge carrier dynamics were quantitatively assessed by state of the art transient absorption spectroscopies covering femtoseconds to 10 seconds and 350~6,600 nm under modified experiment conditions.[2] The quantitative charge carrier separation properties were correlated with interfacial nanostructures.

Results and Discussion

We could successfully synthesized MAPbI_3 nanoplatelets, and moreover found that nanoplatelets or nanocubes can be selectively synthesized by altering the ligand concentration.[3] We also found that the ligand concentration kinetically controls nanoplatelet and nanocube formation. We found that exciton relaxation of PbS QDs are size dependent, and interestingly smaller QD shows faster relaxation compared to a large size.[4] Hot electron injection from PbS QD to TiO_2 was observed. Charge recombination rates are size dependent, that is, the larger QD is, the slower charge recombination is.

References

[1] S. Chan, M. Liu, K. Latham, M. Haruta, H. Kurata, T. Teranishi, **Y. Tachibana**, *J. Mater. Chem. C*, **5**, 2182 - 2187 (2017).

Outcomes

[2] Tachibana et al, *submitted*.

[3] Tachibana et al, *manuscript in preparation*.

[4] Tachibana et al, *manuscript in preparation*.

Dynamics of shear-induced concentration fluctuation in polymer solutions

Maya Endoh Stony Brook University

Introduction. Additive manufacturing (AM) constructing 3-demensinal objects mainly through printing is the one of the most active current technologies. Polymeric materials which are used in AM are exposed in the rapid process in complex 3D geometries and complicated flows, thus exhibit nonlinear dynamics and form non-equilibrium structures that often cause the defects in final structure. Therefore, it is important to understand the physics underlying the flow-induced concentration fluctuation. Theoretically, it is explained that the flow-induced (or shear-induced) concentration fluctuation and phase separation are caused by the effects of “dynamical coupling between stress and diffusion” in the dynamically asymmetric systems by Doi and Onuki. Even though the static characteristics of the shear-induced concentration fluctuation phenomena have been studied, their dynamics have not been well understood for actual materials containing both polymeric and colloidal components.

Experimental Method and Result. To examines the dynamics of the shear-induced concentration fluctuation and/or phase separation in polymer solutions, blends and nanocomposites having a large dynamic asymmetry, we proposed to use X-ray photon correlation spectroscopy (XPCS) technique at National Synchrotron Light Source II (NSLS-II) at Brookhaven National Laboratory (BNL). Due to the COVID-19 pandemic, BNL was closed and we lost the in-person access to conduct the experiment. However, the preliminary XPCS measurement was performed at the CHX beamline at NSLS-II with different system to investigate the nonlinear shear effects on AM materials. Figure 1 exhibits the dynamics of stress relaxation of a silicone/calcium carbonate nanocomposite system. From this two-time correlation function image, we can determine the temporal evolving non-equilibrium dynamics during the stress relaxation of the polymeric nanocomposite system by tracking the speckles from the calcium carbonate as a marker. Unfortunately, the dynamic share mode was unable to determine for this experiment.

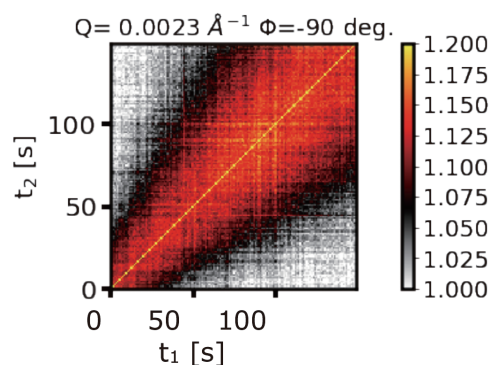


Fig. 1 Two-time correlation function of stress relaxation silicone/calcium carbonate nanocomposite system

GISAXS-CT 法による金薄膜材料におけるナノ粒子の不均一分布評価

藤原明比古 関西学院大学

Grazing Incidence Small Angle X-ray Scattering (GISAXS) 法は、薄膜材料に対して X 線をすれすれに入射することで、散乱体積を稼ぎ、反射 X 線との干渉によって信号増強された小角散乱を得る手法である。これにより、薄膜内部の詳細なナノスケール構造情報を得ることができ、非常に強力な構造解析手段として盛んに研究・利用が進んでいる。しかしながら、試料表面上におけるフットプリントが大きくなることから、マイクロビームを用いた局所構造測定が困難である。そこでこれらの課題を解決するため、GISAXS に CT (Computed Tomography) 法を組み合わせる GISAXS-CT 法の開発が進んでいる。各回転角度及び位置で GISAXS 測定により得られた二次元イメージを CT 法により再構成する GISAXS-CT 法では、基板上的のナノスケール構造の分布状態が得られる。特に、二次元イメージ内の逆空間スケールを表す各 q における散乱強度から CT 像を再構成するため、異なった q の位置から異なったナノスケール情報(例えば、相関、形状、表面フラクタルなど)を再構成することが可能である。CT 像の再構成には、各回転角度において GISAXS 像を得る必要があるため、トータルの測定時間は長くなってしまふ。また、試料への X 線ダメージの影響がある。測定を短時間にするためには、試料の回転角度を間引く必要がある。しかしながら、得られる CT 像の分解能は低くなってしまふ。そこで本研究では、円にパターンした金の微粒子におけるナノスケールの分布状態を回転角度が $3^\circ - 48^\circ$ 間隔で間引いた CT 像をトータルバリエーション (TV) 正則化により画像回復した (図 1)。各制限角度に間引いた Filtered back-projection (FBP) による CT 像 (FBP-CT) と比較した結果、TV 正則化による CT 像 (TV-CT) は、像のシグナル及びアーティファクトのノイズの抑制が可能であることがわかった (図 2)。

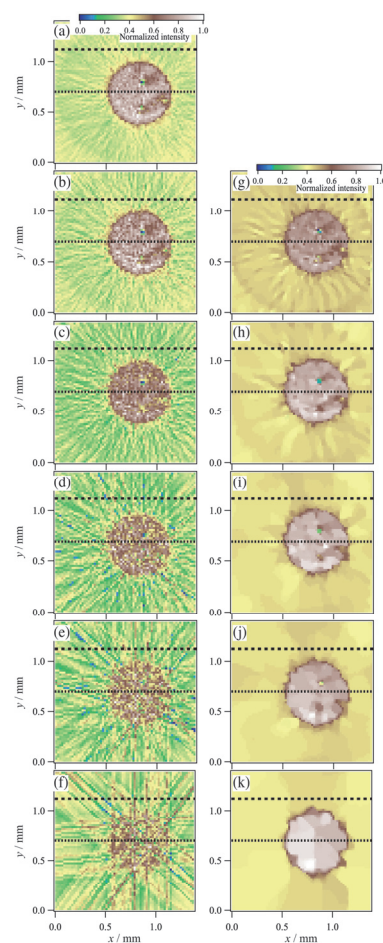


Fig.1 Reconstructed CT images as a function of $\Delta\theta$: (a) $\Delta\theta=1.0^\circ$; (b) $\Delta\theta=3.0^\circ$; (c) $\Delta\theta=6.0^\circ$; (d) $\Delta\theta=12.0^\circ$; (e) $\Delta\theta=24.0^\circ$; and (f) $\Delta\theta=48.0^\circ$. Recovered CT images using TV regularization for downsampling CT images: (g) $\Delta\theta=3.0^\circ$; (h) $\Delta\theta=6.0^\circ$; (i) $\Delta\theta=12.0^\circ$; (j) $\Delta\theta=24.0^\circ$; and (k) $\Delta\theta=48.0^\circ$

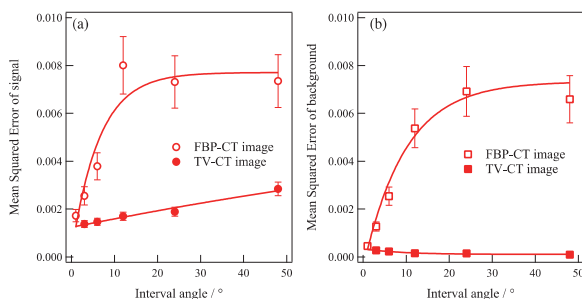


Fig.2 MSE values as a function of $\Delta\theta$ at (a) the circular patterned and (b) background areas obtained from Figures 1. Filled circles were estimated from the line profiles of FBP-CT images with various $\Delta\theta$ angles. Filled squares were estimated from the line profiles of the TV-CT images using TV regularization.

基部陸上植物・ゼニゴケにおける活性型ジベレリンの単離と同定

河内孝之 京都大学

これまで植物ホルモン「ジベレリン(GA)」に関して、主にシロイヌナズナやイネといった被子植物を用いて、生合成遺伝子や受容体など多くの因子が単離され GA によって引き起こされる生理機能が分子レベルで解明されてきた。しかし、このような多様な GA 応答性がどのように獲得され、植物進化に寄与したのかは不明である。GA の起源とそのシグナル伝達系の分子進化について、植物進化の軸に沿って体系的に理解するため、ゼニゴケ (*Marchantia polymorpha* L.) を解析対象とした。ゼニゴケは、系統学的解析により陸上植物進化の基部に位置し、近年ゲノム解読が完了し、ゲノム編集技術が確立され基盤情報や技術を備えた基部陸上植物モデルである。また、予備的な実験からゼニゴケには維管束植物の GA 信号伝達因子が部分的に存在することを見出し、GA の進化的起源が遡る可能性を見出していた。本研究では、陸上植物進化における祖先的な GA 分子 (GAx) の実体とその機能を解明するため、GAx を特定し、物質から個体の生長、基部陸上植物から被子植物への進化といった多様な階層性への理解を目指した。

GAx を特定するため、ゼニゴケのバイオアッセイを立ち上げた。ゼニゴケの GA 生合成変異体は生殖器形成期が遅延することから、一般的な GA 単離法である二相分配法に従って調製した分画を用いた生殖器形成期を指標にしたバイオアッセイを検討した。化学研究所の山口信次郎博士 (共同研究者)、増口潔博士 (研究協力者) との共同研究により、ゼニゴケ抽出物から二相分配法に従って分画サンプルを作成し、生殖器形成時期を指標にしたバイオアッセイを行った。その結果、低極性酸性物質が蓄積する画分に、GA 生合成変異体の生殖器形成遅延効果を回復する効果を持つ物質が含まれていることが明らかになった。今後、質量分析装置や NMR、また必要に応じて予想化合物の有機化学合成を組み合わせることで GAx の構造決定を行う計画である。

近年、モデル・非モデル生物を問わず独自の RNA-seq データを元にした共発現解析から新たな代謝経路の発見が相次いでいる。バイオインフォマティクス情報を利用してゼニゴケの GA 生合成遺伝子・受容体の同定を加速するため、ゼニゴケの公開 RNA-seq データを再解析し、共発現データベースを構築することを進めた。川村 (研究協力者・大学院生) は、公開・集積されるゼニゴケの RNA-seq データを再解析し、共発現ネットワークデータベースを構築した。ゼニゴケの GA 生合成初発酵素との共発現遺伝子を解析したところ、他の既知 GA 生合成遺伝子が複数共発現することを見出した。さらに、共発現遺伝子として機能未知の P450 酵素を見出した。鈴木・孫・王 (研究協力者・大学院生) は、上記 P450 酵素についてその遺伝子破壊株を作成した。その結果、この P450 変異体は他の GA 生合成遺伝子変異体の表現型と同様に、生殖器形成時期の遅延が観察された。吉竹 (研究協力者) は分子系統学的解析に基づいて GA 合成遺伝子群の推定を進め、更に複数の遺伝子が冗長的に機能する可能性を示唆した。

分画とバイオアッセイによりで活性を示した粗抽出物は、その挙動から GA 類縁化合物である可能性が高いと考えられた。バイオインフォマティクスにより候補となった生合成酵素の解析と合わせて、基部陸上植物の GA の同定を進める予定である。尚、今年度は関連した論文公開および学会発表には至っていない。

Origin analysis of atmospheric aerosol of mountainous areas by trace metal analysis

Yuzuru Nakaguchi Kindai University

Purpose) The authors have been studying about cross-border pollution of the Asian Dust in Higashiosaka city from 2017 to 2020. The concentration of Al and Fe in the coarse particles which was supplied from soil increased during Asian Dust event. However, the concentration of Zn, V, and Pb in the coarse particles which was supplied from anthropogenic origin did not increase during Asian Dust event. On the other hand, the concentration of V and Pb in the fine particles increased during Asian Dust. The origin of Al in the atmosphere is the crust, and its dry deposition velocity is used as an index to indicate the scale of Asian Dust. The dry deposition velocity of Al decreased from 2017 to 2020. It is difficult to understand the origin of cross-border pollution because there are many sources of human pollutants since Higashi-Osaka City has many industrial areas and highways around the city. In this study, atmospheric aerosols were collected and analyzed in mountainous areas where the effects of local pollution were small, and the effects of cross-border pollution of Asian Dust were investigated.

Experimental) Atmospheric aerosol samples were collected on the PTFE filter of air sampler (Kimoto-electric co.Ltd, Type AS-9) at the rooftop of the Yamanashi University building during from March 16 to March 24, 2020. The PTFE filter paper was changed every 24 hours. After sampling, the filter is cut into a Fine part (particle size $< 2.5 \mu\text{m}$) and a Coarse part (particle size from 2.5 to $10.0 \mu\text{m}$). The cut filter was transferred to an HDPE bottle, pure water was added, ultrasonic waves were irradiated for 15 minutes to elute, and it was filtered through a $0.45 \mu\text{m}$ filter, and then the ionic components were analyzed by ion chromatography system (Dionex, Type ICS-1500). The cut filter was transferred to a reaction decomposition vessel for microwave ovens (San-ai Kagaku, Type P-25), high-purity nitric acid, high-purity perchloric acid, and high-purity hydrofluoric acid were added and decomposed in the microwave oven, and after decomposition, Trace heavy metals were determined with an inductively coupled plasma emission spectrometer (Thermo Scientific co Ltd., Type iCAP7600). The PM_{2.5} and PM₁₀ were analysed by the automatic fine particulate matter measuring instrument (Kimoto-electric co Ltd, Type SPM-613).

Results and discussions) The Asian Dust event was observed in Kofu city from March 21 to 22, 2020. The results of the backward trajectory analysis showed that this Asian Dust passed over the Mongolian desert and Shanghai, China, and reached Kofu city. The dry deposition velocity of Al and Pb in the Coarse fraction during Asian Dust (AD) event were 249 and $0.93 \text{ mg} / \text{m}^2 \cdot \text{year}$, respectively, and the dry deposition velocity of these elements during non-Asian Dust (nAD) event were 89, $0.37 \text{ mg} / \text{m}^2 \cdot \text{year}$, respectively. It was found that soil-derived (crust) Al during AD was 2.8 times higher than nAD, and Pb, of anthropogenic pollutant during AD was about 2.5 times higher than nAD.

Achievement report) Nakaguchi, Y., Ikeda, Y., Sakamoto, A., Zheng, L., Minami, T., Sohrin, Y., 2020, Distribution and stoichiometry of Al, Mn, Fe, Co, Ni, Cu, Zn, Cd, and Pb in the East China Sea, Journal of Oceanography, <https://doi.org/10.1007/s10872-020-00577-z>

部分フッ素化両親媒性分子の膜物性・構造に対する Rf 鎖長依存性の解析

園山正史 群馬大学

【目的】 私たちは膜タンパク質研究に資する部分フッ素化リン脂質の設計指針を得るための物理化学的な研究により、パーフルオロアルキル基(Rf)を疎水鎖末端に部分的に導入した両親媒性分子が、Rf 鎖長依存的な際だった物性を示すことを明らかにして来た。本研究では、炭素鎖長 $n=5$ および7の Rf 基を有する部分フッ素化ミリスチン酸 F_n -MA とリン脂質 Dimyristoylphosphatidylcholine (DMPC) の部分フッ素化アナログ分子である F_n -DMPC を新たに合成し、表界面物性および分子構造を解析することにより、膜物性・構造の Rf 鎖長依存性を明らかにすることを目的とした。

【方法】 これまでの方法に準じて部分フッ素化したミリスチン酸群 F_n -MA およびリン脂質分子群 F_n -DMPC のグラムスケールでの合成を試みた。脂質二分子膜懸濁液の熱物性の解析には日立ハイテクサイエンス社製示差走査熱量計 DSC6100-Exstar6000 を用いた。

【結果と考察】 $F5$ -MA および $F7$ -MA については、グラムスケールで純度の高い試料が得られた。それらを用いて F_n -DMPC の合成を試みたところ、 $F7$ -DMPC は純度の高い試料を大量合成することに成功したが、 $F5$ -DMPC については小スケールでの合成を終え、現在グラムスケールでの合成を行っているところである。

得られた $F7$ -DMPC 懸濁液の示差走査熱量 (DSC) 測定を行った。結果を下図に示す。24.4 °C のゲル-液晶相転移および 14.2 °C の前転移による2本の吸熱ピークを示す DMPC に対して、 $F7$ -DMPC では 45.0 °C にシャープな1本の吸熱ピークが観測された。 $F7$ -DMPC の相転移温度 T_m は、 $F6$ -DMPC の 19.9 °C と $F8$ -DMPC の 64.4 °C のほぼ中間に位置した。したがって、Rf 鎖長の短い $n=2$ および4では DMPC に比較して T_m が大きく低下する一方、さらに Rf 鎖を伸長した F_n -DMPC では T_m が上昇傾向に転じることが明らかになった。 $F7$ -DMPC の転移エンタルピー ΔH は 11.6 kJ/mol と算出され、 $n=6$ とほぼ同じであった。以上のように、Rf 鎖が $n=6$ よりも長い F_n -DMPC では ΔH は DMPC (18.9 kJ/mol) よりも小さい値を示し、 T_m は上昇するという傾向が顕著に見られた。今後、現在合成中の $F5$ -DMPC を含めて、水面上単分子膜の表面圧-分子占有面積等温曲線および赤外反射スペクトルの測定により、 F_n -DMPC 脂質膜の Rf 鎖長依存性の物理化学的起源を明らかにする予定である。

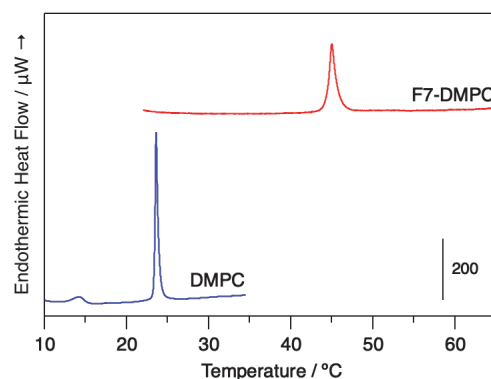


図. $F7$ -DMPC および DMPC 脂質膜の DSC 曲線

【成果報告】

招待講演: Masashi Sonoyama, "Partially Fluorinated Phospholipid Membrane", Symposium 2S-9 "New lipid membrane technologies for reconstitution, analysis, and utilization of 'living' membrane proteins", 58th Annual Meeting of Biophysical Society of Japan (Sep. 16, 2020, online).

Dynamic viscoelasticity and tensile properties of thermoplastic elastomers

Atsushi Noro Nagoya University

Background and objectives: To develop elastomers with excellent toughness and processability, block copolymer-based thermoplastic elastomers (TPEs) with dynamic noncovalent cross-links have been actively studied in recent years; for instance, we developed an ABA triblock copolymer with hydrogen-bonding groups of amide on the B middle block with a glass transition temperature lower than room temperature, and we also evaluated the effects of hydrogen bonds formed in the ABA triblock copolymer-based TPE on the mechanical properties. However, most of the previous studies on noncovalent-bonded TPEs, including our previous reports, mainly focused on the incorporation of hydrogen bonding groups into the rubber-component blocks. Therefore, in this study, an ionically functionalized thermoplastic elastomer (iSIS) was synthesized by incorporating ionic groups into the polyisoprene block of a polystyrene-*b*-polyisoprene-*b*-polystyrene (SIS) triblock copolymer. Mechanical properties of SIS and iSIS were also compared by performing tensile tests.

Experimental methods: Film samples of neat SIS (Fig. 1a) and ionically functionalized iSIS (Fig. 1b) were prepared by using a solution-casting method. Uniaxial tensile tests were performed at room temperature to evaluate the tensile properties, where an initial distance between jigs is ~ 10 mm.

Results and discussion: Fig. 1c shows the stress-strain curves of neat SIS and iSIS. The tensile strength and the toughness of neat SIS were 9.1 MPa and 112 MJ m^{-3} , respectively, where toughness can be estimated from the inner area under the stress-strain curve. On the other hand, iSIS exhibited much higher tensile strength (43.1 MPa) and toughness (480 MJ m^{-3}). This surprising result is attributed to formation of ionic multiplets from ionic groups in iSIS, which serve as strongly associated but reversible, dynamic cross-links. Since the elastomers can be produced at industry scale, they have great market potential for becoming next-generation elastomeric materials.

Publication: “Extremely Tough Block Polymer-Based Thermoplastic Elastomers with Strongly Associated but Dynamically Responsive Noncovalent Cross-Links” Kajita, Takato; Tanaka, Haruka; Noro, Atsushi*; Matsushita, Yushu; Nozawa, Atsushi; Isobe, Kousuke; Oda, Ryoji; Hashimoto, Sadaharu, *Polymer* 2021, 217, 123419, <https://doi.org/10.1016/j.polymer.2021.123419>

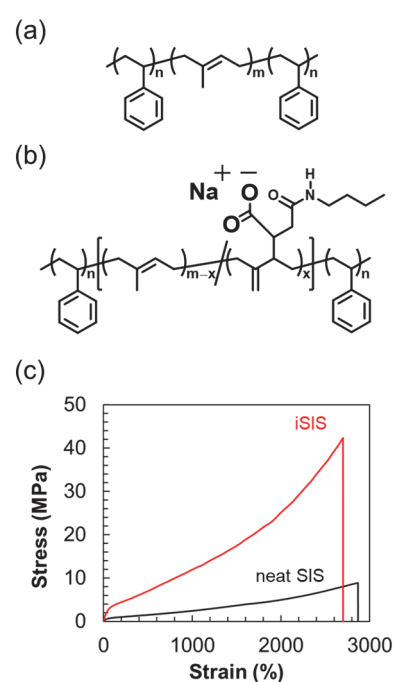


Fig 1. (a) Chemical structure of SIS. (b) Chemical structure of iSIS. (c) Stress-strain curves of SIS and iSIS.

プラズモニック合金ナノ粒子を設計するための理論的指針の構築

飯田健二 北海道大学

[目的] 自然界の限られた資源を有効活用するためには、様々な元素を組み合わせることで高性能な物質・材料を創造していくことが求められる。可視域に局在表面プラズモン共鳴(LSPR)吸収を示す材料の場合、周期表 11 族の単金属 (Cu、Ag、Au) のみが使われてきた。しかし近年、B2 (塩化セシウム) 型合金ナノ粒子が可視域に LSPR 吸収を示すことが発見された。このナノ材料は Pd と In を 1:1 の組成比で有しており、組成比や原子種を改変することで LSPR 吸収波長を制御できると期待される。そこで本研究では、合金ナノ粒子の第一原理計算を行い、LSPR 特性を制御するための理論的指針を構築することを目的とする。

[計算手法] 本研究では、数 nm のナノ粒子の光電子物性を原子・電子のレベルで明らかにすることが求められる。そのために、高い並列化効率を有する第一原理計算プログラム SALMON を用いた大規模計算によって、光励起電子ダイナミクスシミュレーションを行った。対象としたのは、図 1(a)に示した直径約 3 nm の B2 型の $\text{Pd}_{329}\text{In}_{312}$ ナノ粒子である。比較のために、同程度の大きさの Au_{561} (図 1(b))についても計算を行った。

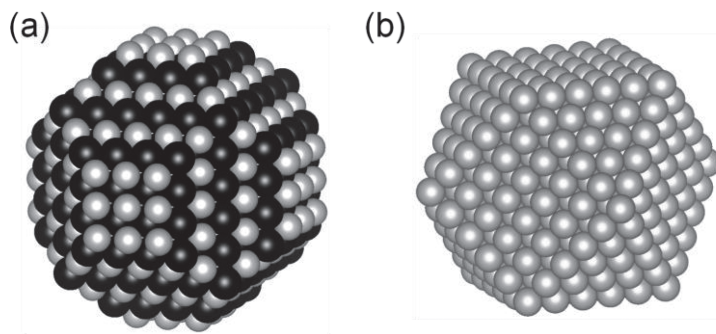


図 1. 対象とした(a) $\text{Pd}_{329}\text{In}_{312}$ ナノ粒子と(b) Au_{561} ナノ粒子。

[結果と考察] 光吸収スペクトルを計算したところ、 Au_{561} では 2.4 eV 付近に LSPR に由来するピークが見いだされた。更に、 $\text{Pd}_{329}\text{In}_{312}$ でも 2.4 eV 付近に Au_{561} と同程度の強い吸収ピークが存在していた。そこで $\text{Pd}_{329}\text{In}_{312}$ について、2.4 eV の光によって誘起される電子ダイナミクスを解析した。その結果、電子の集団振動が励起されることが見いだされた。これによって、 Au_{561} と同じく $\text{Pd}_{329}\text{In}_{312}$ でも可視光で LSPR が励起されることが明らかになった。

Pd や In の単一金属では、可視光領域で LSPR は生じない。そこで、合金化により LSPR が発現するメカニズムを解析した。その結果、Pd と In の間の結合によって Pd 由来の d バンドのエネルギーが下がり、Au に類似の電子構造を取ることが明らかになった。

[成果] 飯田健二, 「ナノ物質系の界面の光や電圧に対する応答の理論計算研究」京都大学福井謙一記念研究センターオンラインシンポジウム, オンライン開催, 2021 年 1 月 25 日 (招待講演)

Study on transportation of metal ions through a polymer membrane containing ionic liquid

Hiroshi Mukai Kyoto University of Education

Introduction Transportation of metal ions using a liquid membrane (LM) of a thin layer is an alternative method of liquid-liquid extraction which use a large amount of harmful organic solvents and valuable carrier molecules, and expected to reduce these risks and costs. However, the thin layer of LM is often mechanically unstable. Therefore, polymer membranes containing liquids have been applied to the LM in order to improve its strength. In our previous work, the active transportation of copper (II) ions using polyvinyl chloride (PVC) membrane containing ionic liquid (IL) was achieved and its almost quantitative transportation for 24 hours was observed. For the purpose of separation of metal ions, the transportation of metal ions through a polymer membrane was studied under the various different experimental conditions in this study.

Experimental (1) Preparation of PVC membrane: 1-Phenyl-3-methyl-4-benzoylpyrazol-5-one (PMBP) or 1,10-phenanthroline hydrochloride monohydrate ($\text{phen} \cdot \text{HCl} \cdot \text{H}_2\text{O}$) were dissolved in 1-hexyl-3-methyl-imidazolium bis(trifluoromethanesulfonyl)imide ($[\text{C}_6\text{mim}][\text{Tf}_2\text{N}]$) or dioctyl phthalate (DOP) at the concentration of $0.005 \text{ mol kg}^{-1}$. This solution of 1.25 g and PVC of 0.1 g for $[\text{C}_6\text{mim}][\text{Tf}_2\text{N}]$ or 0.3 g for DOP were dissolved in tetrahydrofuran of 5 g in the glass petri dish of 49 mm inner diameter and were dried. (2) LM transportation: The membrane was fixed at the center of the U-shaped reaction cell. The 30 or 40 cm^3 of aqueous supplying phase ($[\text{Fe}(\text{NH}_2)_2(\text{SO}_4)_2] = 5.0 \times 10^{-5} \text{ mol dm}^{-3}$, $[\text{CH}_3\text{COONa}] = 0.01 \text{ mol dm}^{-3}$, $[\text{CH}_3\text{COOH}] = 0.01 \text{ mol dm}^{-3}$, pH 4.70) and the 30 or 40 cm^3 of aqueous receiving phase ($[\text{HCl}] = 1 \text{ M}$, pH 0) were poured into each part of the reaction cell separated by the membrane. After 24 hours, the pH values, the volumes and the Fe concentrations of the supplying and receiving aqueous phases were measured.

Results and discussion The membrane worked stably as a separator of two aqueous phases when the membrane left 6 mm margin around the center hole with a diameter of 25 mm in the reaction cell. Table shows the results of LM transportation of Fe^{2+} ions for the different membrane composition. Compared with the LM transportation of Cu^{2+} ions, Fe^{2+} ions were much less transportable due to less stable complex formation according to Irving-Williams rule. It suggests the possibility of metal separation by the LM transportation due to the different stability of metal complex formations. Compared between Nos. 2 and 3, it was found that the transportation rate can be controlled by the choice of carrier molecules. Fe^{2+} ions seem to suit N coordination atoms of phen rather than O atoms of PMBP according to HSAB theory.

Table Results of liquid membrane transportation of Fe^{2+} under the different experimental conditions.

No.	PVC	$[\text{C}_6\text{mim}][\text{Tf}_2\text{N}]$	DOP	PMBP	$\text{phen} \cdot \text{HCl} \cdot \text{H}_2\text{O}$	Time	Transportation Rate
	[g]	[g]	[mol/kg]	[mol/kg]	[mol/kg]	[h]	[–]
1	0.1	1.25	–	–	0.05	24	0.10
2	0.3	–	1.25	–	0.05	24	0.10
3	0.3	–	1.25	0.05	–	24	0.02

Exploration of hierarchical dynamics of amorphous polymers by broadband dielectric spectroscopy

Osamu Urakawa Osaka University

We examined the hierarchical dynamics of a topological network formed by rotaxane-type movable crosslinks consisting of a poly(ethyl acrylate) backbone threaded through peracetylated γ - or β -cyclodextrins (CD) connected to other chains. Figure 1 schematically shows the structure of the movable crosslinking network. These network materials were synthesized by bulk radical copolymerization of ethyl acrylate and peracetylated γ - or β -CD monomers: PEA- γ -CD, or PEA- β -CD. The rotaxane structure was naturally introduced through this synthesis even though the amount of rotaxane type CD moieties is small (22 mol% of the feed CD content, determined from the dielectric intensities). The obtained materials were rubber-like and highly stretchable. We conducted rheological and broadband dielectric spectroscopy measurements to analyze the hierarchical dynamics governing the material properties.

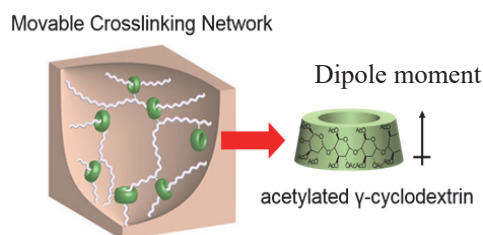


Figure 1. Rotaxane-type movable crosslink network

Figure 2 shows the storage modulus G' (composite curves) as functions of frequency ω for PEA- γ -CD with various CD contents at temperatures 50°C above each glass transition temperature. By increasing the molar fractions of CD (x), the $G'(\omega)$ spectra at low ω change: the terminal slopes change from 2 to 0, suggesting the formation of rotaxane type crosslinks. In the glass to rubber transition region (at $\omega = 10 \sim 10^5 \text{ s}^{-1}$), where network strand dynamics is responsible, a new relaxation process called “slow mode” was detected. Figure 3 shows the corresponding dielectric data (ω -derivative of dielectric permittivity), clearly exhibiting the slow mode indicated by the black arrow. We ascribed this dielectric relaxation mode to the rotational motion of the rotaxane type cyclodextrin moieties via sliding on the polymer backbone accompanied by the chain conformational change. The temperature dependence of this mode relaxation time obeyed the Arrhenius type equation with the activation energy $E_a = 140 \text{ kJ mol}^{-1}$. From this E_a value, we concluded that CD's sliding motion occurs through a distance of about or longer than the Khun length.

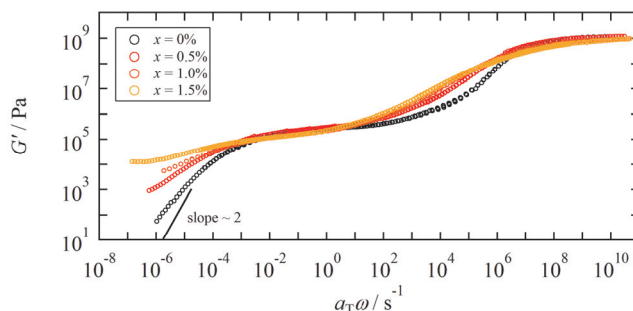


Figure 2. $G'(\omega)$ for PEA- γ -CD with $x=0 \sim 1.5 \text{ mol}\%$.

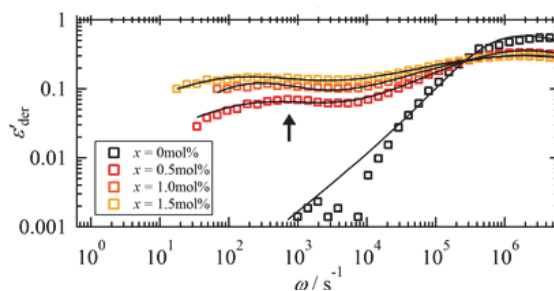


Figure 3. ω dependence of the derivative of dielectric permittivity for PEA- γ -CD with $x = 0 \sim 1.5 \text{ mol}\%$.

Reference) Kashiwagi, Y.; Urakawa, O.; Zhao, S.; Takashima, Y.; Harada, A.; Inoue, T. *Macromolecules* 2021, accepted.

Dielectric relaxation of type-A rouse chain under end-adsorption/desorption equilibrium: Effect of motional coupling

Youngdon Kwon Sungkyunkwan University

Properties of polymer nanocomposites reflect not only those of polymer matrix and nanoparticles but also the behavior of the interface therein.¹⁾ The structure and dynamics of interfacial layers between the bulk polymer phase and the particle surface have been studied with the aid of various experimental techniques, for example, small angle x-ray scattering²⁾ and broadband dielectric spectroscopy.³⁾ However, those studies mainly considered very strong adsorption of the segments, which is equivalent to an assumption of the chains attached to the particle surface through strong bonds. Obviously, this assumption should fail for the adsorption occurring through moderate bonding (for example, hydrogen bonding).⁴⁾ This work is devoted for this case of moderate adsorption, and a mathematical formulation of the unentangled dynamics (Rouse dynamics) for the end-adsorbing type-A chains (Figure 1) has demonstrated a significant effect of adsorption/desorption equilibrium on the end-to-end fluctuation of the chains (detected with a dielectric method).

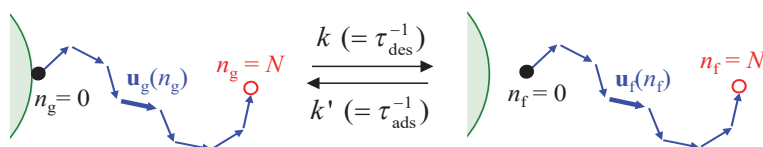


Fig. 1. Illustration of a type-A linear Rouse chain undergoing end-adsorption and desorption. The adsorption occurs on a fixed point in space. Nevertheless, a hypothetical, permeable surface is also illustrated for convenience of distinguishing the desorbed (free) and adsorbed (grafted) chains.

This formulation considered a conformational exchange between the adsorbed and desorbed chains that results in strong a motional coupling between those chains. Eigenmode analysis for those motionally coupled chains⁵⁾ enabled analytical characterization of the time evolution of the chain conformation and the corresponding changes of the end-to-end fluctuation time τ with the adsorption and desorption time constants, τ_{ads} and τ_{des} shown in Figure 1.

A typical result, obtained for a case of $\tau_{\text{ads}} = \tau_{\text{des}}$, is shown in Figure 2. On enhancement of adsorption/desorption (i.e., on a decrease of τ_{des}), the conformational exchange is accelerated so that the fluctuation time τ normalized by τ^0 in the absence of the adsorption decreases and increases, respectively, for the chains in the adsorbed and desorbed states. In an extreme of fast adsorption/desorption ($\tau_{\text{des}} \rightarrow 0$), τ/τ^0 of the chains in those states merge with each other and the two states become indistinguishable. These results demonstrate a new aspect in the dynamics of adsorbed/desorbed chains, a strong effect of their conformational exchange.

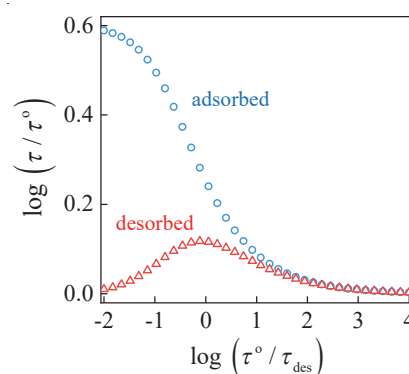


Fig. 2. Changes of fluctuation time of adsorbed and desorbed chains with τ_{des} .

Acknowledgement: This work has been published in *J. Soc. Rheol. Japan*, 48, 27 (2020).

references: 1) Cheng et al, *J. Chem. Phys.*, 146, 203201 (2017). 2) Jouault et al, *ACS Macro Lett.*, 5, 523 (2016). 3) Klonos PA, *J. Phys. Chem. C*, 122, 50 (2018). 4) Srivastava et al, *Curr. Opin. Chem. Eng.*, 16, 92 (2017). 5) Kwon et al, *Macromolecules*, 52, 8484 (2019).

Molecular mechanisms for the inactivation of a growth hormone in rice

Zuhua He Chinese Academy of Sciences

Objectives: Gibberellins (GAs) are a group of diterpenoid carboxylic acids. They act as plant hormones that play critical roles in promoting growth, including internode (stem) elongation of rice. The *elongated uppermost internode 2 (eui2)* mutant of rice shows a tall phenotype due to its elongated uppermost internode. Because of this reason, this mutant has been used in hybrid rice breeding in order to eliminate panicle enclosure in male sterile parents. We have previously identified the *EUI2* gene by map-based cloning, and found that *EUI2* is a functionally-uncharacterized protein that belongs to the α,β -fold hydrolase superfamily. In collaboration with Shinjiro Yamaguchi's group, we have previously characterized the rice *eui* mutant and found that *EUI* encodes a cytochrome P450 enzyme that deactivates GAs via epoxidation. Interestingly, the *eui eui2* double mutant plants are phenotypically indistinguishable from the *eui* single mutant, supporting the idea that *EUI* and *EUI2* act in the same pathway. Based on this notion, we speculated that *EUI2* might act as an epoxy hydrolase and further deactivate epoxidated GAs in the uppermost internode of rice. Our objective of this collaborative research is to prove this hypothesis. First, we need to examine whether *EUI2* protein can hydrolyze epoxy GAs. Second, we determine the levels of endogenous epoxy GAs in wild type and the *eui2* mutant. We would also need to examine the biological activities of epoxy GAs. Because of his expertise in plant hormone biochemistry, especially GAs, we collaborated with Prof. Shinjiro Yamaguchi at ICR in Kyoto University on this project.

Experimental methods: *EUI2* recombinant protein was prepared in bacteria. Epoxy GAs in rice plants were analyzed by LC-MS/MS after derivatization as ethyl esters. Biological activity of epoxy GAs was determined by a micro-drop method using GA-deficient rice seedlings. The physical interaction between the GA receptor *GID1* and epoxy GAs was analyzed by differential scanning fluorimetry (DSF).

Experimental results: We found that the recombinant *EUI* protein is able to hydrolyze epoxy GAs to produce diols *in vitro*. To analyze endogenous epoxy GAs in rice, we could not simply follow the normal method for GA purification because epoxy GAs are not stable under weak acidic conditions during the purification steps. We therefore derivatized epoxy GAs as ethyl esters and purified them as neutral compounds. This method was successful in finding that the *eui2* mutant accumulated epoxy GA₄ at higher levels than did wild type plants. Our biological activity test showed that epoxy GA₄ was weakly active. We chemically synthesized epoxy GA₄. DSF analysis indicated that epoxy GA₄ can physically interact with the GA receptor *GID1*, consistent with its weak biological activity. These results suggest that the accumulation of epoxy GA₄, which is weakly bioactive, is the cause of the tall phenotype of *eui2*.

Publications: In preparation.

Well-defined AIE-based polymer brush for the application of the electrochemical luminescence biosensors

Ying Ma South China University

Electrochemical luminescence (ECL) sensors have demonstrated broad applications in biomedical analysis with high sensitivity, and been applied in clinical diagnosis for a variety of biomarkers. However, the development of new ECL agents with high quantum yields and good stability is the key issue to improve the sensitivity of sensors. Fluorophores with aggregation-induced emission (AIE) property are good candidates to satisfy this requirement owing to their high ECL performance, while their fixation on electrode surface with controlled thickness and density is still a challenge.

In this project, we are working with Prof. Kohji Ohno (ICR partner researcher) to focus on the fixation of AIE dyes on a gold (Au) electrode surface based on the surface-initiated atom transfer radical polymerization (SI-ATRP), and achieved the good ECL signals in terms of high intensity and good stability. The experiment involves in four key sections: (1) synthesis of ATRP initiator with disulfide group to allow its fixation on Au electrode surface; (2) synthesis of tetraphenylethylene (TPE)-carrying monomer and its subsequent graft on electrode surface via SI-ATRP; (3) the ECL behavior of TPE-carrying polymer brush; (4) the ECL detection of alkaline phosphatase (ALP).

The results show that AIE-carrying monomer can be successfully grafted on Au surface via SI-ATRP, and its thickness can be well tuned by the polymerization conditions. The polymer brush has been characterized by the fluorescence and infrared spectra. More importantly, the resulting polymer brush exhibited good ECL behavior in the presence of triethylamine, and its ECL intensity is very dependent on the thickness of polymer brush, which reached a maximal intensity with the polymer molecular weight of 15 kDa. In addition, the ECL signal remained 95% of its intensity after 50 times of cyclic voltammetry scanning, revealing its good ability as an excellent ECL agent for sensors. Furthermore, we developed an ALP sensor based on a bipolar ECL sensing platform with the polymer brush-modified electrode as an ECL reporting electrode and a bare Au electrode as a sensing electrode. The ALP could catalyze its enzymatic substrate into phenol to generate an electrochemical current, which induces the tunable ECL signals. Therefore, the ALP concentration could be readout by ECL signals. Good linearity of the signal in the ranges of 0.1-20 mU/L for ALP was obtained and the limit of detection can reach as low as 0.02 mU/L, which could be well applied in the clinical profiling of ALP.

Role of phosphoinositide signaling in pollen development

Sheng Zhong Peking University

Objectives: Phosphatidylinositol 4,5-bisphosphate [PtdIns(4,5)P₂], one of phosphoinositides, serves as a site-specific signal on biological membranes. PtdIns(4,5)P₂ confines downstream events including actin cytoskeletal reorganization and membrane trafficking to specific subcellular loci *via* its effector proteins, leading to various cell-biological phenomena. In plants, PtdIns(4,5)P₂ has been studied intensively for its involvement in root hair and pollen tube growth as well as those in environmental responses. The model plant *Arabidopsis thaliana* has 11 PIP5Ks, which are classified into type A (PIP5K10 and 11) and type B (PIP5K1–9) based on the absence and presence of membrane occupation and recognition nexus (MORN) repeats at their N-termini, respectively. In this collaboration work, we investigated a role of the PtdIns(4,5)P₂ producing enzyme phosphatidylinositol 4-phosphate 5-kinase (PIP5K) in pollen development and pollen tube growth. We selected a series of PIP5K loss-of-function mutants. Starting with these, we identified a PIP5K gene set that is needed for pollen development or pollen tube growth.

Experimental Methods: Tagging mutant lines of PIP5K genes were obtained from public organizations of biological resources. Null alleles for each type-B PIP5K genes were selected among them. Multiple mutants were constructed by crossing, and examined for their male sterility.

Results and Discussion: Null mutants of type-B PIP5K genes except *PIP5K6* were selected among the lines obtained from Arabidopsis Biological Resource Center. For *PIP5K6*, its null mutant was found among those from RIKEN Biological Resource Center. The *pip5k6* mutant, the genetic background of which is the ecotype of Nossen, was crossed with the Columbia wild 10 times to have almost the same genetic background as that of the other PIP5K mutants. Starting with these mutant lines, multiple mutants were constructed. However, the *pip5k4pip5k5pip5k6* triple mutant could not be obtained by crossing among the *pip5k4pip5k5*, *pip5k4pip5k6*, and *pip5k5pip5k6* double mutants. Mutual crossing analysis between the wild type and *pip5k4pip5k5pip5k6/+* plants revealed that ovules, but not pollens, could carry the *pip5k4pip5k5pip5k6* mutation to progeny. This male sterility was rescued by either transgenes expressing PIP5K4-YFP, PIP5K5-YFP, or PIP5K6-YFP. These results indicate that *PIP5K4*, *PIP5K5*, and *PIP5K6* genes have redundant functions in pollen development and/or pollen tube growth. Detailed mutant analyses of cell biological processes during pollen development and pollen tube growth will be performed in our future study.

Role of PX-PH-type phospholipase Ds in plant intracellular membrane traffic

Yohei Ohashi MRC

Objectives: Phospholipase D (PLD) hydrolyzes glycerophospholipids including phosphatidylcholine (PC), a ubiquitous phospholipid in eukaryotic membranes, to produce phosphatidic acid (PA). Besides phospholipid metabolization, PLD is implicated in promoting various intracellular processes such as membrane traffic, signal transduction, and cytoskeletal reorganization through molecular functions of PA. PLD is requisite for plants in their development according to the genetic program and responses to environmental stimuli. However, particular processes promoted by PLD in plant cells largely remain elusive partly because subcellular loci where each PLD functions for its relevant intracellular process various remain unknown. In this collaboration research, we performed comparative analysis for intracellular localization patterns of PLD ζ 1 and PLD ζ 2, eukaryote-general PX-PH-type PLDs of *Arabidopsis thaliana*, in root tissues for a clue as to their functions in cell biological processes.

Experimental Methods: Transgenic *Arabidopsis* lines, which expressed fluorescence protein fusions of PLD ζ 1 and PLD ζ 2, and their N-terminal partial proteins, were constructed, and then crossed with lines expressing various fluorescence markers for intracellular localization. Root cells of those constructed transgenic lines were observed by confocal laser-scanning microscopy.

Results and Discussion: PLD ζ 1-mCherry co-localized with a *trans*-Golgi network or Early Endosome (TGN/EE) marker, while PLD ζ 2-GFP localized to the tonoplast and punctate structures including the pre-vacuolar compartments or multivesicular bodies (PVCs/MVBs). These localization patterns were reproduced by fluorescent protein fusions of their N-terminal partial proteins containing the PX-PH domains. Domain dissection analysis using an overexpression system revealed that the N-terminal moiety preceding the PX-PH domain of PLD ζ 2 was required for tonoplast-predominant localization, whereas either the PLD ζ 1 or PLD ζ 2 PX-PH domain alone could direct the tonoplast-partial localization, suggesting that PLD ζ 2, but not PLD ζ 1, is actively transferred to the tonoplast depending on its N-terminal moiety. We hypothesize that PLD ζ 1 and PLD ζ 2 target different but consecutive compartments along the membrane traffic pathway to the tonoplast *via* their N-terminal regions, and that they function in post-Golgi membrane trafficking in partially overlapping, but still distinctive manners.

Proteomic approach to discovering specific inhibitors for bile-acid interacting enzymes

Xiaoguang Lei Peking University

Bile acids (BAs) are important amphipathic molecules produced in the liver that improve lipids digestion by emulsification. Bile acid metabolism and signaling have been gaining significance due to the relationship between bile acids and diseases such as cancer, type 2 diabetes, cardiovascular, cholestatic and fatty liver disorders (Thomas et al., 2008). While endogenous receptors for bile acids, in particular the nuclear farnesoid X receptor (FXR) and the plasma membrane bound G protein-coupled receptor (TGR5) have been widely investigated (Thomas et al., 2008), the biological significance of other bile acid-binding proteins remains unexplored.

Our group in Peking University recently discovered more than 600 novel bile acid-interacting proteins (Zhuang et al., 2017). In this project, we collaborated with the Uesugi group in ICR for analyzing those bile acid-interacting proteins and for discovering small molecules that selectively block the interactions. The Uesugi group of ICR has recently developed a chemical library of bile acid analogues. Bile acid analogues have shown to activate or antagonize known bile-acid interacting proteins (Thomas et al. 2008).

In 2020, our collaboration identified an immune receptor X as an unprecedented bile-acid binding protein in immune cells. Intriguingly this highly important protein is not listed in the 600 bile acid-interacting proteins that we previously found in non-immune cells. Uesugi group in ICR experimentally tested its ability to interact with bile acids and found that bile acids physically associate with protein X. The photo-affinity probe of bile acids that was synthesized in our group in Peking University was exploited in ICR for the demonstration of the interaction. Biological significance of the interaction remains unclear at this moment, and experiments using immune cells are currently underway.

It has long been known that bile acids and their metabolites modulate immune responses; however their modes of action remain incompletely understood. Our findings suggest an exciting possibility that bile acids are hitherto unidentified endogenous modulators of protein X for controlling immune responses.

Transfer of redox sensitive elements across the sediment-water interface in a hypoxia area near the East China Sea

Pinghe Cai Xiamen University

Objectives: By working with **Prof. Yoshiki Sohrin at ICR**, this project aims to 1) quantifying benthic fluxes of dissolved trace metals and 2) examining how these fluxes change with varying redox potentials at the sediment-water interface in a seasonal hypoxia area near the Yangtze River Estuary (China).

Experimental methods: Sediment and porewater samples were collected along a transect in the East China Sea in summer 2020 (Figure 1). Exchangeable radium-224 (^{224}Ra) and surface-bound thorium-228 (^{228}Th) in sediments were measured using a RaDeCC system. Porewater profiles of dissolved iron (Fe) was analyzed using an ICP-MS. Phosphate concentrations in porewater were determined as per the classic colorimetric method. Oxygen concentrations in bottom seawater was obtained using the Winkler titration method.

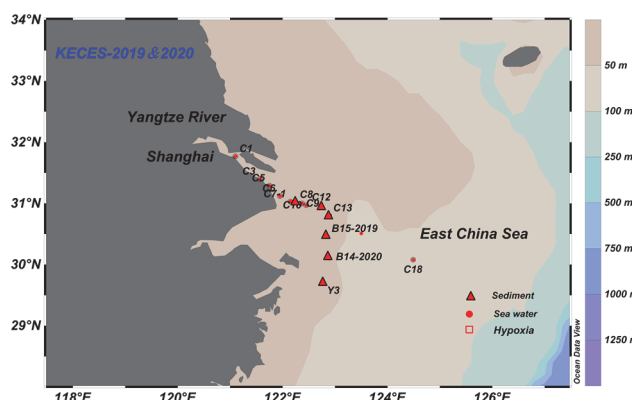


Figure 1. Sampling stations in the East China Sea

Experimental results: Benthic fluxes of dissolved Fe estimated from $^{224}\text{Ra}/^{228}\text{Th}$ disequilibrium in the sediment show an increase with decreasing dissolved oxygen concentration (Figure 2). At bottom seawater dissolved oxygen concentrations lower than $63\ \mu\text{M}$, benthic fluxes of dissolved iron increased to a maximum of $10.8\ \text{mmol m}^{-2}\ \text{d}^{-1}$. When oxygen concentrations were higher than $150\ \mu\text{M}$, benthic fluxes of dissolved iron declined to a level of $<1.0\ \text{mmol m}^{-2}\ \text{d}^{-1}$. In the meantime, benthic fluxes of phosphate display a pattern similar to dissolved Fe.

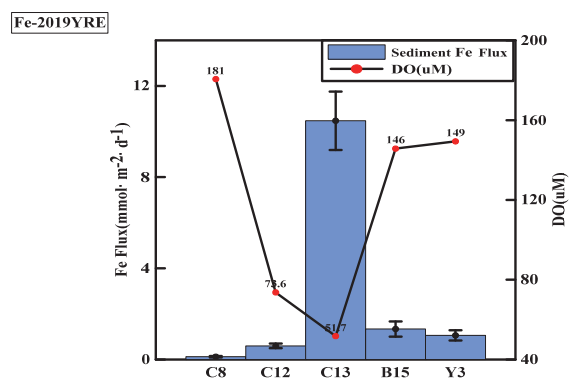


Figure 2 Plot of benthic Fe flux vs. oxygen level

Discussion: Benthic fluxes of dissolved Fe are extremely sensitive to oxygen levels in the bottom water. There is a tight coupling of dissolved Fe and phosphate, probably reflecting the dissolution of poorly crystalline iron oxides in bottom sediments that releases dissolved Fe and phosphate simultaneously into the overlying water column.

Outcome report : Not yet available.

Application of artificial viral capsid to intracellular delivery

Kazunori Matsuura Tottori University

There is increasing interest in the potential of functional proteins such as antibodies and peptides that regulate protein-protein interaction (PPI) as biopharmaceuticals. However, when these are applied intracellularly, it is essential to develop a highly efficient introduction system into cells. On the other hand, our research group reported a 24-residue artificial peptide (INHVGGTGGAIMAPVAVTRQLVGS) derived from the viral backbone forming β -annulus structure [1]. We found that the peptide self-assembled in water, yielding virus-like nanocapsules of 30-50 nm diameters. We also confirmed that the peptide assembly has a hollow structure by small-angle X-ray scattering, and the N-terminal (present inside the assembly) and the C-terminal (present on the surface of the assembly) of this peptide can be selectively modified with various molecules [2]. The purpose of this study is to create a novel intracellular delivery carrier by conjugating the β -annulus peptide with the intracellular delivery peptide HAad developed by ICR partner researcher [3] and to evaluate their applicability to intracellular delivery.

As our first step toward this goal, a HAad-modified artificial viral capsid was prepared that encapsulates the enhanced green fluorescence protein bearing a histidine tag (EGFP-His₆). NTA- β -annulus-C[HAad] which has a nickel-nitrilotriacetic acid (NTA) on the N-terminus of β -annulus peptide and the HAad peptide conjugated at the C-terminus was prepared. NTA- β -annulus-C[HAad] formed a nanoparticle having diameter of ~30 nm. Moreover, efficient encapsulation of EGFP-His₆ was achieved in the presence of Ni²⁺. Marked cytosolic distribution of EGFP-His₆ was also observed to 74% of cells when HeLa cells were treated with Ni-NTA- β -annulus-C[HAad] encapsulating EGFP-His₆ for 1 h. The above results suggested the promise of the use of β -annulus-based artificial viral capsids to intracellular protein delivery.

Our original plan included the invitation of Professor M. Ryadnov, the National Physical Laboratory, UK to Japan. Unfortunately, due to the prevails of COVID-19, that was not possible. However, we had a chance to have his lecture on web to discuss about the refinement of the structure of virus-like nanocapsules and the possibility of collaboration in future.

[1] K. Matsuura et al. *Angew. Chem. Int. Ed.* **2010**, *49*, 9662–9665; [2] K. Matsuura et al. *Org. Biomol. Chem.* **2016**, *14*, 7869–7874; [3] K. Sakamoto et al. *Angew. Chem. Int. Ed.* **2020**, *59*, 19990-19998.

Structural and functional analysis of curvature-inducing peptides and application

Anne S. Ulrich Karlsruhe Institute of Technology

Epsin-1 is a representative protein which induces the positive curvature necessary for the formation of clathrin-coated pits during endocytosis. Modulating the structural dynamics of biomembranes by inducing bilayer curvature and lipid packing defects has been highlighted as a practical tool to modify membrane-dependent cellular processes. Collaborative research of Ulrich research group at KIT with Futaki research group at ICR, Kyoto University has already shown that the N-terminus 18-residue peptide of epsin-1 (EpN18) possess curvature inducing abilities of the parent protein (*ACS Chem. Biol.* **2013**, 8, 1894). We also reported that EpN18 also promotes membrane remodeling including lipid packing defects in cell membranes (*Angew. Chem. Int. Ed.* **2017**, 56, 7644). However, a high concentration is required to exhibit a pronounced effect. In this study, we demonstrate a significant increase in the membrane-remodeling effect of EpN18 by constructing a branched EpN18 homotrimer. Both monomer and trimer could enhance cell internalization of octaarginine (R8), a cell-penetrating peptide. The EpN18 trimer, however, promoted the uptake of R8 at an 80-fold lower concentration than the monomer. Analysis of the generalized polarization of a polarity-sensitive dye (di-4-ANEPPDHQ) revealed a higher efficacy of trimeric EpN18 in loosening the lipid packing in the cell membrane. Circular dichroism measurements in the presence of lipid vesicles showed that the EpN18 trimer has a higher α -helix content compared with the monomer. The stronger ability of the EpN18 trimer to impede negative bilayer curvature is also corroborated by solid-state ^{31}P NMR spectroscopy. Hence, trimerizing peptides can be considered a promising approach for an exponential enhancement of their membrane-remodeling performance.

Site-selective protein acetylation by a small molecule

Lu Zhou Fudan University

Post-translational modifications (PTMs) play essential roles in regulating a myriad of cellular processes in mammalian cells, including signal transduction, metabolism, and gene transcription. Dysregulation of protein modifications causes metabolic diseases, neurodegenerative diseases and cancers. Among protein modifications, acetylation and phosphorylation represents the most critical PTM. In the present research with ICR, we continued to collaborate with the Uesugi research group to design small molecules that specifically acetylate or phosphorylate cellular proteins.

Our collaboration has already led to the discovery of a small-molecule acetylase mimic that specifically acetylates Lys-100 of PGAM1. The molecule, referred to as KHAc, has an acetyl ester group as an acetyl donor. Together with the Uesugi group, we have checked the selectivity of the molecule and found that KHAc is selective to PGAM1 at the proteome level. We have summarized the data which were published in ACS Chemical Biology.

To discover more small-molecule acetylases selective for a number of different proteins, we screened a chemical library of 280 acetyl ester compounds. Each of these molecules was incubated with cell lysates or even live cells, and acetylated proteins were analysed by western blots with a pan-antibody against acetylated lysine. Unfortunately, any of the screening hits failed to exhibited clear acetyl transfer reactions in multiple assays. We therefore decided to design acetylation compounds for protein X, which has recently been shown as an important immune regulatory protein that is controlled by acetylation. We have synthesized a number of compounds and subsequently discovered a compound that is capable of transferring an acetyl group to protein X in a selective way.

In the phosphorylation project, collaboration with Uesugi group allowed us to identify a nitro-benzyl phosphate group as a donor of UV-induced phosphate transfer reactions in aqueous solutions. We conjugated a nitro-benzyl phosphate group to drug A, a known inhibitor of Y kinase. Such hybrid molecules may transfer a phosphate group upon UV irradiation. In other words, this approach converts inhibitors to UV-dependent kinase activators. We are looking forward to continued collaborations with ICR.

Modulation of ferrimagnetic spin waves by electric field

Kab-Jin Kim KAIST

Objective:

The aim of the research is to study the spin wave of ferrimagnetic alloys.

Experimental methods:

For this study, we prepared ferrimagnetic films at prof. Teruo Ono's group in ICR and measured the electrical properties at KAIST. The longitudinal resistance as well as the transverse resistance was measured by sweeping the magnetic field at various temperatures. To characterize the spin wave, we also used Brillouin light scattering measurement technique.

Experimental results:

We investigate the spin wave handedness and magnetoresistance of ferrimagnetic GdFeCo across the magnetization compensation temperature, T_M as well as the angular momentum compensation temperature, T_A . The spin wave handedness was found to reverse at T_M and T_A . The magnetic field dependence of longitudinal resistivity (ρ_{xx}) shows opposite trends below and above T_M , and the variation of ρ_{xx} with B becomes more significant as the temperature decreases. The transverse resistivity (ρ_{xy}) of GdFeCo shows negligible field dependence.

Discussion:

The observed distinct spin wave handedness is attributed to the gyromagnetic reversal of ferrimagnetic alloy. As for the unconventional magnetoresistance, we ascribe it to the sperimagnetism of GdFeCo. We also reveal that, contrary to the recent reports that the transition metal dominates transport of rare-earth transition-metal ferrimagnets, the Gd contribution to magnetoresistance is comparable to the FeCo contribution, showing that the transport of GdFeCo is antiferromagnetic. Our results therefore show that ferrimagnets are a convenient platform for studying antiferromagnetic spin wave as well as antiferromagnetic spin transport.

Publication:

J. Park et al., Phys. Rev. B 103, 014421 (2021).

Novel strategy for intracellular delivery of nanomedicines

Sílvia PUJALS Institute for Bioengineering of Catalonia

Nanomedicine arose 20 years ago with the promise of selectively delivering drugs to target sites, thus increasing their effectivity while minimizing undesired side effects. However, despite the great promise behind nanomedicine for drug delivery, very few products have been approved for patient use. This poor translation into clinic comes from different factors, some of them being a poor characterization of the nanomaterials or a simplistic model to evaluate them. Poor cellular uptake efficacy of these nanomedicines is also a big obstacle. Our research group has a speciality in preparation of nanoparticles being applied for nanomedicine. We also have strong background of nanomaterials characterization and intracellular behavior using various microscopic techniques (including electron microscopy and super resolution microscopy). On the other hand, Professor Futaki at ICR, Kyoto University is an expert on intracellular delivery of nanomedicines.

The successful cytosolic delivery of nanoparticles is hampered by their endosomal entrapment and degradation. To push forward the smart development of nanoparticles we must reliably detect and quantify their endosomal escape process. However, the current methods employed are not quantitative enough at the nanoscale to achieve this. Nanoscopy is a rapidly evolving field that has developed a diverse set of powerful techniques in the last two decades, opening the door to explore nanomedicine with an unprecedented resolution and specificity. The understanding of key steps in the drug delivery process – such as endosomal escape – would benefit greatly from the implementation of the most recent advances in microscopy. Therefore, we have made discussions on the possible design of ideal nanoparticles based on our understanding on the current status of the use of nanoscopy for endosomal escape quantification.¹⁾ Alternatively, Futaki and coworkers developed delivery peptides potentially applicable to cytosolic delivery of nanoparticles.^{2,3)} Studies are underway by merging the above insights.

References

- 1) T. Andrian, R. Riera, S. Pujals, L. Albertazzi, *Nanoscale Adv.*, **2021**, 3, 10-23
- 2) K. Sakamoto, M. Akishiba, T. Iwata, K. Murata, S. Mizuno, K. Kawano, M. Imanishi, F. Sugiyama, S. Futaki, *Angew. Chem. Int. Ed.* **2020**, 59, 19990-19998.
- 3) J. V. V. Arafiles, H. Hirose, Y. Hirai, M. Kuriyama, M. M. Sakyamah, W. Nomura, K. Sonomura, M. Imanishi, A. Otaka, H. Tamamura, S. Futaki, *Angew. Chem. Int. Ed.* in press.

Revealing exciton quenching mechanisms in thermally activated delayed fluorescent devices

Lian Duan Tsinghua University

Organic light-emitting diodes (OLEDs) have become popular in the commercial products such as smart phones, flat-panel displays and solid-state lightings. For further practical applications, one of the challenges is to realize both high efficiency and excellent device lifetime for blue OLEDs, especially at high brightness. Recently, thermally activated delayed fluorescence (TADF) emitters have been reported, showing high device efficiency comparable to phosphorescent OLEDs. This is because TADF emitters have small single-triplet energy gap (ΔE_{ST}), and therefore can convert non-emissive triplet excitons to emissive singlet excitons via reverse intersystem crossing (RISC) process. However, the lifetimes and efficiency at high brightness of the blue OLEDs are still far from satisfaction from the point-view of practical applications and guidelines for efficient and stable blue TADF OLEDs are still rare.

To overcome the above problems, we have developed efficient and stable blue OLEDs using a TADF compound to sensitize a fluorescent dopant, known as TADF-sensitized fluorescence emission (TSF). In this process, the triplet excitons generated on the TADF sensitizer can be up-converted into the singlet ones through RISC process, from where the energy will be transferred to the conventional fluorescent emitters through the long-range Förster energy transfer. Our group have successfully achieved TSF-OLEDs with the external quantum efficiency (EQE) over 20% even at high brightness by combining the sterically hindered fluorescent emitters to avoid the unfavorable energy transfer from triplets of the host and TADF materials to that of the fluorescent emitters by short-range Dexter energy transfer (D. D. Zhang et al., *Adv. Mater.* 2018, 30, 1705250).

It is well known that the major degradation mechanisms in OLEDs are triplet-triplet and triplet-polaron annihilation. These processes originates from Dexter energy transfer from the triplet to triplet and the triplet to the polaron. Thus, the use of TADF emitters with very fast RISC rate constant as sensitizer is expected to suppress these processes and thus simultaneously improve the efficiency roll-off and lifetime of OLEDs. On the basis of the above concepts, we have conducted the collaboration work with Kaji group to develop highly efficient blue stable OLEDs.

In this year, due to COVID-19 related difficulties, our group and Kaji group have independently advanced researches: our group have developed efficient and stable deep blue TSF OLEDs by using wide-energy-gap TADF materials as sensitizer (D. D. Zhang *et al.*, *Adv. Mater.* **2020**, 32, 1908355) and Kaji group have reported a new TADF emitters exhibiting ultrafast RISC rate constant around 10^7 s^{-1} (Y. Kusakabe, *et al.*, *Front. Chem.*, **2020**, 8, [530-1]-[530-9]). We now plan to further improve the efficiency and stability of our blue TSF OLEDs by adopting the ultra-fast RISC TADF materials developed by Kaji group. We anticipate that a breakthrough in blue OLEDs can be achieved by our continuing collaborative work, which is highly desired for both academical and industrial fields.

Fabrication of nanotopographical polymer surfaces for bactericidal properties-II

Maya Endoh Stony Brook University

Introduction. Surface topology is of great interest to develop bactericidal surfaces in place of traditional chemical-based approaches that are often toxic to human beings and environments. A key aspect of bactericidal properties of nanopatterned surfaces is the larger the stretching degree on nanopatterned surfaces, the better the bactericidal efficiency. The so-called stretching theory [1] predicted that the stretching degree of *Escherichia coli* (*E. coli*) and *Pseudomonas aeruginosa* (*P. aeruginosa*) strongly depends on the geometric parameters of nanopatterned surfaces (i.e., pillar size, pillar height, and interpillar spacing). In this research, we aim to develop a new paradigm of designing a nanopatterned polymer surface to control a bacteria-polymer surface interaction.

Experimental Method and Result. We demonstrate that the PS nanopillars with a height of 25 nm, a diameter of about 40 nm, an interpillar spacing of about 60 nm templated using self-assembly of a cylinder-forming polystyrene-*block*-poly(methyl methacrylate) (PS-*block*-PMMA purchased from Polymer Source Inc, $M_{w,PS}=45,900$ g/mol, $M_{w,PMMA}=138,000$ g/mol, polydispersity (M_w/M_n)=1.16) on solid substrates showed a bactericidal property against *E. coli* [2]. The viability of *E. coli* on the samples was assessed using the BacLight Live/Dead staining kit (Molecular Probes, Life Technologies, Carlsbad, CA), and examined with an EVOS Microscope (ThermoFisher Scientific) using a standard green filter set to image live cells and a standard red filter to image dead cells. The results demonstrated that the PS nanopillars suppressed the amount of *E. coli* adsorbed on the patterned surfaces by about 70% compared to that on a 25 nm-thick PS thin film (i.e., a “flat” (control) surface) after 24 h of immersion in a bacteria suspension. Notably, the percentage of dead cells on the patterned surface was nearly 100 % (Fig. 1a), while more than 70 % of *E. coli* adsorbed on the flat surface were still alive under the same conditions (Fig. 1b). Fig. 1c shows a representative SEM image of *E. coli* on the PS nanopillars. It is clear that the bacterium appears to be deflated on the PS nanopillars, as the theory predicted, while the bacteria kept the original rod-shape on the PS flat surface (data not shown).

References

- [1] F. Xue, J. Liu, L. Guo, L. Zhang, and Q. Li, *J. Theor. Biol.*, **385**, 1-7 (2015).
- [2] Y. Morimitsu, D. Salatto, N. Jiang, M. Sen, S. Nishitsuji, B. M. Yavitt, M. K. Endoh, A. Subramanian, C.-Y. Nam, R. Li, M. Fukuto, Y. Zhang, L. Wiegart, A. Fluerasu, K. Tanaka, and T. Koga, *Macromolecules*, **52**, 5157-5167 (2019).

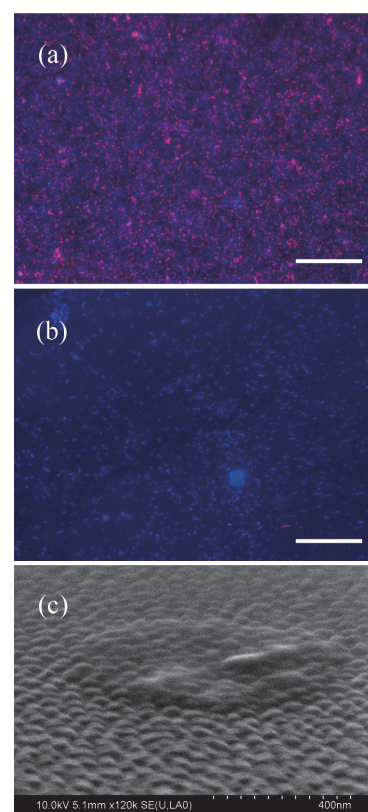


Fig. 1. Fluorescent microscopy image of (a) the PS nanopillars and (b) the PS flat surface after 12 h of immersion in an *E. coli* suspension. Red color indicates dead bacteria. The scale bars represent 100 μm . (c) SEM micrograph of *E. coli* (located near the center) on the nanopillars. The bacteria deflate on the nanopillars.

Synthesis of polyether nanocomposite solid polymer electrolytes for lithium ion batteries

Robert C. Ferrier, Jr. Michigan State University

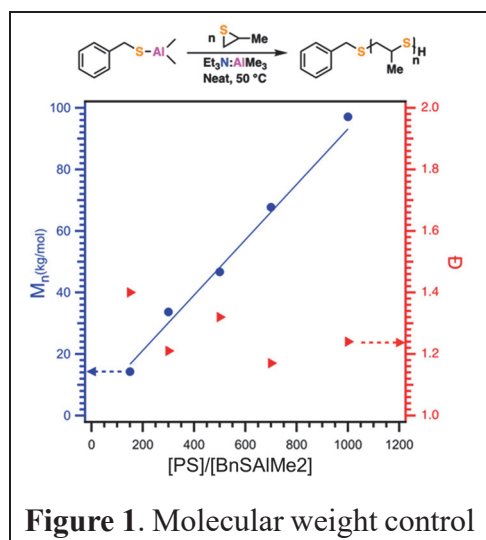


Figure 1. Molecular weight control

Objective. The objective of this work was to develop novel polyether-based nanocomposite materials for lithium ion batteries (LIBs) by combining the epoxide polymerization techniques of the PI and the surface initiated polymerization techniques developed by the ICR partner researcher, Prof.

Ohno from Kyoto University. **Experimental Methods.** Aluminum-based initiators were characterized by ^1H NMR spectroscopy. Polymers were characterized by size-exclusion chromatography (SEC), ^1H and ^{13}C NMR spectroscopy, differential scanning calorimetry (DSC), broadband dielectric spectroscopy (BDS), rheometry, and small angle X-ray

scattering (SAXS). **Experimental Results.** Homopolymers of poly(butylene oxide) (PBO), poly(propylene oxide) (PPO), and polyepichlorohydrin (PECH) were characterized by BDS and found to have room temperature conductivity of 10^{-7} S/cm at 50:1 lithium to oxygen ratio. To improve conductivity, copolymers of the above polymers as well as polymers containing high dielectric constant units have been synthesized. The thiol based initiator developed in last year's grant (2019-74) was used to polymerize propylene sulfide (PS), which can be converted to poly(propylene sulfone). **Figure 1** shows the molecular weight control of PPS to 100 kg/mol with narrow polydispersity (\bar{D}). Copolymers of PS and epoxides PO and ECH were also synthesized. Block and statistical architectures were produced and copolymer structure was confirmed via diffusion ordered spectroscopy (DOSY). Finally, architecture was tuned through the development and utilization of a bi-functional and four-armed initiator. **Figure 2** shows the architecture control. In the future, we will perform surface initiated polymerizations of these polymers from silica nanoparticles and investigate conductivity properties. **Publications.** An article entitled "Aluminum-based Initiators from Thiols for Epoxide Polymerizations" co-authored by the PI and his ICR partner researcher Prof. Ohno was accepted to *Macromolecules* (doi.org/10.1021/acs.macromol.0c00464). Another publication based on the work above is in preparation to be submitted in March. My student, Ms. Niloofar Safaie, will present this work at the April meeting of ACS, held virtually, with a talk entitled: "Aluminum-based initiators from thiols for epoxide polymerizations."

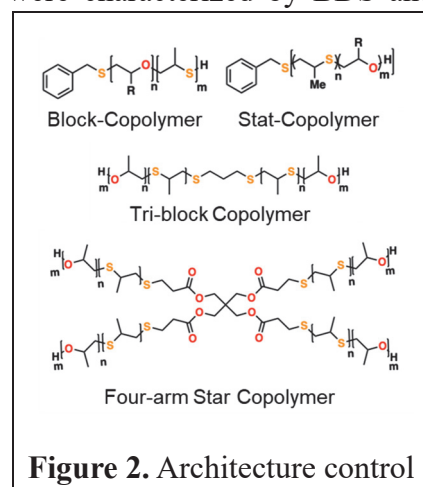


Figure 2. Architecture control

Structural and functional analysis of the surface glycolipids of outer membrane vesicles released by bacteria

Maria Michela Corsaro University of Naples Federico II

Objectives:

Outer membrane vesicles (OMVs) secreted by bacteria to the extracellular space play important roles in intercellular communication, pathogenicity, defense, and so on. The group of the ICR partner researcher (Prof. Tatsuo Kurihara) recently isolated a new bacterial strain named *Shewanella vesiculosa* HM13, which produces OMVs carrying a single major cargo protein named P49. Disruption of *wzx*, which is located in the vicinity of the P49 gene on the genome and codes for a putative flippase involved in oligosaccharide translocation, caused mislocalization of P49, suggesting that P49 interacts with the surface glycolipids of OMVs. The objective of this work has been the isolation and the structural characterization of lipooligosaccharides obtained from the constructed *wzx*-mutant.

Experimental:

Dried cells and OMVs from the *wzx*-mutant (5.1 g and 81 mg, respectively) of *S. vesiculosa* HM13 grown at 18 °C were extracted with phenol/chloroform/light petroleum (PCP) method to recover LOS with a yield 1.9% w/w from dried cells and 19% w/w from dried vesicles. Polyacrylamide gel electrophoresis (PAGE) was performed with sodium deoxycholate (DOC) as detergent, as reported (Casillo, 2019). All the chemical analyses and NMR spectra were obtained as already reported (Casillo, 2019).

Results:

After PCP extraction of cells (*wzx_c*) and OMVs (*wzx_OMV*) from the *wzx*-mutant, both crude extracts were analyzed by DOC-PAGE, and the results compared with those of cells (*wt_c*) and OMVs (*wt_OMV*) from *S. vesiculosa* HM13 wild-type (Di Guida, 2020). No differences related to electrophoretic pattern appeared among the four samples. The samples were then treated with hydrazine and, after that, with 4M KOH, obtaining the corresponding phosphorylated oligosaccharides (OS). The ¹H NMR spectral analysis and a comparison with those obtained from wild-type samples revealed slight differences in the anomeric and carbinolic regions between the samples from the *wzx* mutant and the wild-type ones.

Casillo, A. et al. Marine Drugs (2019), 17, 34.

Di Guida et al. Marine Drugs (2020), 18, 231.

Construction of heterologous protein secretion system at low temperatures by using cold-adapted microorganisms

Xianzhu Dai Southwest University

[Objectives] Gram-negative and Gram-positive bacteria secrete membrane-enclosed nanoparticles called extracellular membrane vesicles (EMVs). EMVs are involved in bacterial survivability, such as intercellular communication, biofilm formation, infection, and defense against bacteriophages. EMVs also have attracted the attention of biotechnological industries for their potential use as a platform for drug delivery system, vaccine development, and secretory protein production. In this study, we used a hyper-vesiculating and cold-adapted bacterium, *Shewanella vesiculosa* HM13. This bacterium isolated by the group of the ICR partner researcher (Prof. Tatsuo Kurihara) secretes an S-layer-like protein, P49, as a single major cargo of the EMVs. This highly selective cargo transportation mechanism is expected to be useful for vesiculation-mediated heterologous protein production and the development of surface engineered vesicles. Here, to examine whether the P49-selective cargo transportation to EMVs is available for secretory production of heterologous proteins, green fluorescence protein (GFP) fused to P49 was expressed in *S. vesiculosa* HM13.

[Experimental methods] A gene coding for GFP was fused to the 3'-terminus of the P49 gene by homologous recombination using a suicide plasmid, pKNOCK-Km. The recombinant strain was cultured at 18 °C, and distribution of the fusion protein in the insoluble fraction of the cells, the soluble fraction of the cells, the culture supernatant after removal of EMVs (PVF), and EMVs was analyzed by western blotting with an anti-GFP antibody. As a control, the recombinant strain producing GFP without being fused to P49 was constructed.

[Experimental results and discussion] GFP without being fused to P49 was detected only from the cellular soluble fraction, whereas GFP fused to P49 was transported to EMVs, indicating that P49 can function as a carrier to deliver the fusion partner to EMVs. On the other hand, P49-free GFP was also detected from the EMVs of the recombinant strain expressing GFP fused to P49, suggesting the occurrence of an unexpected proteolytic cleavage between P49 and GFP. Regulation of this putative proteolytic cleavage is supposed to enable production of P49-free foreign protein by facilitating the cleavage. In contrast, it may be possible to obtain the fusion protein with higher purity by suppressing the cleavage. These findings facilitate the application of the EMV production and the vesiculation-mediated protein secretion of *S. vesiculosa* HM13.

Molecular mechanisms governing gene expression regulation in plant plasticity

Vicente RUBIO National Center of Biotechnology

Objectives: We focus to understand molecular mechanisms bridging proteolysis to pre-mRNA processing in environmental adaptation. Plant plasticity is obtained by orchestrating numerous spatiotemporal gene expressions. CULLIN4 RING ligase complexes (CRL4) mediated proteolysis has been associated to gene expression regulation. We at CNB-CSIC have revealed that one of its subunit, DDB1, associate with DDB1, CUL4-Associated Factors (DCAFs) and others, which directly bind specific targets to promote their ubiquitination and degradation. Dr. Tsuge's group at ICR works on another CRL-interacting complex, COP9 signalosome (CSN) that binds mRNA processing factors. Here, we aim to reveal that, by maintaining accurate levels of regulatory proteins through targeted degradation and transcription control, CRL4, DCAFs, and CSN survey nuclear processes essential for gene expression regulation.

Experimental methods: Arabidopsis was chosen as a model to investigate CRLs, DCAFs, CSN and their binding factors. CFI (cleavage factor I) is a complex that binds CSN in mammals and plants, and is involved in processing 3' UTR ends of pre-mRNAs. As a start, Tandem affinity purification method and protein detection system, at CNB-CSIC was utilized to analyze CFI-interacting proteins under different conditions.

Experimental results: CNB-CSIC revealed that Arabidopsis CFI 25a subunit interacts with CFI 25a, CFI 59, and CFI 68, suggesting, for the first time, that an intact CFI complex could be formed in plants. Furthermore, we identified FIP1, which is involved in pre-mRNA 3' end processing, and CSN subunit, which is involved in signal transduction, as CFI 25 interacting partners. Based on these novel findings, the ICR group established knock out plants for CFI 25, CFI59, CFI 68, etc. to further analyze *in planta* gene expression regulation. This revealed that CFI regulates gene expression through regulating not only the lengths of 3' UTR but also the diversity of the 3' ends in the isoforms of transcripts processed from the pre-mRNA. Further, analyses are being conducted to comprehend the molecular mechanisms of this regulation.

Discussion: These results were unique and were due to the fact that this collaboration was utilizing the plant system as a model to comprehend the universal regulatory system. We favor our hypothesis that diverse yet temporal-regulated transcript usages are key to respond to specific environmental stimuli. Further collaboration will provide understanding for the general platform for gene expression regulation *via* proteolysis and transcriptional regulation.

Publications: *in preparation*, "CFI 25 subunit of Cleavage Factor I is essential for polyadenylation site determination and its diversity in *Arabidopsis thaliana* (L.) Heynh." X. Zhang, M. Garcia-León, V. Rubio, T. Tsuge *et al.*

Formation of supramolecular complexes through a host-guest interaction between cycloparaphenylene and azacorannulenes

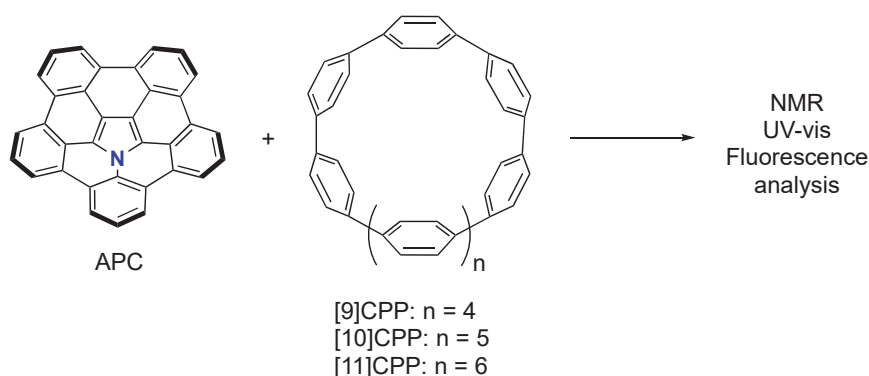
Shingo Ito Nanyang Technological University

Objective

Supramolecular chemistry of polycyclic aromatic compounds has attracted much attention because of the interesting structures and potential applications in material sciences. My research group at NTU previously reported the synthesis of azapentabenzocorannulene (APC) as the first example of nitrogen-containing buckybowls. In this collaboration, we aim at studying supramolecular chemistry between APC and cycloparaphenylenes (CPP), which have been developed and investigated by Prof. Yamago at ICR.

Results and Discussion

First, we have established an efficient method for large-scale synthesis of hydrogen-substituted APC (**Scheme 1**), because it is hardly soluble in common organic solvents. We could obtain a sufficient amount of APC by optimizing recrystallization and HPLC separation. Next, the size and ring number of CPPs suitable for hosting APC as a guest molecule were investigated by molecular modeling and theoretical calculations, which suggested that [10] and [11] are the most suitable fit the core of APC. Therefore, hydrogen-substituted APC was mixed with [9], [10], and [11]CPP and analyzed by NMR, UV-vis absorption, and fluorescence spectroscopy (**Scheme 1**). The NMR spectra showed that there is no change in the chemical shifts of the signals, which indicated that no intermolecular interaction occurred. Further investigation is currently ongoing.



Scheme 1

Reference

- 1) T. Nagano, K. Nakamura, Y. Tokimaru, S. Ito, D. Miyajima, T. Aida, K. Nozaki, *Chem. Eur. J.* **2018**, *24*, 14075–14078.

Research of multi-qubit diamond quantum processors

Marcus W. Doherty Australian National University

Quantum communication and quantum computation are expected to establish a new paradigm and advance our understanding of quantum mechanics. It is considered that they will provide cryptography that can not be decoded and super parallel computation that is much faster than that of ordinary computers. Besides these, technical issues intriguing questions concerning quantum mechanical phenomena can be addressed. NV centers in diamond are significantly interested as a candidate of a resource for demonstration and the realization of them [1]. It is because that single spins can be coherently controlled [2] and electrically driven single photon source are realized at room temperature (RT) in the NV center. In other solid materials such as quantum dot or superconducting devices, those are realized only in extremely low temperature.

In this project, we would like to develop further this system with multi-nuclear spin qubits. We discuss new architectures for enhancement of speed and fidelity of quantum processor by using multi-qubits NV centers in diamond. We discuss the usage and production of isotopically engineered diamonds for the enhancements of speed and fidelity of quantum processor. It is considered that quantum communication and quantum computation will e.g. provide secure data encryption and super parallel computation that in certain cases outperforms classical computers. The realization of them has strong impact not only to science but also to industry and society.

Recently, we proposed a full model of multi-qubit diamond quantum processors and develop a semi-analytical method for designing gate pulses [3]. This method optimises gate speed and fidelity in the presence of random control errors and is readily compatible with feedback optimisation routines. We theoretically demonstrate infidelities approaching $\sim 10^{-5}$ for single-qubit gates and established evidence that this can also be achieved for a two-qubit CZ gate. Consequently, our method reduces the effects of control errors below the errors introduced by hyperfine field misalignment and the unavoidable decoherence that is intrinsic to the processors. Having developed this optimal control, we simulated the performance of a diamond quantum processor by computing quantum Fourier transforms. We find that the simulated diamond quantum processor is able to achieve fast operations with low error probability. We discuss the experimental demonstration of this method in this project.

References

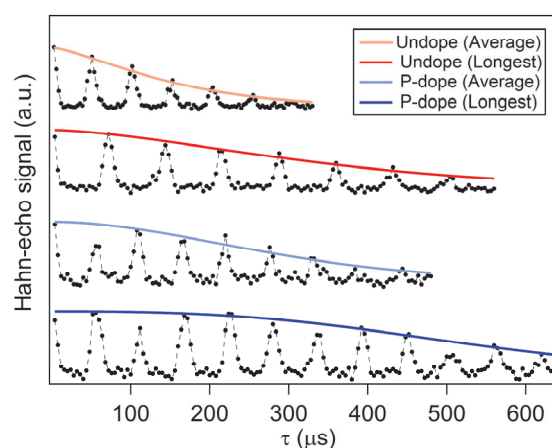
- [1] M. W. Doherty, N. B. Manson, P. Delaney, F. Jelezko, J. Wrachtrup, L. C. L. Hollenberg, *Physics Reports* 528 (1), 1-45 (2013).
- [2] P. Neumann, N. Mizuochi, F. Rempp, P. Hemmer, H. Watanabe, S. Yamasaki, V. Jacques, T. Gaebel, F. Jelezko, J. Wrachtrup. *Science*, 320, 1326 (2008).
- [3] Y. Chen, S. Stearn, S. Vella, A. Horsley, M. W. Doherty, *New J. Phys.* 22, 093068 (2020).

Research toward stable NV centers at shallow region in diamond

Gopalakrishnan Balasubramanian Leibniz institute for surface engineering

A negatively charged NV center in diamond is a versatile atomic-sized spin system for remarkable applications in quantum sensing and quantum-information science. The reason is that it has excellent properties such as long coherence times [1,2] and high sensitivities with nanometer-scale resolution. By utilizing nanoscale shallow NV centers, applications for nanoscale imaging [3] and nanoscale nuclear magnetic resonance were demonstrated. Furthermore, NV centers were successfully integrated into photonic and mechanical structures, and in electronic devices, which expands their versatility.

Toward these issues, Kyoto University group demonstrates the extension of the spin-coherence time (T_2), the stabilization of the charge state, and an improvement of the creation yield of NV centers formed by the ion-implantation technique at a depth of ~ 15 nm in phosphorus-doped n-type diamond [4]. The longest T_2 of about 580 μs of a shallow NV center approaches the one in bulk diamond limited by the nuclear spins of natural abundant ^{13}C as shown in figure. The averaged T_2 in n-type diamond is over 1.7 times longer than that in pure non-doped diamond. Moreover, the stabilization of the charge state and the more than twofold improvement of the creation yield are confirmed. The enhancements for the shallow NV centers in an n-type diamond-semiconductor are significant for future integrated quantum devices.



Figure, Hahn-echo decays of NV centers in undoped and Phosphorus (P) doped diamond samples. Echo decays of the longest and an average length T_2 in each sample are shown. The revivals in echo decays are due to ^{13}C nuclear spin precession, which rate matches the Larmor precession frequency for the ^{13}C nuclear spin.

References

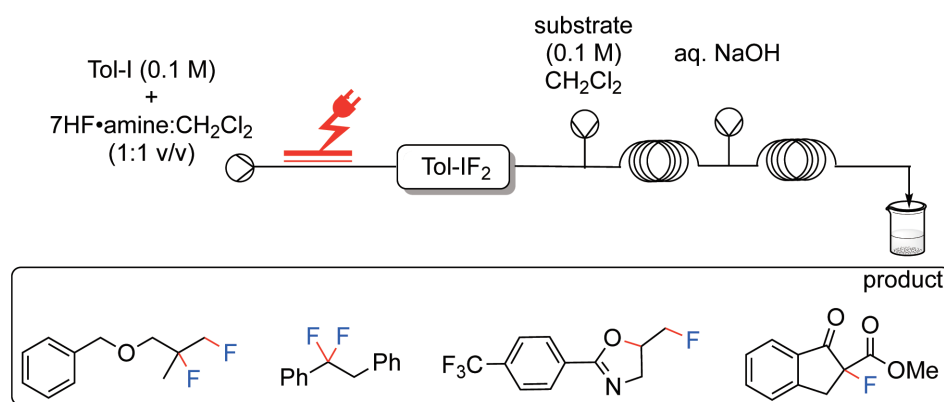
- [1] G. Balasubramanian, P. Neumann, D. Twitchen, M. Markham, R. Kolesov, N. Mizuochi, J. Isoya, J. Achard, J. Beck, J. Tissler, V. Jacques, P. R. Hemmer, F. Jelezko, J. Wrachtrup, *Nature Materials* **8**, 383–387 (2009).
- [2] E. D. Herbschleb, H. Kato, Y. Maruyama, T. Danjo, T. Makino, S. Yamasaki, I. Ohki, K. Hayashi, H. Morishita, M. Fujiwara, N. Mizuochi, *Nature Communications*, **10**, 3766 (2019).
- [3] Balasubramanian, G., et al. *Nature* **455**, 648–651 (2008).
- [4] A. Watanabe, T. Nishikawa, H. Kato, M. Fujie, M. Fujiwara, T. Makino, S. Yamasaki, E. D. Herbschleb, N. Mizuochi, *Carbon*, **178**, 294–300 (2021).

Advanced iodine – mediated stereoselective flow electrochemistry

Thomas Wirth Cardiff University

Objectives: We want to explore the electrochemical generation of iodine(III) reagents in flow. The key requirement for a successful reaction generating and using hypervalent iodine compounds *in only catalytic amounts* is the ability of electrochemical process to make selectively the hypervalent iodine compound in the presence of the substrate. We propose to use a biphasic reaction system which should be able to provide an elegant solution since the iodine(III) reagent can be formed in one phase while the oxidation of the substrate occurs in the other. For this approach we will develop iodine reagents with dual function as they will serve as the precursor for iodine(III) but also as electrolyte.

Results and discussion: Due to the COVID-19 pandemic, Cardiff University was completely closed for 4 months and then gradually re-opened. For the last 6 months (August 2020 – January 2021) our lab could only be occupied with 40%. Therefore, research is very slow, and we were not in a position to tackle the challenging objectives set out in the proposal. We did some preliminary work on fluorination reactions outside this proposal as shown in Scheme 1. This work is still under investigation and not yet published.



Scheme 1. Electrochemical fluorinations of different substrates in a flow electro-microreactor.

We hope that our laboratory work can fully resume in summer 2021.

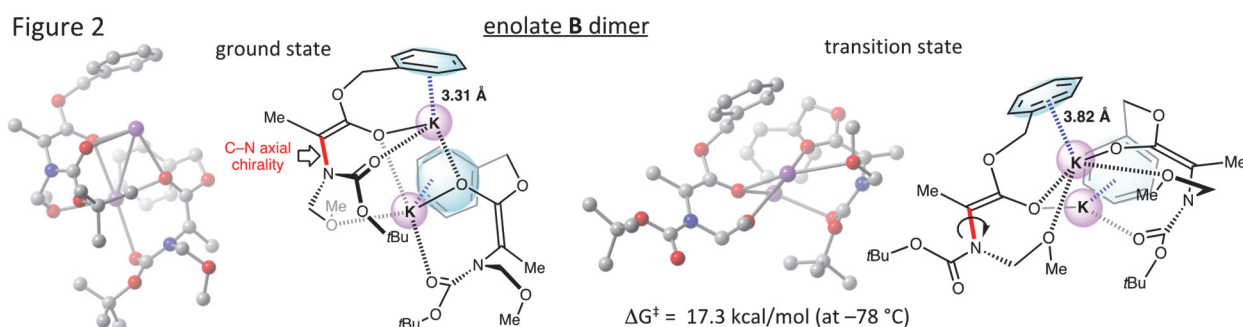
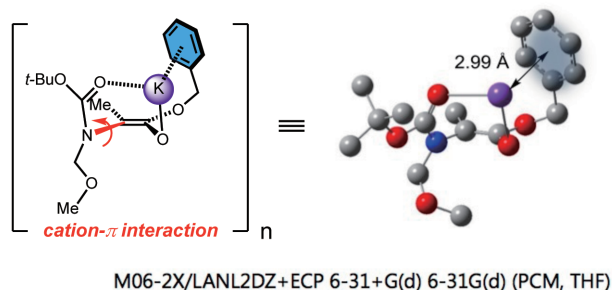
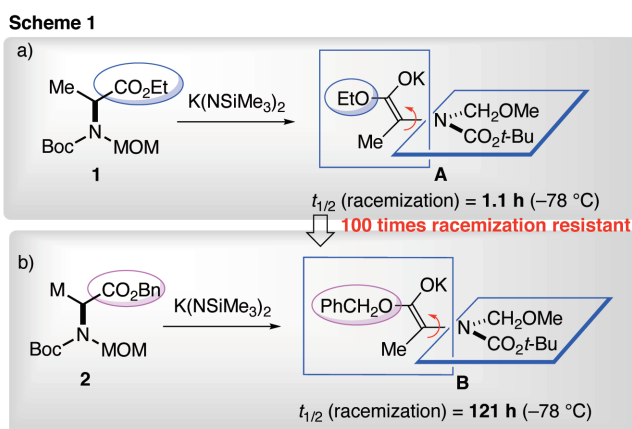
Cation- π interaction in enolate chemistry

Jonathan Clayden University of Bristol

Objectives: Our group and Kawabata's groups have developed unique methods for asymmetric synthesis of unnatural amino acids with tetrasubstituted carbon based on enolate chemistry.^{1,2)} The strategy developed by Kawabata is characteristic in the enolate intermediate with dynamic sp^2 chirality (Scheme 1). Recent interesting finding is that enolate **B** derived from benzyl ester **2** has a ~110 times longer half-life of racemization compared with **A** derived from the corresponding ethyl ester **1**. The origin of elongation of the racemization half-life of the chiral enolate intermediate **B** was assumed to be resulting from the enolate structure, in which axial chirality along the chiral C-N axis is stabilized by cation- π interaction (Figure 1). Our Purpose of this joint research is to clarify the origin of resistance of enolate **B** toward racemization.

1) Clayden, *et. al.*, *Nature*, **2018**, 562, 105. (2) Kawabata, *et al.*, *JACS*, **2013**, 136, 13294.

Results and discussions: Density functional theory (DFT) calculations were performed for the racemization processes of enolates **A** and **B**. The activation energy for the C-N bond (shown in red in Figure 2) rotation of the dimer of enolate **A** was estimated to be 14.9 kcal/mol at -78°C , whereas that of the dimer of enolate **B** was calculated to be 17.3 kcal/mol (Figure 2). The racemization barriers were well compatible with the experimentally determined racemization barriers at -78°C (14.9 and 16.7 kcal/mol for enolate **A** and enolate **B**, respectively). The distance between the potassium cation of the enolate moiety and the benzene ring of the benzyl ester moiety was shown to be 3.31 Å (shorter than the sum of their Van der Waals radii: 3.45 Å) in the ground-state of the dimer of enolate **B**, while that in the transition state of the C-N bond rotation (racemization process of axially chiral enolate **B**) was indicated to be 3.82 Å. These results suggest that the stabilization by the cation- π interaction is more significant in the TS, indicating that the origin of resistance of enolate **B** toward racemization is expected to be ground-state stabilization by the cation- π interaction between the potassium cation and the phenyl ring.



Interdisciplinary approach to nanostructured materials for applications

Jean-Pierre Bucher Université de Strasbourg.

As the research activities were strictly limited in 2020, here we only include an ongoing collaboration with the team of Prof. Jun Onoe (Nagoya University) which constitutes a first step in the interdisciplinary project. For this project, Prof. T. Teranishi is our ICR contact.

The objective is to improve the energy conversion efficiency of organic solar cells by studying the correlation between the photo-current elementary processes and the nano-structural properties. The Onoe team macroscopically examines the external quantum efficiency of organic solar cells made of a hetero-junction of donor (phthalocyanine or porphyrin) and acceptor (C_{60}) films, using *in situ* electrical field modulated spectroscopy. The Strasbourg team on the other hand is using bottom-up fabrication capabilities of model donor (D)/acceptor (A) interfaces and ultrahigh vacuum STM spectroscopy at cryogenic temperatures to detect the spatial modification of electronic properties such as frontier-orbitals, ionization energy and electron affinity in relation to the nano-structural properties such as crystallinity, molecular orientation and environment.

Experimental results show that the local HOMO and LUMO features as detected at interfaces by STM spectroscopy are very different from the ensemble averaging frontier orbitals obtained by optical absorption spectroscopy. In particular, the proximity of an interface or electrode has dramatic effects on the very first interface monolayers. Experiments (Strasbourg) and DFT calculations (Nagoya) show strong hybridization of C_{60} with ZnPc in the buffer layer upon adsorption on Ag(111) thus highlighting the importance of boundary layers where the A-D character is strongly perturbed. The anomalous behavior at the interface is accompanied by a significant charge transfer from the Ag to the molecular complex. Two papers have been published and one submitted prior to the iJURC project. Due to the epidemic situation, no workshops or meetings could be organized.

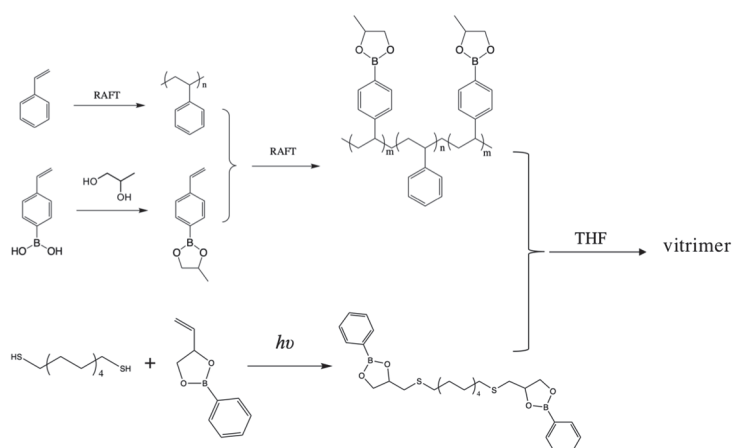
Relationship between chain orientation, amount of defect, and toughness of glassy polystyrene materials

Quan Chen Changchun Institute of Applied Chemistry

Objectives: Polystyrene (PS) is a widely used thermoplastic polymer. Since its glass transition temperature is much higher than the room temperature, it is usually used in the glassy state in our daily life. Nevertheless, its brittleness has limited the potential applications on more occasions. How to improve the toughness of brittle glassy materials is one of the most challenging subjects in polymer science. In this study, we prepare the telechelic PS samples, and examine whether the “anchoring effect” of the end groups would increase the chain orientation during flow, so as to enhance the ductility of the samples that are quenched directly after the flow.

Experimental methods:

The telechelic PS vitrimer samples were obtained from reaction of two precursors, Precursor T and Precursor C, in THF, where Precursor T was prepared via the two-step RAFT polymerization, and Precursor C was prepared via the click reaction, as shown in Scheme 1.



Scheme 1. The synthesis route of telechelic PS vitrimer samples

Experimental results and Discussion:

Figure 1 shows the (pseudo-) master curves of storage and loss moduli, G' and G'' , plotted against frequency, ωa_T , for the PS-T-9.1-C- x system, where T-9.1 means that Precursor T contains 9.1 functional end groups per chain on average, and x means a molar ratio between Precursor C and Precursor T. The precursor chain ($x = 0$) shows a typical Rouse behavior characterized by a Rouse power-law region followed by the terminal relaxation, indicating that this sample is unentangled. Increasing x leads to the sol-to-gel transition, PS-T-9.1-C- x ($x = 0.3, 0.4, 0.9, 2, 3, 4$) show clear plateau, where the amplitude of the plateau increases with increasing x for $x \leq 4$, meaning that they are above the gel point and the network is densifies with increasing the Precursor C/Precursor T ratio. The plateau modulus decreases with increasing x from 4 to 6, indicating a reverse gel-to-sol transition when the Precursor C is in great excess.

In the future, nonlinear elongational rheological and mechanical measurements will be conducted in collaboration with Prof. Yumi Matsumiya in ICR, Kyoto University.

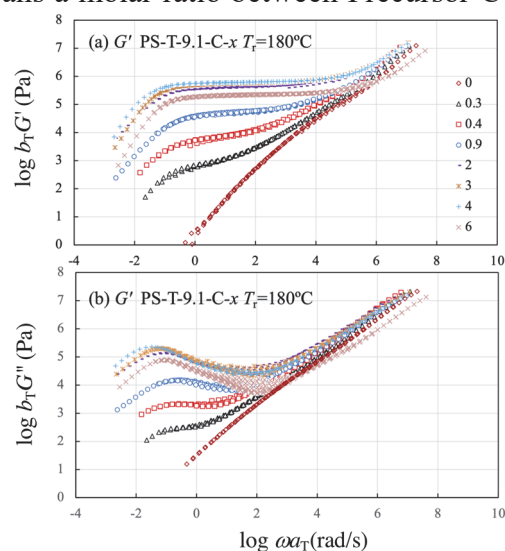


Figure 1: Comparison of the linear viscoelastic behavior of the PS-T-9.1-C- x samples, where panel (a) and (b) shows the storage and loss moduli, G' and G'' , respectively for $x \leq 6$ reduced at 180°C.

Search for four-wave-mixing in the vacuum – Unveiling dark components in the Universe –

Kensuke Homma Hiroshima University

Purpose and Method

The purpose of this study is to search for Four-Wave-Mixing (FWM) phenomena in the vacuum in order to understand dark components in the Universe. So far, we have constructed and improved an ultra-high vacuum chamber in ICR toward the search. In this vacuum chamber, two-color laser pulses are collinearly combined and focused into the vacuum along the same optical axis. If photon-photon interactions occur in the vacuum environment, generation of intrinsic FWM photons via the stimulated interaction $\omega + \omega \rightarrow (2-u)\omega + u\omega$ is enhanced, where ω is the energy of the creation laser pulse and $u\omega$ is the energy of the inducing laser pulse with $0 < u < 1$. The signal photon energy in this scattering process corresponds to $(2-u)\omega$.

Progress and Achievements

We have extended the search by increasing laser intensity by one order of magnitude. Accordingly, quantification of background signal photon yields from the known atomic processes has been further required, because we must subtract them from the signal yield in order to discuss the dark components in the vacuum. We then have established a way to quantify background yields from the surface origin in addition to the residual gas origin.

As the present status, we have succeeded to publish a paper on one of the search results to a journal and we are now preparing for the next submission on the rest of the results. In addition, we have developed an idea to extend the same method to the GHz-band and invented a concept of stimulated radar collider. On this concept we have called a press conference in Hiroshima University and the article has been published in Chugoku Shinbun. We summarize published papers, a relevant invited talk and the press release during FY2020 as follows.

Published papers:

- [1] Extended search for sub-eV axion-like resonances via four-wave mixing with a quasi-parallel laser collider in a high-quality vacuum system,
Akihide Nobuhiro, Yusuke Hirahara, Kensuke Homma*, Yuri Kirita, Takaya Ozaki, Yoshihide Nakamiya, Masaki Hashida, Shunsuke Inoue, Shuji Sakabe, Prog. Theor. Exp. Phys. 20120(2020) 7, 073C01.
- [2] Stimulated radar collider for probing gravitationally weak coupling pseudo Nambu-Goldstone bosons,
Kensuke Homma* and Yuri Kirita, Journal of High Energy Physics volume 2020, Article number: 95 (2020).

Invited talk:

- [1] 多波長電磁波衝突を用いた真空構造への多角的アプローチ –地上散乱実験は重力結合へ到達し得るか?–
本間 謙輔, 東北大学 ELPH セミナー (2021.2.25)

Press release:

- [1] <https://www.hiroshima-u.ac.jp/research/news/60232>

Fine synthesis of polymer brush on ferromagnetic nano-platelet for magnetophotonic LC

Yoshiaki Uchida Osaka University

In response to the rapid spread of automated systems everywhere like factories and vehicles, short-range communication systems using visible light with optical fibers made of inexpensive polymers have recently attracted attention. However, as the communication speed and the number of nodes incorporated in the systems increase, problems arise with the interference between cables, complicated wiring, and the limit of flexibility for bending. To solve these problems, fiber-free short-distance optical transmission systems are promising.

We have focused on the photonic structures of liquid crystalline (LC) phases: cholesteric LC (CLC) materials with flexible one-dimensional periodic structures, nematic LC (NLC) materials showing strong light scattering as random laser resonators, and whispering gallery mode (WGM) in an LC microsphere, where light is trapped inside the sphere by repeated total reflection on the sphere surface. We expect that optical transmission devices using these materials allow the remote control of light using magnetic fields. We have already fabricated CLC capsules that work as three-dimensional laser resonators with three modes: WGM, distributed feedback (DFB) mode and distributed Bragg reflection (DBR) mode [1]. Besides, we have succeeded in switching the random laser action in NLC materials doped with ferromagnetic nanoplates by using a weak magnetic field [2]. To synthesize such nanoplates, we have developed a synthesis method of nanoplate dispersions using the LC phases as templates [3].

We focus on the stable dispersion of the ferromagnetic nanoplates in CLC phases to obtain ferromagnetic CLC materials and the magnetic switching of optical elements that emit lights or receive lights. We have been investigating the dispersion of solid magnet particles with polymer brushes into various liquid crystals. In the previous year, we succeeded in dispersing the nanoplates in NLC materials, and we have been optimizing the condition of the polymer brushes to disperse the nanoplates in CLC materials. Meanwhile, we investigated the NLC droplets in aqueous surfactant solutions as laser resonators that could exhibit laser action at two different wavelengths derived from their random mode and WGM. The two modes have been found to switch depending on the excitation light irradiation position; it is the first example of the coexistence and tunability of the two modes. The origin of the controllability is likely to be attributed to the correlation between the droplet diameter and the lasing threshold.

References

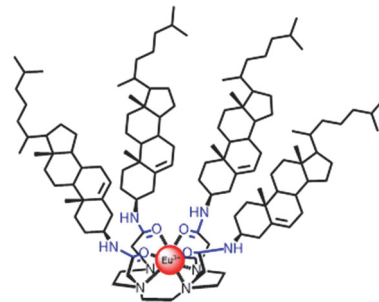
1. Y. Uchida, Y. Takanishi, J. Yamamoto, *Adv. Mater.*, **25**, 3234-3237 (2013).
2. T. Naruta, T. Akita, Y. Uchida, D. Lisjak, A. Mertelj, N. Nishiyama, *Opt. Express*, **27**, 24426-24433 (2019).
3. Y. Uchida, T. Nishizawa, T. Omiya, Y. Hirota, N. Nishiyama, *J. Am. Chem. Soc.*, **138**, 1103-1105 (2016).

自己集積型希土類錯体の薄膜化とその機能解析

三枝栄子 大阪市立大学

【背景・目的】

希土類イオンは、高輝度、長寿命など有機蛍光色素にはない発光特性を示すことから、蛍光体やバイオセンサーなどに応用されている。我々のグループでは疎水性のコレステル基と親水性のポリアミン部位からなる配位子を独自に開発し、特に、可視光発光をもつ Eu 錯体が水溶液中でベシクル状の自己集合体を形成する性質を有し、水溶液中におけるアニオン応答を発光による出力として観測できることを見出した¹⁾。本研究課題では、希土類錯体集積膜を分子認識場として活用し、希土類発光による化学的・物理的環境の変化を可視化する機能を有するケミカルセンサー開発を目指すため、まずは固体状態での構造・物性を明らかにする。今回、Eu 錯体 (**EuL**, Fig.1) の薄膜集積化と赤外分光法による構造評価を行った。

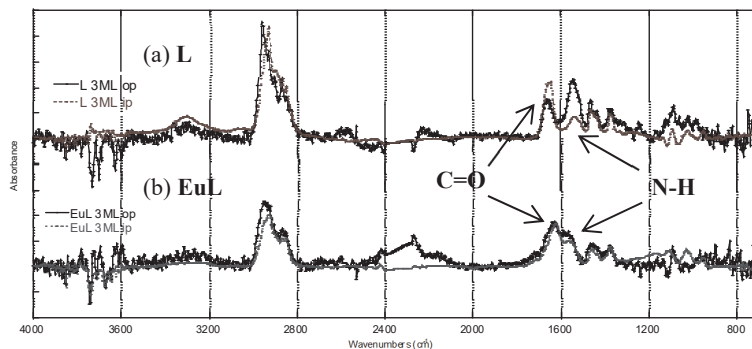
Fig.1 両親媒性希土類錯体 **EuL**.

【実験方法】

配位子 **L** および錯体 **EuL** について、Langmuir-Blodgett (LB) 法により水面上単分子膜の作製、および作製した LB 膜を Si 基板に転写した。**L**、**EuL** の膜構造について MAIRS (偏光多角入射分解分光) 法を用いた赤外分光測定を行った。MAIRS 法は共同研究者の長谷川健教授が開発した分析手法であり、基板に平行/垂直な方向に対する IR スペクトルを分解し同時に解析することが可能で、薄膜中の分子配向を官能基単位で定量的に評価することができる。

【考察】

Fig.2 に **L**、**EuL** 積層膜の赤外 MAIRS スペクトルを示す。Fig.2(a) より、**L** は 1651 cm^{-1} にアミド I の C=O 伸縮が面内方向に強く出ており、 1547 cm^{-1} にアミド II の NH 変角が面外 (OP) 方向に強く出ていることが分かる。これより、膜内に分子配向性があり C=O 結合は基板に対して平行に伸縮振動していると考えられる。一方、**EuL** (Fig.2b) は 1627 cm^{-1} 、 1574 cm^{-1} に観測されるアミド基由来の吸収強度に差がなく、分子配向性は見られなかった。このように、自己集積型配位子およびその錯体が膜内でどのように配向しているか詳細を初めて明らかにした。

Fig.2 Si 基板上 LB 膜の IR-MAIRS スペクトル (a) **L**, (b) **EuL**, OP : —, IP : ----

【文献】 1) T. Sagami *et al.*, *Chem. Commun.*, **2017**, 53, 3967.

Study on the regulatory network of plant epidermal cell differentiation

Rumi Tominaga Hiroshima University

Introduction:

Plant epidermal cell development including root hair and trichome cells represent well-studied model systems for cell-fate specification in *Arabidopsis thaliana*. Some regulatory factors have been shown to contribute to this regulatory network. The CLAVATA3/ESR (CLE) plant polypeptides act as peptide hormones in various physiological and developmental aspects in a diverse array of land plants. One of the CLE family of genes, *CLE14*, is reported to induce root hair formation in *Arabidopsis* roots. Previously, we demonstrated that the application of CLE14 polypeptide induced excess root hairs, and reduced the expression level of the non-hair cell fate determinant gene, *GLABRA2* (*GL2*) in *Arabidopsis* roots. In this study, we investigated the function of CLE14 polypeptide in rice (*Oryza sativa*) and tomato (*Solanum lycopersicum*) roots.

Methods:

Root phenotypes of CLE14-treated 10-day-old rice and tomato seedlings were observed.

Real-time PCR was performed to analyze the expression levels of the *OsGL2* and *SlGL2* genes, i.e., homologs of the *Arabidopsis GL2* gene, in rice and tomato seedlings, respectively.

Results and Discussion:

CLE14 polypeptide treatment clearly induced excess root hair formation in rice roots. Unlike the result seen in rice, the CLE14 treatment did not have a substantial effect on tomato root hair induction. Consistent with the findings of *Arabidopsis*, we detected a significantly lower accumulation of *OsGL2* transcripts in the rice roots treated with the CLE14 compared with those of the control plants. These results suggested that CLE14 is functional in rice roots as well as in *Arabidopsis* roots, where it inhibits the expression of the *GL2* homolog gene *OsGL2* and promotes root hair formation. Unlike the results seen in *Arabidopsis* and rice, CLE14 did not induce root hair formation in tomato seedlings. However, consistent with the results from *Arabidopsis* and rice, a significantly lower accumulation level of the *GL2* homolog gene (*SlGL2*) transcripts was detected in the CLE14 treated tomato roots compared with those of the control plants. These results suggested that regardless of the root hair phenotype, CLE14 polypeptide can suppress the *GL2* homolog gene expression in rice, tomato, and *Arabidopsis* seedlings. Although further investigations of the effects of CLE14 polypeptide on crop plants are required, the present study offers new insights into the molecular basis of CLE peptide signaling in rice and tomato root epidermal cell differentiation.

N. Hayashi, et al., Plant Biotech., 36, 205-208 (2019)

免疫賦活化するナノ集合体

山崎晶 大阪大学

ワクチンは感染症を予防するための最もすぐれた医学的介入である。疾患を引き起こす病原体を弱めた弱毒化ワクチン(生ワクチン)は、自然免疫と獲得免疫の両方の反応を継続的に刺激するため、効果的なワクチンとして作用する。弱毒化ワクチンは効果的な感染症予防の手段だが、生きたウイルスであるため安全面において問題がある。この課題を解決するために病原体の抗原となる部分を取り出した不活性化ワクチンが開発され、ワクチンの主力として臨床的に広く用いられている。しかし、不活性化ワクチンは自然免疫原性を有しておらず、十分な獲得免疫応答を誘導するためにはアジュバントと呼ばれる自然免疫活性化剤との併用が必要。これまでにアラム(アルミニウム塩)や水中油型エマルジョンなどが経験的に利用されているが、事実上この二つだけである。新興ウイルスに対応して効果的なワクチンを準備するためには、アジュバントのレパートリーを増やすことが急務である。

これまでの上杉グループとの共同研究によって、自己集合性ワクチンアジュバント材料を発見し、コリカマイドと名付けた(Angew. Chem. Int. Ed, 2020)。コリカマイドの集合体はTLR7というウイルス受容体に認識される。本共同研究では、上杉グループとコリカマイドの様々な類縁体を化学合成し、より強力かつ安全なアジュバントを見つけ出した。コリカマイドは胆汁酸(デオキシコール酸)2分子が炭素5個のジアミンによって結合した単純な構造である。さらなる有機合成展開により、自己集合性と免疫活性化能に優れた最適化合物を発見した。IL6産生を指標にして樹状細胞の活性化を評価したところ、デオキシコール酸をXに置き換えた化合物1がコリカマイド約3倍の活性を持つことが分かった。リンカー部位を炭素数2~12個に置き換えた化合物を合成して同様に試験したところ、炭素数Y個の化合物2がコリカマイドの約4倍の活性を持っていた。

ポストコロナの時代でも、新たな新興ウイルスが次々と出現するだろう。今回のコロナ禍のように、その都度ワクチンが開発され、アジュバントが組み込まれる。本研究成果が先導して、様々なアジュバントが開発されれば、新興ウイルスに最適かつ安価なアジュバントを選択できるようになる。発展途上国を含めたグローバル社会に貢献すると期待できる。

Functional analysis of non-canonical strigolactones as plant hormones and root-derived signals

Yoshiya Seto Meiji University

【The aim of this study】 Strigolactones (SLs) are plant hormones that regulate shoot branching, as well as being known to be rhizosphere signals that control symbiotic and parasitic relationship with Arbuscular mycorrhizal fungi and root parasitic plants, respectively. SLs are biosynthesized from carotenoids via a key intermediate molecule called carlactone (CL). In a model plant, *Arabidopsis*, CL is further converted into carlactonoic acid (CLA) by a cytochrome P450 monooxygenase, MORE AXILLARY GROWTH1 (CYP711A). We previously identified

methyl esterified derivative of CLA, methylcarlactonoate (MeCLA) in *Arabidopsis*, and found that MeCLA can interact with the *Arabidopsis* SL receptor protein, AtD14. On the other hand, CL and CLA were not able to interact with AtD14, suggesting that the methyl esterification step is critical to convert a biologically inactive precursor to a bioactive hormone molecule. Conventional SL molecules have the tricyclic lactone ring part (ABC-ring) that is connected to another butanolide lactone part (D-ring) via an enol ether bridge. However, CL derivatives lack BC ring system, and possesses only A and D rings. After the discovery of CL derivatives, structurally similar molecules have been isolated from various plant species. Currently, these new types of SL molecules are classified to be ‘non-canonical’ SLs, whereas the conventional SLs are called ‘canonical’ SL (Fig. 1). Although, these new types of SL molecules have been identified, the functional difference between canonical and non-canonical SLs are not fully understood. In this collaborating project with Prof. Shinjiro Yamaguchi in ICR, Kyoto University, we planned to clarify the biological role of non-canonical SL using an important crop, Tomato. MeCLA is thought to be a common precursor for non-canonical SLs, thus we decided to identify the CLA methyltransferase in tomato (*Solanum lycopersicum* CLA methyltransferase; *SiCLAMT*), and analyze its biological function.

【Results】 We have previously identified the *Arabidopsis* CLAMT. Therefore, we performed a BLAST search with tomato genomic database using *Arabidopsis* CLAMT as a query, and found a candidate gene of tomato *SiCLAMT*. The cDNA of *SiCLAMT* was cloned into a protein expression vector, and expressed using *Escherichia coli*. We found that the cell free extract of *E. coli* expressing *SiCLAMT* can convert CLA into MeCLA. We also started to generate the Tomato *SiCLAMT* knockout mutant by using CRISPR-CAS9 method. We cloned multiple gRNA sequences targeting *SiCLAMT* into a genome editing vector. We are going to obtain the knockout mutant, and will clarify the biological function of *SiCLAMT*.

【Publication】 Mashiguchi K, Seto Y, and Yamaguchi S, Strigolactone biosynthesis, transport, and perception, *The Plant Journal*, in press (<https://doi.org/10.1111/tpj.15059>)

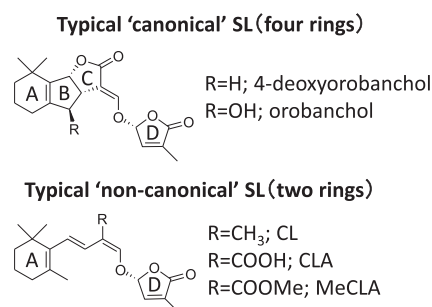


Fig. 1. Structures of ‘canonical’ and ‘non-canonical’ SL

Analysis of phase equilibrium and molecular dynamics in mixture of nematic liquid crystal and solvent

Ryoko Shimada Japan Women's University

Liquid crystalline (LC) molecules exhibit rich behavior when mixed with non-LC molecules, because the free energy of the mixture is contributed not only from the LC free energy determined by the order parameter Q but also from the mixing free energy not directly related to Q .^{1,2)} This free energy has been utilized to discuss complicated phase evolution in LC/solvent mixtures.^{1,2)} A characteristic feature of these mixtures is the coupling between the LC free energy and the mixing free energy that allows the LC transition to trigger the phase separation. This coupling is expected to affect properties of the mixtures even in the isotropic one-phase state, but details of this effect have not been well elucidated. This study attempts to resolve the effect on the static and kinetic properties in the isotropic one-phase state for a mixture of 4-cyano-4'-pentylbiphenyl (5CB) with dimethyl phthalate (DMP; $w_{\text{DMP}} = 3.1$ wt%). Pure 5CB forms nematic LC at $T_{\text{IN}} = 35^\circ\text{C}$.

The DMP/5CB mixture separated into LC and isotropic phases at a transition temperature $T_{\text{IN}}^* = 27^\circ\text{C}$. This T_{IN}^* is lower than T_{IN} of pure 5CB because of the mixing free energy contribution explained above. The mixture and pure 5CB commonly exhibited simple thermal expansion and the Andrade-type behavior of their mass density ρ and kinematic viscosity ν at temperatures T well above T_{IN}^* and/or T_{IN} . However, at T just moderately above T_{IN}^* and/or T_{IN} (still in the *isotropic one phase regime*), non-trivial deviations from this high- T asymptote were observed.

This observation is demonstrated in Figures 1 and 2 where the deviations $\Delta\rho$ and $\Delta\nu$ are normalized by the high- T asymptotes $\rho^{\text{iso-high } T}$ and $\nu^{\text{iso-high } T}$ and plotted against T . Filled and unfilled symbols show that the materials were in the LC and isotropic one-phase state, respectively, and the circles with inner dot indicate that the DMP/5CB mixture was phase separated into LC and isotropic phases. For pure 5CB, the positive deviations $\Delta\rho/\rho^{\text{iso-high } T}$ and $\Delta\nu/\nu^{\text{iso-high } T}$ in the isotropic state emerge only at T in a close vicinity of T_{IN} because of the first-order nature of its isotropic-nematic transition. In contrast, for the 5CB/DMP mixture, the deviation emerges in a considerably wide range of T spanning almost 10K. This remarkable deviation is attributable to the concentration fluctuation not existing in pure 5CB. Namely, the fluctuation of the 5CB concentration due to a small amount of DMP (3.1 wt%) induces correlation between 5CB molecules locates at distant points in the mixture thereby enhancing the density and viscosity, as deduced from the statistical theory of Helfand.³⁾

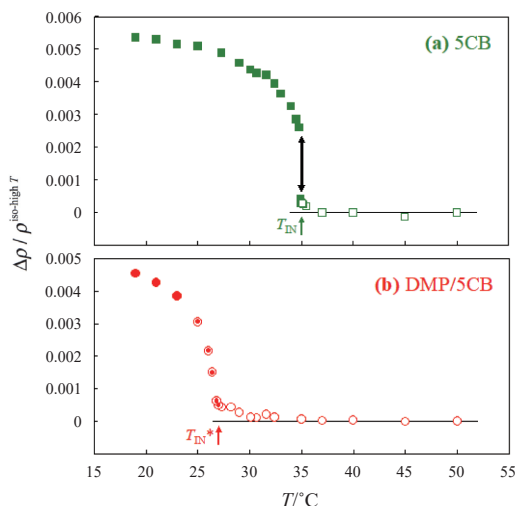


Fig. 1. Density change of 5CB and DMP/5CB mixture with T .

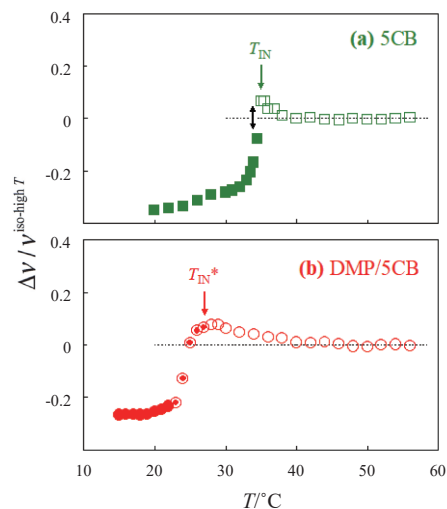


Fig. 2. Viscosity change of 5CB and DMP/5CB mixture with T .

Acknowledgement: This work has been published in *J. Soc. Rheol. Japan*, 48, 199 (2020).

References: 1) Araki and Tanaka, *Phys. Rev. Lett.*, 93, 015702 (2004). 2) Reyes et al, *Soft Matter*, 15, 6044 (2019). 3) Helfand, *Phys. Rev.*, 119, 1 (1960).

イネのストリゴラクトン生合成における CYP711A ファミリーの機能解析

井澤毅 東京大学

ストリゴラクトン (SL) は植物の枝分かれなどを制御する植物ホルモンである。また、SL は根圏アレロケミカルとしても機能しており、アーバスキュラー菌根菌の菌糸分岐誘導作用や、アフリカなどで甚大な農業被害をもたらす根寄生植物の種子発芽誘導作用を有している。近年、SL 生合成に関する研究は飛躍的に進展し、その全容が明らかになりつつある。しかし、SL のホルモン作用を理解する上で、最も重要な「植物ホルモンとしての活性本体」は未解明である。本研究では、イネを材料として、活性型 SL の生合成に重要な役割を果たすと考えられる CYP711A ファミリーの遺伝学的および生化学的な機能解析の共同研究を行い、植物ホルモンとしての活性型 SL 分子種を明らかにすることを目的とする。

本年度、井澤グループでは、イネの施肥に応答する遺伝子として同定した CYP711A ファミリーに属する遺伝子について、CRISPR-Cas9 システムを用いて、単独破壊株や二重破壊株を作出した。表現型解析の結果、二重破壊株において分げつ（枝分かれ）が増加したことから、これらの CYP711A 遺伝子が活性型 SL 分子種の生合成に重要な機能を有することが示唆された。

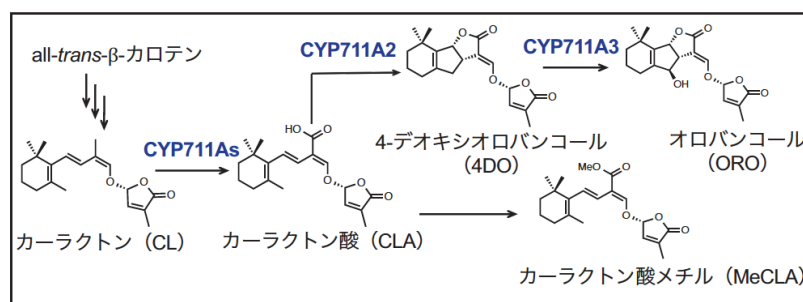


図1. イネの推定SL生合成経路

結果、二重破壊株において分げつ（枝分かれ）が増加したことから、これらの CYP711A 遺伝子が活性型 SL 分子種の生合成に重要な機能を有することが示唆された。

CYP711A ファミリーは、リコンビナントタンパク質を用いた実験などから、SL 生合成中間体であるカーラクトン (CL) からカーラクトン酸 (CLA) への変換が主要な酵素機能であると考えられている (図 1)。しかし、イネには CYP711A ファミリーに属する遺伝子が 5 つ存在し、CLA だけではなく四環性 SL である 4-デオキシオロバンコール (4DO) やオロバンコール (ORO) の生合成にも関与することが報告されており、それら生理機能には不明点が多い (図 1)。そこで、化学研究所の山口信次郎博士 (共同研究者)、増口潔博士 (共同研究者) との共同研究により、二重破壊株における CL や CLA の内生量を、高速液体クロマトグラフ質量分析計を用いて定量した。その結果、二重破壊株の地上部において CLA が減少し、CL が過剰に蓄積していることが明らかとなった。このことから、これらの CYP711A 遺伝子は、イネ生体内でも CL から CLA への変換を担っていることが示唆された。

以上のことから、イネにおいて枝分かれ抑制作用を有する活性型 SL は CLA 以降に存在することが示唆された。今後、CYP711A の二重破壊株における、四環性 SL である 4DO や ORO、非四環性 SL のカーラクトン酸メチル (MeCLA) の内生量を定量し、SL の「活性本体」についてのさらなる知見を得たいと考えている。なお、今年度は本研究課題に関する論文発表および学会発表は行っていない。

Analysis of the physiological functions of extracellular vesicles produced by intestinal bacteria and fermented food-derived bacteria and their application

Atsushi Kurata Kindai University

Introduction:

The gastrointestinal tract is inhabited by a complex community of bacteria, the gut microbiota. The gut microbiota and its host are exchanging various molecules, resulting in a complex interrelationship. The gut bacteria-produced modulator toward host cells are not fully understood. Most bacteria release extracellular vesicles (EVs) with the size ranging from 50 to 400 nm. The EVs released by intestinal bacteria may play critical roles in the host-bacteria interactions. Against this background, the first objective of this study is to analyze functional characteristics of EVs from intestinal bacteria and fermented food-derived bacteria. The second objective is to develop novel expression systems for heterologous proteins using EVs-producing bacteria.

Results:

1. Functional characterization of EVs produced by intestinal bacteria

Lactobacillus plantarum isolated from human intestines produces EVs with the size of 50-100 nm. Proteins of EVs were analyzed by LC-MS/MS. As the results, five kinds of lipoproteins were detected in the EVs. EVs from *L. plantarum* stimulated toward Raw264 cells to produce IL-1, IL-6, and IL-10, and toward Peyer's patch cells to produce IgA. The EVs and one of the purified lipoproteins from *L. plantarum* were recognized by human Toll-like receptor 2 of HEK293 cells. These findings elucidated the relationship of Toll-like receptor 2 and the lipoprotein of EVs as a novel modulator in the gut immune responses toward *L. plantarum*.

2. Analysis of regulatory mechanism for production of EVs

Shewanella vesiculosa HM13 isolated from intestinal contents of horse mackerel (*Trachurus japonicus*) abundantly produces EVs and is considered useful as a host for production of heterologous proteins as cargoes of EVs. It was revealed that production of EVs by this bacterium is enhanced by increasing the concentration of lysine in the culture medium. A putative sensor protein with typical sensing and signaling domains was found to play a major role in lysine-inducible EV production. This protein was also shown to be involved in lysine-responsive suppression of biofilm formation. These results suggest that regulations of EV production and biofilm formation of this bacterium share a common mechanism to sense nutrients in the environment.

自己集合性分子による心筋細胞移植の効率化

柴祐司 信州大学

日本における心不全患者数は全癌患者数よりも多く、約 120 万人と推定され、今後もさらに増加することが確実である。現在の内科的、外科的治療法は心不全患者の症状の緩和と、病気の進行抑制に有効であるが、病気を治癒させることは出来ない。これは、心臓を構成する心筋細胞が分裂・増殖能をほとんど持たず、傷害によって失われた心筋細胞が回復しないことに起因している。重症心不全に対する唯一根本的な治療は心臓移植であるが、ドナー不足は深刻である。近年、多能性幹細胞から心筋細胞を作製するプロトコールが複数報告され、比較的容易に大量の心筋細胞を作製することが可能となってきた。

本研究では、京都大学化学研究所の上杉グループと共に、心筋細胞分化を誘導する化合物 KY02111 のメカニズムを解明した。本化合物は上杉グループと中辻グループによって発見された化合物であり、強力な心筋分化能力をもつ。現在、心筋分化の大量調整に利用されている。しかし、そのメカニズムは解明されていなかった。これまでの共同研究により、KY02111 の標的タンパク質として酵素 X を同定した。さらに KY02111 が X に結合して Y との相互作用を阻害することが確認された。Y の変異は主に心臓疾患に見られるため、X と Y の相互作用の心筋発生に影響している可能性が高い。実際、Y の変異は X との相互作用を阻害した。我々のグループは、心筋分化の様々なタイミングで KY02111 を添加し、その影響を観察した。KY02111 を心筋分化プロトコールの初期から培養液に入れ続けると、心筋分化から脂肪細胞分化へと移行した。この効果は Y の変異による病態と一致する。

一方、新学術領域「先端モデル動物支援プラットフォーム」で KY02111 の生理活性を評価して頂いたところ、KY02111 が Z 刺激による A の発現を抑制することが見出された。また、X や Y のノックダウンでも、Z 刺激による A の発現が抑制された。これに対し、心筋分化促進活性を有さない KY02111 の類縁体は、X と Y の結合を阻害せず、Z シグナルにも影響を及ぼさなかった。以上の結果より、KY02111 は X と Y の結合を阻害することで、Z シグナルを抑制し、心筋分化を促進することが示唆された。

以上の成果は上杉グループと論文にまとめ、現在投稿中である。

Observation of spin wave propagation in polycrystalline YIG thin films prepared by co-precipitation method

Keisuke Yamada Gifu University

【Introduction】 Recently, $\text{Y}_3\text{Fe}_5\text{O}_{12}$ (YIG) is one of the most prominent materials for spintronic device applications that utilize the spin pumping and spin Seebeck effects with its low Gilbert damping constant α . This paper reports our latest experimental findings on the variation of longitudinal spin Seebeck (LSSE) voltage with microstructural change in YIG films chemically synthesized onto a Si substrate as a function of annealing temperature.

【Experimental Method】 YIG-film samples were synthesized by co-precipitation and spin-coated onto Si substrates. The samples were subsequently annealed at temperatures ranging from 1073 K to 1273 K for 0.5 hour in an ambient atmosphere. Their structure and magnetic properties were characterized by X-ray diffractometry (XRD), scanning electron microscopy (SEM), ferromagnetic resonance (FMR) measurements and LSSE measurements. FMR measurements were performed at ICR of Kyoto Univ.

【Results and Discussion】 The diffraction peaks associated with the garnet phase are observed in all the YIG samples measured by XRD. When the annealing temperature T_a increases from 1073 K to 1273 K, the average particle size $\langle D \rangle$ of the YIG crystals estimated by SEM increases from 50 nm to 68 nm which increases by 36%, as shown in the left axis of Fig. 1. The areal fraction of voids v obtained from the SEM surface images is represented in the right axis of Fig. 1. The values of v are in the range of $36 \leq v \leq 42\%$, it indicates that the v is slightly dependence on the annealing temperature. The value of thermoelectric performance (TP) estimated by LSSE measurements decreases monotonically with increasing T_a from 1073 K to 1273 K, and it decreases by up to 24% (64%) in the YIG films with Pt = 5 nm (10 nm) (see Fig. 2). These results indicate the microstructural changes in the YIG films by annealing temperature cause the decreased TP, which are corresponded with a reduced coherence of the magnons in the YIG films. This result indicates that the coherence of the spin waves propagated in the YIG films confirmed nanocrystal is affected on the magnitude of TP.

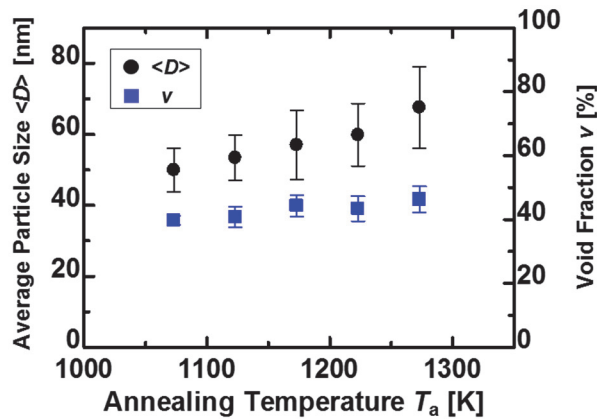


Fig. 1 $\langle D \rangle$ and v of the samples plotted as a function of T_a .

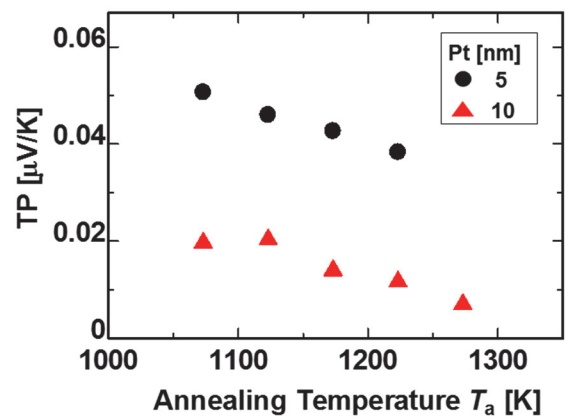


Fig. 2 Variation of TP with T_a for each Pt thickness.

【Achievement report】 This research has been submitted to a journal as a manuscript which title is “Change of longitudinal spin Seebeck voltage with annealing in $\text{Y}_3\text{Fe}_5\text{O}_{12}$ films formed by densely packed nanocrystals” .

抗腫瘍性膜透過ペプチドによるがん進展調節

大橋若奈 慶應義塾大学

【目的】正常組織に見られるような組織幹細胞様の細胞集団が腫瘍組織にも存在し、この細胞集団は自己を複製する能力や様々な種類のがん細胞を生み出す能力を有し、少数存在するだけで腫瘍組織を構築しがんの再発や転移の進行につながると考えられている。このような細胞集団をがん幹細胞と呼ぶ。がん幹細胞集団の存在とこれによる腫瘍組織の形成と転移の誘発は生命予後を悪化させる要因であることからこれらの細胞集団の完全な除去はがんの完治に向けての重要な課題である。がん幹細胞集団の駆逐の難しさの一つとしてがん幹細胞集団は抗がん剤治療に対する抵抗性がある。この要因としてはがん幹細胞が細胞周期の静止期にあることや、腫瘍組織深部は血管形成の乏しさなどから十分に化学療法剤ががん幹細胞集団へ到達しない、等があげられている。本課題では、がん幹細胞除去のアプローチとして三次元細胞塊（スフィア）に効果的な導入が可能な膜透過ペプチドに抗腫瘍配列を付与し深部がん細胞死誘導に向けての検討を行った。深部がん細胞の生存制御が可能となれば、深部がん幹細胞の効率的除去法の開発へとつながることが期待される。

【実験方法】スフェロイド形成プレート(EZSPHERE, IWAKI)にヒト大腸がん由来細胞 HT29 細胞を播種し三次元細胞凝集塊（スフィア）を得た。細胞死誘導配列を付加した種々の膜透過ペプチド（CPP）をスフィアに投与し、細胞死誘導領域の評価を行なった。全ての CPP は共同研究者の二本教授（京都大学化学研究所）より提供を頂いた。

【実験結果と考察】細胞死誘導配列を連結した CPP をスフィアに投与後、ホルマリン固定スフィア切片のヘマトキシリン-エオジン染色像を示す(図)。スフィア表層及び内側領域は空隙なく密に細胞同士が接着して構成されているのが分かる。細胞死誘導配列連結 CPP を投与したスフィアでは内部にヘマトキシリン強陽性の斑点を有するアポトーシス様細胞の存在を認めた。細胞死誘導 CPP 投与はスフィア生存率を有意に低下させ、またスフィア周囲に不透明なデ

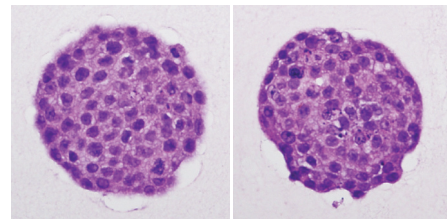


図. ヒト大腸がん細胞株HT29が形成する3次元細胞塊（スフィア）薄切標本HE染色像。未処理スフィア（左）と比較して細胞死誘導CPP処理スフィア(右)では、スフィア内部にヘマトキシリン強陽性の斑点を認める。

ブリスが増加した。これらのことから、細胞死誘導 CPP はスフィアの細胞死を誘導し、この細胞死誘導はスフィア内部においても起こっていることが示唆された。腫瘍深部組織へ到達可能な薬物輸送法は腫瘍の縮小化及び駆逐に重要であり、ここに腫瘍選択性を高める介入により有害事象の軽減が期待される。スフィアは腫瘍組織と類似した内部環境を有するとされ、本検討にて検証した腫瘍組織内部移行型細胞死誘導 CPP に腫瘍標的化を行うことにより、組織内部の腫瘍形成制御が可能とする薬物送達法の構築へとつながることが期待される。

Giant exchange reaction from H to D terminating on nanocrystalline silicon surface and their use

Takahiro Matsumoto Nagoya City University

The deuterium is attracting special interest for the manufacturing of silicon (Si) semiconductors, Si-microchips and optical fibers as well as the synthesis of isotopically-labeled compounds. However, the facile production of deuterium in a controlled manner is a challenging task.

In this collaborative research program (grant # 2020-97), we determined the surface-localized vibrational modes for hydrogen- and deuterium-terminated n-Si using inelastic neutron scattering (INS) spectroscopy. Because the determination of surface vibrational energies in the lower wavenumber region below 600 cm^{-1} is difficult using FTIR spectroscopy as the localized modes completely overlap the bulk Si phonon bands.

Figure 1 shows the contour plot for n-Si:H_{0.15}D_{0.85}. In addition to the spectrum originating from the H vibration (H2B), spectra are clearly observed at energy levels of $\hbar\omega = 67\text{ meV}$ (D2B), 60 meV (D1S), and 51 meV (D1B). These spectra and the energies are well described by harmonic oscillators with the same force constant as H. Thus, the energy levels of Si-D vibrations can be expressed as $E_i^{(D)} = (n_i^{(D)} + 1/2)\hbar\omega_i^{(D)}$. Here, we note that the scattering cross section of the H atoms in the INS measurements is more than 10 times larger than that of the D atoms ($\sigma_{\text{scatt}}(\text{D})/\sigma_{\text{scatt}}(\text{H}) \approx 7.64/82.03$); therefore, despite the lower concentration of H atoms (<10%), the Si-H mode results in an intense S(Q, $\hbar\omega$) spectrum, as shown by the H2B mode.

By determining the energy of surface vibrational modes for both Si-H and Si-D as shown in TABLE I, we found that the physical mechanism responsible for this enrichment originates from the quantum resonance between the bending modes of Si-deuteride and n-Si phonons.

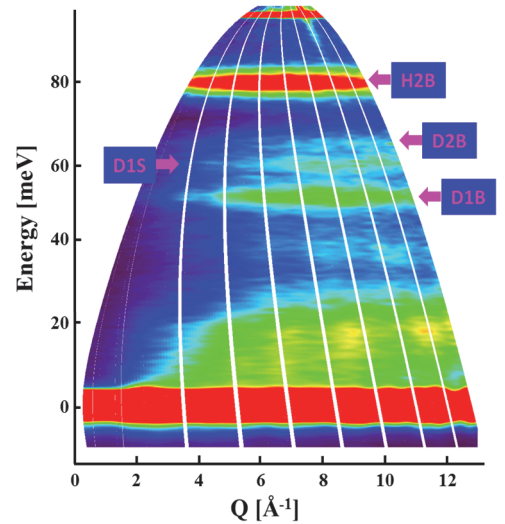


Figure 1. Localized vibrational modes for n-Si:D obtained by INS spectroscopy. B and S denote bending and stretching modes, respectively.

TABLE I. Surface vibrational energies for Si-D and SiH. The values are given in meV.

	Bend1	Bend2	Stretch1	Stretch2
SiD	51	67	60	190
SiH	59	79	61	261

界面活性剤を用いた溶媒含浸樹脂による金属イオンの固相抽出

倉橋健介 大阪府立大学工業高等専門学校

1. 目的

希土類元素である Eu は発光材料としてその需要の高まる一方、主な産出国が海外であり、その供給の不安定さから、廃棄物からのリサイクルが注目されている。主要なレアメタル分離法の一つである溶媒抽出法は、安価かつ簡便な操作で比較的高い選択性が得られる利点があるが、人体や環境に有害な有機溶媒を大量に用いる問題がある。そこで、人体や環境に有害な有機溶媒の暴露が少ない分離法として、多孔性樹脂に抽出剤を含浸させた溶媒含浸樹脂に着目した。先行研究では、溶媒含浸樹脂の調製を行う際に、抽出剤とともに界面活性剤を含浸させると、樹脂に含浸させた他の抽出剤による希土類抽出率を向上させるだけではなく、陰イオン性界面活性剤を含浸させた場合は、他の抽出剤を含浸させなくても希土類元素を樹脂相へ抽出可能であることを見出した。界面活性剤は安価で多様な種類の試薬が市販されており、界面活性剤単独で希土類金属を抽出できれば、高価な抽出剤の使用を削減し、分離コストを大きく下げることができる。そこで本年度は、この界面活性剤単独の溶媒含浸樹脂を用いた Eu の抽出について、界面活性剤の物性の検討を行った。

2. 実験方法

母材とする多孔性樹脂としてオルガノ株式会社製の Amberlite XAD-7HP を用いた。含浸する界面活性剤は親水基が陰イオン性である Sodium Dodecylsulfate (SDS) と Sodium Tetradecylsulfate (STS) を使用した。エタノールで洗浄後、乾燥した樹脂 1.0 g に対して 0.01 M 界面活性剤を含むエタノール溶液 10 mL を加え、1 日含浸させた。ロータリーエバポレーターで溶媒を減圧留去し、50℃で 1 日真空乾燥させ、目的の溶媒含浸樹脂を調製した。Eu を 0.2 mM 含む水溶液 2.5 mL を HCl と NaOH で任意の pH に調整した。この水相に SIR を 0.1 g 加え、2 時間振とうした。振とう後、遠心分離した後、水相を分取し、pH を測定した。分取した水相は Ni を内標準として、誘導結合プラズマ発光分光分析装置(ICP-OES)を用いて Eu 濃度を測定した。

3. 結果と考察

親水基が共通でアルキル鎖長のみが異なる界面活性剤である SDS および STS を含浸させた樹脂による Eu 抽出の結果を図 1 に示す。多孔性樹脂に界面活性剤のみを含浸させた場合、界面活性剤のアルキル鎖長は Eu 抽出率にほとんど影響を与えないことがわかった。これは、多孔性樹脂に含浸された陰イオン性界面活性剤の対カチオンである Na イオン 3 個と水相中の Eu イオン 1 個が交換されることで、Eu 抽出が起こるためと考えられる。

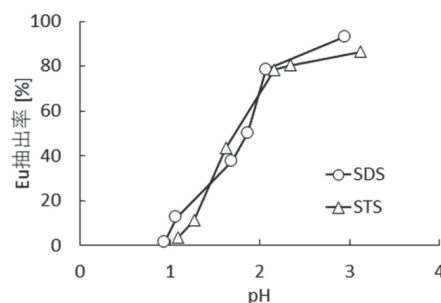


図 1 アルキル鎖の異なる界面活性剤を含浸させた溶媒含浸樹脂による Eu 抽出

4. 成果報告

- 1) 金村英雄ら, 第 80 回分析化学討論会, 北海道教育大学札幌校, 2020.5.
- 2) 金村英雄ら, 第 23 回化学工学会学生発表会, オンライン開催, 2021.3.

Anomalous Hall effect of ultrathin Pt films grown on magnetic oxide

Taro Nagahama Hokkaido University

Introduction: Recently, Spin Hall effect has been utilized to generate pure spin current, in particular, Pt is the most important element due to large spin-orbit interaction which is the source of the spin Hall effect. Additionally, Pt is well known as the material which exhibits a large magnetic proximity effect. It is purely an interface effect based on exchange interaction between magnetic and non-magnetic material, which could cause novel spintronic phenomena at the interface.

In this study, we investigated the magnetic proximity effect and anomalous Hall effect in Pt/CoFe₂O₄. As a result, the anomalous Hall effect was observed, which was sensitive to the interface states significantly.

Experiment: The films were grown on MgO(001) substrates by the molecular beam epitaxy (MBE) method with the base pressure of 8×10^{-8} Pa. The film structures were Al₂O₃(0001)/Pt(111)/ CoFe₂O₄ (111). The epitaxial growth and the surface morphology were confirmed by reflection high energy electron diffraction (RHEED) and the crystal structures were investigated by X-ray diffraction (XRD). The anomalous Hall measurements were carried out in the cryostat.

Results and discussions: Results and discussions: By the Hall measurement of Pt(2nm)/ CoFe₂O₄ (50nm), anomalous Hall effect that followed the magnetic hysteresis of CoFe₂O₄ was observed. Since CoFe₂O₄ is an insulator, the AHE is considered to be originated from the electric current in Pt layer in which small magnetic moments were induced by the magnetic proximity effect. To see the interface importance, we prepared the samples with and without CoFe of 0.5nm (1~2ML) and post oxidation. The AHE of the samples is shown in Fig.1. For the sample with CoFe and post oxidation, clear AHE was observed, on the contrary, no AHE was observed for the sample without interface treatment. In

the CoFe₂O₄ deposition process, the Co and Fe were deposited in an oxygen radical atmosphere, therefore, the oxygen layer could exist at the interface between Pt and CoFe₂O₄. The interface oxygen layer is considered to disturb the proximity effect, meaning that the direct exchange between Pt and the Fe and Co ions is important.

Publication and Conference: 1. S. Nodo et al., "Voltage Control of Magnetic Proximity Effect and Anomalous Hall Effect in CoFe₂O₄/Pt Bilayer by Ionic Liquid Gating" APEX, 13, 063004 (2020). 2. S. Nodo et al., "Voltage Control of Magnetic Proximity Effect and Anomalous Hall Effect in CoFe₂O₄/Pt Bilayer by Ionic Liquid Gating" 65 th MMM, online.

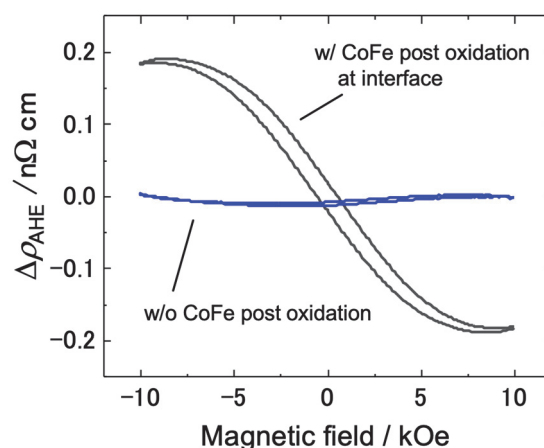


Fig.1 Anomalous Hall effect measurement of Pt(111)/ CoFe₂O₄ (111) films with or without CoFe deposition and post oxidation at the interface.

異常高原子価イオンを含む機能性酸化物合成とその構造物性研究

齊藤高志 高エネルギー加速器研究機構

遷移金属酸化物は幅広い機能を示す物質群であるが、その機能発現において遷移金属イオンの価数状態や電子状態が非常に重要な役割を果たしている。*A* サイト秩序型ペロブスカイト $\text{LaCu}_3\text{Cr}_4\text{O}_{12}$ は異常高原子価イオン $\text{Cu}^{3+}/\text{Cr}^{4+}$ を含む物質であり、*Cu-3d*、*Cr-3d*、*O-2p* 軌道が強く混成した特徴的な電子状態を持つために低温で *Cu-Cr* サイト間電荷移動転移に伴い反強磁性金属状態となる[1]。一方、申請者は最近 $\text{LaCu}_3\text{Cr}_4\text{O}_{12}$ における La^{3+} を Pb^{2+} で置換した $\text{PbCu}_3\text{Cr}_4\text{O}_{12}$ を合成し、これが *A* サイト秩序型ペロブスカイト構造を持ち、また低温で強磁性的な振舞を示すことを見出した。

$\text{LaCu}_3\text{Cr}_4\text{O}_{12}$ が反強磁性体である一方で $\text{PbCu}_3\text{Cr}_4\text{O}_{12}$ が強磁体であることは興味深く、その原因を理解する上でその結晶構造や電子状態を明らかにすることが重要である。 $\text{La}^{3+}\text{Cu}_3\text{Cr}_4\text{O}_{12}$ と同様、 $\text{Pb}^{2+}\text{Cu}_3\text{Cr}_4\text{O}_{12}$ も異常高原子価 $\text{Cu}^{3+}/\text{Cr}^{4+}$ を含むと期待される。 $\text{PbCu}_3\text{Cr}_4\text{O}_{12}$ の価数状態や電子状態を理解するためには精度の高い結晶構造情報が必要であるが、重元素 *Pb* を含むため、酸素原子位置を X 線回折から正確に求めることは難しい。そこで $\text{PbCu}_3\text{Cr}_4\text{O}_{12}$ の粉末中性子回折を行った。

J-PARC/MLF の BL09 に設置された粉末中性子回折装置 SPICA を用い、化学研究所・島川研究室の高圧合成装置を利用して作製した $\text{PbCu}_3\text{Cr}_4\text{O}_{12}$ の粉末試料について 300 K、100 K、50 K、4 K における粉末中性子回折実験を行った。室温構造の解析結果の BVS 計算から金属イオンの価数を見積もったところ、*Pb*、*Cu*、*Cr* 値の BVS はそれぞれ 3.2、2.3、3.4 であった。*Cu*、*Cr* の BVS 値がそれぞれ 2、3 より大きいことから、異常高原子価 $\text{Cu}^{3+}/\text{Cr}^{4+}$ を一部含むと考えられる。また *Pb* の BVS 値が 3 に近いということは、*A'* サイトにおいて $\text{Pb}^{2+}/\text{Pb}^{4+}$ が混在している可能性を示唆している。また図 1 に示す通り、100K 以下において室温では見られない 001 反射が観測された他、4 K において $d=4.86\text{\AA}$ 付近にも新たな反射が出現した。 $\text{PbCu}_3\text{Cr}_4\text{O}_{12}$ では約 150 K、20 K において強磁性的な磁化の増加がみられることから、これらは磁気秩序によって出現した磁気反射であると考えられる。今後、結晶構造と磁気構造の詳細を明らかにする。

[1] T Saito, Y. Shimakawa, et al., Phys. Rev. B, 95, 041109 (2017).

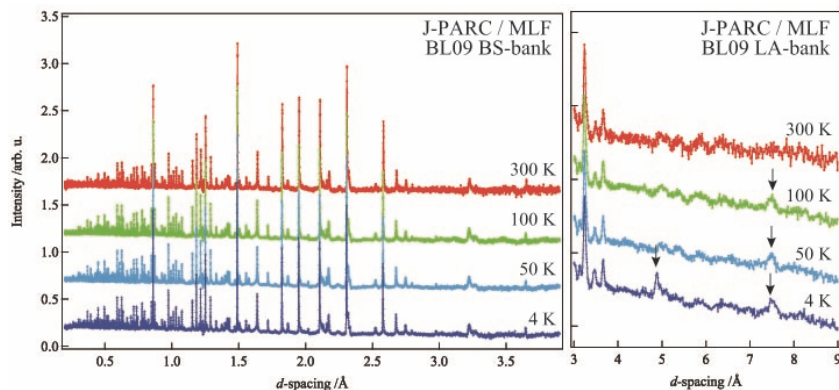


図 1. 300 K、100 K、50 K、4 K における $\text{PbCu}_3\text{Cr}_4\text{O}_{12}$ の粉末中性子回折データ。

メビウストポロジーを有する環状パラフェニレンの芳香族性の検討

藤塚守 大阪大学

シクロパラフェニレン(CPP)はベンゼン環オリゴマーであるパラフェニレンが環状に結合した分子であり、高い歪みと環状に整列した p 軌道に由来する興味深い物性により関心を集めている。われわれは、化学研究所の山子教授ならびに茅原助教らが合成した種々の CPP 類に時間分解分光等を適用することで、CPP 類の励起状態およびラジカルイオン状態などに関する新たな知見を報告してきた。¹⁾ 近年、山子グループは CPP 内にエチニル基を導入することに成功している。本化合物は π 電子の数から励起一重項状態において反芳香族性を示すが、励起三重項状態において芳香族性を示すことが予想される。本研究ではスピン多重度の変化に伴う芳香族性の変化を明らかにすることを目的とし、過渡吸収測定等を行うことで新たな知見を得たので報告する。

本研究で用いた CPP 類の分子構造を Fig. 1 に示す。これらの分子に対し、フェムト秒またはピコ秒パルスレーザーを照射することで可視近赤外過渡吸収測定を行った。

本研究で測定した[6]CPP-DPA-1 の過渡吸収スペクトルを例として Fig. 2 に示す。励起直後において 600 および 1360 nm に極大を有する過渡吸収が生じ、これらの減衰に伴い新たな吸収が 530 nm に生成することが確認された。過渡吸収変化の時定数は 1.3 ns であり蛍光寿命と一致したことから、測定された過渡吸収変化は項間交差による励起三重項生成過程であることが示された。同様に他の Fig. 1 の CPP 類についても項間交差にともなう過渡吸収変化を観測することに成功した。本測定等より項間交差に伴う過渡吸収帯の吸光係数の変化を求めたところ、メビウストポロジーを有する CPP 類は、同様の π 電子数を有する[6]-および[7]CPP よりも励起三重項における吸光係数が大きいことが示された。本結果は、スピン多重度の変化によりメビウストポロジーを有する CPP 類が芳香族性の変化を示すことを実証するものである。

文献: 1) Fujitsuka, M.; Cho, D. W.; Iwamoto, T.; Yamago, S.; Majima, T. *Phys. Chem. Chem. Phys.* **2012**, *14*, 14585-14588.

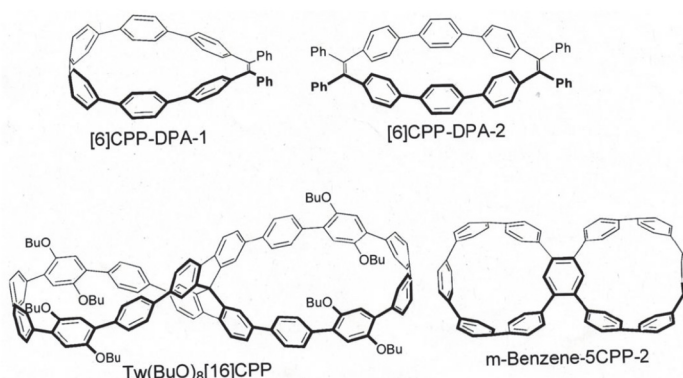


Fig. 1. 本研究で用いた CPP 類の分子構造

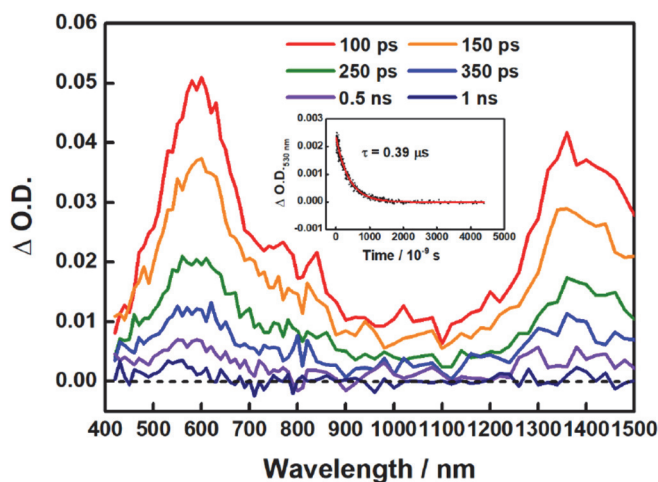


Fig. 2. 355 nm ピコ秒レーザー励起により得られた [6]CPP-DPA-1 の過渡吸収スペクトル

Study on electronic and magnetic behavior of perpendicularly magnetized cobalt ferrite films

Masaaki Tanaka Nagoya Institute of Technology

The spin-filtering effect where the spin current is generated using the electron tunneling through a ferromagnetic insulator is one of the candidates for the spin injection method. It has been reported that magnetic insulator $\text{Co}_x\text{Fe}_{3-x}\text{O}_{4+\delta}$ (CFO, $0 < x < 1$) films grown epitaxially on MgO (001) substrates with nonmagnetic metal TiN buffer layers have large perpendicular magnetic anisotropy (PMA)[1], which means that they can be applied for PMA spintronics devices. In this study, the spin-filtering effect of CFO films with PMA was investigated.

TiN (20 nm)/CFO ($x=0.53$, 3.5 nm)/MgO (1.0 nm)/CoFe (1.5 nm)/ $\{\text{Tb/Co}\}_n$ (13 nm)/Pt (5 nm) films were prepared on MgO (001) substrates using the pulsed laser deposition and electron beam deposition technique. CFO films were grown at the substrate temperature of 300°C in background oxygen pressure of 6.0 Pa. The magnetic tunnel junctions (MTJs) with a junction diameter of 6 μm were fabricated using photolithography and dry etching by an ion-milling method. This microfabrication was carried out at ICR, Kyoto University. The current-voltage and magnetoresistance measurements of the MTJs were performed using a four-probe method at various temperatures.

The current-voltage measurements indicated that the CFO/MgO layer shows good tunneling properties. The resistance increased dramatically with decreasing temperature, which indicates that the conductivity of the junction is governed by the tunneling current. Figure 1 shows the magnetoresistance of the MTJs at 100 K at the bias voltage of 70 mV. The tunnel magnetoresistance (TMR) effect caused by the magnetization switching of CFO and CoFe layers was observed. The TMR ratio was about 10 %, and the ratio of the spin-polarization caused by the spin-filtering effect of the CFO layers was about 18%.

Reference

- [1] K. Naruse, M. A. Tanaka, K. Nomura, T. Taniguchi, S. Honda, T. Ono, and K. Mibu, J. Magn. Magn. Mater., **475**, 721 (2019).

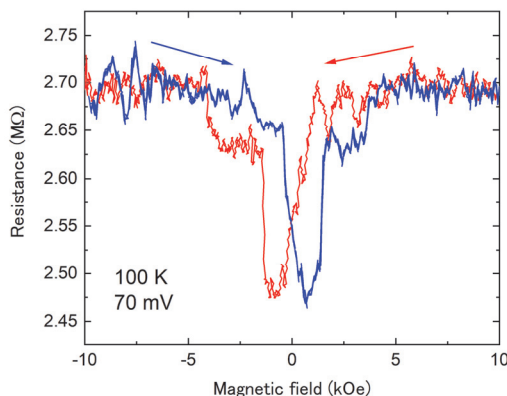


Fig. 1 Magnetoresistance of the MTJ at 100 K at the bias voltage of 70 mV.

マルチスケールシミュレーションによる p 型有機半導体材料群の電荷移動度予測

城戸淳二 山形大学

【目的】

有機半導体材料の電荷移動度は、有機 EL や有機太陽電池、有機トランジスターなどの有機半導体デバイスの性能を決定する重要な因子の 1 つである。電荷移動度解析では、Gaussian Disorder Model (GDM) が一般的に使われているが、このモデルでは、分子構造をあらわに考慮しないため、電荷移動特性と分子構造を直接関連付けることはできず、分子レベルでの解析が不可能といった問題点がある。この問題を解決する手法として、梶らのマルチスケールシミュレーションがある¹。本手法では、有機半導体分子の化学構造を頭に考慮し、任意性のある可変パラメータを用いることなく最終的な移動度を正確に予測することができる。城戸らは、最近、ヘキサフェニルベンゼン骨格を有する新規ホール輸送材料群を開発し、第三世代の有機 EL である熱活性化遅延蛍光素子の長寿命化を実現した。その特性としては、緑色 TADF 有機 EL 素子において 1000 cd/m² 時、外部量子効率 20%、1 万時間以上の素子寿命を実現している²。さらなる素子特性の向上のためには、輸送材料の高移動度化が次の課題である。本研究では、マルチスケールシミュレーションを行うことにより、これまで明確でなかった上記材料群の移動度の大きな違いを分子構造と関連づけて理解する。

【実験方法・結果】

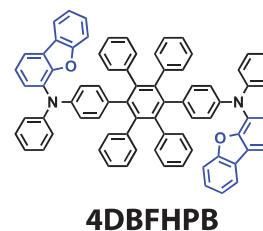
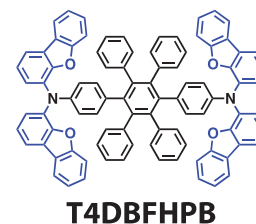
新規材料 T4DBFHPB と比較材料 4DBFHPB は Buchwald-Hartwig アミノ化反応によって合成し、各種スペクトル及び元素分析により同定した。TGA、DSC により熱物性を、UV-vis、PL スペクトル、光電子収量分光法 (PYS) により光学特性を評価した。ついで、マルチスケールシミュレーションを用い、Time-of-Flight (TOF) 法で得られた移動度とシミュレーションの比較を行った。

【結果・考察・今後の展望】

評価した結果、新たな材料 T4DBFHPB は -5.7 eV のイオン化ポテンシャル、-2.4 eV の電子親和力、2.8 eV の高い三重項エネルギー、171°C の極めて高いガラス転移点を有していた。このことから、三重項励起子を活用するリン光と TADF 型有機 EL で、高効率・長寿命が期待される。TOF 法による移動度評価では、電界強度 5.6 x 10⁵ V cm⁻¹ 時の移動度は、T4DBFHPB が 6.0 x 10⁻⁴ cm² V⁻¹ s⁻¹、4DBFHPB が 1.5 x 10⁻⁴ cm² V⁻¹ s⁻¹ であった。マルチスケールシミュレーションとの結果を比較したところ、極めて近い値を与えた。今後、得られた知見に基づき、材料の高移動度化を図る。

【参考文献】

1. H. Kaji *et al.*, *Sci. Rep.* **2018**, 8, 13462.
2. J. Kido *et al.*, *J. Mater. Chem. C* **2020**, 8, 7200.



DArP 法を用いた新規 π 共役系ポリマーの開発と 有機薄膜太陽電池への応用

尾坂格 広島大学

【研究背景と目的】

半導体ポリマーは有機エレクトロニクスにおいて重要な材料群である。我々は以前、ナフトビスチアジアゾール (NTz) を有する半導体ポリマー (PNTz4T) (Figure 1) が、有機薄膜太陽電池 (OPV) にて 10%を超える高い変換効率を示すことを報告した。本研究では、NTz にチオフェン環が二つ縮環した新規骨格であるジチエノナフトビスチアジアゾール (TNT) を合成し、これを有するポリマー (PTNT2T) を Stille カップリング重合 (SP) 法および直接アリール化重合 (DArP) 法により合成した (Figure 1)。TNT は拡張された π 共役系を有するため、これを基調とするポリマーは強い分子間相互作用を持ち、高い結晶性を有することが期待できる。

【実験結果と考察】

SP 法にて合成した PTNT2T の数平均分子量は 40~50 kDa であったのに対し、DArP 法にて合成した PTNT2T は 15 kDa 程度であった。これは、チオフェン環の β 位での副反応が起こったことなどが原因と考えられる。サイクリックボルタメトリーから見積もった PTNT2T の HOMO 準位は -5.32 eV と、PNTz4T と比べて -0.18 eV 低い値を示した。ポリマー薄膜の X 線回折測定を行ったところ、PNTz4T が Edge-on 配向を示すのに対して、PTNT2T は Face-on 配向を示すことが分かった。PTNT2T を p 型半導体、PC₆₁BM を n 型半導体として用いた OPV 素子を作製したところ、DArP 法で合成したポリマーでは変換効率は 5~6%程度であったが SP 法で合成したポリマーは変換効率 11%以上と、PNTz4T の約 9%に比べて

顕著に高い値を示した (Figure 2)。DArP 法にて合成したポリマーの特性が低い要因は、分量が低いことにあると考えられる。以上の結果から、PTNT2T は極めて有望な半導体ポリマーであることが示唆された。今後、さらに DArP 法による合成検討を行い、高量化と高効率化を目指す。

【成果報告】

<論文> (1) M. Wakioka, N. Torii, M. Saito, I. Osaka, F. Ozawa, *ACS Appl. Polym. Mater.*, **2021**, 3, 830.

<学会発表> (1) 尾坂格「分子内非結合性相互作用を駆使した半導体ポリマーの精密分子設計」, 第 69 回 高分子討論会 (オンライン)

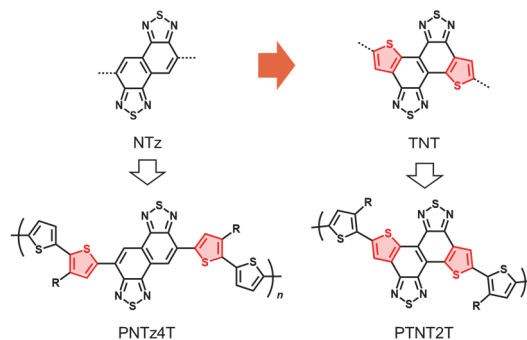


Figure 1. Chemical structure of NTz and TNT (upper), and PNTz4T and PTNT2T (lower).

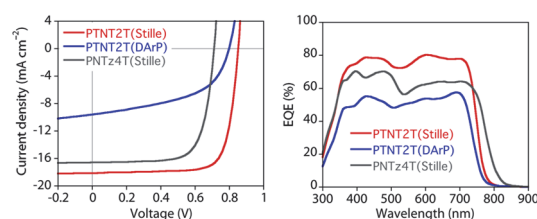


Figure 2. Current-voltage curves (left) and external quantum efficiency spectra (right) of the OPV cells based on PNTz4T and PTNT2T.

Au₂₅ スピン・価数依存強磁性単電子トランジスタ

真島豊 東京工業大学

本研究では、強磁性非対称ナノギャップ電極間に1つの Au₂₅ クラスタを化学吸着したデバイス構造を作製するプロセスを確立し、スピンに依存する単電子トンネル磁気抵抗効果を利用する Au₂₅ 強磁性単電子トランジスタを創製することを目的とした。本研究では、研究代表者のこれまでの単電子トランジスタ造形プロセスに関するノウハウ知見を生かし、電子線リソグラフィを用いて、8 nmのギャップ長を有する強磁性材料による非対称ナノギャップ電極を造形するプロセスを確立し、共同研究者の寺西教授が合成する Au₂₅ クラスタを、自己組織化プロセスによりナノギャップ電極間に1つ化学吸着することにより、強磁性ソース電極/Au₂₅ クラスタ/強磁性ドレイン電極からなる磁化の向き（平行・反平行）の組み合わせに起因したスピン・価数依存単電子トンネル磁気抵抗効果を誘起し、1電子が持つ電荷とスピンの両方を利用した次世代ナノデバイスとしての Au₂₅ 強磁性単電子トランジスタを創製することを目指した。

電子線ビームリソグラフィによりサイドゲート付き L₁₀CoPt 強磁性ナノギャップ電極の作製に向けて、Si 基板上に形成した Pt/Co 二層薄膜をアニールにより L₁₀CoPt 規則相を得ることを試みた。すれすれ入射 X 線回折法(Grazing Incidence X-ray Diffraction: GI-XRD@KEK 8B)により、GI-XRD パターンを測定したところ、アニール温度 800℃において、CoPt 001 あるいは 100 に起因する超格子反射を確認した。001 あるいは 100 ピークは、L₁₂-CoPt₃、L₁₀-CoPt、L₁₂-Co₃Pt に分離することが可能であり、それぞれの比率は、41、36、23%であることを見出した。このことより、Pt/Co 二層薄膜をアニールすることにより Si 基板上で L₁₀CoPt 強磁性体を形成できることを確認した。この試料の磁化特性を測定したところ、図 1 に示すように保磁力 2.1kOe、飽和磁化 600 emu/cm³であった。L₁₀CoPt 強磁性体が形成される本条件を用いて、L₁₀CoPt 強磁性ナノギャップ電極と、Au₂₅ 単電子トランジスタの作製にそれぞれ取り組んでいる。

成果報告（論文、学会発表等）

1. R. Toyama, S. Kawachi, S. Iimura, J. Yamaura, Y. Murakami, H. Hosono and Y. Majima, *Mater. Res. Express* **7**, 066101 (2020).
2. R. Toyama, S. Kawachi, J. Yamaura, Y. Murakami, H. Hosono and Y. Majima, *Jpn. J. Appl. Phys.* **59**, 075504 (2020).

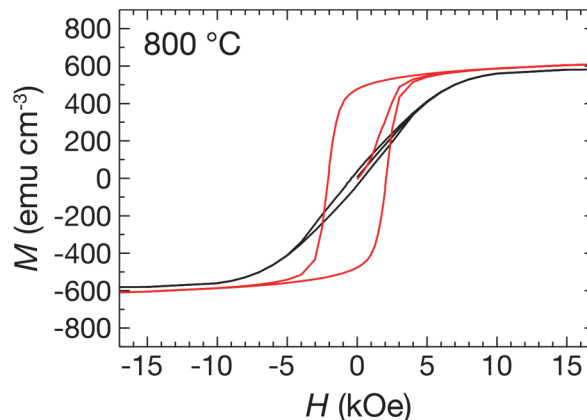


図 1 CoPt アニール膜の磁化特性

高強度レーザーと構造的媒質の相互作用による高エネルギー密度 プラズマの生成・保持に関する実験研究

岸本泰明 京都大学

【計画全体の目的】集光強度が $1\sim 10^{18-20}$ W/cm² の高強度レーザーをサブ μ m オーダの微細構造を有する物質（構造的ターゲット）に照射することにより高エネルギー密度状態のプラズマを生成するとともに、その過程において現出するプラズマの自己組織化機能や構造形成機能を制御することにより、kT オーダの準定常強磁場の生成やそれによる生成プラズマの慣性時間を超えた保持（閉込め）を実現できる可能性が提案者等のシミュレーション研究により示されている。これが実現すれば、中性子を出さない究極の核融合である陽子・ホウ素（P-B）反応など、これまでにない新たな応用が期待される。本研究では、上述の仮説を検証することを目的に、ナノ工学と材料工学を用いて構造的ターゲットを作製するとともに、これに京大化研 T6 レーザーを照射する実験を行う。このため、高アスペクト比のロッド集合体（シリコン）を作製するとともに、T6 レーザーとの相互作用特性の詳細を同定するため、ロッド集合体の上面および側面からの電子エネルギー分布を同時測定する電子スペクトルメータ (ESM) 系を構築する。

【得られた成果】(1) 構造的ターゲット(高アスペクト比ロッド集合体)の作製：R2 年度までの実績をもとに、電子線リソグラフィによる描画を含むドライプロセスであるプラズマエッチング技術を使用し、エッチング時の諸条件（蒸着クロムの膜厚、エッチング時の電圧や回数等）を洗い出す詳細なデータベースを構築するとともに、それに基づいて実験目的に沿ったロッド集合体の作製条件の最適化を行った。図1はその一例（左図：上面、右図；レーザー照射側の側面）を示し、直径 $R=1.0\mu\text{m}$ 、長さ $h=50\mu\text{m}$ （アスペクト比 $A=h/R=50$ ）のシリコン(Si)のロッドからなるレーザー照射領域 ($20\mu\text{m}\times 20\mu\text{m}$) と周辺領域 ($80\mu\text{m}\times 80\mu\text{m}$) の二重構造を有するロッド集合体（構造的ターゲット）を作製することに成功した。図中の赤領域は T6 レーザーパルス (FWHM $\sim 5\mu\text{m}$) を表し、基板を避けてロッド側面へのレーザー照射が可能であることが分かる。両サイドの直方体ブロックはレーザーアライメント時のマーキング用に今回初めて導入した。

(2) 照射配位の検討と電子スペクトルメータ (ESM) 作製：

化学研究所(井上助教)の協力を得て、MeV オーダの高エネルギー電子を計測する電子スペクトルメータ (ESM) を作製した。磁場測定の結果（図2 参照）、京大化研の保有する ESM とほぼ同一の精度で電子の温度が測定可能であることを確認した。

また、レーザーのターゲットへの照射配位について検討した結果、ロッドの上面と側面の両方向での ESM による電子温度の同時測定が可能な照射配位と設置場所の検討を行った。これらを踏まえ、R3 年度の共同研究(申請済)では、(1) (2) で準備したターゲットと ESM を用いた T6 レーザー照射実験を実施予定である。

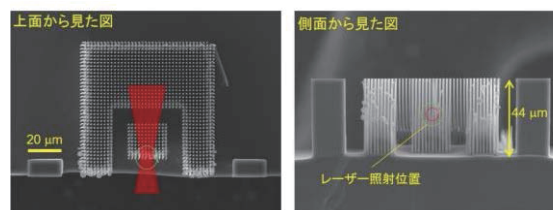


図1 シリコンロッド集合体の電子顕微鏡画像。左図はロッド軸(上面)方向、右図はレーザー照射側(ロッド側面)方向。直径 $1\mu\text{m}$ 、ロッド間隔 $2\mu\text{m}$ で配列、ロッドの局所的な空間充填率は $p\sim 0.2$ 。

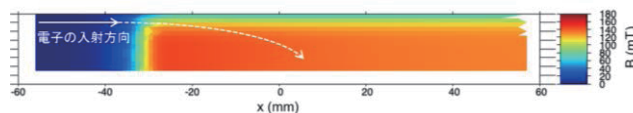


図2 作製した ESM の磁場測定結果。白線は電子の軌跡(概略)。

参考文献：岸本泰明，松井隆太郎，深見一弘，坂口浩司，福田祐仁，今寺賢志，「高強度レーザーと構造的ターゲットとの相互作用による高エネルギー密度プラズマ生成とその特性① —背景の物理と展開—」，日本物理学会 2020 年秋季大会，2020.9.8，online

酢酸菌の外的ストレス耐性における膜脂質の機能解析

豊竹洋佑 立命館大学

【目的】「酢酸発酵」は酢酸菌を代表する発酵プロセスである。内膜結合型のアルコール脱水素酵素 (ADH) とアルデヒド脱水素酵素 (ALDH) が関与し、ペリプラズム領域でエタノールを基質として酢酸が生産される。酢酸は培養液中にほぼ定量的に蓄積され、極めて強い抗菌活性を示すが、酢酸菌は高濃度の酢酸共存下でも生育を可能とする独自の生理メカニズムを有している。

酢酸菌の発酵生理と細胞構造には密接な関係があると考えられることから、その1つとして酢酸菌の膜脂質の分子機能が注目されてきた。酢酸菌細胞膜を構成する脂質分子のうち、50%以上を占める主要分子が膜リン脂質である。中でもホスファチジルコリン (PC) が高い比率で生産され、酢酸菌の酢酸ストレス耐性への関与が示唆されている。

そこで酢酸菌由来 PC 欠失株を相同組換えによって作製し、その表現型を解析することを本研究の目的の一つとした。一方、酢酸発酵の過程で特に重要な酢酸菌膜リン脂質は同定されていない。そこで、酢酸発酵の過程で変動する膜リン脂質を明らかにし、その生理的意義を解明することも目指した。

【方法・結果】研究対象には、*Acetobacter* 属酢酸菌の一種である *Acetobacter pasteurianus* SKU1108 を用いた。Phathanathavorn らの方法 [*J. Biosci. Bioeng.* (2019) 127, 690-7] に従って、ホスファチジルエタノールアミン-*N*-メチル基転移酵素 (PmtA) をコードする遺伝子を欠失させ、SKU1108 株由来 PC 欠失株 ($\Delta pmtA$) を作製した。実際に PC が欠失しているかは、培養した $\Delta pmtA$ 株から抽出した膜脂質を TLC 展開することで確認した。続いて、PC 欠失株を 4%のエタノール、または 0.4%の酢酸を含む培地で培養し、その表現型を解析した。その結果、親株と比較して $\Delta pmtA$ 株は酢酸存在下で著しい生育遅延を示した。一方、エタノール存在下では $\Delta pmtA$ 株も酢酸発酵可能であり、生育特性も親株とあまり差がなかった。以上の結果から、PC は酢酸菌が急に酢酸に晒された場合における酢酸に対する防御機構に関与しており、本菌の酢酸発酵能や酢酸発酵の過程で自身が生産する酢酸に対する応答には関与しないことが示唆された。

SKU1108 株を 4%のエタノールもしくは 0.4%の酢酸含有培地で培養し、得られた菌体から膜脂質を抽出した。続いて、抽出した脂質を TLC 展開し、プリムリン発色させたリン脂質画分を分取した。各リン脂質は湿式分解リン定量法により定量し、菌体の膜リン脂質組成を算出した。その結果、0.4%の酢酸存在下では、何も添加しなかった場合と比較して PC のみが増加した。この結果からも、PC が酢酸に対する防御機構に関与していることが示唆された。一方、4%のエタノール存在下 (酢酸発酵条件下) では、何も添加しなかった場合と比較してホスファチジルエタノールアミン (PE) のみが増加した。しかし、上記と同様に相同組換えによって作製した ADH 欠損株では、エタノール含有培地で培養しても PE の増加が認められなかった。以上の結果から、酢酸発酵の過程で特に重要な膜リン脂質は PE であることが示唆された。

セルロースの氷形成挙動の解明と表面修飾による着氷防止制御

榊原圭太 産業技術総合研究所

緒言：水が氷点下で長期間にわたり凍らない表面があれば、着氷、着霜、着雪など氷が付着する現象を防げるため、様々な産業分野に応用できる。固体表面上にポリマー鎖が高密度にグラフトされた表面、濃厚ポリマーブラシ (concentrated polymer brush; CPB) は、低い氷付着強度が保たれるといった報告例があり、防雪・防水コーティングへの応用に期待がもたれる。著者は、京都大学化学研究所の辻井敬亘教授らとともに、親水性 CPB 内部における水の過冷却特性の解明を企図して、高圧表面開始原子移動ラジカル重合 (HP-SI-ATRP) により厚膜親水性 CPB を合成し、ブラシ内部における水の示差走査熱量測定 (DSC) を遂行した。その結果、ブラシ内部の水の融解ピークに起因すると推定される、 -30°C 付近の吸熱ピークを確認した。これは、親水性 CPB 層内部における水の過冷却と見なされた。一方、グラフェンなどのナノ材料による氷核形成効果が近年報告される。天然のナノ材料としてセルロースナノファイバー (CNF) が注目されており、その親水性 CPB 表面修飾による氷核形成／抑制機能の付与は興味深い。本研究では、CPB を表面に付与した CNF (CPB 付与 CNF) を作製し、着氷防止表面の創製を目指す。

実験：(1) CNF の作製 粉末セルロース (日本製紙製 KC フロック) を *N*-methylpyrrolidone (NMP) に分散させ、遊星型ボールミルに供することで CNF を作製した。(2) 重合開始基の導入 2-bromoisobutryl bromide (1.5 等量/OH) と pyridine (2 等量/OH) を添加し、Ar 雰囲気下、室温一昼夜反応させることで、開始基導入 CNF (Br-CNF) を得た。(3) グラフト化 表面開始原子移動ラジカル重合 (SI-ATRP) 法により親水性モノマー (poly(ethylene glycol)methyl ether methacrylate (PEGMA)) のグラフト重合に供した。

結果・考察：従来、CNF 表面への CPB 付与は、予め水中で解繊した CNF を非水溶媒に置換した後に、無水条件下で重合開始基である 2-bromoisobutryl 基を導入する反応から始めるが、溶媒置換に大量の溶媒と遠心分離工程を必要とするため、大きな課題であった。本研究では、非水溶媒である NMP 中での直接解繊を試みたところ、繊維径 20nm 程度 (図 1) の高分散性 CNF 懸濁液が得られた。この懸濁液を次の反応に供したところ、2-

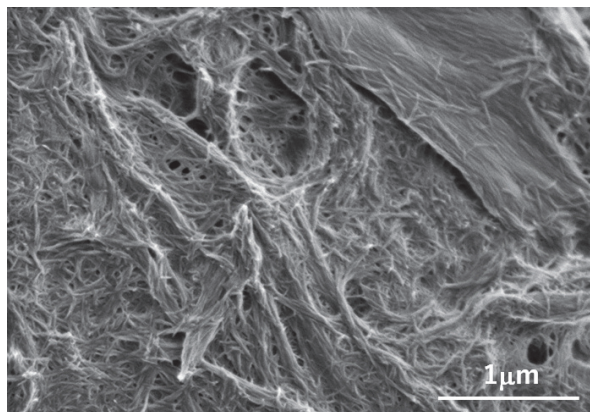


Figure 1. FE-SEM image of CNF prepared in NMP.

bromoisobutryl 基を高置換度かつ高分散で導入可能であることが、FT-IR 測定等により確認された。また、SI-ATRP 法により構造明確な PolyPEGMA ブラシを良好に導入できた。本研究で得られた材料は着氷防止表面の開発に寄与するものと期待される。

ダイヤモンドの数ナノレベルにおける表面近傍の NV 中心作製

徳田規夫 金沢大学

【緒言】

ダイヤモンド中の単一窒素 - 空孔複合体 (NV) 中心は優れたスピン特性及び光学特性を有する。他材料と比べ特筆すべき点は、NV 中心では単一スピンを室温において光検出・操作できる点である。その単一スピンをプローブとし、単一 NV 中心を用いた磁気センサ、電場センサ、温度センサに関して、近年、優れた実証研究がなされてきた。NV 中心のセンサ応用において、NV 中心は感度向上のため数ナノレベルの浅い領域に存在していることが望ましい。しかし、ナノレベルでの表面付近では、センサとして使える電荷状態が -1 価に荷電した NV^- の電荷状態が不安定になることや、スピンコヒーレンス時間の短時間化によりセンサ感度が著しく低下するなど、重要な克服すべき課題がある。この原因の有力な候補の一つとして表面付近の常磁性欠陥や不純物の存在が考えられる。本提案では、課題克服のため常磁性欠陥の極めて少ない原子レベルでの表面平坦化合成技術を用いることによる、表面から数ナノレベルの浅い NV 中心作製を目指した。

【実験と結果】

ダイヤモンドにおいて、ある CVD 合成条件を満たすと、数十 μm 四方の面積において、原子レベルでフラットな表面を持つ試料を作成することができる。成膜プロセスの提案や合成条件における窒素濃度の制御の条件出しを、共焦点レーザ顕微鏡によって行った。我々は原子レベル平坦となっていると考えられる領域において、レーザ掃引した。ここでスポットの形状から単一 NV 中心と思われる蛍光は複数観測されたが、蛍光強度もバルク中の NV 中心よりも 1 桁ほど弱かった。短時間で蛍光が消滅してしまうため、現状では ODMR やパルス波測定、PL スペクトル測定など NV であることを証明できる測定が実現していないが、その実現に向け議論を継続している。課題として、新たな表面処理等を施して更なる安定化を行い、それらの測定を目指している。

また、共同研究成果として、我々はドレスト状態生成によるスピンコヒーレンス時間の桁違いの長時間化を実現し、それを用いて温度感度向上の実証研究を行った[1]。ダイヤモンド中の NV 中心は、細胞内部の温度分布の不均一性や局所的な温度変化によって引き起こされる細胞の生理機能の研究における高感度量子温度センサとしての応用が期待されている。また、Autler-Townes Splitting (ATS) 法により生成したドレスト状態では磁場ノイズによる共鳴周波数の変化の影響を受けにくくなり、コヒーレンス時間が長くなることが知られ、温度センシングにおける高感度化が期待される。今回、我々は金沢大グループで作製した、多数の NV 中心からなるアンサンブル系の試料で ATS 法によりドレスト状態を生成し、その共鳴周波数の温度依存性を測定した。ドレスト状態の共鳴周波数の温度変化が理論とほぼ合う結果が得られ、ドレスト状態の温度センサとしての有用性を示した。

【成果報告】

[1] 中村将也, 山下峻吾, 森下弘樹, 藤原正規, 大木出, Ernst David Herbschleb, 徳田規夫, 水落憲和、第 68 回 応用物理学会 春季学術講演会、2021 年 3 月 18 日

ダイヤモンド中の NV 中心スピンの電氣的制御と電氣的検出

牧野俊晴 産業技術総合研究所

【緒言】ダイヤモンド中の複合欠陥である窒素 - 空孔複合体 (NV) 中心は、量子科学技術分野において研究が精力的に行われ、優れた特性が明らかにされてきた。特に、NV 中心は固体中のスピンとしては群を抜く長いスピンコヒーレンス時間 (T_2) を持つことにより高い感度が実現し、磁場、電場、温度、圧力、pH などの高感度センサとして幅広い分野での応用が期待される。

【実験と結果】

NV 中心は高感度な量子センサとしての応用が期待されているが、従来の量子センサでは、高感度化とダイナミックレンジを広げることを両立することに難点があった。今回、パルス間隔の異なるパルス系列を組み合わせ、それをベイズ推定によるアルゴリズムにより最適化することにより、高い感度を維持しつつ、室温における単一 NV 中心において 7 桁程度のダイナミックレンジを実現した (図 1, [1])。これは単一 NV 中心の低温 (8 K) における最高報告値より、2 桁も広い値である。また、パルス間隔の異なるパルス系列を組み合わせた研究では、測定時間に対する感度の依存性が古典での限界を超えるようにも見られる結果も報告され、学術的に関心が持たれていたが、今回我々はこの現象についてもシミュレーションにより現象の解明を行った。今回考案した手法は他の量子センサにも適用でき、量子センサの計測範囲を、感度を維持しつつ広げた今回の成果は、量子センサの応用環境を広げる成果として期待される。また、測定対象物との間の相互作用の大きさは距離に大きく依存するため、今回の成果は測定空間の領域を広げることにもつながると期待される。

また、これまで産総研グループが合成した n 型ダイヤモンド中の NV 中心を用いて、単一 NV ダイヤモンド量子センサで世界最高磁場感度を実現していたが、今回、リンドーブ n 型ダイヤモンドにイオン注入を行って作製した NV 中心の T_2 が、ドーブしていない試料中に同じ条件で作製した NV 中心の T_2 に比べ長くなることも実証した[2]。イオン注入法は局所的な NV 中心作製に重要な技術であり、将来の集積化にとって重要である。また、電荷状態制御などの成果もまとめることができた。[3]

【成果報告】

- [1] E. D. Herbschleb, H. Kato, T. Makino, S. Yamasaki, N. Mizuochi, *Nature Communications*, 12, 306 (2021).
- [2] A. Watanabe, T. Nishikawa, H. Kato, M. Fujie, M. Fujiwara, T. Makino, S. Yamasaki, E. D. Herbschleb, N. Mizuochi, *Carbon*, 178, 294-300 (2021).
- [3] T. Makino, H. Kato, M. Shimizu, M. Hatano, N. Mizuochi, *Semiconductors and Semimetals*, 103, part 1, Chapter 5, Pages 137-159 (2020). Edited by C. Nebel, I. Aharonovich, N. Mizuochi, M. Hatano, Elsevier.

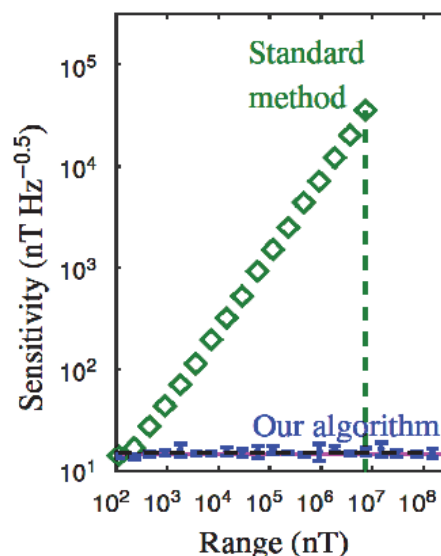


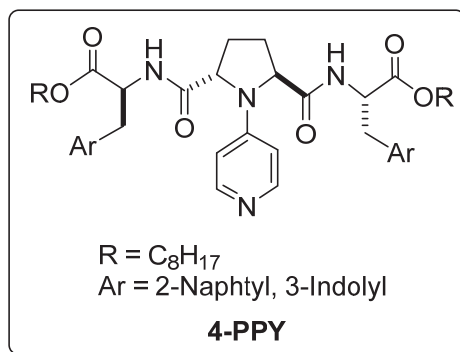
図 1、測定結果 (青点) と既存の手法の結果 (緑点) の比較図。縦軸は感度。横軸は測定範囲で単位はナノテスラ (nT)。

4-ピロリジン-ピリジン型分子触媒による 化学選択的アシル化反応の理論的解析

山中正浩 立教大学

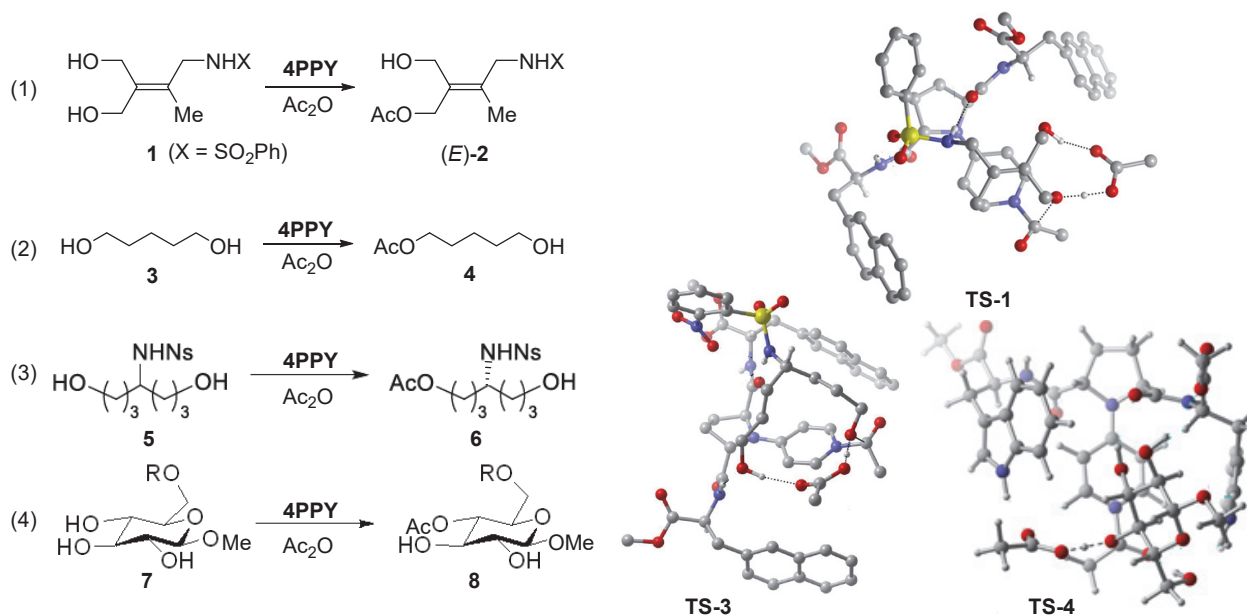
【目的】

我々は本申請課題を通して、川端らによって開発されたピロリジノピリジン触媒 (**4-PPY**) の触媒機能について分子レベルで理解することを目的として研究を進めてきた。これまでに、(1) 四置換アルケンジオールの幾何異性選択的アシル化、(2) 1,5-ヘキサジオールの化学選択的アシル化、(3) 4-ノシルアミノ-1,7-ヘキサジオールの不斉非対称アシル化、(4) β -L-グルコース誘導体に対する 4 位選択的モノアシル化について理論的検討を行っており、本年度は **4-PPY** の触媒機能について総括した。



【結果・考察】

(1) ~ (4) について、**4-PPY** のエステル部位をメチルエステルとし、酸無水物に Ac₂O を用いた計算モデルによって遷移状態 (TS) の探索を行い、いずれの場合も実験事実と合致した計算結果を得た。主生成物を与える TS 構造の共通した特徴として、**4-PPY** のアミド基と基質の配向基 (NH 基や OH 基) との間に強い水素結合が形成している。さらに配向基を認識点として、エステル基や選択性インドリル基などの **4-PPY** 上の置換基との間に水素結合ネットワークを構築することによって、TS を安定化していることが分かった。**4-PPY** が有する特異的な分子認識能は、この基質/触媒間の水素結合ネットワークの効果的な構築に由来しており、TS 構造を確認すると、アシル化する O 原子と認識点までの距離は約 5Å であることが分かった。実験的にも、配向基から反応点までの距離が約 5Å となる基質において、最も高い選択性が発現することが見出されている。これは、**4-PPY** の立体制御能が立体障害ではなく分子認識に基づくことを示しており、一連の研究を通して、遠隔位不斉誘導の戦略として、分子認識による特定の TS の安定化が有効であることが分かった。



動的不斉の発現を基盤とする不斉極性転換型炭素—炭素結合形成反応の開発

森山克彦 千葉大学

現代の有機合成化学において、グリーンサステナブルケミストリーに基づいた反応開発による新規機能性有機分子の創製の研究は重要課題である。申請者は、これまでに官能基極性転換型有機反応剤となる新規超原子価ヨウ素化合物の創製研究に従事してきた。特に、複素環骨格を有する窒素—ヨウ素結合型超原子価ヨウ素化合物の合成に成功し、これを利用した複素環化合物の直截的アミノ化を伴う二重官能基化反応を達成した(*Org. Lett.* **2012**, *14*, 946, *Chem. Commun.* **2015**, *51*, 2273, *Chem. Commun.* **2018**, *54*, 4258)。一方、超原子価ヨウ素化合物を利用したエナンチオ選択的炭素—炭素結合形成反応は挑戦的課題である。これまでの方法では、光学活性な遷移金属錯体を触媒とする反応が殆どであり、遷移金属フリーな不斉炭素—炭素結合形成反応は未だ未開拓である。本研究では、動的な不斉場を構築する動的な不斉エノラトを経由した不斉記憶型結合形成反応による極性転換型結合形成反応を検討した。

アミノ酸から誘導化した N-Boc(MOM)アミノ酸(1)を基質として、ジアセトキシードベンゼン及びジアリルヨードニウム塩を用いたα位アセトキシ化及びα位アリール化を行ったところ目的の化合物(2)を得る事ができ

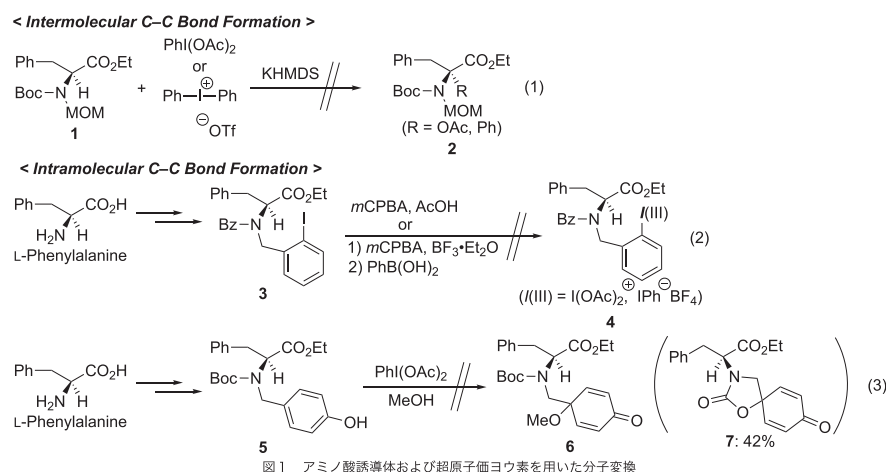


図1 アミノ酸誘導体および超原子価ヨウ素を用いた分子変換

なかった(図1-式1)。また、分子内環化反応の原料である超原子価ヨウ素化合物の合成の検討を行なった。前駆体(3)を効率的に合成する事ができたものの、対応する超原子価ヨウ素化合物(4)を得る事ができなかった(図1-式2)。さらに、フェノール誘導体(5)のジアセトキシードベンゼンによる脱芳香族化を検討したところ、目的の化合物(6)は得る事ができず、スピロジエノン(7)が42%収率で得られた(図1-式3)。本研究達成するために、引き続き検討を行う。

一方、動的な結合軸を有するアニリン型超原子価ヨウ素の創製研究を検討し、(ジアセトキシ)N-ベンゾイル-N-メチル-2-アミノヨードベンゼンの合成に成功した。さらに、この反応剤を用いたスルホンアミド(8)の直截的分子内アミノ化反応を行ったところ、反応は円滑に進行し、目的のピロリジン誘導体(9)が高収率で得られた(図2)。

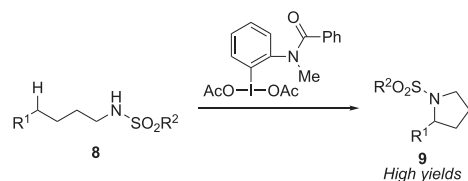


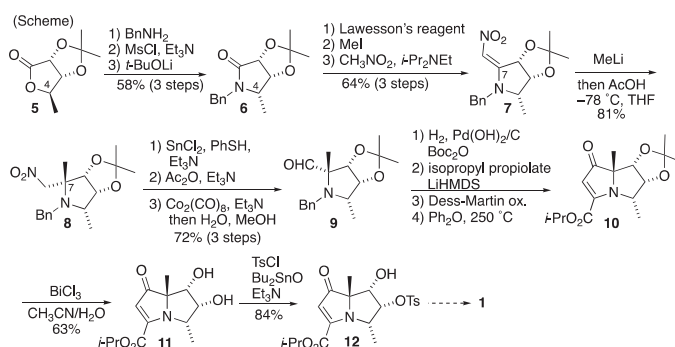
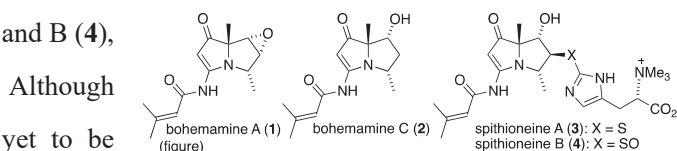
図2 動的超原子価ヨウ素を用いたスルホンアミドの直截的分子内アミノ化反応

Studies on the enantioselective total synthesis of marine natural product bohemamines and their derivatives

Tomoyuki Yoshimura Kanazawa University

Bohemamines A (**1**) and C (**2**), which contain tetrasubstituted carbon in the pyrrolizidine framework, were isolated from marine *Streptomyces spinoverrucosus* strain SNB-048 (figure).¹⁾ Compound **1** is thought to be a biosynthetic intermediate of spithioneines A (**3**) and B (**4**), which possess an amino acid, L-ergothioneine. Although significant biological activities of **1–4** have yet to be reported due to limited research, L-ergothioneine has attracted attention due to its relationship with chronic inflammatory diseases such as rheumatism and Crohn disease. Compounds **1–4** have potential for discovering new biological activities against inflammatory diseases. To synthesize bohemamines and their derivatives, we initially planned the synthesis of bohemamine A (**1**).

The synthetic studies on **1** began from chiral lactone **5**²⁾ (Scheme). Amidation of **5** with benzylamine and subsequent mesylation afforded *sec*-alcohol. Then intramolecular cyclization with inversion at C (**4**) gave lactam **6**. The lactam was converted into nitroolefin **7** by thiolactamization, formation of sulfonium



salt with iodomethane, and condensation with nitromethane. Stereoselective construction of tetrasubstituted carbon was achieved by convex-face selective 1,4-addition reaction of MeLi to nitroolefin **7**. Treatment of nitroolefin **7** with MeLi in THF at -78°C followed by the addition of acetic acid gave pyrrolidine **8** in 81% yield as the sole product. Reduction of nitro compound **8** into oxime followed by *O*-acetylation of the resultant oxime and hydrolysis of *O*-acetyl imine provided aldehyde **9**. Aldehyde **9** was converted into pyrrolizidine **10** in four steps: 1) change of the *N*-protective group from benzyl to Boc, 2) addition of the propiolate ester at the aldehyde, 3) oxidation of the resultant *sec*-alcohol, and 4) cyclization under high temperature. Deacetalization of **10** with protic acids such as HCl and TFA was problematic due to stereoisomerization of **11**. By contrast, deacetalization with BiCl_3 gave diol **11** in 63% yield. Regioselective tosylation of diol **11** gave tosylate **12** in 84% yield. The conversion from **12** to **1** is currently being investigated.

References

- 1) Fu, P.; MacMillan, J. B. *Org. Lett.* **2015**, *17*, 3046-3049.
- 2) Suh, H.; Wilcox, C. S. *J. Am. Chem. Soc.* **1988**, *110*, 470-481.

再生可能資源・木質バイオマスの先端化学材料への効率的変換法の開発

秦野修 奈良県立医科大学

目的:

研究代表者は、カルボニル基をもつ化合物（ステロイド等）を誘導体化し、化学研究所の FT-ICR MS 装置を用いることにより、極めて高分解能（質量分解能 100 万）かつ高感度な質量分析検出、及び、イメージング解析を行なう系を構築している。又、スギ木幹部の光学顕微鏡切片の組織切片上で化学反応を行い、反応行程の前後変化を、光学/蛍光顕微鏡、及び、電子顕微鏡（無蒸着 SEM 観察）レベルで追跡する実験系を構築した。本年度は、これらの手法に加えて、木材の主要成分である Lignin, Cellulose 等のイメージング検出が可能な、顕微 FT-IR イメージング実験系の構築を行うことにより、化学研究所・中村研究室が行っている再生可能バイオマス資源であるスギ等の人工森林木材から有用化合物生産を行う研究に適用することを目的として行った。

実験方法、実験結果、考察:

本年度は、新たに顕微 FT-IR イメージング実験系の構築を行ない、木材の主要成分である Lignin, Cellulose, Hemicellulose の含有量を、スギの木口断面において晩材部と早材部との比較を行った。スギ木幹（心材部）の木口断面の光学顕微鏡切片（15 μm 厚）を作成して、FT-IR の ATR 法、透過法で、木材の主要成分である Lignin, Cellulose, Hemicellulose の検出を行った。又、顕微 FT-IR 機（日本分光 IRT-7200：最高空間分解能 1 μm ）を用いて、50 μm 空間分解能で晩材部、早材部の境界領域を含む 400 μm x 1200 μm 平面（50 μm 平方の FT-IR スペクトルを 8 X 24 個スキャン）の顕微 FT-IR イメージング測定（透過法）を行なった後、Lignin（1265.1 cm^{-1} , 1511.9 cm^{-1} ）、Cellulose(+Hemicellulose)（1029.8 cm^{-1} , 1160.9 cm^{-1} , 1103.1 cm^{-1} , 1153.2 cm^{-1} ）、Hemicellulose（810.0 cm^{-1} , 1731.8 cm^{-1} ）の各スペクトル値を平面ヒートマップ表示を行った結果、Lignin, Cellulose, Hemicellulose の 3 物質ともに、晩材部において、早材部よりも含有量が多い結果を得た。又、晩材部と早材部における含有量の差は、Lignin と Cellulose において、Hemicellulose における差よりも大きかった。今後は、更に空間分解能を高めると共に、透過法のみならず、切片の厚さの影響を受けない ATR 法を用いて、Lignin, Cellulose, Hemicellulose 等の含有量の変化をイメージング解析する系を確立すると共に、共同研究者、研究協力者の中村、磯崎らが行っている触媒を用いたスギ等の木質バイオマス分解系の分解過程の解析に、顕微 FT-IR イメージング法を導入すると共に、他のイメージング検出系（MS Imaging, SEM, 超解像顕微鏡法など）と組み合わせて、解析を行っていききたい。

成果報告:

Osamu Hatano, Masumi Hayazaki, Akie Hamamoto, Hiroshi Takemori, Hikaru Takaya, Takafumi Shanoh, Ken Ohnishi, Masaharu Nakamura. CLEM imaging of rhododendrol-induced leukoderma in zebrafish and catalytic oxidation of Japanese cedar wood. ABiS Symposium: Forefront and Future of Electron Microscopic Imaging. Feb.14-15, 2020 Okazaki, Japan

Armouti M, Winston N, Hatano O, Hobeika E, Hirshfeld-Cytron J, Liebermann J, Takemori H, Stocco C. Salt-inducible Kinases Are Critical Determinants of Female Fertility. Endocrinology. 2020 Jul 1;161(7):bqaa069. doi: 10.1210/endocr/bqaa069.

Determine the three-dimensional structure of ^{13}C labeled α -synuclein(61-95) in the Langmuir-Blodgett film and supported phospholipids bilayers by pMAIRS FT-IR

Chengshan Wang Middle Tennessee State University

A. Objectives:

1. ^{13}C labeled α -syn(61-95) containing residues 61-95 of α -synuclein will be synthesized and purified.
2. Screen the conformation and orientation of specific amino acid residue of α -syn(61-95) in Langmuir-Blodgett film.
3. Screen the conformation and orientation of specific amino acid residue of α -syn(61-95) in supported phospholipids bilayers.

B. Experimental methods:

Peptide of ^{13}C labeled α -syn(61–95) at position 93G was synthesized via solid phase (Fmoc) chemistry and purified by semipreparative reversed-phase high-performance liquid chromatography (RP-HPLC) on Waters Breeze 2 separation system equipped with 1525 EF binary pump. The success of the synthesis and the purity of the peptide were confirmed by a Waters SYNAPT q-TOF tandem mass spectrometer. The surface pressure-area (π -A) isotherm of α -syn(61–95) were conducted in a A Kibron μ trough. The Langmuir-Blodgett (LB) films of α -syn(61–95) were made by transferring the α -syn(61–95) Langmuir monolayers to quartz slides and silicon (Si) slides under the surface pressure 10 mN/m. The circular dichroism (CD) spectra of the LB films of the ^{13}C labeled α -syn(61–95) were measured by a JASCO J-810 spectropolarimeter. p-Polarized Multiple-Angle Incidence Resolution Spectroscopy (pMAIRS) measurements were performed on the Nicolet IS50 FT-IR spectrometer (Thermo Scientific, Waltham, MA) equipped with a pMAIRS accessory. The LB film monolayer of the ^{13}C labeled α -syn(61–95) at position 93G on Si substrate was put in the pMAIRS accessory and the IR beam transmitted through the sample.

C. Experimental results:

The ^{13}C labeled α -syn(61–95) was synthesized and purified. Figure 1A shows the π -A isotherm of the ^{13}C labeled α -syn(61–95) and the isotherm is very similar to that of the unlabeled α -syn(61–95). This is not a surprise because replacement of a ^{12}C by ^{13}C in the backbone carbonyl (i.e., C=O) should not change the overall biophysical behavior of the peptide, which contains hundreds of carbon atoms in it. Thus, the CD spectrum of the ^{13}C labeled α -syn(61–95) is also similar to that of unlabeled peptide as shown in Figure 1B. For the LB films of the ^{13}C labeled α -syn(61–95), two negative peaks at 222 and 208 nm in addition to one positive peak at 192 nm are detected. Therefore, the ^{13}C labeled α -syn(61–95) also transforms to α -helix at the

interface. On the other hand, pMAIRS was used to determine the tilted angle of the axis of α -syn(61–95) at 93G and is very different to that of the unlabeled peptide. As shown in Figure 1C, The In-plane Spectrum (S_{IP}) result of the ^{13}C labeled α -syn(61–95) was shown as the top curve in Figure 1C. Both regular amide I and II bands were detected at 1655 and 1535 cm^{-1} , respectively. A very strong ^{13}C amide I band was also detected at 1625 cm^{-1} in the S_{IP} . The position at 1625 cm^{-1} shows that the 93G is in α -helical conformation in the LB film. In addition, the ^{13}C amide I band in the S_{IP} result is even more intensive than the regular amide I band which is the absorption sum of all the other thirty-four residues in the sequence of α -syn(61–95). Such an intensive ^{13}C amide I band suggests a very small tilt angle (i.e., parallel orientation) of the ^{13}C amide I transition moment. The out-of-plan Spectrum (S_{OP}) shown in the bottom curve of Figure 1C also detects the amide I band at 1659 and 1645 cm^{-1} . More importantly, the ^{13}C amide I band at 1625 cm^{-1} was not detected in the S_{OP} result, even though the ^{13}C label does exist at position 93G. According to the selection rule of pMAIRS, the tilt angle of the ^{13}C amide I transition moment at 93G is $\sim 0^\circ$. Because the tilt angle of the axis of α -helix is equal to that of the ^{13}C amide I transition moment, the tilt angle of the axis of α -helix at 93G is also $\sim 0^\circ$.

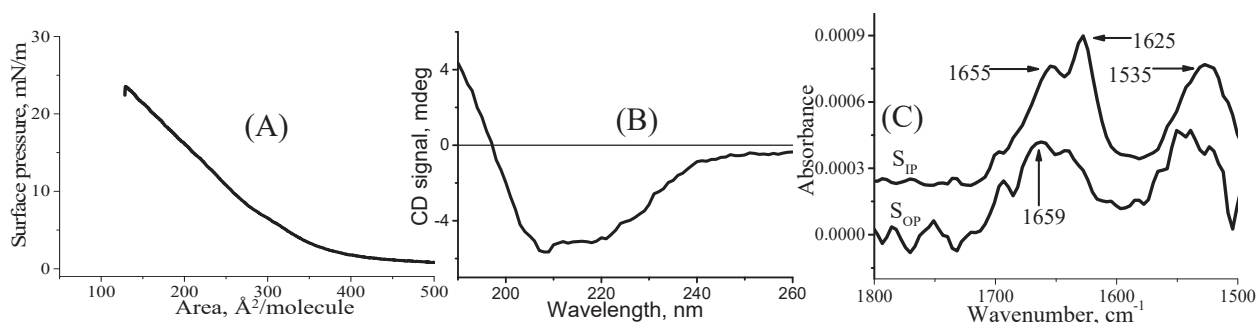


Figure 1. (A) Surface pressure-area isotherm of the ^{13}C labeled α -syn(61–95) on pure water, (B) CD spectra of the LB films of the ^{13}C labeled α -syn(61–95) on quartz slides. (C) p-MAIRS results of the LB monolayer of the ^{13}C labeled α -syn(61–95) transferred under 10 mN/m.

D. Discussion

X-ray crystallography and NMR are two major methods to determine protein's structure. However, neither of them can elucidate the high resolution structure of membrane proteins, which weighs ~ 30 - 35% of the total proteins, in monolayer structure. Dr. Wang and Dr. Hasegawa are developing a method for membrane proteins in monolayer structure with residue resolution by pMAIRS, which will be a supplement to X-ray crystallography and NMR.

E. Publication.

One paper about Figure 1 was submitted to *Colloids & Surfaces B: Biointerfaces*. Positive comments was received and the revision has been submitted for the final decision.

Hydrophilic dendrimers as additive for polyvinylidene difluoride based membranes

Mona Semsarilar University of Montpellier

This project is a collaboration between Dr. Mona Semsarilar from University of Montpellier (France), Prof. Shigeru Yamago and A/Prof. Yangtian Lu from University of Kyoto (Japan).

Objectives:

The aim of this project is to prepare porous polyvinylidene difluoride (PVDF) membranes with hydrophilic character for water filtration. PVDF is hydrophobic and incompatible (immiscible) with all other polymers apart from polymethyl methacrylate (PMMA). PVDF is normally blended with hydrophilic polymers in order to confer hydrophilicity to the prepared membranes. However, due to the immiscibility of PVDF with other polymers this method would result in membranes with inhomogeneous and short-lived hydrophilic character. To solve this major problem in preparation of hydrophilic PVDF membranes, the idea here is to synthesize an amphiphilic block copolymer where one block is a linear hydrophobic PMMA or PVDF (miscible with the membrane forming high molecular weight PVDF) and the other block is a dendritic hydrophilic polymer. The linear PMMA or PVDF block will fully blend with the high molecular weight PVDF and allow the homogeneous dispersion of the hydrophilic polymer segments within the PVDF matrix.

Experimental methods and results:

As per the original design of the project, Prof. Yamago's team was in charge of synthesis of the

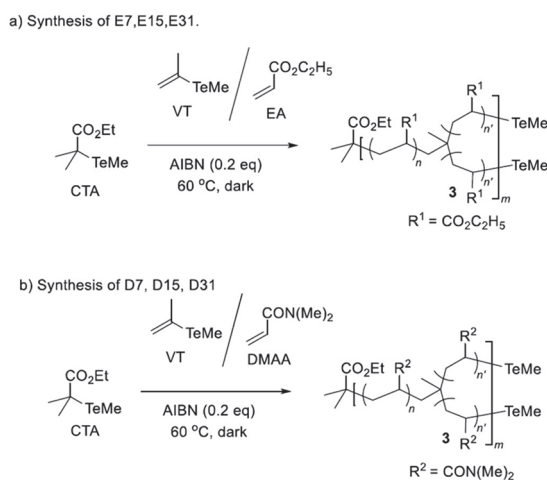


Figure 1. Synthesis route of a) hyperbranched ethyl acrylate (HB-PEA: E7, E15, E31), b) hyperbranched *N,N*-dimethyl acrylamide (HB-PDMAA: D7, D15, D31).

amphiphilic dendritic block copolymers. These block copolymers are prepared using TERP controlled polymerization (Figure 1). Up to now, a library of six polymers (fully characterized) have been prepared (Table 1). Now a second library containing three other block copolymers are in the course of being prepared.

Meanwhile the French team has been studying the blending properties of the synthesized block copolymers with the high molecular weight PVDF used for membrane fabrication using thermogravimetric analysis (TGA) and differential scanning calorimetry (DSC). The block copolymer samples that gave better blends (samples D7, 15 and 31) with PVDF were used to prepare the porous membranes using solvent/ non-solvent phase inversion method (SNIPS). The

Table 1. Characterization of HB-PEA and HB-PDMAA.

Sample number	Composition ratio [VT]/[EA/DMAA]	Generation (G)	$M_n(\text{Theo}) (\times 10^4)$	$M_n(\text{SEC}) (\times 10^4)$	\bar{D}	$M_n(\text{mals}) (\times 10^4)$
E7	7/475	3	5.0	3.7	1.71	6.5
E15	15/479	4	5.2	3.3	1.73	6.4
E31	31/475	5	5.3	2.6	1.93	6.8
D7	7/475	3	5.0	4.4	1.73	5.2
D15	15/479	4	5.2	3.5	1.98	5.6
D31	31/475	5	5.3	1.9	1.82	5.3

performance of the resulting membranes were verified via a dead-end filtration set-up. Currently, aging tests are being performed to evaluate how long the added copolymers would stay in the membrane matrix. In the next step, the same sequence of experiments will be carried out on blend samples that would be prepared using the polymers currently being synthesized in the team of Prof. Yamago (the second sample library).

Publications:

The start of this collaborative project was March 2020, which was coincided with COVID19 pandemic. As in both countries (France and Japan), travelling were banned and in France universities were closed for long period between March-June and October-December, 2020, the proposed tasks in the project could not be carried as planned. Despite these restrictions, we decided to start the collaboration and do as much as we could in each team (with some imposed modifications) and exchange samples via post. This has affected the progress of the project vastly. Up to date we have managed less than 50% of the work initially planned. Regardless of the unfortunate circumstances, both partners are enthusiastic about the project and are committed to carry on with the collaboration and take the project to completion. We are positive that during the course of 2021 we will be able to complete the study and prepare an article based on the work performed. We hope that we would be able to present this joint work to the scientific community in the next coming year.

Resolving percolation dynamics responsible for mechanical reinforcement in polymer nanocomposites under uniaxial stretching

Tadanori Koga Stony Brook University

Introduction. The addition of nanoparticles (NPs) to a polymer matrix impacts the mechanical properties of polymers, leading to a significant increase in the modulus (“reinforcement”). Understanding the reinforcement mechanisms is necessary to improve the design of advanced polymeric materials in the future. There is growing evidence to suggest that mechanical reinforcement in polymer nanocomposites (PNCs) occurs when NPs with polymer chains adsorbed (physically) on filler surfaces percolate over large length scales [1]. At high NP loadings, the bound chains are expected to adsorb on more than one NP simultaneously, resulting in “bridges” that effectively transmit the stress from a weak and deformable polymer matrix to a strong and hard filler. A critical, but unanswered question in the relatively mature field arise: What are the effects of external stimuli on the structure-dynamics-property relationship? To tackle this, we propose to use a model PNC where silica (SiO_2) nanoparticles can be dispersed in a (poly(2-vinylpyridine) (P2VP) matrix with filler loadings up to 27%. The model PNCs are subjected to uniaxial elongation at high temperatures above the glass transition temperature of P2VP ($T_g \sim 105^\circ\text{C}$). We aim to understand the structures and dynamics of filler network in the melts using small-angle X-ray scattering (SAXS) and X-ray Photon correlation spectroscopy (XPCS), mapping them out as a function of temperature, stretching ratio, filler loading, filler size, and molecular weights of the matrix polymer. However, due to the COVID, all allocated SAXS/XPCS experiments under uniaxial elongation at National Synchrotron Light Source-II (NSLS-II, USA) had been cancelled since March 2020 (until at least Aug. 2021). Here I summarize the preliminary XPCS results for the model PNCs without uniaxial stretching.

Experimental. SiO_2 NPs with an average radius of $R_N = 9.1$ nm was dispersed in a P2VP matrix with molecular weight $M_w = 38$ kg/mol (we hereafter assign it as P2VP38k). A series of PNCs with increasing volume fraction of NPs ($\phi = 0.01, 0.06, 0.16$, and 0.27) were prepared by dropcasting and subsequent solvent evaporation [1]. SAXS measurements were also conducted at 160, 170, and 180°C at Beamline 11-BM of National Synchrotron Light Source-II (NSLS-II, BNL). The details of the SAXS experiments have been described elsewhere [1]. Temperature dependent XPCS measurements were conducted at Beamline 11-ID, NSLS-II at three temperatures of 160, 170, and 180°C . A partially coherent X-ray beam with energy of 9.65 keV (wavelength of $\lambda = 0.128$ nm) and unattenuated flux of 3×10^{11} photons/s was used. The beam size was approximately $40\ \mu\text{m} \times 40\ \mu\text{m}$ (full width half maximum).

Results. The collective NP dynamics in the P2VP matrix are investigated with in-situ XPCS to measure the local motions of “markers” (i.e., SiO_2 NPs which have a high X-ray contrast with the polymer) over a wide range of q space ($q = 0.05 - 0.4\ \text{nm}^{-1}$) and timescales ($10^{-3} < t < 10^3$ s). The XPCS intensity-intensity autocorrelation function g_2 is calculated from the intensity of pixel variations in the time series of the speckle patterns collected during the measurement. The experimentally determined $g_2(q, t)$ is fit to a Kohlrausch-William-Watts (KWW) type exponential in the form of Eq. (2) with a relaxation time, τ , and stretching exponent, α . The Seigert factor (B), which depend on the experimental set up, and the baseline (c) is additional fit parameters [2]:

$$g_2(q, t) = B \left(\exp \left(-2 \left(\frac{t}{\tau} \right)^\alpha \right) \right) + c, (1)$$

An example of dynamics resolved by XPCS in terms of $g_2(q, t)$ and the fit with Eq. (1) are shown in Figure 1a for the PNC with P2VP38k. Here, g_2 is normalized by B and the baseline for clarity ($g_2 - c/B$). Over the limited amplitude (vertical) scale probed in the measurement (shown on a linear scale in Figure 1a), the correlation functions decay on an observable time scale and can be reasonably well fit to Eq. (1) with $\alpha = 1 \sim 1.5$. It is likely that $\alpha = 1$ can be justified for the $\phi = 0.01, 0.06$, and 0.16 samples regardless of q used in this study, while compressed relaxations ($\alpha > 1$) are seen for the P2VP38k samples at $\phi = 0.27$.

From Figure 1b one sees that the τ values for the P2VP38k samples increase with ϕ . Figure 1b also shows the q dependence of τ for the P2VP38k series at 180 °C. For the dilute P2VP38k sample at $\phi = 0.01$, one sees $\tau \sim q^{-\gamma}$ (q is the scattering vector) with $\gamma = 2$, which corresponds to a simple diffusive motion. We found that the collective dynamics detected by XPCS in the dilute NP limit tracks the self-diffusion of individual NPs coated with the bound polymer layer (the thickness is about the radius of polymer gyration) embedded in the viscous polymer matrix.

On the other hand, it is clear from Figure 1b that the collective NP dynamics in the PNCs qualitatively deviate from the simple diffusive behavior as NP loading increases. It is notable that the relaxation time grows monotonically with decreasing wavevector except for the 16% and 27% samples in the q region around the peak of the collective static structure factor $S(q)$ (obtained from SAXS) at $q \sim q^*$. In addition, τ becomes less dependent on q at the higher loadings for high and intermediate wavevectors, but shows an interesting *non-monotonic* variation of the local strength of the q -dependence at the lowest wavevectors probed. Further data analysis demonstrated that τ across all temperatures are collapsed onto a single master curve as a function of the reduced dimensionless wavevectors (i.e., qD) with τ normalized by its value at $qD = 4$ (arbitrary choice) within the experimental uncertainties. This likely reflects normalizing out (to zeroth order) the elementary ensemble-averaged polymer time scale in the PNCs.

References

- [1] Y. Zhou, B. Yavitt, Z. Zhou, V. Bocharova, D. Salatto, M. Endoh, A. Ribbe, A. Sokolov, T. Koga, and K. S. Schweizer, *Macromolecules*, **53**, 6984–6994 (2020).
- [2] A. Nogales, and A. Fluerasu, *Eur. Polym. J.*, **61**, 494–504 (2016).

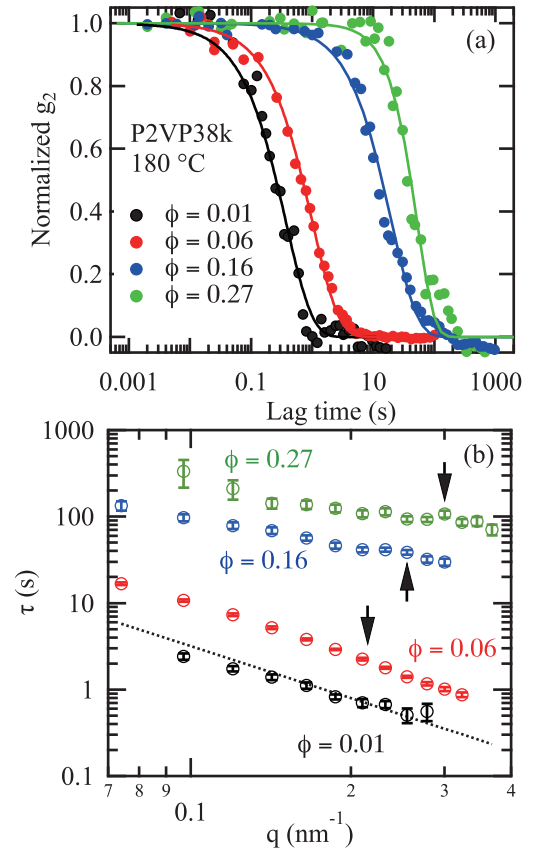


Figure 1. (a) Representative XPCS data for the P2VP38k samples at representative $q = 0.23 \text{ nm}^{-1}$ and 180 °C. The solid lines correspond to the best-fits of Eq. (2) to the data. $\alpha=1$ for $\phi = 0.01, 0.06$, and 0.16 , while $\alpha=1.35$ for $\phi = 0.27$. (b) Relaxation time τ vs. q for the P2VP38k series at 180 °C. The dotted line shows the time scale associated with Stokes-Einstein limit of diffusivity. The arrows correspond to the q^* positions.

Rheology Symposium in IUMRS-ICA 2020 - MRS THAILAND 2021 Instead of the 16th International Workshop for East Asian Young Rheologists

Tadashi Inoue Osaka University

【Purpose of project】 The i-JURC/ICR budget was initially proposed for organization of the 16 International Workshop on Young Rheologist in East Asia (IWEAYR-16, Thailand). This workshop has a mission to promote international exchange among young faculties and graduate students in cooperation with researchers from various countries in East Asia, in several research fields such as polymer science and materials science. The workshop is anticipated to deepen our research activities and form the basis for future cooperation. Unfortunately, COVID-19 prevented to have the workshop on site. Considering the importance of the workshop, we had decided to have an alternative meeting. Fortunately, Prof. Visit Vao-soongern, one of the core members of our society, was planning to have a rheology symposium in IUMRS-ICA 2020 - MRS THAILAND 2021 on line. Therefore, we joined his rheology symposium to support his task and also to complete our mission. The participation of many undergraduate and graduate students fulfilled our original mission to enhance shearing new research results. The budget was effectively utilized to support the participation of as many Japanese researchers as possible.

【Place and schedule of workshop】 Instead of IWEAYR-16, we had a special international rheology symposium in IU-MRS, which was held on Feb 24 and 25, 2021 on the web, chaired by Prof. Visit Vao-soongern of Suranaree University of Technology, Thailand.

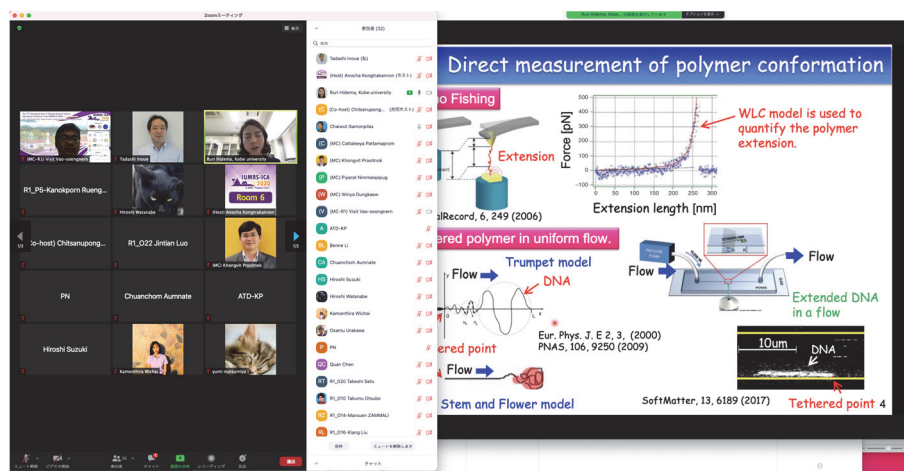
【Purpose of the symposium】 From the beginning, the purpose of this workshop is to promote international exchange and collaboration among young faculties and graduate students who will be the main researchers in the field of rheology and material science in the near future, and therefore, to provide a place for research presentation and discussion, and to revitalize related fields. The symposium provides an opportunity for participants to present their research results, discuss and exchange research ideas in a very friendly atmosphere. At the same time, in order to further develop joint research activities among several research groups, it is to provide a place for people exchange.

【Background of workshop】 This workshop has been held annually since the first IWEAYR in Seoul (February 2006). After that, it has been organized in Kyoto (January 2007), Shanghai (January 2008), Nakhon Ratchasima (January 2009), Busan (January 2010), Yamagata (January 2011), Beijing (February 2012), Phuket (January-February 2013), Seoul (February 2014), Fukuoka (February 2015), Shenzhen (January 2016), Pattaya (February 2017), Jeju Island (January 2018), Nagoya (January 2019), and Changchun (January 2020), in a circulating order of Korea, Japan, China, and Thailand.

【Participants】 The number of participants in this rheology symposium was over 40, which was about one-third of the average in recent years, from seven countries, USA, Japan, Korea, China (Tunisia), Thailand, and Colombia. The main participants were:

Jaewook Nam, Professor,	Seoul National University,	Korea
Youngdon Kwon, Professor,	Sungkyunkwan University,	Korea
Wei Yu, Professor,	Shanghai Jiaotong University,	China
Kang Sun, Professor	Shanghai Jiaotong University,	China
Quan Chen, Professor,	Changchun Institute of Applied Chemistry	China

Exkarach Deenang, Assoc. Professor,	Udon Thani Rajabhat University	Thailand
Hiroshi Watanabe, Professor,	Kyoto University	Japan
Yuichi Masubuchi, Professor,	Nagoya University	Japan
Takashi Taniguchi, Assoc. Professor,	Kyoto University	Japan
Hiroshi Suzuki, Professor,	Kobe University	Japan



A snapshot of the meeting on screen. Left side: participants. Right side: PowerPoint by the presenter (by the invited speaker, Prof. Hidema, Kobe University).

【Overview of the symposium】 Total number of submitted papers was 30, including one keynote and two invited talks. On the first day, Prof. Ronald Larson, University of Michigan, provided a plenary lecture on “Progress in Modeling Polymer Melt Rheology and Crystallization”. After this plenary lecture, a Keynote lecture was presented by Professor Ruri Hidema (Kobe University), long invited presentations by Professor Jaewook Nam (Seoul National University) and Professor Quan Chen (Changchun Institute of Applied Chemistry), and 27 short presentations by mostly doctoral students. 5 poster presentations were also given on web throughout the symposium. The best presentation award was celebrated by participant's vote.

In the symposium, there were many rheological studies on new polymer materials such as nanocomposite and associating polymers. In addition, there were many kinds of basic research on the analysis of various physical and rheological properties and hierarchical structure of reinforcing materials such as particle dispersion systems. Some issues such as theory, simulation, and flow control of soft matter were presented.

【Summary】 In spite of the web style, the discussion was very active. It was an excellent opportunity for students to learn new ideas and deepen their research. Last year, we heard the first report of coronavirus, COVID-19, when leaving from Japan for the IWEAYR-15 venue, Changchun, China. Since then, COVID-19 has been significantly affecting our life and research. However, I strongly felt the high activity of the field during the rheology symposium. Success of this symposium was very helpful to keep our community. We appreciate the financial support from i-JURC/ICR. I would like to finish this report hoping to have IWEAYR-16 on-site, in Udon Thani, Thailand, in the next year.

Study on the mechanism of the crystal structural evolution of polydimethylsiloxane

Liangbin Li University of Science and Technology of China

Objective: Crystallization of polydimethylsiloxane (PDMS) is mysterious. Professor Tosaka, Institute for Chemical Research (ICR), Kyoto Univ., found unusual transformation of the 2D WAXS patterns of PDMS crystal, and subsequently, four crystal forms based on the electron diffraction of the single crystals. The transformation of the 2D WAXS patterns was tentatively explained considering coexistence of the four crystal forms. More detailed studies by Professor Liangbin Li gave the structural evolution diagrams in strain-temperature space and clarified pathways of transformation between the different structures (forms) during the stretching process through in-situ synchrotron radiation experiments. However, the crystallization of PDMS is still difficult to understand by the existing concept of structure formation. Therefore, Prof. Tosaka and Li planned to collaborate on researching the evolution of crystal structure during the crystallization process of PDMS.

Experimental method: The nano-scale dynamic structural analysis X-ray system in ICR was planned to be used for the research. The SAXS experiments about the crystallization of PDMS in the wide range of temperature were expected to reveal the mechanism of the dynamic structure evolution. The cryo TEM in ICR (JEM-2100Plus equipped with a cryo sample holder) was also planned to be used for more detailed observation of single crystals. Based on the obtained data, the structural analysis of the PDMS crystal was expected. In order to build the molecular model to explain the mechanism of the structural transitions, the software of Materials Studio was planned to be used. A post-doctor Jingyun Zhao was scheduled to visit ICR and perform these studies with the help of Professor Tosaka.

Results: Because of the worldwide pandemic of COVID-19 diseases, the international travel to perform the experiments in ICR was not possible during the period of the Joint/Usage Research 2020. Therefore, some other experiments related to this theme were performed in individual countries. For example, cooling experiment of PDMS sample under constant strain by Professor Tosaka revealed increase of tensile stress after the onset of crystallization, which seems to be inconsistent with the proposed crystal structures. The influence of filler contents has been found to significantly influence the crystallization of PDMS at low temperature region, while the detailed formation mechanism requires further investigation.

Discussion: Some of experimental results related to crystallization of PDMS were very difficult to explain according to the currently-proposed crystal structure models. Further refinement of the models is required for consistent understanding of all the experimental results.

High-pressure synthesis of potential multiferroic oxides

Kunlang Ji & J. Paul Attfield University of Edinburgh

Objectives: High pressure-high temperature (HPHT) synthesis is used to stabilize unusual oxidation states and coordination environments in transition metal oxides, resulting in interesting physical properties. In collaboration with Professor Shimakawa in ICR at Kyoto University, a unique high-pressure multianvil apparatus which reaches up to 20 GPa and 2273 K is available to use. This equipment provides a good opportunity for synthesize the double corundum/perovskite with small tolerance factor and develop their potential multiferroics.

Experimental methods: Due to the Covid-19 special circumstance, we developed our collaboration by communicating e-mails. We focus on writing paper of the new double corundum $\text{Co}_2\text{InSbO}_6$ synthesized at Kyoto University during early 2020, while Professor Shimakawa providing very useful scientific guidance for the paper through emails.

Experimental results: A new double corundum $\text{Co}_2\text{InSbO}_6$ has been successfully synthesized with polar NTO-type $R3$ symmetry and lattice parameters $a = 5.28813(3)$ Å and $c = 14.0294(1)$ Å. Magnetic susceptibility and hysteresis loops indicated ferrimagnetic like behavior with $T_C = 40$ K. Temperature dependent synchrotron x-ray diffraction show a dynamic cation site exchange at all temperatures and particular a phase transition to ordered ilmenite type structure above 850 K, inducing the unit cell shrink along the a and b directions, show in Fig.1. The compound was turned back to NTO-type above 950 K with normal thermoal expansion.

Discussion: The selective site exchange only between Co^{2+} and In^{3+} at different temperatures results from the small size and charge mismatch between Co^{2+} ($r^{\text{VI}} = 0.745$ Å) and In^{3+} ($r^{\text{VI}} = 0.8$ Å), compare to that between Co^{2+} and Sb^{5+} ($r^{\text{VI}} = 0.6$ Å).

Publication: K. Ji, M. Amano Patino, E. Solana-Madruga, Y. Shimakawa and J. Paul Attfield, Pressure and temperature induced order-disorder double corundum $\text{Co}_2\text{InSbO}_6$, in preparation

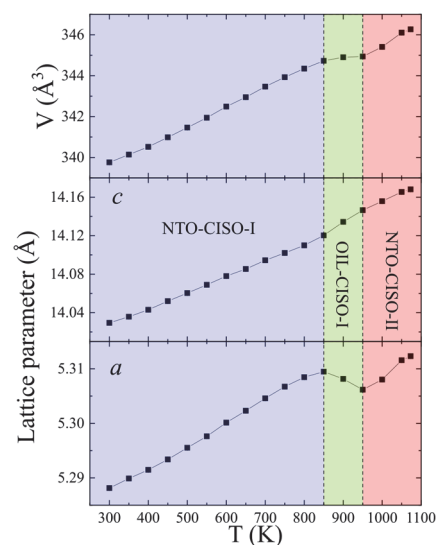


Fig. 1 Temperature dependent lattice parameters and cell volume from SXRD data show phase transition from NTO-OIL-NTO at higher temperatures.

Micro- and nano-structural characterization by advanced transmission electron microscopy of novel functional materials for battery development

Torranin Chairuangsrri Chiang Mai University

Our research group in Thailand has been collaborating with researchers at the ICR including Hiroki KURATA, Mitsutaka HARUTA and Tsutomu KIYOMURA in micro- and nano-structural characterization by advanced transmission electron microscopy of novel functional materials for battery development. Two publications have been completed as summarized below;

I. Novel $\text{TiO}_2(\text{B})/\text{Nitrogen-doped Graphene Hybrid-composites (TNG)}$ as Anode in Advanced Power Batteries

(Ultrafast -charging and long cycle-life anode materials of TiO_2 -bronze/nitrogen-doped graphene nanocomposites for high-performance lithium-ion batteries, T. Autthawong, Y. Chimupala, M. Haruta, H. Kurata, T. Kiyomura, A. Yu, T. Chairuangsrri and T. Sarakonsri, *RSC Adv.*, 2020, 10, 43811-43824)

Novel $\text{TiO}_2(\text{B})/\text{Nitrogen-doped graphene hybrid-composites (TNG)}$ were prepared by hydrothermal method and investigated by TEM at the ICR. Different morphologies of TiO_2 dispersed on nitrogen-doped graphene sheet were confirmed as anatase nanoparticles, TiO_2 nanotubes and TiO_2 depending on the reaction time. The best battery performance was obtained from the nanorods $\text{TiO}_2(\text{B})/\text{nitrogen-doped graphene (TNG-24h)}$ electrode with high specific capacity of 500 mAh g^{-1} at 1C (539.5 mA g^{-1}).

II. Novel $\text{Sn}(\text{SnO}_2)\text{-SiO}_2/\text{Graphene-based nanocomposites}$ as Anode in Lithium-ion batteries

(Improved electrochemical performance of anode materials for high energy density lithium-ion batteries through $\text{Sn}(\text{SnO}_2)\text{-SiO}_2/\text{graphene-based nanocomposites}$ prepared by a facile and low-cost approach, O. Namsar, T. Autthawong, V. Laokawee, R. Boonprachai, M. Haruta, H. Kurata, A. Yu, T. Chairuangsrri and T. Sarakonsri, *Sustainable Energy Fuels*, 2020, 4, 4625-4636)

Novel $\text{Sn}(\text{SnO}_2)\text{-SiO}_2/\text{Graphene-based nanocomposites}$ were prepared by facile and low-cost technique. The materials were studied by TEM at the ICR. The successfully synthesized materials can be confirmed by distribution of Sn, Si, C and O elements (Fig 1). The highest capacity was achieved in the $\text{Sn}(\text{SnO}_2)\text{-SiO}_2/\text{rGO}$ composite. The enhancement of electrochemical characteristics of the nanocomposites was due to the combined advantages of graphene and the nanoparticles with high theoretical capacity (Sn , SnO_2 , SiO_2). Moreover, the flexible graphene matrix was capable of buffering the volume change of the nanoparticles during the discharge-charge process, resulting in the enhanced electrochemical properties.

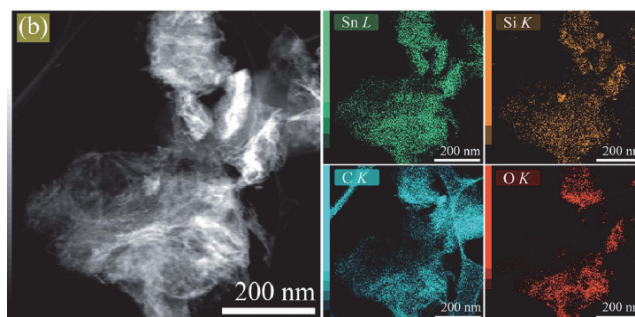


Fig. 1 elemental maps of Sn, Si, C and O for the $\text{Sn}(\text{SnO}_2)\text{-SiO}_2/\text{NrGO}$ nanocomposite and the corresponding high-angle annular dark-field (HAADF) STEM image

Two manuscripts are being prepared for publication in refereed journals. The results can be summarized as follows:

I. Novel Zn-Mg Alloys as Anode in Metal-Air Batteries

Zn-(0-5wt.\%Mg) and $\text{Zn-3Mg-(0-3wt.\%Bi)}$ alloys were investigated. ZnO , ZnO_2 and amorphous ZnO were found as surface oxides on the pure zinc, whereas MgO_4 has been found in addition as a surface oxide on Mg-rich phases ($\text{Mg}_2\text{Zn}_{11}$ and MgZn_2) on the Zn-Mg alloys. The corrosion current density of the ternary alloys significantly increased with increasing Bi content. The highest corrosion current density was from $\text{Zn-3wt.\%Mg-0.5wt.\%Bi}$ alloy, which is about 15.8 A/m^2 . For self-corrosion test, the alloys were immersed in 6 M KOH solution. It was found that self-corrosion rate of the alloys significantly increased with increasing Bi content as compared with the cases of pure zinc and Zn-3wt.\%Mg alloy. The findings are useful for enhanced understanding on passivation behavior of these novel Zn-Mg-Bi alloys as compared to that of the pure zinc and binary system Zn-Mg alloys.

II. Novel Nano Crystalline/Amorphous Vanadium Lithium Borate Glasses as Cathode in LIBs

Structural and local chemical analyses of vanadium-lithium-borate glasses containing V_2O_5 35-60 mol.% and prepared by a melt-quenched method were studied. Nanocrystalline phase of LiV_3O_8 was found by HRTEM. The size of the crystalline phase depends on the vanadium content. It seems likely that the larger amount of vanadium, the larger the crystalline size is as can be compared. The oxidation state of vanadium was confirmed by XANES showing the majority of V^{5+} . These evident can support the presence of vanadium in two environments as in amorphous matrix and nano-crystalline LiV_3O_8 .

Electron energy loss spectroscopy analysis of hexagonal multilayer graphene

Cheng-Yen Wen National Taiwan University

Objective: Multilayer graphene sheets prepared by chemical vapor deposition (CVD) is generally regarded as the Bernal type, of which the stacking order of graphene sheets follows that in natural graphite, so called the AB type stacking. It is recently found that the multilayer graphene prepared by CVD exhibits the primitive hexagonal unit cell (AA-stacked). The optical and electrical properties of such AA-stacked multilayer graphene should be different from those theoretically predicted based on the Bernal stacking. We therefore initiate collaborative research with Prof. Kurata and Prof. Haruta to characterize the AA-stacked CVD graphene and further explore its phonon dispersion properties.

Experimental Methods: The graphene samples were prepared by CVD using Cu as the growth substrate and hydrogen and methane as the gas precursors. Oxygen was also intentionally flowed into the CVD reactor prior to graphene growth (OCVD), for investigating the factors leading to the unusual AA-stacked growth. The graphene layers were wet-transfer method to supporting Cu grids and oxidized Si substrates for transmission electron microscopy analysis and Raman spectroscopy analysis, respectively. Cross-sectional specimens were prepared by a focused ion beam system.

Outcomes: The layer number of CVD graphene can be quickly counted by the contrast change in optical microscopy and scanning electron microscopy, and conveniently determined by Raman spectroscopy based on an empirical rule. However, the layer number of graphene is underestimated. Figure 1 illustrates the inconsistency: the area in Figure 1(a) is regarded as monolayer graphene, in agreement with Raman analysis, but the cross-sectional TEM analysis in Figure 1(b) shows that the area

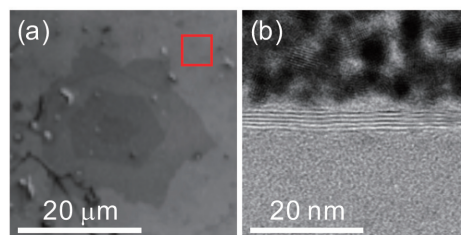


Figure 1. (a) SEM image of CVD multilayer graphene. (b) Cross-sectional TEM image of graphene in the region labeled in (a)

is actually multi-layer graphene. Such inconsistency also appears in the graphene prepared by OCVD. The multilayer regions in Figure 1(a) exhibits even larger numbers of graphene sheets. The CVD graphene prepared in this study could have a different stacking order, so that the Raman empirical rule is not applicable. The stacking order is characterized by diffraction analysis. The results show that the relative diffraction intensity between $\{10\bar{1}0\}$ and $\{11\bar{2}0\}$, no matter what the layer number is, is close to 1.1, which is the ratio for monolayer graphene. The intensity ratio should quickly drop down with the increasing layer number for the stacking orders other than the AA stacking.

Analysis: AA-stacked graphene is found in both regular CVD and OCVD. Such growth is suggested to be attributed to incorporation of oxygen in the growth substrate. The hexagonal (AA stacking) multilayer graphene has been overlooked for a long time. Theoretical calculation shows that hexagonal graphene has better carrier transport property. Production of such hexagonal multilayer graphene can be generalized for application.

Electronic excitations in charge-density-wave systems

Ming-Wen Chu National Taiwan University

This proposed research aims at tackling the electronic excitations in charge-density wave (CDW) systems. CDW instabilities have been a well-accepted notion in electronic phase transitions of solids and are generally considered to be entangled with the characteristic Fermi surface nesting (FSN). In recent years, systematic examinations of the established CDW phases such as NbSe₂, however, revealed that FSN is not a robust ingredient to the electronic transition, but possibly the concomitant electron-phonon coupling. The establishment of a firm methodology in sorting out a relevant electron-phonon coupling, therefore, becomes growingly important and electron energy-loss spectroscopy (EELS) that can capture excited phonon and electronic characteristics in matters turns out to be a plausible solution in addressing the correlated physics.

The realization of such EELS experiments calls for the simultaneous achievement of two essential aspects, (i) a high energy resolution of better than 50 meV in order to picture the spectral features of phonon excitations and (ii) a cryogenic specimen environment considering the typical CDW onset at low temperatures. The two tasks are no routine and expected to be tested together with Profs. Kurata and Haruta in ICR in 2020. Nevertheless, the COVID-19 pandemic prevents this current PI from travelling to ICR for the experiments. It is hoped that the upcoming availability of safe vaccines can twist the situation and international travels to ICR will become possible again in late 2021 for the proposed research. If not, this PI will try to conduct some preliminary remote experiments under the assistances of Profs. Kurata and Haruta. Indeed, this PI deeply appreciates the support of this joint initiative and does look forward to fruitful collaboration results in the near future.

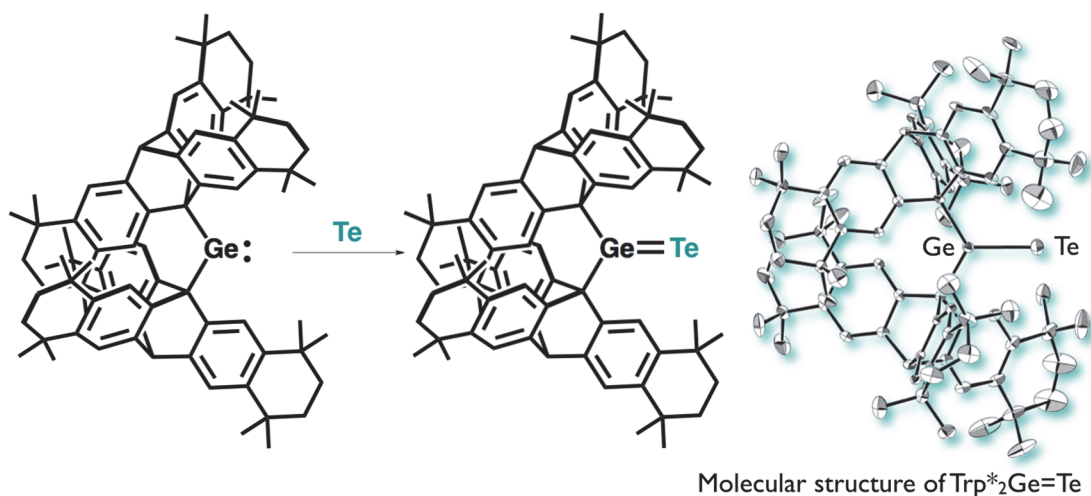
Synthesis and characterization of novel organoselenium and -tellurium compounds

Mao Minoura Rikkyo University

In recent years, organoselenium and -tellurium compounds have attracted an explosive increase in research interest regarding their synthesis, structural characterization, reactivity not only in chemistry but also in biological application.¹⁾ It is generally known that germanium-selenium and -tellurium double bond compounds are highly reactive species and such double bond compounds can easily dimerize. By utilizing the bulky protecting group, it is possible to synthesize and isolate the germanium-chalcogen double bond compounds. Tokitoh *et al.* reported the synthesis of the germanium-chalcogen double bond compounds bearing large aromatic Tbt group. However, in the case of alkyl substituted species, the stable germanium-chalcogens double bond compound has never been reported due to the difficulty of the ligand design. Recently, our group has designed and synthesized Trp*, *i.e.*, a novel triptycene (Trp)-based aliphatic bulky group that bears bulky fused ring-type substituents at the periphery of the Trp framework. In the present study, we took advantage of the steric protection of the Trp* group to synthesize the thermally stable germylene Trp*₂Ge: and the corresponding germanium-tellurium double bond compounds.

The treatment of the Trp*₂Ge:, which was synthesized by the reaction of Trp*Li and GeCl₂, with elemental tellurium afforded the germanetellone (Trp*₂Ge=Te). The isolated Trp*₂Ge=Te is thermally very stable and moisture sensitive, the molecular structure was determined by X-ray crystallographic analysis.

We thank Professors Norihiro Tokitoh, Yoshiyuki Mizuhata, Mariko Yukimoto (ICR, Kyoto University) and Professor David G. Churchill (KAIST, Korea) for their kind discussions.



1) David G. Churchill *et al.* *Molecules*, **2021**, 26, 692. doi:10.3390/molecules26030692

単結晶 X 線構造解析を用いた、含フッ素共役分子の結晶構造におけるフルオラス相互作用の解明

吾郷友宏 茨城大学

フッ素置換基は化合物の電子受容能を向上させるのみならず、結晶中での分子配列制御にも寄与するため、n 型有機半導体材料の開発において含フッ素共役化合物が注目されている。しかし、含フッ素共役分子の構造と分子間相互作用の関係には未解明の点が多く、クリスタルエンジニアリングにフルオラス相互作用を積極的に活用するまでに至っていない。特に、アセン類やポルフィリン、フタロシアニンといった平面 π 共役分子は有機半導体の重要な構造モチーフであるが、微小単結晶を形成しやすいため単結晶 X 線構造解析は困難であることが多く、これらの平面 π 共役分子にフッ素置換基を導入した含フッ素共役分子におけるフルオラス相互作用の実験的知見はほとんど無い。

本研究では、化学研究所の極微小結晶用 X 線単結晶 X 線構造解析装置である VariMax を用いて、研究代表者が合成した含フッ素アセン、ポルフィリンやフタロシアニンの構造を解析し、フルオラス相互作用に基づいた π 共役系の配列制御に必要なフッ素置換基の構造を明確化する。この知見に基づいて、フルオラス相互作用を活用した含フッ素 π 共役分子の構造制御と物性発現を目指す。

本年度の研究では、ペルフルオロオクチル基に代表される既存の長鎖フッ素置換基が「残留性有機汚染物質に関するストックホルム条約第 9 回締約国会議 (COP9)」で廃絶対象物質に追加されたことを受けて、長鎖フッ素置換基の撥水・撥油性、電子求引性、クリスタルエンジニアリング特性を維持しつつ環境負荷低減が可能な新規フッ素置換基の開発を検討した。検討した新規フッ素置換基はペルフルオロアルキレンユニットがビニレンユニットで架橋された構造であり、COP9 で指定された長鎖ペルフルオロアルキル基と異なり、ペルフルオロオクタン酸 (PFOA) 等の生物濃縮性物質は生じない一方で、長鎖フッ素置換基に期待される特性は維持されると考えられる。この予想を実証するために本フッ素置換基を導入したポリ (メタ) アクリレート樹脂を合成したところ、PFOA 発生源となる長鎖ペルフルオロアルキル基を持つ既存のフッ素樹脂と同等の撥水・撥油性、耐熱性を持つことが明らかとなり、本フッ素置換基がフルオラス相互作用発現のために有効であることが示唆された。今後は、本フッ素置換基を導入した含フッ素共役分子を合成し、単結晶 X 線構造解析によるフルオラス相互作用評価を実施する。



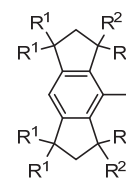
【成果報告】 Shirai, T.; Fukumoto, H.; Kanno, Y.; Kubota, T.; Agou, T. *Polymer (Elsevier)* 2021, 217, 123478.

Synthesis and structural characterization of low-valent species of heavier group 14 elements

Tsukasa Matsuo Kindai University

In this collaborative research, we have planned to investigate the synthesis and structures of low-valent species of the heavier group 14 elements by taking advantage of the steric protection using the fused-ring bulky Rind group (Rind = 1,1,3,3,5,5,7,7-octa-R-substituted *s*-hydrindacen-4-yl).

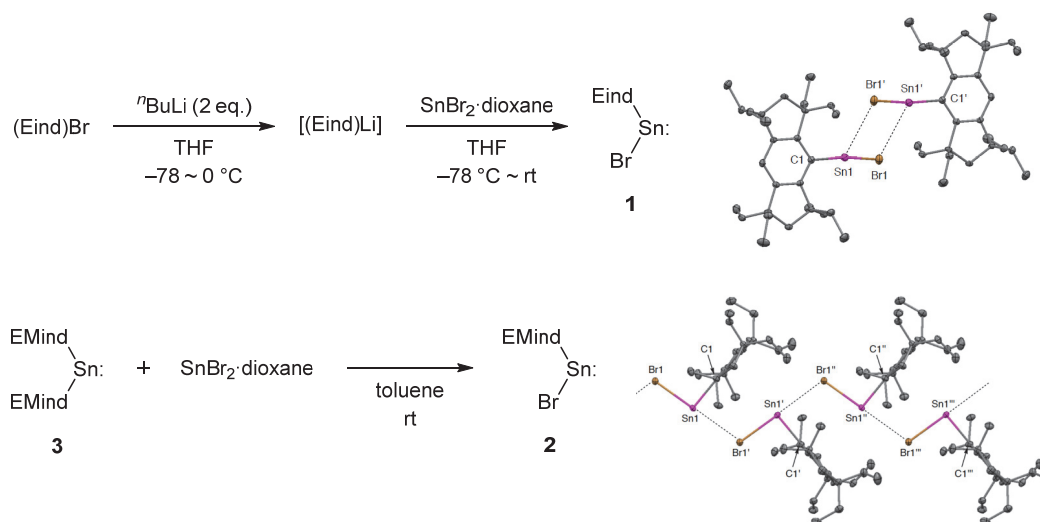
The bulky Eind-based bromostannylene, (Eind)BrSn: (**1**), has been synthesized by the reaction of SnBr₂·dioxane with 1 equiv. of (Eind)Li in THF (Scheme 1). In contrast, the less bulky EMind-based bromostannylene, (EMind)BrSn: (**2**), has been obtained by the ligand redistribution between the diarylstannylene, (EMind)₂Sn: (**3**), and SnBr₂·dioxane in toluene. The arylbromostannylenes **1** and **2** can be isolated as room-temperature-stable orange crystals, and their structures have been clearly determined by X-ray diffraction methods. While the dimer formation is found for the bulky Eind-based **1** in which two Sn atoms are asymmetrically bridged by two Br atoms, the less bulky EMind-based **2** shows a unique one-dimensional polymeric structure with alternating Sn and Br atoms, supported by the perpendicularly-oriented EMind groups.



Rind

EMind: R¹ = Et, R² = Me

Eind: R¹ = R² = Et



Scheme 1. Synthesis of **1** and **2**.

DNP-NMR を利用した炭素材料表面官能基解析法の開発

後藤和馬 岡山大学

ナノカーボン材料の一つとしてグラフェンや薄膜炭素が注目されており、その応用に関して数多くの研究が行われている。化学的にグラフェン系材料を大量合成可能な手法として、黒鉛を酸化して炭素層を剥離することで酸化グラフェン(GO)を得る方法がある。GO は金属ナノ粒子担持体や、ポリマー等との複合体として化学反応触媒、燃料電池電極触媒、バイオマテリアルなど多種多様な応用が期待されている。また酸化グラフェンの表面を還元した「還元酸化グラフェン(rGO)」についても、樹脂用フィラーなどへの利用が検討されている。GO や rGO の表面には数多くの欠陥構造があり、そこには水酸基やカルボキシル基、エポキシ基などの末端官能基が存在している。そのためこの表面官能基の状態を把握し、制御することが材料開発において重要となっている。従来、炭素薄膜の表面官能基については X 線光電子分光(XPS)や核磁気共鳴(NMR)が用いられてきたが、これらの方法では官能基の量が少ない rGO 表面の解析は不可能であった。本研究では、従来の NMR に比較して飛躍的な検出感度向上が得られる動的核偏極(DNP)法を用いて、rGO の表面官能基解析を試みた。

粉末黒鉛を Hummers 法により酸化して合成した GO を、メタノールまたはヒドラジンをを用いて還元することで 2 種類の rGO (MeOH-rGO、Hyd-rGO)を得た。これらについて外部磁場 9.4 T 下にて ^{13}C DNP-NMR 測定を行った。分極剤には[1-(3,6,9,12-テトラオキサトリデカン-1-イル)ウレイレンビス(3,11-ジオキサ-7-アザジスピロ[5.1.5.3]ヘキサデカン-15,7-ジイルオキシ)]ラジカル(AMUPol)を用いた。MeOH-rGO の ^{13}C DNP-NMR 測定を行った結果、通常の ^{13}C NMR 測定で得られたスペクトルと比べて、S/N 比が 1.5~2 倍程度のみ改善されることが確認できたが、Hyd-rGO ではほとんど信号強度の増強が確認できなかった。rGO は炭素層末端のダングリングボンドに起因する不対電子を有しているため分極移動に最適な外部磁場の大きさが変化したことが考えられるため、外部磁場の大きさを変化させながら DNP-NMR 測定を行った結果、S/N 比が改善し、 ^{13}C NMR に比較して最大で 2~3 倍程度の感度上昇を達成することができた(図 1)。

本年度は、2020 年春頃や 2021 年初頭~現在(2 月末)の緊急事態宣言など、新型コロナウイルスの感染拡大による度重なる出張制限があったため実験を進展できない期間が半年以上に亘った。そのため、rGO 測定における S/N 比改善という成果までは得られたものの、残念ながら詳細な官能基分析まで研究を進めることができなかった。2021 年度も本研究テーマを京都大学化学研究所との共同研究として継続できるならば、各種還元手法により rGO にどのような官能基が残存するかを明らかにし、様々なナノカーボンの表面官能基解析手法として確立することを目指してさらに研究を進めたいと考えている。

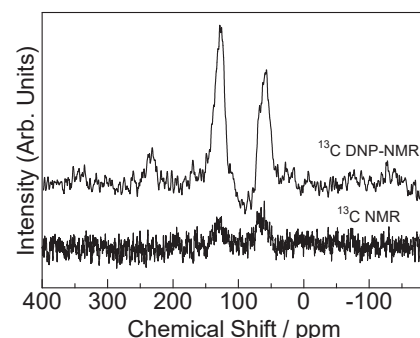


図 1 MeOH-rGO の ^{13}C DNP-NMR および ^{13}C NMR スペクトル

平面シリセンナノリボンの理論設計と新しい動作原理の探究

高橋まさえ 東北大学

【目的】本研究は研究代表者が設計した平面構造のケイ素六員環からなるシリセン分子[M. Takahashi Sci. Rep. 2017, 7, 10855.]をベースに二次元に拡張し、平面構造のナノスケール幅を持つ帯状物質シリセンナノリボンを構築し、既存の動作原理とは異なる動作原理の探究を目的としています。「ケイ素版グラフェン」とも呼ばれる新材料「シリセン」は、炭素原子の代わりに同じ 14 族であるケイ素原子を使ったシートです。グラフェンは電子構造にエネルギーギャップがないため、論理回路への応用が望めなく、シリセンの実現が切望されています。しかし、シリセンは、平面構造のグラフェンとは異なり、一部の原子が浮き上がって座屈した凹凸構造をとるため、空气中できわめて不安定です。多くの研究者の努力にもかかわらず、これまで、平面構造のシリセンおよびシリセンナノリボンは理論的にも実験的にも得られていません。

【方法】京都大学化学研究所スーパーコンピュータシステムの Materials Studio を用いて第一原理計算を行いました。シリセンナノリボンの設計には、格子定数、原子座標ともに構造全最適化を行い、得られた構造は振動解析により安定構造であることを確認しました。

【結果と考察】2018 年度より本共同利用に採択していただき、研究代表者が見出した平面構造のシリセン分子をもとに平面ケイ素 2 次元シートの設計を進めてまいりました。研究代表者が見出した平面シリセン分子を単純に二次元へ拡張しただけでは目的とする平面二次元シートは得られず難航しました。しかし、新しい着想によりようやく平面構造のナノリボンの設計にたどりつきました。2020 年度はコロナ感染症拡大のため、思うように共同研究を進めることができませんでしたが、解析をすすめる中で、この平面シリセンナノリボンが興味深い物性を有することがわかってきました。バンド構造から、得られた平面シリセンナノリボンは負の間接バンドギャップを有する半金属であることがわかりました。非平面のジグザグシリセンナノリボンが磁性を有するのとは異なり、今回設計した平面シリセンナノリボンは非磁性を示しました。ケイ素の 3p 軌道に由来する面外の π および π^* 軌道による明瞭な直線的分散特性がバンド構造に観測され、フェルミ準位のわずかに上にディラク点の存在が見出されました。

【成果報告】

発表論文

- ・ M. Takahashi, M. Kowada, H. Matsui, E. Kwon, Y. Ikemoto, *J. Phys. Chem. A* **2021**, in press.

核融合プラズマ対向材料中の水素・ヘリウム挙動の高精度測定

宮本光貴 島根大学

核融合炉発電の実現には、高性能プラズマの安定維持に加え、それを取り囲む材料との相互作用を正確に把握する必要がある。特に、プラズマ対向材料中の水素同位体およびヘリウムの挙動の理解は、プラズマ制御および材料の健全性に関わる極めて重要な課題である。本研究では、主に現在建設中の国際熱核融合実験炉（ITER）のプラズマ対向材料に利用が予定されているベリリウムを対象として、そこでの重水素およびヘリウムの挙動を微細組織変化と関連付けて評価した。

図 1 に 3 keV-D₂⁺、および 3 keV-He⁺を室温で 1×10^{21} ions/m² 照射したベリリウムからの昇温脱離ガス測定の結果を示す。いずれにおいても 2 つの主要な放出ステージを確認できるが、ヘリウムはその放出温度が重水素と比較して高く、ヘリウムが材料中に安定に保持されていることを示している。透過型電子顕微鏡を用いた照射後試料のその場観察から、昇温過程において、いずれの試料においても、ガス放出温度に対応したガスバブルの成長や消失が見られた。さらに重水素、およびヘリウムバブルの昇温下での消失挙動は大きく異なり、重水素は昇温に伴いバブル内から乖離し、バブルが縮小し消滅するのに対し、ヘリウムバブルは、縮小することなく移動を伴う合体成長を続け、試料表面に到達することで消失することが明らかになった。これらの試料について、京都大学化学研究所のモノクロメータ搭載低加速原子分解能分析電子顕微鏡により電子エネルギー損失分光測定（EELS）を行った結果、バブル中の重水素とヘリウムの存在状態に明瞭な違いが確認された。図 2 には、一例として、重水素照射後にヘリウム照射したベリリウム試料内部の (a) HAADF 像、および EELS スペクトルのマッピング解析から得られた (b) 重水素と (c) ヘリウムの濃度分布像を示す。HAADF 像中の黒いコントラストは、試料中に形成したバブルを示している。ヘリウムはバブル内部に均一に存在しているのに対し、重水素はバブルの表面近傍に局在していることが確認できる。これは、水素とヘリウムがバブル内部において、捕捉状態が異なることを示しており、放出挙動の相違の主要因であると考えられる。今後、実験パラメータを拡張し、照射量、温度等の依存性を調べるとともに、重水素・ヘリウムの相乗効果等について引き続き評価を行う。

なお、本研究は、倉田博基教授、治田充貴准教授（京都大学化研）、杉本有隆、原一智（島根大学）らとの共同研究として実施されたものである。また、本成果は、来年度開催予定の核融合炉材料国際会議 ICFRM-20 にて報告予定である。

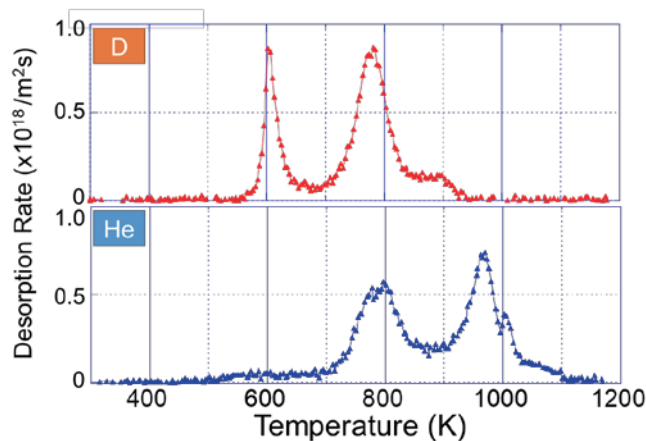


図 1 重水素（上）、およびヘリウム（下）照射したベリリウム試料からの昇温脱離ガススペクトル。

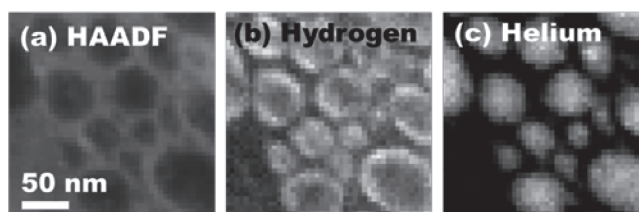


図 2 重水素・ヘリウム複合照射したベリリウム試料の STEM-EELS による (a) HAADF 像、および (b) 重水素と (c) ヘリウムの濃度分布像。

Synthesis and structures of cationic aromatics bearing thiopyrylium units

Noriyoshi Nagahora Fukuoka University

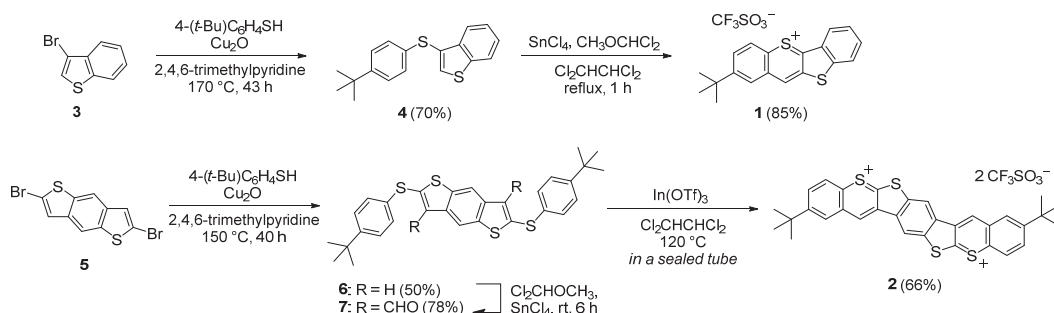
Introduction

A variety of organoelectronic devices are based on thiophene derivatives and therefore thiophene derivatives/analogues with improved properties are highly sought after. In this regard, thiophene-fused thiopyrylium salts can be expected to exhibit promising potential. However, examples on the synthesis of thiophene-fused thiopyrylium compounds have so far remained scarce. In this work, we present the synthesis of a new family of thiophene-fused thiopyrylium salts **1** and **2** together with the experimental and theoretical examination of their electronic structures.

Results and Discussion

The reaction of bromothiophene **3** with 4-*tert*-butylbenzenethiol provided thioether **4** in moderate yield. We attempted the synthesis of thiopyrylium salt **1** via a Rieche formylation followed by a Friedel–Crafts cyclization. Thioether **4** was treated with $\text{Cl}_2\text{CHOCH}_3$ in the presence of the Lewis acid SnCl_4 , which afforded thiopyrylium salt **1**. Subsequently, we performed the Lewis-acid-promoted intramolecular reaction of **7**. In a sealed vessel, we carried out a literature method for the $\text{In}(\text{OTf})_3$ -induced cyclization on **7** in $\text{Cl}_2\text{CHCHCl}_2$. Cold hexane was added dropwise to the resulting solution and the thus obtained reddish brown powder of stable bithiopyrylium salt **2** were isolated in 66% yield by centrifugation.

Crystallization from a saturated solution of **1** in CH_3CN afforded single crystals. The molecular structure of **1** was determined by X-ray diffraction analysis using a high-flux diffractometer for single crystals in Institute for Chemical Research, Kyoto University. The sum of the internal bond angles of all the 5- and 6-membered rings in **1** are close to 540° and 720° , respectively, which indicates that the ring framework of **1** exhibits a highly planar structure in the solid state.



Publications

- Nagahora, N.; Kitahara, K.; Mizuhata, Y.; Tokitoh, N.; Shioji, K.; Okuma, K. *J. Org. Chem.* **2020**, *85*, 7748–7756.
- Nagahora, N.; Tanaka, R.; Tada, T.; Yasuda, A.; Yamada, Y.; Shioji, K.; Okuma, K. *Org. Lett.* **2020**, *22*, 6192–6196.

FT-ICR-MS を用いた湖沼及び土壌環境中溶存有機物の 化学特性および起源解析

布施泰朗 京都工芸繊維大学

【目的】 環境中の難分解性溶存有機物（Dissolved Organic Matter：DOM）は、水生生態系や水質汚濁を引き起こす物質として、その影響が懸念されており、このような難分解性 DOM の増加は、琵琶湖などの閉鎖性水域にて観察されている。我々は、これまでに琵琶湖北湖における DOM の分子量分布や蛍光特性等の動態を明らかにしてきたが、近年、環境水中の DOM がクラスターを形成していることなどが明らかとなっており、DOM の化学特性や起源について詳細な解析を行っていく上では、DOM の詳細質量を明らかにし、元素組成を詳細に解析することが重要となる。FT-ICR-MS は近年開発された、分子のミリマス測定を可能とする、他の質量分析法をはるかに超える高分解能・高精度な分析技術である。本研究では、環境水中の DOM の化学特性および起源解析を行うことを目的として、FT-ICR-MS を用いる特性解析法について検討を行った。

【実験】 標準試料は、日本腐植学会頒布の標準フルボ酸（褐色森林土：Dando）を用いた。いくつかの濃度の標準フルボ酸溶液を調製し、FT-ICR-MS による測定に最適な試料条件について検討を行った。

【結果と考察】 標準フルボ酸による FT-ICR-MS のマススペクトルを Fig.1 に示す。Negative ion mode で測定した結果、フルボ酸濃度 100ppm 未満では良好なマススペクトルが得られなかった。このことより、FT-ICR-MS による質量分析には、試料条件として、おおよそフルボ酸濃度 100ppm（炭素濃度にして、約 50 mgC/L）程度まで濃縮する必要があることが示唆された。また、マススペクトルによるイオンピークは m/z 200～1000 までの範囲で検出され、これまでに GPC 等により推定されてきたフルボ酸分子量（数千～数万 Da）は、分子量 200～1000 程度の小分子がクラスターを形成し、見かけ分子量を増大させていたことが推測された。Dando FA の van Krevelen diagram を Fig.2 に示す。Van Krevelen diagram は得られたイオンピークごとの水素炭素比及び酸素水素比をプロットしたものであり、得られる位置により、リグニン様、脂質様などの特性に応じた評価が報告されている。今後、これらの解析手法を元に、琵琶湖水中溶存有機物の特性および起源について検討していく予定である。

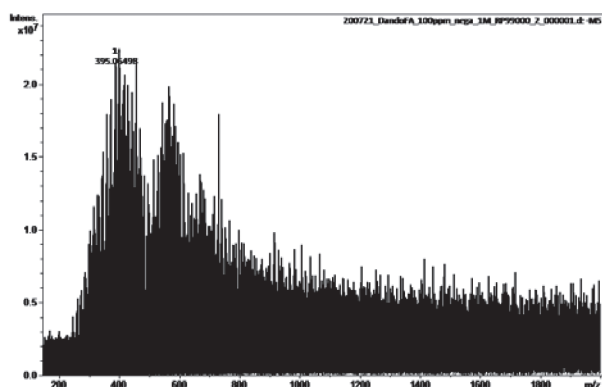


Fig.1 MS spectrum of Dando FA (negative ion mode)

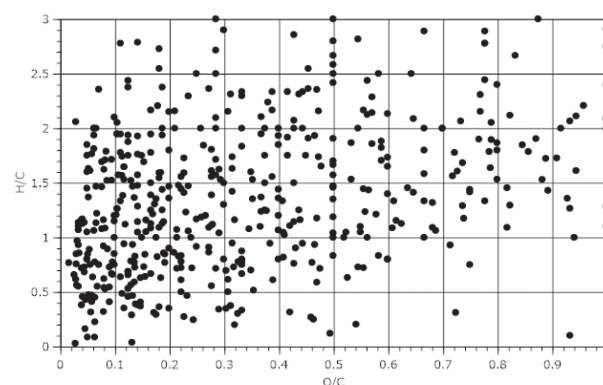


Fig.2 van Krevelen diagram of Dando FA

2 次元物質欠陥の束縛励起子の STEM-EELS 解析

齊藤光 九州大学

極性ハニカム構造をもつ単層遷移金属ダイカルコゲナイド(TMD)は2種類の原子から構成され、逆格子の $K(K')$ 点でバンドギャップが開いた直接遷移型の半導体である。 $K(K')$ 点付近の谷の形状をしたバンド分散面はバレーと呼ばれ、 K バレーと K' バレーとで電子の軌道角運動量が反転していることから、円偏光によって各バレーの電子を選択的に励起することができる。さらに、TMD は一般にスピン軌道相互作用が強く、軌道角運動量の選択はすなわちスピンの選択となる。このようなスピン選択性をデバイスとして利用するには、格子との相互作用による減偏極の影響を低減する必要がある。例えば、これまでに、スピン偏極情報を素早く表面プラズモンに変換することで減偏極の害が克服された例がある[1]。

本研究では、TMD とプラズモン共振器の相互作用の詳細を走査透過電子顕微鏡-電子エネルギー損失分光(STEM-EELS)を用いてナノメートルスケールで明らかにすることを目的とし、TMD とプラズモン共振器の複合構造を作製した。TMD として WS_2 を選定し、単層試料を化学気相成長(CVD)により合成した。プラズモン共振器としてナノギャップ構造を有した金属円柱配列(ププラズモニック結晶:PIC)を選定し[2]、真空蒸着およびスパッタリング、電子線リソグラフィによる作製した。作製した PIC は Al 円柱配列/ SiO_2 (20 nm)/Ag 基板の多層構造を有しており、単層 WS_2 は SiO_2 ギャップ層の中心、すなわち Ag 基板表面から 10 nm の高さに位置するように埋め込んだ。Al 円柱配列は三角格子型の周期配列になっており、直径 150 nm、高さ 20 nm の Al 円柱が周期 600 nm で配列された。

Fig. 1 は作製した構造の励起子発光をフォトルミネセンスで評価した結果である。 WS_2 は視野の上半分(水色線より上側)に位置し、Al 円柱配列は視野の左側(ピンク色線より左側)に位置している。 WS_2 の励起子発光のピーク波長 645 nm の発光強度をマップとして表示すると(Fig. 1 上)、 WS_2 と Al 円柱配列が重なった領域(視野の左側)が、 WS_2 のみの領域(視野の右側)よりも明るく表示されていることがわかる。すなわち、PIC による WS_2 の発光増強が確認された。今後、同試料を STEM-EELS により解析し、TMD とプラズモン共振器の相互作用の詳細をナノメートルスケールで明らかにする。

[1] S. H. Gong et al., Science. 359, 443 (2018). [2] H. Saito et al., ACS Photon. 6, 2618 (2019).

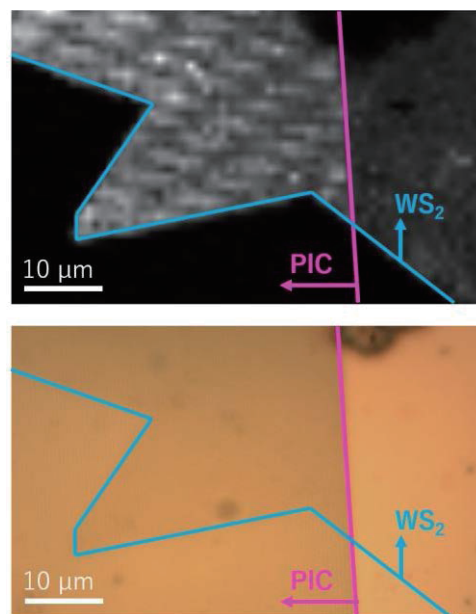


Fig. 1 (上)フォトルミネセンスによる単層 WS_2 の励起子発光の顕微分光. (下)同一視野の光学顕微鏡像.

2. 国際会議、シンポジウム・研究会報告

新型コロナウイルス感染症拡大防止のため、令和2年度は開催せず。

3. 成果発表論文

紙数の都合により、目次に記載した論文の一部についてのみ、別刷りを次頁以降に掲載する。

(別刷りは印刷体のみに掲載する)

4. 參考資料

京都大学化学研究所
化学関連分野の深化・連携を基軸とする先端・学際グローバル研究拠点
令和2年度国際共同利用・共同研究公募要領

京都大学化学研究所は、「化学に関する特殊事項の学理及び応用の研究を掌る」ために、化学を中心とする分野で基礎研究に重点を置いた先端研究に進捗してまいりました。平成22～30年度の期間には、文部科学大臣から国立大学共同利用・共同研究拠点としての認定を受け、化学研究所の活性を基盤とする「化学関連分野の深化・連携を基軸とする先端・学際研究拠点」として国内外の化学関連分野の研究者との共同利用・共同研究を推し進めてまいりました。この拠点活動におけるグローバル共同利用・共同研究が評価され、平成30年化学研究所は文部科学省から国際共同利用・共同研究拠点に認定されました。これを受けて、平成31年度からの国際共同利用・共同研究拠点活動においては、多様でグローバルな化学分野の共同研究を一層強力に推進すべく、さらなる事業展開を図っております。

つきましては、化学に関わる分野でご活躍の皆様のご意見・ご要望を尊重しつつ、世界の化学の基礎・応用研究を皆様とともに一層推進することを念頭に置き、下記の要領で令和2年度の拠点共同利用・共同研究の課題公募をさせていただきます。

この公募に当たりましては、分野選択型（計画研究型）、課題提案型、連携・融合促進型および施設・機器利用型の四つに分けて研究課題を募集いたします。これらの課題の実施に際しては当研究所の専任教員または客員教員との共同研究を基調といたしますが、いずれの課題でも後述の共通設備・機器・資料等のご利用が可能です。なお、各課題とも、海外研究者を研究代表者あるいは研究協力者とする国際共同研究（この場合、英語フォームで申請下さい）と、国内研究者を研究代表者とする国内共同研究を実施致します。これらの点も勘案いただき、本公募要領の詳細について十分ご確認の上、期日までにご申請下さいますようお願いいたします。

京都大学化学研究所長 辻井敬亘
共同研究ステーション長 寺西利治

1. 研究期間

1年間（令和2年4月1日から令和3年3月31日まで）。

2. 研究課題分類

下記のような分類（型）ごとに研究課題を募集いたします。いずれの課題についても、分類ないし分野の担当者もしくは当研究所で対応する共同研究者にご一報の上、ご申請下さい。また、研究経費に関しては、p.3の表をご覧ください。

2-1. 分野選択型（計画研究型）研究課題

分野選択型（計画研究型）研究課題は、あらかじめ設定された分野に関して化学研究所内の研究者と共同で遂行する課題です。令和2年度は下記の5分野について課題を公募いたします。5分野を合わせて、萌芽的な課題と発展的な課題をそれぞれ20件程度、採択の予定です。

ビーム科学分野（担当者：若杉 昌徳；wakasugi.masanori.8z@kyoto-u.ac.jp）

基本テーマ：先進量子ビームの開発と新奇診断分析手法の創出

趣旨：レーザー、X線、電子線、イオンビームなどの量子ビームの高度化とその先端的診断分析法への応用を進めます。また、これらの量子ビームを複合的に用いて、極微細領域での超高速化学・物理現象の解明を目指します。

元素科学分野（担当者：中村 正治；masaharu@scl.kyoto-u.ac.jp）

基本テーマ：元素科学に基づく物質創製・機能創出

趣旨：元素の新たな特性を引き出し、この特性をもとに優れた機能を有する新物質を創製します。元素と社会との関わりを俯瞰した元素戦略研究も推進します。物質の機能は、構成元素の特性を相乗的に反映して発現します。この発現機構を明らかとし、望みの機能を意のままに創出することを目指します。

バイオ情報学分野（担当者：緒方 博之; ogata@kuicr.kyoto-u.ac.jp）

基本テーマ：バイオ情報を含む複合情報の融合解析

趣旨：ゲノムやメタゲノムに代表される最新バイオ情報に立脚して、バイオ情報がいかに生体内や自然環境における化学現象と関わっているかを明らかにし、生命システムについての化学的理解の深化を図ります。さらに、その成果を応用して、ゲノム創薬やパーソナライズド医療などへの展開も目指します。

物質合成分野（担当者：村田 靖次郎; yasujiro@scl.kyoto-u.ac.jp）

基本テーマ：複合機能材料の戦略的創製

趣旨：異種材料のハイブリッド化・複合化ならびにナノサイズ化に重点を置き、新規な機能をもつ新世代材料の創製を目指すとともに、生体の認識、応答、反応などの諸機能を担う例えば生体膜等も複合機能材料と捉え、機能物質と生命現象の化学的相関の解明も目指します。

現象解析分野（担当者：寺西 利治; teranisi@scl.kyoto-u.ac.jp）

基本テーマ：複合測定に基づく物質解析

趣旨：化学を基盤とする多種の分光学的手法・解析的手法を複合的に駆使して、天然および人工物質の構造・性質を分子レベルから巨視的レベルまで階層的に理解・記述することを目指し、一方、その結果を還元することによって新たな物質科学の枠組みを構築する取り組みも目指します。

2-2. 課題提案型研究課題（担当者：梶 弘典; kaji@scl.kyoto-u.ac.jp）

課題提案型研究課題は、前項 1 で設定した一つの分野に留まらない分野、あるいはそれ以外の分野について、化学関連分野の研究者から自由にご提案いただく課題です。萌芽的な課題と発展的な課題を、それぞれ 20 件程度、採択の予定です。新分野の開拓につながるような課題を特に歓迎いたします。なお、緊急性・重要性が極めて高いと判断した課題については、前記の応募期日にかかわらず、直ちに採択することもあります。

2-3. 連携・融合促進型研究課題（担当者：渡辺 宏; hiroshi@scl.kyoto-u.ac.jp）

連携・融合促進型研究課題は、化学関連分野における国内外の研究連携の強化を主目的とする共同研究課題です。国外も念頭に置く場合は、化学研究所の部局間国際学術交流締結先 (http://www.kuicr.kyoto-u.ac.jp/sites/international_exchange/agreement/ 参照) との共同研究を開始する場を求めていることも可能です。また、この目的に沿った研究集会の開催も本課題として応募いただけます。5 件程度を採択する予定です。

2-4. 施設・機器利用型研究課題（担当者：倉田 博基; kurata@eels.kuicr.kyoto-u.ac.jp）

施設・機器利用型研究課題は、http://www.kuicr.kyoto-u.ac.jp/sites/research_activities/joint_research/kaken_kyodo_instr/ (拠点ホームページ) に記載の共通設備・機器・資料等の利用を主とする共同研究課題です。15 件程度を採択する予定です。

令和2年度国際共同利用・共同研究経費概算値

	経費上限／件 [*] （千円）	
	国際共同研究	国内共同研究
分野選択型萌芽的研究	1,000	800
分野選択型発展的研究	2,000	1,500
課題提案型萌芽的研究	1,000	800
課題提案型発展的研究	2,000	1,500
連携・融合促進型研究	1,000	800
施設・機器利用型研究	1,000	800

^{*}表中の金額は目安です。予算の状況に応じた減額もありえますことをご了解下さい。
経費内での備品費、消耗品費、旅費の配分は、申請者と化学研究所の共同研究者が協議して決定下さい。特に、旅費については、地域性を勘案してご決定下さい。

3. 共同研究応募方法

3-1. 申請資格

国公立大学、国公立研究機関、独立行政法人等の専任研究者、または、これに準ずる者。

3-2. 申請書記入要領

申請に当たっては、該当する募集分類・分野の担当者もしくは当研究所で対応する共同研究者と、事前に研究課題、研究内容、研究経費に関して、必ずご協議下さい。対応する共同研究者は、当研究所の専任教員または令和2年度客員教員からお選び下さい。なお、教員のリストは下記の化学研究所ホームページをご参照下さい。

教員リスト http://www.kuicr.kyoto-u.ac.jp/sites/research_activities/chemist/

また、対応する共同研究者をお決めになれない場合は、各分類・分野の担当者に、まず、ご相談ください。
上記の表の経費上限は目安です。特に、経費内での備品費、消耗品費、旅費の配分については、当研究所で対応する共同研究者と十分にご協議の上で申請下さい。特に、旅費については、地域性を勘案してご申請下さい。

課題申請は、本要領に添付の分野選択型共同利用・共同研究申請書（様式1）、課題提案型共同利用・共同研究申請書（様式2）、連携・融合促進型共同利用・共同研究申請書（様式3）、施設・機器利用型共同利用・共同研究申請書（様式4）に必要事項を記入し、下記の要領で、化学研究所共同研究推進室にご提出下さい。

なお、各課題とも、海外研究者を研究代表者あるいは研究協力者とする国際共同研究も実施可能です。この場合、英語フォーム（Forms 1~4）の左肩の欄にチェックを入れて、ご申請下さい。

<記入上の注意事項>

- ※を付した事項は当研究所で記入します。
- 当研究所で対応する共同研究者は必ずご記入下さい。
- 申請者（研究代表者）と共同研究者の役割分担を明記して下さい。事前に共同研究者の承諾を得ていただくことが必要です。
- 申請書は3頁以内にまとめて下さい。

3-3. 提出期限および提出先

応募に当たっては、前記の申請書にご記入の上、令和2年1月20（月）までに、WEB申請して下さい。

問い合わせ先

京都大学化学研究所共同研究推進室 国際共同利用・共同研究係

E-mail: icr-hub@scl.kyoto-u.ac.jp, 電話: (0774)38-3121

4. 課題選考と採択通知

応募課題の採否は、当研究所の共同研究委員会で審査し、運営評議会の承認を経て決定されます。審査に際しては、共同研究の申請内容だけでなく、予算枠や、共通設備・機器・資料の使用時間等も考慮いたします。採否の結果（内定）については、令和2年3月に当研究所の所長から研究代表者に通知いたします。

5. 研究の実施および研究成果報告

5-1. 研究経費等

研究代表者と当研究所で対応する共同研究者には、予算の範囲内で、研究経費（備品費および消耗品費）と旅費が支給されます。また、研究協力者（学生も含めることが可能です*）にも予算の範囲内で旅費が支給されます。共同研究の実施に当たっては、まず対応する共同研究者にご連絡下さい。なお、当研究所には、共同研究者のための宿泊施設はありません。

* 研究協力者について、学生の場合は原則として大学院生といたします。なお、傷害保険等に参加していることが必要です。

5-2. 研究成果報告

採択された研究課題については、研究成果報告書を次に記す作成要領に従って記載・提出していただきます。その報告書は、まとめて当研究所の国際共同利用・共同研究報告書集として公開させていただく予定です。また、その内容を研究成果報告会でご報告いただくことがあります。なお、報告会についての詳細は、採択課題の研究代表者に後日お知らせいたします。

5-3. 研究成果報告書の作成要領

分野選択型研究、課題提案型研究、施設・機器利用型研究については1頁、連携・融合促進型研究については2頁の報告書を（様式5）を用いて作成下さい。A4版の用紙には1頁あたり1,200字程度が記載できます。図表などカラーを用いても構いませんが、報告書集刊行の際はモノクロ印刷になることもありますので、その点をお含み置き下さい。

1頁の1行目の中央に研究課題名、3行目に右詰めで研究代表者の氏名と所属、5行目から本文を記載して下さい。なお、当研究所で対応した共同研究者は報告書の共著者とはせず、必要に応じて本文中に明記して下さい。また、国際共同研究の場合、報告書は英文でご作成ください。

5-4. 報告書の内容

形式は自由ですが、例えば、実験的研究では、目的、実験方法、実験結果、考察、成果報告（論文、学会発表等）をお書き下さい。なお、連携・融合促進型研究で研究集会を開催した場合には、研究集会のプログラム、参加者名簿（所属機関・部局・職名を明記）、および、作成された場合は要旨集またはプロシーディングスを添付して下さい。

5-5. 報告書の提出

提出締切日は、令和3年2月末日とします。電子ファイル（Word ファイルと PDF ファイル）を、WEBから提出してください。なお、ファイル名は「課題番号+代表者名（姓）」として下さい（例：2020-1 田中.doc、2020-1 田中.pdf）。

問い合わせ先

京都大学化学研究所共同研究推進室 国際共同利用・共同研究係

E-mail: icr-hub@scl.kyoto-u.ac.jp, 電話: (0774)38-3121

5-6. 研究成果の公開

学術論文などによる研究成果の公開に際しては、京都大学化学研究所の国際共同利用・共同研究として行われたことを明記して下さい。英文での謝辞例を次に示します。

謝辞例: This work was supported by the International Collaborative Research Program of Institute for Chemical Research, Kyoto University (grant # XXXX).

日本語での謝辞は、この英文表記に準ずるものとして下さい。

化学研究所 国際共共拠点 R2年度採択課題(応募203件, 採択 132件)

課題番号	研究代表者	研究代表者所属	化研内 研究協力者	型	選択 分野	実施 状況	国際	課題名(和文・英文)
2020-1	中川 充	地方独立行政法人 大阪産業技術研究所	倉田 博基	分野選択型	1	萌芽的		化学的手法に基づくキラルプラズモンニックナノ構造体の作製および設計技術 Fabrication and design of chiral plasmonic nanostructures based on chemical methods
2020-2	平井 健二	北海道大学・電子科学研究所	金光 義彦	分野選択型	1	発展的		中赤外レーザーを用いた振動強結合による反応性変化の解明 Unveil the effect of vibrational strong coupling on molecular reactivity
2020-3	老川 典夫	関西大学・化学生命工学部	藤井 知美	分野選択型	1	発展的		マレイル酢酸還元酵素リガンド複合体のX線構造研究 X-Ray Structural Studies on Ligand Complexes of Maleylacetate Reductase
2020-4	草場 光博	大阪産業大学・工学部	橋田 昌樹	分野選択型	1	発展的		レーザープラズマ密度制御による金属表面機能性付与加工 New functionalities on metal surface with controlling laser plasma density
2020-5	長島 健	摂南大学・理工学部	橋田 昌樹	分野選択型	1	萌芽的		2色パルス誘起微細周期構造形成過程の研究 Study of formation of fine periodic structures induced by two color optical pulses
2020-6	大西 哲哉	理化学研究所・仁科加速器科学研究センター	若杉 昌徳	分野選択型	1	萌芽的		ナノ構造を持つ ISOL 用標的の開発 Development of new nano-structure target for ISOL
2020-7	須田 利美	東北大学・電子光理学研究センター	若杉 昌徳	分野選択型	1	萌芽的		電子散乱による短寿命不安定核の希少な構造の解明
2020-8	Haichuan Guo	Ningbo Institute of Industrial Technology (ONITECH) of the Chinese Academy of Sciences	島川 祐一	分野選択型	2	萌芽的	国際	遷移金属酸化物におけるガスセンサー性能研究 Gas sensing properties research of transition-metal oxides
2020-9	Yuichi Negishi	Department of Applied Chemistry, Tokyo University of Science	高谷 光	分野選択型	2	萌芽的	国際	チオラート保護金属クラスターのLC/MSを駆使した原子精度分離と評価 Separation and evaluation of thiolate protected metal clusters with atomic precision by using LC/MS
2020-10	Rainer Streubel	Institute for Inorganic Chemistry, University of Bonn	時任 宣博	分野選択型	2	発展的	国際	新規なアニオン性FLPを用いた小分子活性化 Small molecule activation using anionic crypto-FLPs
2020-11	Wei-Tin Chen	National Taiwan University	島川 祐一	分野選択型	2	発展的	国際	Design and Tailoring Advanced Functional Materials: Symmetry Operation and High Pressure Synthesis
2020-12	Takeaki Iwamoto	Tohoku University, Department of Chemistry	時任 宣博	分野選択型	2	発展的	国際	非対称型高周期典型元素 π 電子系の開拓と物性解明 Development of Unsymmetrical π -Electron Systems of Heavier Main Group Elements and Elucidation of Their Property
2020-13	Shunsuke A. Sato	1Max-Planck Institute for structure and dynamics of matter, Visiting scientist, 2University of Tsukuba	金光 義彦	分野選択型	2	発展的	国際	固体高次高調波発生光制御 Optical control of high-order harmonic generation from solids
2020-14	Alakananda Hajra	DEPARTMENT OF CHEMISTRY, VISVA-BHARATI UNIVERSITY, SANTINIKETAN-731235, INDIA	中村 正治	分野選択型	2	萌芽的	国際	Iron-Catalyzed C-H Borylation
2020-15	Apurba K. Das	Department of Chemistry, Indian Institute of Technology Indore	中村 正治	分野選択型	2	萌芽的	国際	Electrochemically Engineered Peptide based Organic-Inorganic Nanohybrids for Electrocatalytic Conversion of Biomass into Value Added Chemicals
2020-16	Laksmikanta Adak	Department of Chemistry, Indian Institute of Engineering Science and Technology	中村 正治	分野選択型	2	萌芽的	国際	Iron-Catalyzed Enantioselective Carbometallation and Ring-Opening Reactions of Oxabicycloalkenes and other Related Substrates and Mechanistic Consideration

2020-17	立津 慶幸	名古屋大学・リベラルアーツ機構	寺西 利治	分野選択型	2	発展的	第三元素添加による新奇三元系ナノ粒子形成の安定性に関する研究 Study on the stability of novel ternary nanoparticles by doping 3rd elements
2020-18	石井 順久	量子科学技術研究開発機構・関西光学科学研究所	金光 義彦	分野選択型	2	発展的	固体における高効率極端非線形光学のための極短中赤外光源の開発 Development of an ultrashort mid-infrared light source for highly efficient extreme nonlinear optics in solids
2020-19	佐藤 琢哉	東京工業大学・理学院	廣理 英基	分野選択型	2	発展的	マルチフェロイック物質における高強度テラヘルツパルスを利用したマグノン・フォノン励起 Magnon-phonon excitation in multiferroic materials by intense terahertz pulses
2020-20	中村 泰之	国立研究開発法人 物質・材料研究機構	山子 茂	分野選択型	2	発展的	ラジカル重合停止反応機構の包括的な理解とモデル化 Comprehensive understanding and modeling of the termination mechanism in radical polymerization
2020-21	山口 佳隆	横浜国立大学・大学院工学研究院	中村 正治	分野選択型	2	発展的	モノニオン性3座ピンサー型配位子を基盤とする複核ニッケル錯体の開発 Development of dinuclear nickel complexes based on a monoanionic tridentate pincer-type ligand
2020-22	橋 洋一	京都市産業技術研究所・高分子系チーム	中村 正治	分野選択型	2	萌芽的	磁性微粒子を用いたウルシオール塗膜の機能発現 Functionalization of urushiol coating film using magnetic particles
2020-23	笹森 貴裕	筑波大学・数理物質系化学域	若宮 淳志	分野選択型	2	発展的	高性能ペロブスカイト太陽電池作成に有効な高活性酸化スカベンジャーの開発 Creation of Effective Oxidation Scavenger for Efficient Perovskite-based Solar Cells
2020-24	Masayuki Karasuyama	Nagoya Institute of Technology, Department of Computer Science	馬見塚 拓	分野選択型	3	萌芽的 国際	統計的機械学習による効率的なグラフ構造データ解析法の開発 A Study on Statistical Machine Learning for Efficient Graph Structured Data Analysis
2020-25	Jinn-Moon Yang	National Chiao Tung University, Department of Biological Science and Technology	阿久津 達也	分野選択型	3	発展的 国際	深層学習を用いたオミクスデータとモジュールに基づくネットワークデータの統合解析による腫瘍細胞分類 Integrating omics data and module-based network with deep learning to develop cancer type predictive models
2020-26	Jiangning Song	Monash University, Biomedicine Discovery Institute	阿久津 達也	分野選択型	3	発展的 国際	タンパク質分解酵素による切断部位の高精度予測のための次世代バイオフィンフォマティクス技術 Next-generation bioinformatics approaches for the accurate identification of protease-specific cleavage sites
2020-27	Samuel Chaffron	LSRN, CNRS UMR6004	遠藤 寿	分野選択型	3	萌芽的 国際	群集ネットワーク推定とマニングを用いた全球海洋における巨大ウイルスの宿主生物予測 Revealing associations between giant viruses and eukaryotes in the global ocean through community networks inference and mining
2020-28	Tom Delmont	CNRS/Genoscope/UMR8030	緒方 博之	分野選択型	3	萌芽的 国際	生態学的に重要な海洋巨大ウイルスのゲノムの解明 Unveiling the genomic contents of ecologically important marine giant viruses
2020-29	富井 健太郎	産業技術総合研究所・人工知能研究センター	緒方 博之	分野選択型	3	萌芽的	リモートセンシングデータに基づく海洋微生物群集の予測法の開発 Development of predictive methods for marine microbial communities based on remote sensing data
2020-30	ホセ ナチエル	東邦大学・理学部情報科学科	阿久津 達也	分野選択型	3	萌芽的	確率的最小支配集合による複雑ネットワークの制御と解析 Control and Analysis of Complex Networks via Probabilistic Minimum Dominating Sets
2020-31	武村 政春	東京理科大学・理学部	緒方 博之	分野選択型	3	萌芽的	巨大ウイルスのゲノム・トランスクリプトーム解析 Genomics and transcriptomics of giant viruses
2020-32	片岡 剛文	福井県立大学・海洋生物資源学部	遠藤 寿	分野選択型	3	萌芽的	海産細菌捕食性原生生物の全ゲノム解析 Whole genome analyses of marine bacterivorous heterotrophic nanoflagellates
2020-33	佐藤 晋也	福井県立大学・海洋生物資源学部	緒方 博之	分野選択型	3	萌芽的	ハルマ藻・珪藻の祖先的形質の解明に向けた比較ゲノム解析 Comparative genome analysis of Parmales and diatoms: Looking for the ancestral genomic feature
2020-34	茅野 光範	帯広畜産大学・グローバルアグリメディン研究センター	馬見塚 拓	分野選択型	3	発展的	分子ネットワーク解析の統計的機械学習による解法と応用 Statistical machine learning methods and applications in molecular network analysis

2020-35	Ru-Shi Liu	National Taiwan University, Department of Chemistry	金光 義彦	分野選択型	4	発展的	国際	ハロゲン化物ペロブスカイトおよび関連材料からの発光 Light emission from halide perovskites and related materials
2020-36	Margetic, Davor	Rudjer Boskovic Institute, Bijenicka c. 54, 10000 Zagreb, Croatia, Division of organic chemistry and biochemistry, Laboratory for physical organic chemistry, Prof. PhD, head of Division	村田 靖次郎	分野選択型	4	萌芽的	国際	グアニジン修飾アントラセンの付加環化反応の開発 Exploration of Cycloaddition Properties of Guanidine Functionalized Anthracenes
2020-37	Eli Zysman-Colman	University of St Andrews, Organic Semiconductor Centre, EaStCHEM School of Chemistry	梶 弘典	分野選択型	4	発展的	国際	分子配向を制御した新規青色TADF発光材料の開発 Development of new blue TADF emitters with horizontal molecular orientations
2020-38	Akimitsu Narita	Okinawa Institute of Science and Technology Graduate University (OIST), Organic and Carbon Nanomaterials Unit	廣瀬 崇至	分野選択型	4	発展的	国際	ナノグラフエンと湾曲 π 系のカップリングと電子的光学的相互作用の解明 Coupling of nanographenes and curved π -systems and elucidation of their electronic and optical interactions
2020-39	Ak(nori) Saeki	Department of Applied Chemistry, Graduate School of Engineering, Osaka University	若宮 淳志	分野選択型	4	発展的	国際	スズペロブスカイトに特化したホール輸送材の開発と素子評価 Development of hole transport materials for tin-perovskite and device characterization
2020-40	村田 理尚	大阪工業大学・工学部応用化学科	村田 靖次郎	分野選択型	4	発展的		π 共役ニッケル錯体を用いた高性能n型熱電材料の開発 Development of π -Conjugated Nickel Complexes for High Performance n-Type Thermoelectric Materials
2020-41	黒飛 敬	久留米工業高等学校・一般科目(理科系)	村田 靖次郎	分野選択型	4	発展的		ヘテロアズレンの特性を活かした新規機能性色素の創製 Synthesis of Novel Organic Functional Dye bearing heteroazulene unit
2020-42	平井 智康	大阪工業大学・応用化学科	竹中 幹人	分野選択型	4	萌芽的		ブロック共重合体の動的誘起螺旋構造形成とその支配因子の解明 Preparation of dynamic induced-helical conformation in block copolymer and investigation of its dominant factor
2020-43	安倍 学	広島大学・大学院理学研究科	山子 茂	分野選択型	4	発展的		マクロ環骨格内に導入れた反応中間体の化学 A Study of reactive intermediates in macrocyclic systems
2020-44	吉田 圭佑	名城大学・薬学部	川端 猛夫	分野選択型	4	萌芽的		有機分子触媒を用いるN-M軸不斉化合物の速度論的光学分割法の開発 Development of kinetic resolution for N-N axial chirality by organocatalyst
2020-45	VaoVisit-soongnem	Suranaree University of Technology, Chemistry	渡辺 宏	分野選択型	5	萌芽的	国際	イオン性末端会合高分子の構造とダイミックスの分子描像 Molecular understanding on the structures and dynamics of ionic end-aggregation polymers
2020-46	Sanghoon Kim	University of Ulsan, Department of Physics	小野 輝男	分野選択型	5	発展的	国際	Observation of orbital Hall effect in ferromagnet/nonmagnet bilayers
2020-47	Sathish K. Sukumaran	Graduate School of Organic Materials Science, Yamagata University	渡辺 宏	分野選択型	5	発展的	国際	高分子液体の高周波応答: レオロジーおよび誘電緩和 High Frequency Response of Polymeric Liquids: Rheology and Dielectric Relaxation
2020-48	H0, Tung-Yuan	Academia Sinica, Research Center for Environmental Changes	宍林 由樹	分野選択型	5	発展的	国際	北太平洋における微量金属の元素・同位体組成: 起源と内部循環 Trace metal elemental and isotopic composition in the North Pacific Ocean: sources and internal cycling
2020-49	Ifor D. W. Samuel	Organic Semiconductor Centre, SUPA, School of Physics and Astronomy, University of St. Andrews	梶 弘典	分野選択型	5	発展的	国際	熱活性化遅延蛍光素子における励起子消滅機構の解明 Revealing exciton quenching mechanisms in thermally activated delayed fluorescent devices
2020-50	Yasuhiro Tachibana	RMIT University, School of Engineering	寺西 利治	分野選択型	5	発展的	国際	狭バンドギャップ半導体膜の作製とその光誘起電荷移動・輸送ダイミックスの評価 Fabrication of low bandgap semiconductor films and their light induced interfacial charge transfer and charge transport dynamics
2020-51	Maya K. Endoh	Stony Brook University, Department of Material Science and Chemical Engineering	竹中 幹人	分野選択型	5	発展的	国際	高分子溶液における流動誘起濃度揺らぎのダイミックス Dynamics of Shear-Induced Concentration Fluctuation in Polymer Solutions
2020-52	藤原 明比古	関西学院大学・理工学部	竹中 幹人	分野選択型	5	発展的		GISAXS-QT法による硫黄系高分子薄膜材料における硫黄元素の不均一分布評価 Visualization of sulfur distribution in polymer thin films using GISAXS-QT

2020-53	河内 孝之	京都大学・生命科学研究所	山口 信次郎	分野選択型	5	萌芽的	基部陸上植物・ゼニゴケにおける活性型ジベレリンの単離と同定 Identification of an active gibberellin compound in the basal land plant Marchantia polymorpha
2020-54	中口 謙	近畿大学・理工学部	宗林 由樹	分野選択型	5	発展的	微量金属分析による山岳地帯大気エアロゾル中の起源解析 Origin analysis of atmospheric aerosol of mountainous areas by trace metal analysis
2020-55	園山 正史	群馬大学・大学院理工学府	長谷川 健	分野選択型	5	発展的	部分フッ素化両親媒性分子の膜物性・構造に対する付着長依存性の解析 Analysis of membrane structure and properties of partially fluorinated amphiphilic molecules
2020-56	野呂 篤史	名古屋大学・大学院工学研究科	渡辺 宏	分野選択型	5	萌芽的	熱可塑性エラストマーの動的粘弾性と引張特性 Dynamic Viscoelasticity and Tensile Properties of Thermoplastic Elastomers
2020-57	飯田 健二	北海道大学・触媒科学研究所	寺西 利治	分野選択型	5	発展的	プラズマモンテカルロ法を設計するための理論的指針の構築 Construction of Theoretical Guidelines for Designing Plasmonic Nanoalloys
2020-58	向井 浩	京都教育大学・教育学部理学科	宗林 由樹	分野選択型	5	萌芽的	イオン液体含有高分子膜を用いた金属イオンの液膜輸送に関する研究 Study on transportation of metal ions through a polymer membrane containing ionic liquid
2020-59	浦川 理	大阪大学・大学院理学研究科	松宮 由美	分野選択型	5	発展的	ブロードバンド誘電分光法による非晶性高分子の分子運動の階層性解明 Exploration of Hierarchical Dynamics of Amorphous Polymers by Broadband Dielectric Spectroscopy
2020-60	Youngdon Kwon	Sungkyunkwan University (Korea), School of Chemical Engineering	松宮 由美	課題提案型		萌芽的 国際	末端吸着平衡下におけるA型 Rouse 鎖の誘電緩和・動的カップリングの効果 Dielectric Relaxation of Type-A Rouse Chain under End-adsorption/desorption Equilibrium Effect of Motional Coupling
2020-61	Zuhua He	Chinese Academy of Sciences, CAS Center for Excellence in Molecular Plant Sciences, Institute of Plant Physiology and Ecology	山口 信次郎	課題提案型		発展的 国際	イネの成長ホルモンの不活性化機構の解析 Molecular mechanisms for the inactivation of a growth hormone in rice
2020-62	Ying Ma	South China University of Technology, Chemistry and Chemical Engineering	大野 工司	課題提案型		発展的 国際	電気化学発光・バイオセンサーの開発を指向した凝集誘起発光性ポリマーベースの精密合成 Well-defined AIE-Based Polymer Brush for the Application of the Electrochemical Luminescence Biosensors
2020-63	ZHONG, Sheng	Peking University, School of Life Sciences	青山 卓史	課題提案型		発展的 国際	花粉形成におけるホスホリノシグナルの役割 Role of Phosphoinositide Signaling in Pollen Development
2020-64	OHASHI, Yohei	MRC Laboratory of Molecular Biology	青山 卓史	課題提案型		萌芽的 国際	植物細胞内の膜交通におけるPX-PHタイプホスホリノラーゼの役割 Role of PX-PH-type Phospholipase Ds in Plant Intracellular Membrane Traffic
2020-65	Xiaoguang Lei	Peking University, College of Chemistry and Molecular Engineering	上杉 志成	課題提案型		発展的 国際	プロテオーム解析による胆汁酸結合酵素の阻害剤探索 Proteomic Approach to Discovering Specific Inhibitors for Bile-Acid Interacting Enzymes
2020-66	Pinghe Cai	Xiamen University, Department of Marine Chemistry and Geochemistry	宗林 由樹	課題提案型		発展的 国際	Transfer of redox sensitive elements (Fe, Mn, Zn) across the sediment-water interface in a hypoxia area near the East Chia Sea
2020-67	Kazunori Matsuura	Tottori University, Department of Chemistry and Biotechnology	二木 史朗	課題提案型		萌芽的 国際	人工ウイルスコアの細胞内送達への応用 Application of artificial viral capsid to intracellular delivery
2020-68	Anne S. Ulrich	Karlsruhe Institute of Technology (KIT), Institute of Organic Chemistry (IOC) and Institute of Biological Interfaces (IBG-2), Chair of Biochemistry at IOC	二木 史朗	課題提案型		発展的 国際	曲率誘導ペプチドの構造活性相関と応用 Structural and functional analysis of curvature-inducing peptides and application
2020-69	Lu Zhou	Fudan University, School of Pharmacy	上杉 志成	課題提案型		発展的 国際	小分子化合物による選択的タンパク質アセチル化 Site-Selective Protein Acetylation by a Small Molecule
2020-70	Kab-Jin Kim	Korea Advanced Institute of Science and Technology, Department of Physics	小野 輝男	課題提案型		発展的 国際	フェリ磁性体でのスピン波の電圧変調 Modulation of ferrimagnetic spin waves by electric field

2020-71	Silvia Pujals	Nanoscipy for Nanomedicine Group, Institute for Bioengineering of Catalonia (IBEC)	二木 史朗	課題提案型		萌芽的	国際	ナノ医薬の新規細胞内効率的送達法 Novel strategy for intracellular delivery of nanomedicines
2020-72	Lian Duan	Tsinghua University, Department of Chemistry	梶 弘典	課題提案型		発展的	国際	迅速な逆項間交差を有する熱活性化遅延蛍光材料を用いた高効率・高耐久青色有機EL素子の開発 Development of highly efficient and stable blue organic light emitting diodes using thermally activated delayed fluorescent materials with ultrafast reverse intersystem crossing
2020-73	Maya K. Endoh	Stony Brook University, Department of Material Science and Chemical Engineering	竹中 幹人	課題提案型		発展的	国際	高分子ナノ表面構造による殺菌効果-II Fabrication of nanotopographical polymer surfaces for bactericidal properties-II
2020-74	Robert C. Ferrier, Jr.	Michigan State University, Chemical Engineering and Materials Science	大野 工司	課題提案型		発展的	国際	リチウムイオン電池用ポリエーテル系ナノコンポジット固体電解質の合成 Synthesis of Polyether Nanocomposite Solid Polymer Electrolytes for Lithium Ion Batteries
2020-75	Maria Michela Corsaro	University of Naples Federico II, Department of Chemical Sciences, Professor	栗原 達夫	課題提案型		発展的	国際	細菌が放出する外膜小胞の表層糖脂質の構造機能解析 Structural and functional analysis of the surface glycolipids of outer membrane vesicles released by bacteria
2020-76	Xianzhu Dai	College of Resources and Environment, Southwest University, Chongqing, P. R. China	栗原 達夫	課題提案型		萌芽的	国際	低温適応微生物を用いた低温異種タンパク質分泌生産系の構築 Construction of heterologous protein secretion system at low temperatures by using cold-adapted microorganisms
2020-77	RUBIO, Vicente	National Center of Biotechnology (CNB-CSIC), Plant Molecular Genetics Department	柘植 知彦	課題提案型		発展的	国際	植物の可塑性を支える遺伝子発現を制御する分子機構 Molecular mechanisms governing gene expression regulation in plant plasticity
2020-78	Shingo Ito	Division of Chemistry and Biological Chemistry, School of Physical and Mathematical Sciences, Nanyang Technological University (NTU)	山子 茂	課題提案型		萌芽的	国際	シクロラファエニレンと含窒素コラニレンのホスト-ゲスト相互作用による超分子構造体の生成 Formation of Supramolecular Complexes Through a Host-guest Interaction Between Cycloparaphenylene and Azacoronulenes
2020-79	Marcus W. Doherty	Research School of Physics and Engineering, Australian National University	水落 憲和	課題提案型		発展的	国際	ダイヤモンド多量子ビット量子プロセッサの研究 Research of multi-qubit diamond quantum processors
2020-80	Gopalakrishnan Balasubramanian	Max-Planck Institute for Biophysical Chemistry, Göttingen, Germany	水落 憲和	課題提案型		発展的	国際	表面近傍のNV中心の安定化へ向けた研究 Research toward stable NV centers at shallow region in diamond
2020-81	Thomas Wirth	Cardiff University, School of Chemistry	川端 猛夫	課題提案型		発展的	国際	超原子価ヨウ素化学とフローケミストリーの融合による新合成 Advanced Iodine - Mediated Stereoselective Flow Electrochemistry
2020-82	Jonathan Clayden	School of Chemistry, University of Bristol	川端 猛夫	課題提案型		発展的	国際	カチオン-π 相互作用を利用するエノラト化学の新展開 Cation-π Interaction in Enolate Chemistry
2020-83	Jean-Pierre Bucher	Université de Strasbourg, Institut de Physique et Chimie des Matériaux (IPCMS)	寺西 利治	課題提案型		萌芽的	国際	Interdisciplinary Approach to Nanostructured Materials for Applications
2020-84	Quan Chen	Changchun Institute of Applied Chemistry, Chinese Academy of Sciences (CAS)	松宮 由美	課題提案型		萌芽的	国際	ガラス状ポリスチレンにおける鎖配向、欠陥、強靱性の相関 Relationship between chain orientation, amount of defects, and toughness of glassy polystyrene materials
2020-85	Kensuke Homma	Hiroshima University, Physics	井上 俊介	課題提案型		発展的	国際	宇宙暗黒成分解明へ向けた真空内四光波混合の探索 Search for four-wave-mixing in the vacuum - Unveiling dark components in the Universe -
2020-86	内田 幸明	大阪大学・大学院基礎工学研究科	大野 工司	課題提案型		発展的		ポリマーブラシ付与強磁性ナノプレートの精密合成による磁性フォトニック液晶の実現 Fine synthesis of polymer brush on ferromagnetic nano-platelet for magnetophotonic LC
2020-87	三枝 栄子	大阪市立大学大学院・理学研究科物質分子系専攻	長谷川 健	課題提案型		萌芽的		自己集積型希土類錯体の薄膜化とその機能解析 Fabrication of thin films and structural characterization of self-assembled lanthanoid complexes
2020-88	富永 るみ	広島大学大学院・統合生命科学研究科	青山 卓史	課題提案型		萌芽的		植物表皮細胞の分化における制御ネットワークの研究 Study on the Regulatory Network of Plant Epidermal Cell Differentiation

2020-89	山崎 晶	大阪大学・微生物病研究所	上杉 志成	課題提案型		萌芽的	免疫賦活化するナノ集合体 Immune-Stimulatory Nano-Assemblies
2020-90	瀬戸 義哉	明治大学・農学部	山口 信次郎	課題提案型		発展的	「非典型的」ストリゴラクトン類の植物ホルモンおよび根圏シグナルとしての機能解析 Functional analysis of non-canonical strigolactones as plant hormones and root-derived signals
2020-91	島田 良子	日本女子大学・理学部数物科学科	渡辺 宏	課題提案型		萌芽的	ナマチック液晶-溶媒混合系における相平衡と分子ダイナミクスの解析 Analysis of phase equilibrium and molecular dynamics in mixture of nematic liquid crystal and solvent
2020-92	井澤 毅	東京大学・農学生命科学研究所	増口 深	課題提案型		萌芽的	イネのストリゴラクトン合成におけるCYP711Aファミリーの機能解析 Functional analysis of the CYP711A family in strigolactone biosynthesis of rice
2020-93	倉田 淳志	近畿大学・農学部 応用生命化学科	栗原 達夫	課題提案型		発展的	腸内細菌および発酵食品由来細菌が生産する細胞外膜小胞の生理機能解析と応用 Analysis of the physiological functions of extracellular vesicles produced by intestinal bacteria and fermented food-derived bacteria and their application
2020-94	柴 祐司	信州大学・医学部	上杉 志成	課題提案型		萌芽的	自己集合性分子による心筋細胞移植の効率化 Self-Assembling Molecules for Improvement of Cardiomyocyte Engraftment
2020-95	山田 啓介	岐阜大学・工学部・化学・生命工学科	小野 輝男	課題提案型		発展的	共沈法を用いて作製した多結晶YIG薄膜のスピン波伝搬の観測 Observation of spin wave propagation in polycrystalline YIG thin films prepared by coprecipitation method
2020-96	大橋 若奈	慶應義塾大学・薬学部・生化学講座	二木 史朗	課題提案型		発展的	抗腫瘍性膜透過ペプチドによるがん進展調節 Control of malignant behavior of colorectal cancer by anti-tumoral cell penetrating peptide (CPP)
2020-97	松本 貴裕	名古屋市立大学・芸術工学科	金光 義彦	課題提案型		萌芽的	水素終端ナノ結晶シリコン表面における巨大重水素置換反応の分光学的解明とその応用 Giant exchange reaction from H to D terminating on nanocrystalline silicon surface and their use
2020-98	倉橋 健介	大阪府立大学工業高等専門学校・環境物質化学コース	宗林 由樹	課題提案型		萌芽的	界面活性剤を用いた溶媒含浸樹脂による金属イオンの固相抽出 Solid phase extraction of metal ion by solvent impregnated resin using surfactant
2020-99	長兵 太郎	北海道大学・工学研究院応用化学部門	小野 輝男	課題提案型		発展的	磁性酸化物絶縁体上に接合したP超薄膜の異常ホール効果 Anomalous Hall effect of ultrathin Pt films grown on magnetic oxide
2020-100	齊藤 高志	高エネルギー加速器研究機構・物質構造科学研究所	鳥川 祐一	課題提案型		発展的	異常高原子価イオンを含む機能性酸化物合成とその構造物性研究 Synthesis and study of oxides with unusually high-valent cation
2020-101	藤塚 守	大阪大学・産業科学研究所	山子 茂	課題提案型		萌芽的	メビウストポロジーを有する環状パラフェニレンの芳香族性の検討 Studies on aromaticity of cyclic paraphenylenes with Möbius topology
2020-102	田中 雅章	名古屋工業大学・物理工学科	小野 輝男	課題提案型		萌芽的	垂直磁化を有するコバルトフェライト薄膜の電気・磁気的挙動の解明 Study on electronic and magnetic behavior of perpendicularly magnetized cobalt ferrite films
2020-103	城戸 淳二	山形大学・大学院有機材料システム研究科	梶 弘典	課題提案型		発展的	マルチスケールシミュレーションによるp型有機半導体材料群の電荷移動度予測 Prediction of Charge Transport Mobilities of Organic p-Type Semiconductors based on Multiscale Simulation
2020-104	尾坂 格	広島大学・大学院工学科	脇岡 正幸	課題提案型		発展的	DAP法を用いた新規π共役系ポリマーの開発と有機薄膜太陽電池への応用 Development of novel π-conjugated polymers by DAP and their application to organic photovoltaics
2020-105	真島 豊	東京工業大学・フロンティア材料研究所	寺西 利治	課題提案型		発展的	Au ₂₃ スピン・価数依存強磁性単電子トランジスタ Spin and Valence Electron Dependent Au ₂₃ Ferromagnetic Single-Electron Transistor
2020-106	岸本 泰明	京都大学大学院・エネルギー科学研究科	井上 俊介	課題提案型		萌芽的	高強度レーザーと構造物媒質の相互作用による高エネルギー密度プラズマの生成・保持に関する実験研究 Study of the generation and sustainment of high energy density plasmas due to the interaction between high power laser and structured medium

2020-107	豊竹 洋佑	立命館大学・生命科学部生物工学科	小川 拓哉	課題提案型	萌芽的	酢酸菌の外的ストレス耐性における膜脂質の機能解析 Functional analysis of membrane lipids on environmental stress tolerance in acetic acid bacteria
2020-108	榊原 圭太	産業技術総合研究所・中国センター	辻井 敬亘	課題提案型	萌芽的	セルロースの氷形成挙動の解明と表面修飾による着氷防止制御 Study on water freezing with cellulose and their anti-icing control by surface modification
2020-109	徳田 翔夫	金沢大学・理工研究域 電子情報学系	水落 憲和	課題提案型	発展的	ダイヤモンドの数ナノレベルにおける表面近傍のNV中心作製 Manufacture of nano-scale shallow NV centers in diamond
2020-110	牧野 俊晴	産業技術総合研究所・先進パワー・エレクトロニクス研究センター	水落 憲和	課題提案型	発展的	ダイヤモンド中のNV中心スピンの電氣的制御と電氣的検出 Electrical control and detection of spin of NV center
2020-111	山中 正浩	立教大学・理学部化学科	川端 猛夫	課題提案型	発展的	4-ピロリジン-ピリジン型分子触媒による化学選択的アリル化反応の理論的解析 Theoretical Study on Chemoselective Acylation Catalyzed by 4-Pyrrolidinopyridine Derivatives
2020-112	森山 克彦	千葉大学・大学院理学研究院	川端 猛夫	課題提案型	萌芽的	動的不斉の発現を基盤とする不斉極性転換型炭素—炭素結合形成反応の開発 Asymmetric Umpolung C-O Bond Formation via Expression of Dynamic Chirality
2020-113	吉村 智之	金沢大学・医薬保健研究域薬学系 機能性分子合成学	川端 猛夫	課題提案型	萌芽的	海産天然物ボヘマミン類およびその誘導体の不斉全合成研究 Studies on enantioselective total syntheses of marine natural product boheminamines and their derivatives
2020-114	秦野 修	奈良県立医科大学・医学部	中村 正治	課題提案型	萌芽的	再生可能資源・木質バイオマスの先端化学材料への効率的変換法の開発 Development of efficient conversion method of woody biomass, renewable biological resources, to advanced chemical materials
2020-115	Chengshan Wang	Middle Tennessee State University, Chemistry	長谷川 健	連携・融合促進型	国際	Determine the three-dimensional structure of ^{13}C labeled α -synuclein(61-95) in the Langmuir-Blodgett film and supported phospholipids bilayers by p-MAIRS FT-IR
2020-116	Mona Semsarilar	ONRS, Institut European des Membranes (IEM)	山子 茂	連携・融合促進型	国際	Hydrophilic Dendrimers as Additive for Polyvinylidene fluoride Based Membranes
2020-117	Tadanori Koga	Stony Brook University, Department of Material Science and Chemical Engineering	竹中 幹人	連携・融合促進型	国際	高分子ナノコンポジットの延伸過程における補強メカニズムの解明 Resolving percolation dynamics responsible for mechanical reinforcement in polymer nanocomposites under uniaxial stretching
2020-118	Tadashi Inoue	Osaka University, Department of Macromolecular Science	松宮 由美	連携・融合促進型	国際	東アジア圏の若手レオロジストのための第16回ワークショップ The 16th International Workshop for East Asian Young Rheologists
2020-119	Liangbin Li	University of Science and Technology of China, National Synchrotron Radiation Laboratory	登坂 雅聡	施設・機器利用型	国際	Study on the Mechanism of the Crystal Structural Evolution of Polydimethylsiloxane
2020-120	Kunliang Ji	Centre for Science at Extreme Conditions and School of Chemistry, University of Edinburgh	島川 祐一	施設・機器利用型	国際	High-pressure synthesis of potential multiferroic oxides
2020-121	Torranin Chairuangsr	Chiang Mai University, Industrial Chemistry	倉田 博基	施設・機器利用型	国際	Micro- and Nano-structural Characterization by Advanced Transmission Electron Microscopy of Novel Functional Materials for Battery Development
2020-122	Cheng-Yen Wen	National Taiwan University, Department of Materials Science and Engineering	倉田 博基	施設・機器利用型	国際	Electron energy loss spectroscopy analysis of hexagonal multilayer graphene
2020-123	Ming-Wen Chu	Center for Condensed Matter Sciences, National Taiwan University, Research Fellow	倉田 博基	施設・機器利用型	国際	Electronic Excitations in Charge-Density-Wave Systems
2020-124	Mao Minoura	Rikkyo University, College of Science, Department of Chemistry	時任 宣博	施設・機器利用型	国際	新規有機セレンおよびテルル化合物の合成と性質解明 Synthesis and Characterization of Novel Organoselenium and -tellurium Compounds

2020-125	吾郷 友宏	茨城大学・工学部物質科学工学科	時任 宣博 水畑 吉行	施設・機器利用型			単結晶X線構造解析を用いた、含フッ素共役分子の結晶構造におけるフルオラス相互作用の解明 Elucidation of the fluoruous interactions in the crystal structures of fluorine-containing conjugated molecules by the single-crystal X-ray structural analysis
2020-126	松尾 司	近畿大学・理工学部	時任 宣博	施設・機器利用型			高周期14族元素低原子面化学種の合成と分子構造の解明 Synthesis and Structural Characterization of Low-Valent Species of Heavier Group 14 Elements
2020-127	後藤 和馬	岡山大学・大学院自然科学研究科	梶 弘典	施設・機器利用型			DNP-NMRを利用した炭素材料表面官能基解析法の開発 Development of functional group analysis on the surface of carbon materials using DNP-NMR
2020-128	高橋 まさえ	東北大学・大学院農学研究科	時任 宣博	施設・機器利用型			平面シリセンナノリボンの理論設計と新しい動作原理の探究 Theoretical design of planar silicene nanoribbons and search for new operating principles
2020-129	宮本 光貴	島根大学・総合理工学部	倉田 博基	施設・機器利用型			核融合プラズマ対向材料中の水素・ヘリウム挙動の高精度測定 High accuracy measurement of hydrogen and helium behavior in plasma facing materials for nuclear fusion devices
2020-130	長河 記嘉	福岡大学・理学部化学科	時任 宣博	施設・機器利用型			チオピリリウム骨格を組み込んだカチオン型芳香族化合物の合成と構造解析 Synthesis and structures of cationic aromatics bearing thiopyrylium units
2020-131	布施 泰朗	京都工芸繊維大学・分子化学系	中村 正治	施設・機器利用型			FT-ICR-MSを用いた湖沼及び土壌環境中溶存有機物の化学特性および起源解析 Analysis of chemical properties and origins of organic matter in lakes and soils using FT-ICR-MS
2020-132	斉藤 光	九州大学・大学院総合理工学研究院	倉田 博基	施設・機器利用型			2次元物質欠陥の束縛励起子のSTEM-EELS解析 STEM-EELS analysis of bound excitons at defects in two-dimensional materials

